Targeting Aneuploidy, CIN and Mechanisms of DNA content reduction in cancer

Maria Mandelia

A thesis submitted for the degree of Doctor of Philosophy

Breast Cancer Now Research Centre
The Institute of Cancer Research
237 Fulham Road London

This thesis was completed under the supervision of Professor Spiros Linardopoulos. The work described here was carried out in the Breast Cancer Now Research Centre, The Institute of Cancer Research, 237 Fulham Road, London SW3 6JB.

I, Maria Mandelia confirm that the work presented in this thesis is my own. Where information has been derived from other sources, I confirm that this has been indicated in the thesis.

Date: November 13th, 2020

…Maria Mandelia……..

Abstract

Chromosomal instability (CIN) and aneuploidy are distinct events that can coexist in a tumour and one can result from the other. They can arise through direct errors in mitosis or in DNA damage repair and response machineries, DNA replication or chromatin remodelling that may allow damaged DNA to progress through cell cycle. Importantly, both CIN and aneuploidy can promote tumour initiation, progression and resistance to cancer therapies. Moreover, cell fusion is another mechanism that can lead to CIN or aneuploidy after chemotherapy or irradiation treatment. However, it can also cause tumour resistance and relapse, independently of aneuploidy and CIN, but currently, little is known about these mechanisms.

The overall aim of this PhD study was to identify novel targets in CIN and aneuploidy and to elucidate and target the mechanisms by which cell fusion can promote tumour relapse after chemotherapy treatment. Generation of different CIN and aneuploid models through errors in mitosis, DNA damage response/repair machineries or impaired chromatin remodelling, allowed the identification of hits dependent or independent of specific chromosome and gene alterations. Screening of CIN and aneuploid clones using a custom sgRNA library and confirmation by gene silencing and chemical inhibition, led to identification of synthetically lethal interactions between SETD7 depletion and BRG1 defects, TEX14-depletion and CENP-E-defects, HELQ-depletion and SWI/SNF-mutated models and PRIM1 depletion and CHK1-defective or SWI/SNF-mutated complex. In addition, we confirmed the induction of cell fusion due to Paclitaxel treatment and we identified and targeted, by screening of a small molecule library, the events by which tumour relapse occurs. Finally, we identified Crenolanib in sequential treatment with Paclitaxel as a new therapeutic approach in clinic to delay tumour recovery after Paclitaxel treatment.

In summary, this PhD project proposes novel potential therapeutic targets and approaches in CIN and cell recovery after drug treatment, to improve cancer patient outcome.

Acknowledgements

I would first like to thank my supervisor Professor Spiros Linardopoulos for giving me the opportunity to carry out my PhD in his laboratory. I am truly grateful for his insight, guidance and support throughout the duration of this study and the writing of this thesis. His contribution with knowledge, passion for science and time have been essential for inspiring and motivating me during the past four years.

I would also like to thank my associate supervisor Kostas Drosopoulos for his guidance, support and help from the first day of this project. His ideas and advice have been essential to this project and my personal scientific development.

To all the members of the Linardopoulos lab in Sutton; Grace, Katrin, Lisa and Yiannis and in Chelsea; Kostas, Oliver and Romana: thank you all for your scientific assistance and the valuable discussions as well as the fantastic working environment that you created. In particular, I would like to thank Oliver and Romana for their day to day scientific and personal support. It was a pleasure working with you!

In addition, I would like to thank Professor Jessica Downs lab, at ICR, for providing me with the SWI/SNF mutated CIN models and the past and present members of Flow Cytometry and Microscopy Facility in Chelsea, for their assistance with the microscopy and FACS experiments.

Thank you, to all of my friends at ICR and in particular to Aaron, Amanda, Andri, David, Doug, Erik, Ioanna, Joe, Laura, Liam, Nikos, Rebecca, Sarah and Yiannis, for their advice, support and the incredible time at ICR and out of the ICR!

To all of my Greek friends, who are supporting me the last 10 years (Chrysa, Maria, Michalis and Sophia), or from my childhood (Athina, Elena and Vasia): thank you

for being there for me, understanding and always thinking of me, even with so many kilometres and countries, separating us!

To Nikos: thank you for supporting me psychologically the last three years of my PhD. Your patience and constant will to learn inspired me and continues to inspire me every day to evolve and become a better scientist and person.

Finally, I would like to thank my parents and sister, Yiannis, Vaso and Ioanna, for believing in me and supporting me in every possible way from the beginning of my studies. I am truly thankful for your endless encouragement!

Table of contents

List of figures

List of tables

List of videos

List of abbreviations

Å	angstrom
APC/C	Anaphase-promoting complex/cyclosome
APS	Aneuploidy-associated protein signature
ARID	AT-rich interactive domain
ART1	ADP-ribosyltransferase 1
ASCT2	Alanine, Serine, Cysteine Transporter 2
ATIP3	AT2 receptor-interacting protein 3
ATM	Ataxia-Telangiectasia Mutated
ATR	ataxia telangiectasia and Rad3-related
bp	Base pare
BUB1	Budding uninhibited by benzimidazoles 1
BUB1B,BUBR1	Budding uninhibited by benzimidazoles 1 Homolog Beta
BUB3	Budding uninhibited by benzimidazoles 3
Cas9	CRISPR associated protein 9
CCLE	from Cancer Cell Encyclopedia
CDK	cyclin dependent kinase
cDNA	Complementary DNA
CENP	Centromere-associated protein
CFS	common fragile sites
CGH	Comparative genomic hybridization
CHK	Checkpoint kinase
CIN	Chromosomal instability
CoCl2	Cobalt chloride
CRISPR	clustered regularly interspaced short palindromic repeats
CSCs	Cancer stem cells
CTG	CellTiter-Glo
DAPI	4’,6-diamidino-2-phenylindole
DDR	DNA damage response
DMEM	Dulbecco’s Modified Eagle's Medium
DMSO	Dimethyl sulfoxide
DNA	Deoxyribonucleic acid
Dox	Doxycycline
DSB	Double strand break
DTT	Dithiothreitol
EMT	Epithelial to mesenchymal transition

F1	Filial generation 1
FACS	Fluorescence-activated cell sorting
FBS	Foetal bovine serum
FDA	Food and drug administration
FF	Fusion family
FLT3	Fms Related Receptor Tyrosine Kinase 3
GIN	Genomic instability
G1	Gap 1
G2	Gap 2
gDNA	Genomic DNA
HELQ	Helicase, POLQ Like
HIV	Human immunodeficiency virus
HPV	Human papillomavirus
Hoechst	Trihydrochloride, Trihydrate
HR	Homologous recombination
HSP90	Heat shock protein 90
HST	Heterokaryon to synkaryon transition
ICLs	Interstrand crosslinks
IL	Interleukin
kDa	kilodaltons
KMN	Knl1/ Mis12/ Ndc80 complex
KO	Knockout
KT	Kinetochore
LSS	Laboratory Support Services, in ICR
M	Mitosis
MAD2	Mitotic arrest deficient 2
MCM2-7	Minichromosome maintenance complex component 2-7
MEFs	mouse embryonic fibroblasts
MIN	Microsatellite instability
MPS1	Monopolar spindle 1
mRNA	Messenger RNA
MT	Microtubule
N	haploid number of chromosomes (23 in human cells)
NEDD4	neural precursor cell expressed developmentally down-regulated protein 4
NGS	Next generation sequencing
NHEJ	Non-homologous end joining
NIN	Nucleotide instability

PAGE	Polyacrylamide gel electrophoresis
PBS	Phosphate-buffered saline
PCM	Pericentriolar material
PCNA	Proliferating Cell Nuclear Antigen
PCR	polymerase chain reaction
PDGFR	Platelet derived growth factor receptor
PGCCs	Polyploid giant cancer cells
PI	Propidium iodide
PRIM1	DNA primase subunit 1
RNA	Ribonucleic acid
ROCK	Rho-associated protein kinase
RPMI	Roswell Park Memorial Institute
RT	Room temperature
S	Synthesis
S-CIN	Structural chromosomal instability
SAC	Spindle assembly checkpoint
SARS-CoV-2	Severe acute respiratory syndrome coronavirus 2
SDS	Sodium dodecyl sulfate
SETD	SET-Domain
sgRNA	Single guide RNA
siRNA	Small interfering RNA
SIV	Simian immunodeficiency virus
SMARCA	SWI/SNF Related, Matrix Associated, Actin Dependent Regulator Of Chromatin, Subfamily A
SNPs	Single nucleotide polymorphisms
SSB	Single Strand Break
STEDV	Standard deviation
SWI/SNF	SWItch/Sucrose Non-Fermentable
TBS	Tris Buffered Saline
TCGA	The cancer genome atlas
TEX14	Testis expressed 14
TNF	intracellular domain (ICD) form
USP10	Ubiquitin specific peptidase 10
WT	Wild Type
17-AAG	17-N-allylamino-17-demethoxygeldanamycin

Chapter 1 - Introduction

1.1 Worldwide and UK cancer incidence

Cancer is a term that describes a large group of complex diseases which each have their own sub-classifications, diagnosis and treatment. Cancer, can initiate in almost every tissue of the human body, in which the abnormal, cancer cells may acquire novel characteristics, which allow them to grow uncontrollably and invade locally or spread to other parts of the body. Worldwide, in 2018, 17 million new cases of cancer were diagnosed, 9.6 million deaths were caused and in the same year, cancer was one of the highest cause of mortality, globally. The number of new cancers is predicted to increase by over half a million every year with a total of 30 million new cancer cases and approximately 16 million new cancer related deaths, by the end of 2040 (Cancer Research UK statistics 2018, World Health Organization statistics 2018).

Cancer can be categorised as many different diseases and distinct subtypes. Nevertheless, in every cancer type, it is required that cells acquire genetic and epigenetic alterations in order to obtain tumorigenic potential. These alterations occur gradually, providing the transformed cells with advantageous properties. In line with Darwinian evolution, the transformed cells with advantageous characteristics will outcompete the rest and grow into the main cell population in a specific organ and eventually they can expand in other areas of the human body. In 2000, Hanahan and Weinberg described the first model according to which the transformed cells need to acquire six essential properties in order to become malignant: self-sufficiency in growth signals, insensitivity to growth-inhibitory signals, evasion of programmed cell death, limitless replicative potential, sustained angiogenesis, and tissue invasion and metastasis (Hanahan and Weinberg, 2000).

Progress in cancer research, led to the enrichment and refinement of the model, which was updated in 2011. The originally six essential properties were transformed into

10 categories that until today compose the hallmarks of cancer: sustained proliferative signalling, loss of growth suppressors, avoided immune destruction, replicative immortality, tumour-promoted inflammation, increased invasiveness and metastatic potential, induced angiogenesis, genomic instability and mutation, evasion of apoptosis and deregulated cellular energetics (Hanahan and Weinberg, 2011).

In the UK, in 2017, there were 367,000 new cancer cases and 165.000 cancer related deaths. From these cases, breast cancer accounts for the largest proportion of all new cancer diagnoses each year (15%) with an estimated 55,000 new cases, and is responsible for ~11,000 deaths per year. It is estimated that 1 to 7 women in UK will be diagnosed with breast cancer in their lifetime. Another common cancer in the UK, is colorectal cancer, accounting for 42,000 new incidents every year, placing it in the third most common cancer in UK for both men and women, after lung cancer. However, colon cancer is the second most common cause of cancer death, reporting 16,300 new deaths every year (10% of all cancer deaths) (Cancer Research UK statistics, 2015-17).

Cancer is characterised by a high and distinct degree of genetic alterations as a result of genomic instability in the different subtypes. Genetic alterations are used for cancer's classification into subtypes, which can also determine the prognosis and the treatment that will be followed. This thesis sets out to investigate genomic instability in cancer in order to identify potential novel anti-cancer targeted therapies. In addition, it aims to define specific gene alterations and their role in stability and integrity of the cancer genome.

1.2 Genomic instability

Genomic instability (GIN) is a common characteristic for almost all of the human cancers. It refers to a range of genomic alterations from point mutations to changes of the chromosome arrangement and number (Aguilera et al., 2008, Negrini et al., 2010). As described above, in the section 1.1, GIN is one of the ten hallmarks of cancer, capabilities that are required for a tumour to initiate and progress. It provides the cancer cells with the genetic variation, accelerating the accumulation of favourable genotypes which allow cancer cells to acquire functional capabilities such as survival, increased proliferation and escaping cell death. Therefore, it is considered as an enabling characteristic in cancer that drives the accumulation of emerging features that are functionally important for tumour progression (Hanahan and Weinberg, 2011, Negrini et al., 2010).

1.2.1 Genomic instability: causes and consequences

Depending on the different genomic alterations, GIN is divided in three subcategories: nucleotide instability (NIN), microsatellite instability (MIN) and chromosomal instability (CIN). NIN includes base nucleotide substitutions and small deletions or insertions of one or a few nucleotides, while MIN characterizes the expansion or contraction of the oligonucleotide repeats in the microsatellite regions. Lastly, CIN is a major form of GIN that describes the structural and numerical alterations in the chromosomes of a cancer cell, compared to a normal cell (Giam and Rancati, 2015, Pikor et al., 2013, Negrini et al., 2010).

Human cells accumulate daily up to 10^4-10^5 DNA lesions, which if not corrected appropriately, may interfere with important cellular processes, such as DNA replication or mitosis and lead to genomic instability. Exogenous and endogenous factors, such as environmental and chemical agents, electromagnetic radiation or mutations and loss or gain of function in tumour suppressor genes and oncogenes, respectively, can increase the rate of DNA error accumulation, driving GIN and tumour initiation. Loss or gain of

function in genes involved pathways such as a) DNA damage response and repair; b) DNA replication and transcription; c) telomere maintenance; d) mitosis and e) checkpoint machineries, can potentially lead to genomic instability. (Burrell et al., 2013, Hanahan and Weinberg, 2011, Ribeiro-Silva et al., 2019).

1.2.1.1 The DNA damage response and repair pathways as causes of genomic instability

Human cells contain multiple pathways of DNA damage response and repair machineries to recognize and resolve different types of DNA damage. Each of these pathways is essential for maintaining the genomic integrity of the cells. There are three major groups of DNA damage repair. The first is the excision repair, in which damaged nucleotides are excised from a DNA strand and replaced using the complementary strand as a template. The second includes repair through homologous recombination (HR) and the third, through non-homologous end-joining repair (NHEJ). The latter two, are involved in repairing DNA breaks, either by using undamaged homologous DNA as a template (HR) or by simply ligating the DNA ends with no regard to homology (NHEJ). Additionally, in case of intracellular crosslinks, the Fanconi aneamia repair pathway is activated, in combination with NER and HR (Figure 1.1) (Chatterjee and Walker, 2017).

In more detail, the excision repair pathways are focused on sensing and repairing damaged nucleotides, incorrect base pairing or single strand breaks (SSBs). Depending on the disruption in the DNA sequence, there are three distinct pathways that can be activated, however, in case of an impaired pathway any of the other two might be able to take over. The nucleotide excision repair (NER) pathway is involved in sensing and repairing nucleotide damage that causes distortion of the DNA helix, for example by environmental and chemical agents or ultraviolet (UV) light. NER can be divided in two subpathways: the global genome NER (GG-NER), which detects and repairs inaccurate base pairing in all of the genome and the transcription-coupled NER (TC-NER), which is focused in repairing DNA lesions during transcription. The main difference between the two subpathways is that in GG-NER the DNA damage is sensed by the XPC protein in complex with RAD23B and centrin 2 (CETN2), while in TC-NER the damage is

recognized during transcriptional elongation indirectly by stalling of RNA polymerase II (RNA Pol II). The stalling increases the affinity of the RNA Pol II to Cockayne syndrome protein CSB, which allows the DNA to be accessed by other repair proteins. However, in both subpathways, the repair initiates after TFIIH (transcription initiation factor IIH) is recruited to the lesion. Then, RPA covers the undamaged DNA strand and XPD, XPA, XPF, the trimeric proliferating cell nuclear antigen (PCNA) ring and DNA polymerase accumulate on the damaged strand in order to cut and replace the damaged area. The repair is completed with the ligation of the two DNA strands. Notably, XPA is the main coordinator and interacts with almost every protein in NER while RPA protects the undamaged strand and guides XPG and XPF to cut the correct strand. Thus, if XPA, XPG or RPA proteins are impaired, the excision step would be done incorrectly, leading to R-loop formation (a three stranded nucleic acid structure, consisting of a DNA-RNA hybrid and a vulnerable single DNA strand) and to transcription stress, and thus to genomic instability (Marteijn et al., 2014, Lans et al., 2019).

Similarly, a second excision pathway, the base excision repair (BER), can be activated following generation of SSBs or DNA damage caused by alkylation. Alkylation can be caused by proteins or compounds that add alkyl groups (for example methyl or ethyl groups) in biological molecules and impair their function by changing their structure. These agents can be components of environmental factors such as fuels or cigarette smoke, or naturally occurring metabolic products of the existing molecules into the cell, such as methylating agents. When in contact with DNA, they can generate different base adducts and compromise the integrity of the genome. In the presence of simple alkyl lesions, BER is activated by poly(ADP-ribose) polymerase 1 and 2 (PARP1 and PARP2) enzymes, which act as sensors for recruitment of an alkyladenine DNA glycosylase (AAG), APE, XRCC1 and DNA polymerase β complex to repair the damaged area. The repair is completed after a DNA ligase joins the two strands together (Fu et al., 2012, Lord and Ashworth, 2012, Alhumaydhi et al., 2010). Notably, every step in BER pathway generates SSBs which can increase the rate of mutagenesis and genomic instability in the cell (Permata et al., 2019, Fu et al., 2012). Moreover, GIN can occur by

overexpression of AAG glycosylase, which can increase the rate of frameshift mutations. In addition GIN can be caused by loss of function or expression of XRCC1, scaffolding enzyme that interacts with DNA processing enzymes and is necessary for repair. (Horton et al., 2008, Fu et al., 2012).

The last excision repair pathway is the mismatch repair (MMR) that is directed to repair DNA mismatches, mainly generated by DNA replication. In MMR, the mismatched base pair is recognized by MutSα complex which is formed by MSH2 and MSH6, while the presence of multiple mismatches is recognized by MutSβ complex that includes MSH2 and MSH3 proteins. Either MutSα or MutSβ can recruit MutLα complex, formed by MLH1 and PMS2 proteins. In order to promote excision of the mismatch segment, several other factors are recruited, such as PCNA, replication factor C (RFC) and exonuclease EXO1. In addition, RPA protects the ends of the correct strand and after the removal of the mismatched base, DNA polymerase δ is 'filling the gap' in the DNA strand, where a DNA ligase will seal the strands at the end of the repair (Jiricny, 2006, Gupta and Heinen, 2019, Liu et al., 2017). Unsurprisingly, impaired MMR induces MIN or CIN in multiple types of cancers (e.g. colon, breast) and it has been shown that mutated MLH1 causes genomic instability and infertility in mice. Moreover, deletion of MSH2 and MSH3 promotes instability through incorrect processing of Z-DNA, a left handed helix that is generated at sequences of purinepyrimidine repeats (e.g. TG or GC) (McKinney et al., 2020, Pasanen et al., 2020, Wong et al., 2020, Li, 2008, Matsuno et al., 2019).

In the presence of single strand DNA lesions, the NER, BER or MMR repair pathways are activated as discussed previously. However, in the presence of double strand breaks, which can be generated by ionizing radiation, collapse of DNA replication forks, chemical agents or impaired repair pathways of other DNA lesions, two other distinct repair pathways are activated. The non-homologous end-joining repair (NHEJ) pathway is activated when the Ku70/80 heterodimer is recruited to the area of the DSB. It restrains the breaks and forms a complex with DNA-PK, which is stabilized by PAXX. Then, the core machinery of NHEJ pathway is recruited, mainly consisted of Artemis,

XRCC4, XLF and DNA ligase 4, in order to align and ligate the ends of the broken strand, independently of sequence homology (Blackford and Jackson, 2017, Han et al., 2017, Balmus et al., 2019) (Figure 1.2). There are cases when an alternative NHEJ pathway is activated, however it is not yet understood when the classical or the alternative pathway is preferred. The alternative NHEJ pathway is based on the same concept with the classical, but it involves localization of PARP1 at the DSBs and the ligation by DNA ligase 1 or 3 (Han et al., 2017, Li et al., 2016). The NHEJ repair pathway can be activated in any phase of the cell cycle, nevertheless, because there is no need of a repair template, it is error prone, highly mutagenic and predisposed to cause genomic instability (Blackford and Jackson, 2017, Li et al., 2016).

The second pathway that responds to DSBs is homologous recombination (HR), which can be activated only during the S and G2 phases of the cell-cycle, where a sister chromatid is used as a template. In HR, the MRE11-RAD50-NBS1 (MRN) complex senses the break and recruits ATM kinase for the initiation of the repair pathway. Recruitment of CtIP, ATRIP and ATR guarantees the resection of DSBs and the generation of singe stranded DNA which is protected by RPA. Upon removal of RPA, RAD51 is loaded on the singe strands with the aid of BRCA1 and BRCA2 to direct the strand into the homologous sister chromatid. A DNA polymerase synthesizes any missing information and a DNA ligase joins the strands, completing the repair mechanism (Balmus et al., 2019, Peng and Lin, 2011, Whelan et al., 2018) (Figure 1.2). Notably, mutations in ATM, MRN complex or BRCA1 and BRCA2 are linked to genomic instability in a variety of cancers, including breast, ovarian and pancreatic cancers, as their impairment prevents the initialization of the HR pathway. In addition, impairment of RAD51 protein prevents the inversion of the single strand that is necessary for the repair process (Drosos et al., 2017, Koh et al., 2005, Li et al., 2016, Whelan et al., 2018, Lord and Ashworth, 2012).

Exogenous carcinogens such as cigarette smoke, alcohol, or DNA intercalating agents, such as cisplatin, can cause intracellular crosslinks (ICLs) promoting replication fork stalling due to prevention of strand separation. ICLs repair occurs through activation

of the Fanconi anaemia pathway and its interactions with NER and HR. Initially, ICLs are recognised by the FANCM–FAAP24–MHF1–MHF2 complex which recruits the Fancony anaemia core complex that includes 14 proteins (FANCA, FANCB, FANCC, FANCE, FANCF, FANCG, FANCL, FANCM, FANCT, FAAP100, MHF1, MHF2, FAAP20 and FAAP24). The core complex together with UBE2T and BRCA1 interact and activate the FANCD2- FANCI complex, which promotes DNA incision and removal of the ICL from the one of the two parental strands through activation of NER pathway, while it generates a DSB to the second. The incision leaves the crosslinked nucleotide bound to the complementary strand. Then, REV1 or DNA polymerase ζ continue with lesion bypass by adding nucleotides and extending the broken strand, with increased possibility to introduce mutations to the genome. The ligation generates a DNA duplex which functions as template for HR repair of the DSB that DNA incision created. In addition, inactivation of the Fanconi anaemia genes causes a genomically unstable disease, Fanconi aneamia, after which the genes were named, that shows high predisposition to cancer. Additionally, deletion of FANCA, BRCA1 or FANCD2 promote genomic instability due to replication stress (Ceccaldi et al., 2016, Nalepa and Clapp, 2018, Taylor et al., 2019).

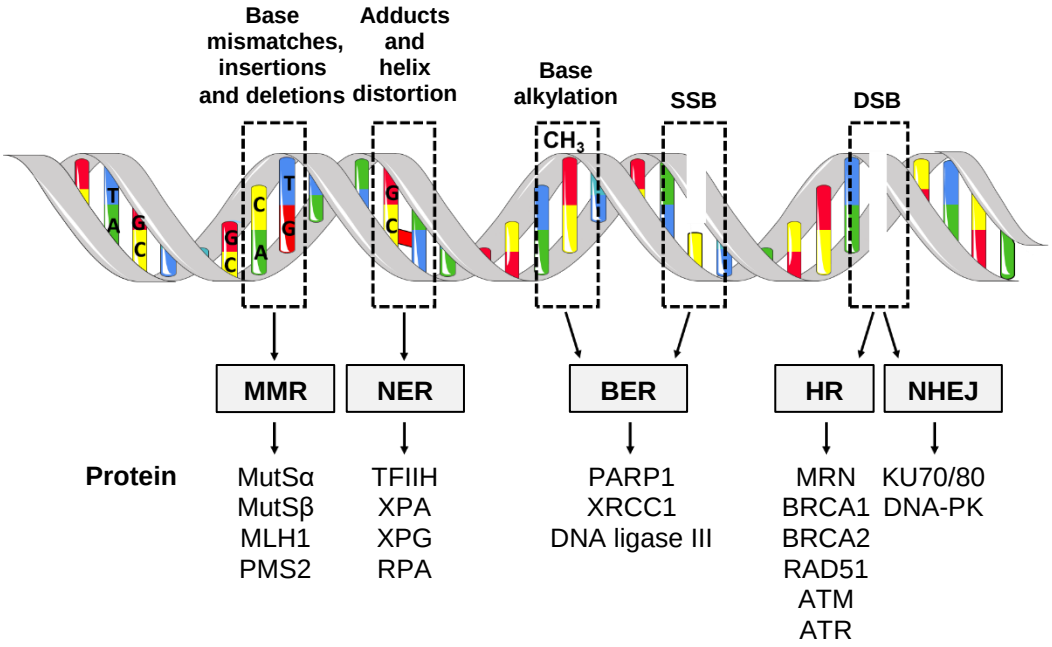

Figure 1.1: The DNA damage repair mechanisms. Different types of DNA lesions are repaired by distinct mechanisms. Each mechanism utilises key proteins for the recognition and the repair of each DNA error. SSB: single strand break, DSB: double strand break, MMR: mismatch repair, BER: base excision repair, NER: nucleotide excision repair, HR: homologous recombination, NHEJ: non-homologous end-joining.

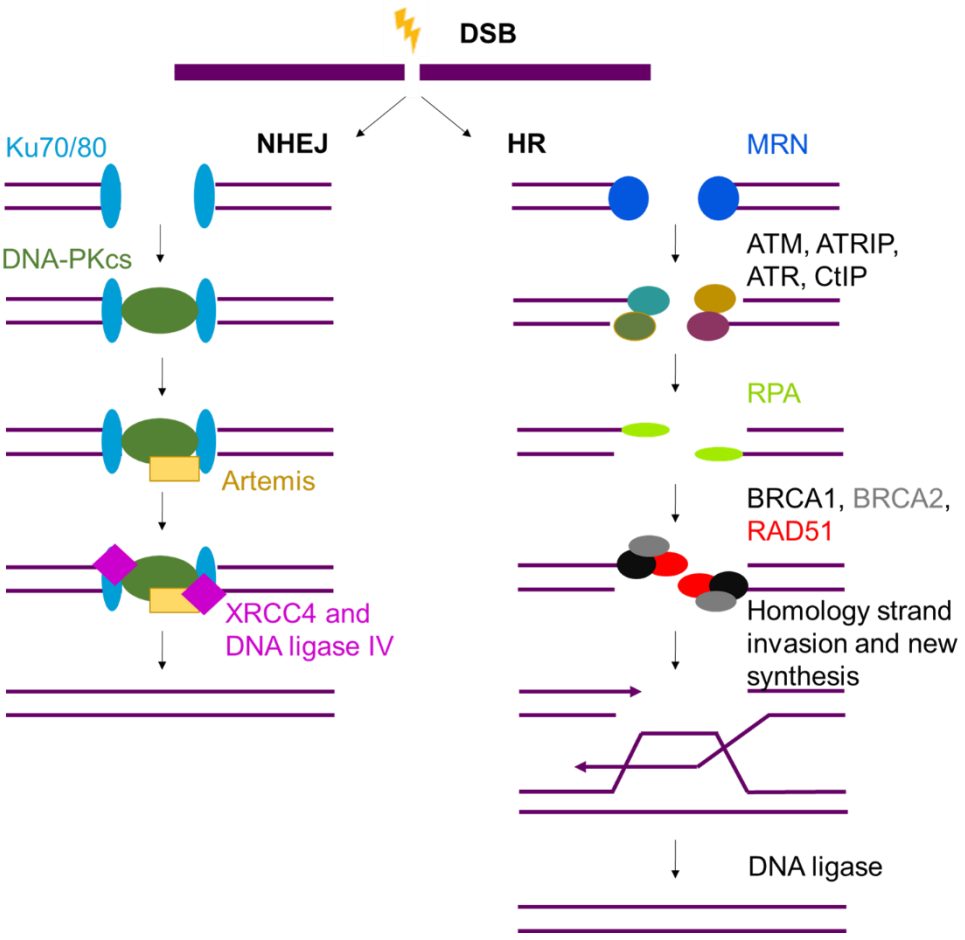

Figure 1.2: The DNA damage response/repair mechanisms of double strand breaks. The classical non-homologous end-joining (NHEJ) repair mechanism initiates with recognition of the DNA ends by Ku70/80, which recruit DNAPkcs and Artemis to trim the DNA ends and XRCC4

and ligase IV to seal the break. In the homologous recombination repair (HR) pathway, the MRN complex senses the break and recruits ATM, ATRIP, ATR and CtIP in the damaged area that generate single stranded DNA (ssDNA). RPA coats and protects the ssDNA until it is replaced by RAD52 with the help of BRCA1 and BRCA2. RAD51 is responsible for strand invasion on the homogenous template. A DNA polymerase synthesizing any missing information and a DNA ligase joins the strands, completing the repair mechanism.

1.2.1.2 DNA replication stress and transcription-replication collisions cause genomic instability

In the concluding remark in the paper published by Watson and Crick announcing the discovery of the structure of DNA (Watson and Crick, 1953) it was noted “It has not escaped our notice that the specific pairing we have postulated immediately suggests a possible copying mechanism for the genetic material.”

DNA replication is a process by which DNA is duplicated in the S phase of the cell cycle, in a semiconservative manner. During DNA replication, each strand of the double helix functions as a template for the synthesis of a new complementary daughter strand. However, initiation of DNA replication requires the double helix to unwind and a Y structure to be formed, named the replication fork, in order for DNA polymerases to synthesize the complementary strand (Alberts, 2003). The proteins, required for unravelling the DNA, are called chromatin remodellers. The most well-described chromatin remodelling complexes belong to the SWI/SNF (switch/sucrose non-fermentable) family. In human, the SWI/SNF family contains three complexes, which will be discussed in more detail in section 1.3.1.4. The SWI/SNF complexes promote access of the DNA replication machinery to the DNA, however, they are not involved in the direct biding of the replication machinery to the DNA. Furthermore, mutation or deletion of BRG1 (the catalytic subunit in two of the three SWI/SNF complexes) in mice or human cervix cancer cells, decreases to a half the efficiency of replication fork progression, indicating that SWI/SNF complexes are also important for the process of replication elongation (Cohen et al., 2010, de Cubas and Rathmell, 2018). In previous studies has been demonstrated that in the presence of DNA damage, BRG1 facilitates the recruitment of BRCA1 and ATR in the damaged area for DNA damage repair initiation

(Zhang et al., 2013). In general, DNA damage or any other disruption of DNA replication, generates replication stress and stalling - until the damage is repaired - or the replication fork collapses, leading to genomic instability (Lambert and Carr, 2013, Taglialatela et al., 2017). Moreover, common fragile sites (CFS) are areas at the genome with large genes, which undergo slow replication and upon replication stress, are prone to breakages during mitosis and generation of chromosomal rearrangements. Thus, replication stress due to increased stalling or collapse of replication forks, can generate under-replicated DNA and subsequent genomic instability will arise (Gaillard et al., 2015, Matsuno et al., 2019, Wilhelm et al., 2019, Mukherjee et al., 2019, Brison et al., 2019).

Nevertheless, DNA is not only a substrate for replication but also for transcription, and it has been shown that they can occur in the same genomic area at the same time, generating collision, DSBs and genomic instability. Often, the collision occurs in the CFS due to the large size of the genes (more than 300kb long). Transcription of these genes often need more than one cell cycle and subsequently, replication and transcription machineries can be concurrent during S phase. The replication and transcription collisions can be co-directional or in head-on orientation. The co-directional orientation may occur if the replication machinery follows the transcription machinery in the same direction and the replication fork progress faster than the RNA polymerase. In that case, the collision can be resolved if the DNA polymerase displaces the RNA polymerase and the replication continues. The head-on orientation collisions are caused, when the replication fork and the RNA polymerase progress on opposite directions. Then, the DNA between the two machineries can be supercoiled and thus, induces stalling of the replication fork, possible collapse and generation of DNA breaks. Collisions between the two machineries can induce genomic instability through collapse of replication forks and DSBs, generation of under-replicated DNA or transcription associated recombination (Helmrich et al., 2013, García-Muse and Aguilera, 2016, Duch et al., 2018, Brison et al., 2019).

1.2.1.3 Disruption of telomere maintenance pathways cause genomic instability

Telomeres are regions of repetitive nucleotide sequences at the end of the chromosomes that protect the latter from degradation or fusion and thus, are essential for maintenance of genomic stability. Telomeres consist of repetitive DNA sequences and shelterin, a multisubunit complex, which protects the chromosome ends from DNA damage response. Additionally, there are specific mechanisms that the human cells use in order to prevent telomere shortening and avoid genomic instability. During the S and M phases of cell-cycle, telomerase, a ribonucleoprotein complex, synthesises new telomeric sequences. The telomerase complex includes TERT, the telomerase reverse transcriptase, and telomerase RNA (TR) that contains the template for the addition of the repeat sequence. Another complex, dyskerin, stabilizes TR and together with TERT form the Cajal body, where the new sequences are synthesized (Armanios and Blackburn, 2013, Roake and Artandi, 2020).

Apart from the classical machinery of telomere elongation, alternative pathways may be activated in order to prevent telomere shortening. The alternative lengthening of telomeres (ALT) machinery mediates telomere synthesis through homologous recombination (HR) of a DNA telomeric template, by using the mechanism described in section 1.2.1.1. Furthermore, telomere length can be regulated by histone modifications in the telomeric area. For example, trimethylated histone H3 at lysine 9 (H3K9me3) and trimethylated histone H4 at lysine 20 (H4K20me3) regulate the telomeric elongation machinery or the ALT through recombination. Additionally, cancer cells with impaired DNA methylation, in particular reduced H3K9me3 and H4K20me3 methylation, have been shown to contain shortened telomeres. (Yu et al., 2019, Benetti et al., 2007, Conomos et al., 2013). Thus, deregulation of TERT, shelterin, HR or specific chromatin remodelers (e.g. ATRX, DAXX, PWP1) results in altered telomere length, loss of genome stability and cancer (Roake and Artandi, 2020, Yu et al., 2019,Clynes et al., 2015, Heaphy et al., 2020).

1.2.1.4 Mitosis and genomic instability

The cell cycle consists of four phases: G1, S, G2 and mitosis (M) (Figure 1.3 A). The G1 phase is the pre-replicative stage in which chromosomes are in the form of single DNA duplexes. DNA replication takes place in the S phase, but it can continue into the G2 phase in which the doubled sister chromatids are held together by cohesins. In particular, in the case of DNA damage occurring during S phase, replication can finish in the beginning of G2. If the cells enter mitosis, while carrying unresolved DNA damage from S or G2 phase, then, proper separation of the sister chromatids to the daughter cells can be impaired. (McIntosh, 2016, Yanagida, 2014).

Mitosis means 'thread' in Greek, named by researchers in the 19th century, who observed thread-like structures before the division of dyed cells. These structures are now known to be condensed chromosomes (Yanagida, 2014). Mitosis is a complex, highly dynamic process which requires careful coordination of multiple protein complexes, in order to ensure a bipolar mitotic spindle and subsequent proper separation of the daughter cells and it is organized into five stages: prophase, prometaphase, metaphase, anaphase and telophase. In prophase, the nuclear membrane is dissolved and the sister chromatids condense by decreasing their length and increasing their thickness. In prometaphase, the chromosomes are organised into twofold-symmetric structures, which consist of the chromosome arms, telomeres and the centromeres. Each sister chromatid is composed of two chromosome arms, a short-p- and a long -q- arm, at the end of which are the telomeric regions that protect the chromosome ends and prevent chromosomal fusions. The area that holds the two sister chromatid together is named centromere and contains the two sister chromatid kinetochores (Figure 1.3 B). Moreover, in prometaphase, the mitotic spindle is formed, a bipolar complex of microtubules and proteins at the two opposite sides of the cell that are essential for the correct separation of the sister chromatids. The two poles of the mitotic spindle are formed by one centrosome each, which consists of two centrioles surrounded by the pericentriolar material (PCM) and is the main microtubule-organising centre. Microtubules are formed by aligned filaments of α- and β- tubulin, and are divided

in two subcategories depending their attachment or not to the sister chromatid kinetochores. The kinetochore microtubules that form parallel bundles and are initiating from the mitotic poles and bound at the kinetochores, are known as kinetochore fibers or k-fibers and are essential for correct chromosome segregation. The non-kinetochore microtubules consists of three different types: the astral, the polar and the overlap microtubules. All of the three types of microtubules are nucleated from the spindle poles, but astral microtubules grow towards the cell cortex, the polar microtubules towards the middle of the spindle and have free ends, while the overlap microtubules form antiparallel overlaps in the central part of the spindle. As the cell progresses through metaphase, the kinetochores on the sister chromatids are attached to microtubules that are nucleated from the two opposing spindle poles. When the chromosomes are aligned in the metaphase plate and the kinetochores in each sister chromatid pair are attached correctly to microtubules from the opposing poles, the cells progress to anaphase. In anaphase, the sister chromatids are separated and move towards the opposite poles (Figure 1.3 C) (McIntosh, 2016, Ohta et al., 2011, Naumenko et al., 2015, Yanagida, 2014, Wieser and Pines, 2015, Tolić, 2018).

Finally, in telophase, the separated chromosomes are de-condensed, the nuclear membrane starts to form again and the two daughter cells, still connected, undergo cytokinesis. A contractile ring of actin-myosin filaments is organised in the middle of the dividing cell and leads to the formation of the cleavage furrow (plasma membrane ingression). Then, the spindle microtubules are moving and attaching to the farrow. Lastly, the two daughter cells undergo complete separation (Figure 1.3 C) (Glotzer, 2017, Lens and Medema, 2019).

Defects in mitosis are often linked with genomic instability and in particular to CIN. In particular, incorrect sister chromatid cohesion, impaired attachment of the microtubules to the chromatids' kinetochores, defective structure or geometry of mitotic spindle or cytokinesis failure are some common defects that may lead to loss, gains, breakages or translocations of chromosomes (Burrell et al., 2013, Bakhoom and Compton, 2012).

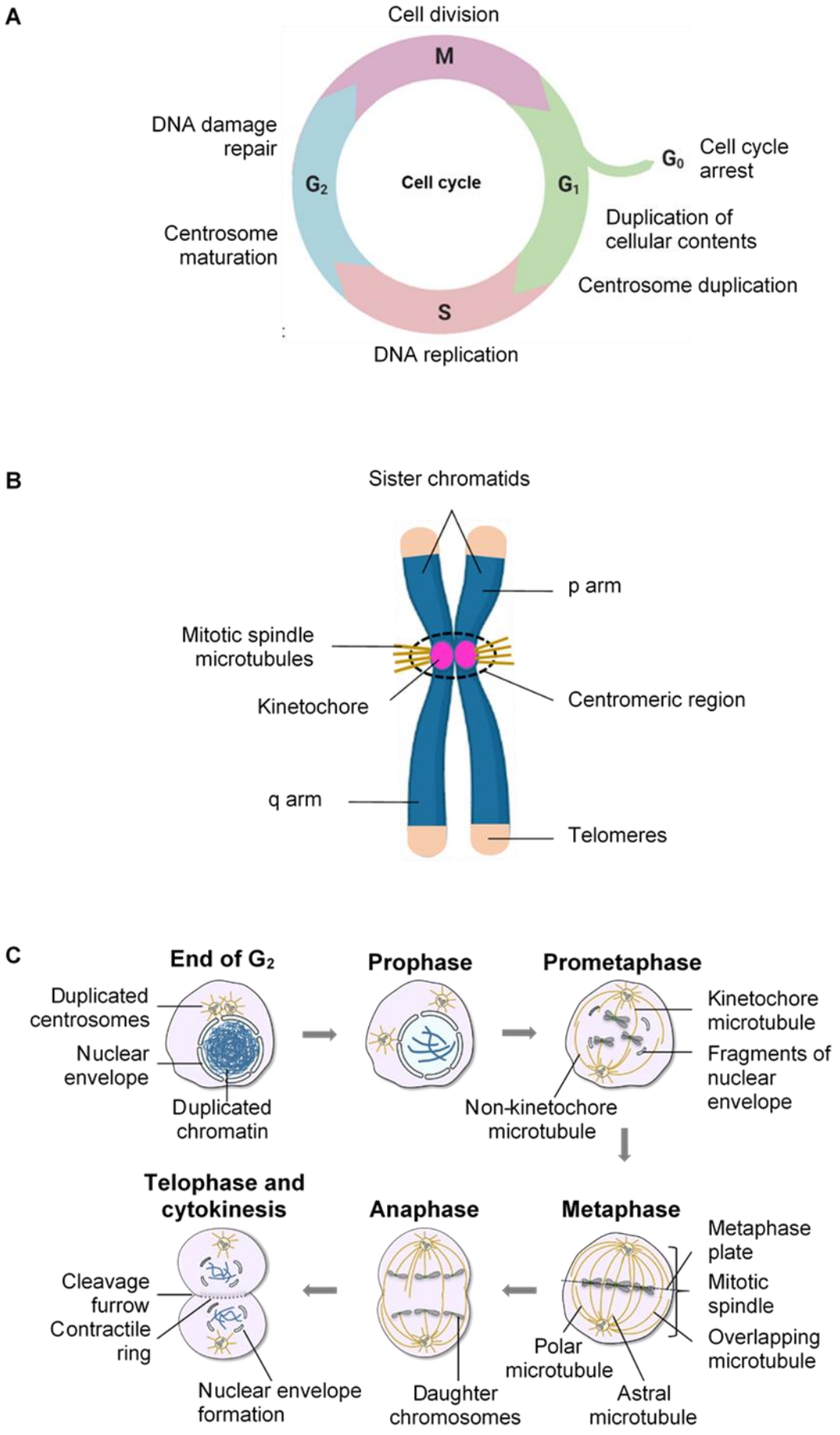

Figure 1.3: Mitosis, the mitotic stages and the metaphasic chromosome. (A) The cell cycle phases. **(B)** The metaphasic chromosome and **(C)** overview of chromosome reorganisation during the mitotic stages and the mitotic spindle formation.

1.2.1.5 Deregulation of cell-cycle checkpoint pathways can lead to genomic instability

During the cell cycle, cells have to ensure genomic integrity and propagate accurate copies of the genome to daughter cells. Thus, in case of damaged, abnormally structured DNA or errors in chromosomes during mitosis, the cell cycle is delayed until the damage is repaired. When DNA damage is beyond repair, programmed cell death is induced or the cell cycle can be permanently arrested, avoiding cell proliferation, a mechanism known as cellular senescence (Lukas et al., 2004). The mechanisms that ensure cell cycle delay, arrest or cell death are named cell cycle checkpoints. There are four major checkpoints in the cell cycle: before the entrance in the S phase (G1/S checkpoint), during the S phase (intra-S checkpoint) after the G2 phase and before the cells enter mitosis (G2/M checkpoint) and during mitosis, before the cell enters anaphase (mitotic checkpoint, also known as spindle assembly checkpoint-SAC) (Löbrich and Jeggo, 2007, Faisal et al., 2017).

In unstressed cells the transition from the G1 to S phase is regulated by activation of CDK4-cyclinD and CDK2-cyclinE proteins which phosphorylate and inactivate Retinoblastoma (pRB) protein, inhibiting its interactions with E2F, a regulator for S transition (Iliakis et al., 2003). However, in the presence of DNA damage, the tumour suppressor protein p53 mediates the expression of p21, which inhibits the CDK2-cyclinE complex, the subsequent phosphorylation of RB and the entry to S phase. Moreover, p21 intervenes directly to inhibit DNA replication by binding to PCNA through its PCNA-binding domain, and antagonizes the interaction of PCNA with DNA polymerase δ, thus inhibiting DNA synthesis and arrest cell cycle during S phase. Apart from p53-depedent activation, expression of p21 can be induced by growth factors like transforming growth factor β (TGFβ) (Abbas and Dutta, 2010, Sheahan et al., 2007). Additionally, activation of CDK2 kinase, can be induced through CDC25A (Cell division cycle 25 A). CDC25A is a dual-specificity protein phosphatase that activates CDK4 and CDK2 and mediates G1/S transition. DNA damage lead to ubiquitination and subsequent degradation of CDC25A, preventing the transition to S phase. Notably, p21 and CDC25A are also regulators of G2/M checkpoint, by inhibiting the activity of CDK1-cyclinB1, a crucial

complex for G2/M transition. Transition to mitosis, requires ubiquitination and degradation of p21 and CDC25A by APC/C (anaphase promoting complex/cyclosome) (Shen and Huang, 2012, Abbas and Dutta, 2010).

DNA breaks are the most common cause of cell cycle checkpoint activation. In case of single strand breaks, the DNA damage response pathway initiates accumulation of ATR protein to the sites of the breakage. In addition to the role of ATR to recruit proteins at the SSBs, it phosphorylates and activates the CHK1 and WEE1 kinases. CHK1 activates NEK11 and promotes degradation of CDC25A, while WEE1 is crucial for regulating entry into mitosis, as it also inhibits the CDK1-cyclinB complex. Thus, ATR and CHK1 can regulate the intra-S and G2/M checkpoints. In the presence of DSBs, ATM is the protein that initiates the repair pathway. ATM phosphorylates and activates CHK2 kinase, which again leads to CDC25A degradation through p53 activation (Lukas et al., 2004, Shen and Huang, 2012, Stathis and Oza, 2010, Pilié et al., 2018). ATM and ATR DDR pathways function with the same principle, but, the former is essential for response to DSBs while the latter for response to SSBs. Nevertheless, during DSBs, ATM together with NBS1 activate the ATR/CHK1 response, by regulating the RPA accumulation to single strand DNA, which is required for ATR recruitment (Jazayeri et al., 2006, Mladenov et al., 2019, Girard et al., 2002).

In mitosis, another checkpoint is activated to prevent the generation of daughter cells with abnormal number or structure of chromosomes. Thus, due to impaired chromosome alignment, defective attachment of microtubules in kinetochore or irregular mitotic spindle poles, progression to anaphase is prevented by spindle assembly checkpoint (SAC) activation. The core of SAC machinery includes MAD1, MAD2, MAD3 (BUBR1), BUB1, BUB3, and MPS1 proteins that directly regulate the checkpoint activity. Kinetochores are the focal point for checkpoint activation and function. On kinetochores that are not correctly attached to microtubules, SAC signalling initiates with the formation of the KMN complex, consisting of KNL1, MIS12 and NDC80, which acts as a scaffold on unattached kinetochores for the recruitment of other SAC proteins. MPS1 kinase binds to NDC80 and allows the attachment of BUB3-BUB1 to KNL1. BUB1 further

recruits BUB3-BUBR1 to KNL1 and a MAD1-MAD2 heterodimer is joining BUB1. At that point, MAD2 changes conformation from an open (O)-MAD2 to a closed (C)-MAD2. (C)-MAD2 binds and inactivates CDC20 by recruiting additional BUB1-BUB3 complexes. This formation is named mitotic checkpoint complex (MCC) and prevents the binding of CDC20 to APC/C, thus preventing the transition from metaphase to anaphase. When there is proper attachment of microtubules to the kinetochores, the above structures are removed from the kinetochores and CDC20 is free to bind to APC/C. Activated APC/C-CDC20 complex targets SAC proteins for proteasome degradation in addition to securin, which protects the sister chromatid cohesion, and cyclin B which interacts with CDK1 for mitotic entry. As a result, SAC is inactivated and progression through mitosis is allowed (Shi et al., 2019, London and Biggins et al., 2014, Bharadwaj and Yu, 2004, Lok et al., 2020, Richeson et al., 2020).

Cell cycle checkpoints are crucial for retaining genome integrity and stability. Deregulation of proteins involved in any of the checkpoints discussed above, are linked to genomic and chromosomal instability. For example, inactivation or missregulation of SAC or DDR pathways, drive genomic instability and are linked with several different types of cancer, including breast (Löbrich and Jeggo, 2007, Deng et al., 2010, Bower et al., 2017, Jang et al., 2020, Marangos et al., 2015, Vogel et al., 2004, Faisal et al., 2017, Drosopoulos, et al., 2014).

1.2.1.6 Genomic instability, a driver for tumour heterogeneity and evolution

Cancer is a dynamic disease. Transformation of a non-malignant cell to malignant requires continuous accumulation of genomic alterations that provide the cell with characteristics that gradually lead to accumulation of the hallmarks of cancer. Thus, presence of these hallmarks is not due to one alteration but through continuous destabilization of key cellular processes. Nevertheless, initiation of a tumour not only does not inhibit the accumulation of new alterations but it increases the rate of genomic changes happening as it progresses. Between patients with a specific type of cancer, the tumour genotypes may be distinct, even if the category of the tumour, as defined by

the histological characteristics, is the same. This type of heterogeneity is named intertumoural heterogeneity. A second type of heterogeneity, named intratumoural heterogeneity, refers to the differences between the cancer cells in the same tumour. Itratumoural heterogeneity can be further classified into spatial heterogeneity, differences between cells from different sites of the same tumour, or temporal heterogeneity, referring to the genetic variation between cancer cells of the same tumours over time (Dagogo-Jack and Shaw, 2017). This study is focused on temporal intratumoural heterogeneity.

Within a tumour, genetically and phenotypically distinct subpopulations of cells (subclones), can emerge. Moreover, cells from the same subclone exhibit genetic or non-genetic variations (mutations, copy number variations, epigenetic modifications) that promote phenotypic diversity. Thus, genomic instability is the driver of intratumoural and subclonal heterogeneity (Burrell et al., 2013, Dagogo-Jack and Shaw, 2017). As described before, elevated mutational frequencies and changes in the chromosomal number or structure can occur when the telomere maintenance, DNA replication, mitosis, cell-cycle checkpoints or DNA damage response and repair pathways are defective. However, GIN is ongoing in the progressing tumour, as it has been shown that culture of single-cell clones quickly become genetically and phenotypically heterogeneous (Ben-David et al., 2018, Ben-David et al., 2019).

Intratumoural heterogeneity, through genomic instability, promotes selection of specific subclones that are phenotypically advantageous within a given tumour-environmental context and guarantees the existence of cells with the appropriate genetic alterations to overpass selective barriers (e.g. malnutrition, immune system response, therapeutic drugs) (Burrell et al., 2013, Cahill et al., 1999). Therefore, heterogeneity enables positive selection for tumour evolution and tumour progression. Selection is a key force in evolution and leads to adaptation. However, excessive instability can be a driver of negative selection, in which cells with decreased fitness are eliminated from the tumour population. GIN contributes to tumour heterogeneity but it is also able to generate deleterious alterations that can shift the balance towards cell death. Additionally,

evidence shows that there is a threshold of genomic instability that the cell can tolerate, above which, accumulation of more genetic alterations becomes detrimental (Turajlic et al., 2019, Andor et al., 2017, Andor et al., 2016).

1.2.2 Summary

In this part of the introduction, the term of genomic instability was introduced and its causes and consequences were presented. GIN refers to the elevated rate of mutations and the structural or numerical chromosomal changes that underlie the genomic alterations responsible for the cell's malignant transformation. Depending on the genomic alterations, GIN can be subcategorised into nucleotide, microsatellite and chromosomal instability, and provides the tumour with genomic changes for its progression and evolution. In particular, unrepaired DNA due to errors in DNA replication, collision of DNA replication and transcription machineries, shortened telomeres, impaired DDR and repair pathways or dysfunctional cell cycle checkpoints, will generate genomically unstable cells. Moreover, direct errors in mitosis will also produce genomically unstable cells. Thus, GIN is able to drive tumour initiation and fuel the intratumour heterogeneity to enable positive selection for tumour evolution. This research study is focusing on targeting GIN and particularly chromosomal instability, generated through direct or indirect errors in mitosis.

1.3 Chromosomal instability

Chromosomal instability (CIN) is a form of GIN and refers to a dynamic state in which the cells are constantly changing the number and/or the structure of their chromosomes. Typically, CIN tumours contain both whole and structural chromosomal alterations. Whole chromosomal instability (W-CIN) describes whole chromosome gains or losses, while structural chromosomal instability (S-CIN) characterises amplifications, deletions, breakages or translocations of chromosomal regions (Sansregret et al., 2018, Zhang et al., 2016, McGranahan et al., 2012).

1.3.1 Causes and consequences of chromosomal instability

The main direct cause of CIN is mitotic errors that can arise either due to defects in the mitotic machinery, for example by impaired SAC or centrosome amplification, or errors in DDR and repair pathways, such as in DNA replication errors or impaired chromatin remodelling (Storchova and Pellman, 2004, Zhang et al., 2016, Bakhoum et al., 2016). This study is focused on investigating both W-CIN and S-CIN after mitotic stress induction, through different errors during mitosis, chromatin remodelling, DDR and repair pathways or polyploidization.

1.3.1.1 Mitotic errors: a direct cause of chromosomal instability

During mitosis, the mitotic spindle is organised by two centrosomes at opposite poles of the cells, where microtubule nucleation takes place. The opposing kinetochores of each mitotic chromosome are attached to kinetochore microtubules from the opposing spindle poles and are pulled towards the equatorial plane of the mitotic cell. Then, the sister chromatids are separated and segregated to the opposite poles. Finally, the two daughter cells are separated completely through cytokinesis with one full set of sister chromatids each (Figure 1.4 A) (Petry, 2016). However, in cancer cells, a number of defects during mitosis can lead to irregular chromosome segregation. Most common

defects are impaired microtubule-kinetochore attachments, defects in sister chromatid cohesion, SAC dysfunction or centrosome amplification (Thompson et al., 2010).

A weakened SAC can allow the transition from metaphase to anaphase even in the presence of an unattached or misaligned chromosome. As a result, one of the daughter cells may gain a chromosome, while the other will lose one (Fig. 1.4 B). Previous studies have suggested a connection between homozygous deletion of the SAC proteins BUBR1 and MAD2, with embryonic lethality due to increased level of missegregated chromosomes. However, heterozygous deletion of either gene is not lethal and can increase chromosome missegragation bellow a lethal threshold due to SAC failure to maintain mitotic arrest in the presence of misaligned chromosomes (Huang et al., 2019, Thompson et al., 2010). Moreover, the SAC related kinase, mitotic spindle 1 (MPS1) is highly expressed in multiple cancers, like glioblastoma, breast, pancreatic and thyroid. MPS1 kinase is a core regulator of SAC as it senses the unattached kinetochores and recruits more SAC proteins at the area, forms the mitotic checkpoint complex and promotes inactivation of APC/C-CDC20. Moreover, MPS1 is required for proper chromosome alignment. Thus, MPS1 inhibition with a selective inhibitor (CCT271850), abrogates SAC and generates high rate of misaligned chromosomes and cell death (Faisal et al., 2017, Maia et al., 2018, Xie et al., 2017, Gurden et al., 2015). Another mitotic protein crucial for the correct alignment of chromosomes is the centromere-associated protein-E (CENP-E), which is a kinesin-7 motor protein that localizes at the kinetochore of mitotic chromosomes. Similarly to MPS1, CENP-E expression is low in the G1 phase of the cell cycle but it is increased at the end of G2 phase and during mitosis where it is necessary for proper attachments of microtubules to the kinetochores and the correct chromosomal alignment at the metaphase plate (Itoh et al., 2018, Kumar and Purohit, 2012, Wood et al., 2010). The C-terminus of CENP-E is crucial for localization to the kinetochores and for its interactions with mitotic checkpoint proteins, such as the serine threonine kinase BUBR1 which inhibits the activity of the anaphase promoting complex APC/C-CDC20 in the absence of stable kinetochore-microtubule attachments (Wood et al., 2010). Studies of

CENP-E depletion in human cervical cancer HeLa cells have shown a prolonged mitotic delay, while deletion of CENP-E has been shown to promote errors in the congression of chromosomes to the metaphase plate (Tanudji et al., 2004, Yao et al., 2000, Kapoor et al., 2006). Indeed, experiments in cervical and colorectal cancer cells, treated with the CENP-E inhibitor GSK923295 showed prolonged mitotic delay and failure in chromosome alignment. Importantly, the effects of GSK923295 treatment are reversible and therefore, after its removal, the cells progress through mitosis (Bennett et al., 2015).

In addition, chromosome missegregation errors can be caused by defects in sister chromatid cohesion, the physical connection between sister chromatids (Fig. 1.4 B). Cohesion of sister chromatids initiates in G1 phase of cell-cycle by cohesion loader proteins, NIPBL and MAU2, but it is established in S phase by the activities of ESCO1 and ESCO2. Cohesion is regulated by cohesion complex, a quaternary ring-like structure, which consists of SMC1A, SMC3, RAD21 and one of STAG1, STAG2 or STAG3, and it is important for tethering the sister chromatids together. Before anaphase, chromatid cohesion is lost along the chromosome length but it is still retained in the centromeric area by RAD21, which is cleaved in the beginning of anaphase for initiation of sister chromatid segregation. Cohesion cleavage is mediated by separase (ESPL1), a protease that is regulated by securin (PTTG1), which in turn, is degraded by ubiquitination mediated by APC/C-CDC20. Deletion or gain of these genes are present on various cancers, like breast, colon, ovarian, skin, lung and leukaemia. Moreover, it has been shown that decreased levels of SNC1A, SMC3 and RAD21 promote improper separation of sister chromatids, chromosome missegregation and generate formation of micronuclei, which are indicative of CIN. Similarly, non-functional ESCO2 and NIPBL formed micronuclei but in less degree (Leylek et al., 2020, Sajesh et al., 2013).

Additionally, impaired attachments between kinetochores and microtubules can lead to syntelic attachments, in which both kinetochores of the sister chromatids are attached to microtubules from the same pole, or merotelic attachments, in which one kinetochore is attached to two microtubules from opposite poles (Fig. 1.4 C and D). If not corrected, the erroneous attachments will lead to chromosome missegregation and

chromosome breaks. For example, if a merotelic attachment is retained through anaphase, the lagging chromosome can be missegragated or completely excluded from both daughter cells. Aurora B is a kinase localized at the inner side of the kinetochore, with a crucial function in correction of these erroneous attachments. In the presence of syntelic attachments, Aurora B senses the lack of high tension between sister kinetochores, phosphorylates the KMN (KNL1, MIS12, NDC80) complex and activates SAC, leading to microtubule destabilization. As soon as correct attachments are established, the spindle poles pull away the kinetochores from the inner centromere, and Aurora B cannot phosphorylate KMN. However, in case of merotelic attachments, SAC is not activated. In contrast, Aurora B regulates the microtubule depolymerases MCAK and KIF2B and inhibits the merotelic kinetochore attachments (Gregan et al., 2011, Krenn and Musacchio, 2015).

Multipolar divisions due to supernumerary centrosomes is another major cause of chromosome missegregation. In mammalian cells, centrosomes are the major microtubule-organization centre and play a role in cell shape, motility, polarity, spindle and cilia formation. Centrosomes are composed of a pair of cylindrical structures, called centrioles that are surrounded by pericentriolar material (PCM), which harbours proteins that are essential for microtubule nucleation and cell cycle regulation (Nigg and Holland, 2018, Chou et al., 2016). In a typical non transformed cell, the pair of centrioles is duplicated only once during cell cycle (through centrosome associated proteins, like CDC6, PLK4, STIL, SAS-6, CPAP, and CEP135) to form two centrosomes, which function as spindle poles during mitosis. In G1 phase, the pair of centrioles is disengaged and duplicated during S and G2 phases, while during the G2/M transition, the duplicated centrioles mature and the two pairs are separated to form two distinct centrosomes (Xu et al., 2017, Chou et al., 2016).

Nevertheless, human cancers may demonstrate centrosome abnormalities, usually amplifications, but also centrosome loss. Incorrect centrosome number can be caused by amplifications or deletions of genes expressing centrosome associated proteins, by cytokinesis failure or by endoreplication. For example, previous studies have

shown that deletion of CDC6 gene, an inhibitor of centriole duplication, or amplification of PLK4 gene, a promoter of centriole duplication, result to centrosome amplification, while amplification of CDC6 or deletion of PLK4 have the opposite effect (Xu et al., 2017, Godinho et al., 2014, Mariappan et al., 2019, Bakhoom et al., 2014, Chou et al., 2016).

Supernumerary centrosomes can result in the formation of multiple spindle poles and usually unviable daughter cells. Nevertheless, it has been observed that the amplified centrosomes frequently cluster at the two spindle poles and the cells proceed to divide in a bipolar fashion. In the presence of supernumerary centrosomes, merotelic attachments arise at an increased frequency, which can result in lagging chromosomes (Fig. 1.4 E) (Sansregret et al., 2018, Thompson et al., 2010, McGranahan et al., 2012, Holland and Cleveland, 2009, Ganem et al., 2009, Sansregret et al., 2011). KIFC1, which encodes the microtubule motor kinase HSET, is a gene that plays an important biological role in the event of centrosome amplification. Inhibition of HSET in centrosome amplified cancers, such as triple-negative breast, brain, lung, colon and cervical cancers, induces cell death through increasing the frequency of multipolar divisions. However, its inhibition does not affect cells with correct number of centrosomes, establishing it as a selective target for therapy of centrosome amplified cancers (Patel et al., 2018, Watts et al., 2013).

Complete loss of centrosomes is not very common in human cancer, however evidence suggest a role in prostate cancer progression. Cancer cells with lack of centrosomes accumulate an acentrosomal microtubule assembly pathway to form a bipolar spindle. There are two main ways for activation of the acentrosomal microtubule pathway. The first initiates by the kinetochores and is dependent on RAN (Ras-related nuclear protein)/GTP complex leading to correct microtubule attachments, while the second drives microtubule nucleation through the augmin pathway. However, acentrosomal spindles induce mitotic delay and errors during mitosis, including anaphase lagging chromosomes. In vivo studies demonstrate, that loss of centrosomes in non-transformed epithelial cells results in chromosomal alterations and generation of malignant tumours in xenografts (Wang et al., 2019, Meunier and Vernos, 2016).

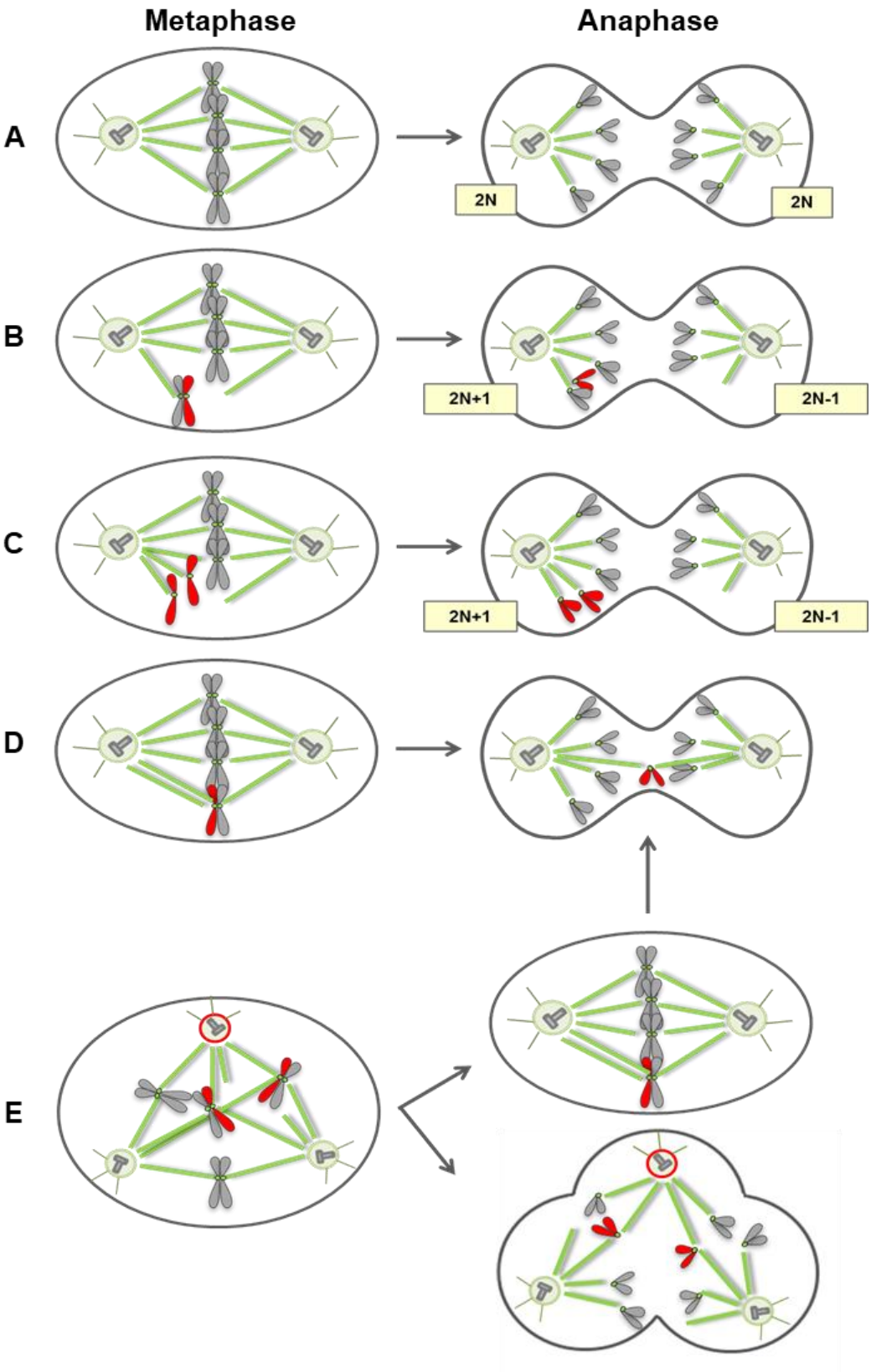

Figure 1.4: Pathways to chromosomal instability through mitotic defects. (A) Normal mitosis, **(B)** weakened mitotic checkpoint or sister chromatid cohesion defects **(C)** syntelic attachments, **(D)** merotelic attachments and **(E)** multipolar divisions. Each defect may lead to the loss of a chromosome from the one daughter cell and gain of a chromosome from the second daughter cell. In case of a lagging chromosome, it may be lost from both daughter cells. The haploid number of chromosomes is represented by N (23 in human cells).

1.3.1.2 Tetraploidization and chromosomal instability

Ploidy is a term that describes the number of complete chromosome sets in a cell. A human cell includes two sets of chromosomes and it is characterised as diploid, while a polyploid cell has more than two sets. Polyploidy naturally exists in nature, for example in plants, insects or amphibians and reptiles. In mammals, polyploidy is rarer but, programmed polyploidy can be found in specific tissues during development, like in heart or placenta, and is a feature of differentiation. Nevertheless, non-programmed polyploidization is a cause of chromosomal instability and is able to trigger cancer initiation (Donne et al., 2020, Peer et al., 2017, Tanaka et al., 2018).

Tetraploidy is a form of polyploidy, in which a single cell contains four complete sets of chromosomes. A tetraploid cell can arise through mechanisms of cell fusion, cytokinesis failure, endoreplication or mitotic slippage. Cell fusion is a mechanism, naturally occurring during development, for example in skeletal muscle cells, for generation of differentiated cells. However, unscheduled cell fusion due to viral infections or spontaneously, leads to tetraploid cells with two nuclei that may fuse and enter the cell cycle with two centrosomes, both of which will duplicate promoting multipolar divisions or lagging chromosomes, as explained previously (Figure 1.4 D and E) (Storchova and Pellman, 2004, Ganem et al., 2007). Cell fusion will be discussed in more detail, in section 1.5.

Cytokinesis failure is a feature frequently observed in cancer cells. After anaphase, the sister chromatids have been segregated to the opposite poles of the mitotic spindle and cytokinesis initiates. In the first step, the dense array of antiparallel microtubules between the two separating spindle poles and the astral microtubules around the centrosomes, activate specific proteins (ECT2/RHOA), which initiate a signalling cascade that results in the formation and contraction of an actin-myosin ring in the middle of the spindle, attached to the cell membrane. The second step is including the formation of the cleavage furrow (plasma membrane ingression) and accumulation of the central spindle microtubules at the farrow, to form the midbody. The last step is called abscission and is the actual separation of the two newly formed daughter cells

(Lens and Medema, 2019). Deregulation of cytokinesis by inhibition of cytokinesis regulators at the end of anaphase, incorrectly formed cleavage furrow or inhibition of abscission regulators, will result in generation of one tetraploid cell with two nuclei and two centrosomes, which will further promote chromosomal instability through centrosome amplification (Figure 1.5 A). Moreover, it has been reported that cytokinesis failure induction can occur after elevated rate of chromosome missegregation or chromatin trapping in the division site (Ganem et al., 2007, Lens and Medema, 2019, Tanaka et al., 2018).

Unscheduled tetraploidization can also occur through endoreplication or mitotic slippage. Endoreplication refers to DNA replication in the absence of mitosis, which generates a tetraploid cell with one nucleus but whole genome duplication. Mitotic slippage, can occur after a prolonged arrest in mitosis and inactivation of the SAC in the presence of mitotic errors. Thus, mitotic slippage also results to a tetraploid cell with one nucleus (Figure 1.5 B). Tetraploid cells generated either by endoreplication or mitotic slippage will undergo centrosome duplication in the next cell cycle, leading to multipolar division or lagging chromosomes (Holland and Cleveland, 2009, Ganem et al., 2007).

Tetraploid cells generated by cell fusion, cytokinesis failure, endoreplication or mitotic slippage may arrest in G1 through activation of the tetraploidy checkpoint. The tetraploidy checkpoint is similar to the G1/S checkpoint, involving p53, p21 and RB proteins. However, it has been disputed whether it is a distinct checkpoint of the cell cycle. Recent reports suggest the existence of a distinct checkpoint for tetraploid cells that results to G1 arrest, but due to supernumerary centrosomes rather than the number of chromosomes. Thus, after generation of tetraploid cells with excessive number of centrosomes and activation of the tetraploidy checkpoint, the cells may remain in G1 or undergo apoptosis. However, in most cancers, p53 function is lost through mutations or deletion of the gene or by perturbations in p53 signalling pathways (Margolis et al., 2002, Vitale et al., 2011, Muller and Vousden, 2013, Gupta et al., 2019, Lens and Medema, 2019). As a result, the tetraploid checkpoint is inactive and the binucleated or mononucleated tetraploid cells can continue to proliferate. Moreover, previous studies

have shown that these tetraploid cells can undergo malignant transformation at a higher rate than diploid cells. However, proliferation of tetraploid cells often produces cells with whole chromosome gains/losses, or other structural abnormalities (Holland and Cleveland, 2008, Storchova and Kuffer, 2008). Lastly, depolyploidization can occur through multipolar divisions, or continuous erroneous mitotic divisions, which can generate pseudodiploid cells that are often unviable due to enormous chromosomal aberrations. However, when viable, these can be highly tumorigenic (Figure 1.5 A and B) (Vitale et al., 2011).

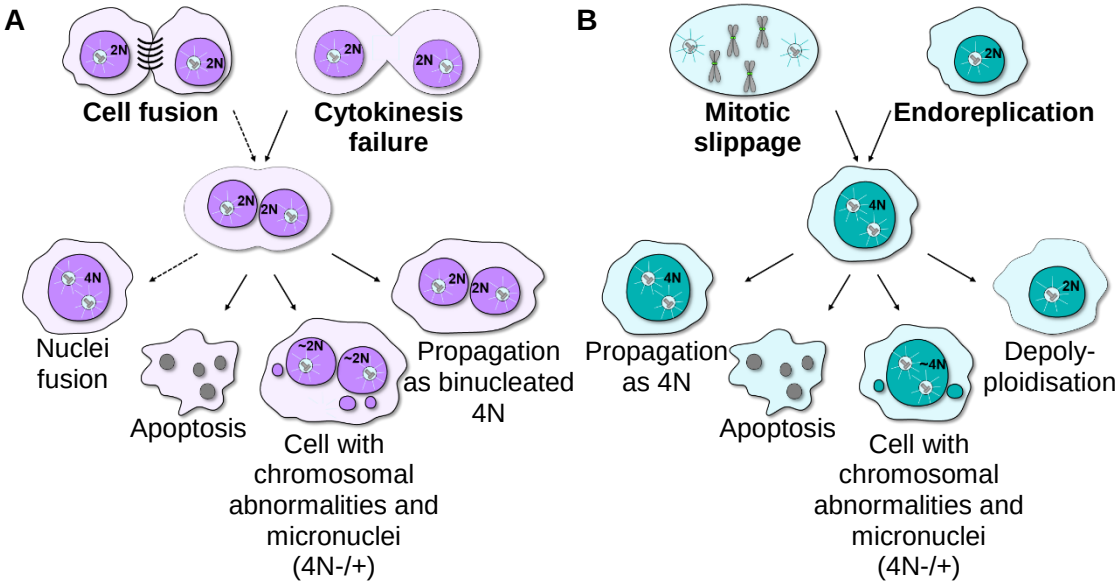

Figure 1.5: Pathways to generation of tetraploid cells and their fate. (A) Generation of binucleated tetraploid cells by cell fusion and cytokinesis failure. Tetraploid cells with two nuclei, formed by fusion, may also fuse their nuclei in the beginning of mitosis, or may remain and propagate as binucleated cells, similar to the tetraploid cells generated by cytokinesis failure. Binucleated tetraploid cells may undergo apoptosis or generate chromosomal unstable cells with micronuclei, through centrosome amplification and lagging chromosomes. **(B)** Generation of mononucleated tetraploid cells by mitotic slippage or endoreplication. The tetraploid cells may continue to propagate as tetraploid, undergo apoptosis or generate chromosomal unstable cells through centrosome amplification. Additionally, tetraploid cells may generate diploid or near diploid cells through depolyploidisation. The haploid number of chromosomes is represented by N (23 in human cells).

1.3.1.3 Impairment of DNA damage response and repair pathways as a driver of chromosomal instability

As mentioned before, different types of DNA lesions can arise through replication stress, telomere erosion, nuclease activity or environmental stress. Occurrence of DNA damage activates the G1/S and G2/M checkpoints through activation of ATM/CHK2 and

ATR/CHK1 DDR pathways, until the damage is repaired. DSBs are the most detrimental form of DNA damage, and are repaired trough NHEJ or HR repair pathways. Even if NHEJ pathway can be activated at any phase of the cell cycle, DSBs during replication stress are repaired from HR pathway as it can guarantee errorless repair. However, when the replication fork encounters a SSB, it collapses and generates a one-ended DSB. Any attempt of repair through end-joining mechanisms may result to chromosomal rearrangements and translocations. Moreover, excessive replication fork collapse, DNA breaks and repair through end-joining mechanisms or impaired DNA damage repair pathways may lead to intensive fragmentation of a chromosome or a chromosomal region. This event was first observed in 2011 and named chromothripsis, from the Greek for 'chromosome' (chromo) and 'shattering into pieces' (thripsis). The chromosomal fragments can be re-ligated by impaired repair pathways and generate extensive chromosomal translocations, deletions, lagging chromosomes or formation of double-minute chromosomes (acentric extra-chromosomal DNA). Double-minutes or anaphase lagging chromosomes are often kept outside of the nucleus in separate structures called micronuclei, and can co-exist with or reincorporate back in the main nucleus (Ichijima et al., 2010, Forment et al., 2012, Ly and Cleveland, 2017, Cortes et al., 2020).

Furthermore, DNA damage can occur during mitosis, for example after ionizing radiation and activation of the primary DNA damage response, with recruitment of ATM and MRN complex. However, the DNA repair pathway does not continue through phosphorylation and inactivation of RNF8 and 53BP1 proteins and the damaged DNA is ‘marked’ for repair after the end of mitosis, in G1 phase. However, active RNF8 and 53BP1 can initiate a secondary repair mechanism by recruiting BRCA1 and proceed with DNA damage repair during mitosis. In that case, due to sister chromatid telomere fusions, chromosome rearrangements generate dicentric chromosomes, which can break during anaphase, and form micronuclei after cytokinesis (Petsalaki and Zachos, 2020, Orthwein et al., 2014).

Recently, studies have shown that the DDR and repair machinery interacts with the mitotic machinery to maintain the genomic integrity, even in the absence of DNA

damage. In human cells, CHK2 is localised at the centrosomes and phosphorylates and activates BRCA1 in order to promote proper mitotic spindle assembly. Moreover, previous studies suggest that CHK2 localises to the kinetochores in early prometaphase, where it interacts with Aurora B in the presence of unattached kinetochores and promotes localization and stabilisation of MPS1, and thus activation of SAC. (Stolz et al., 2010, Ertych et al., 2014, Petsalaki and Zachos, 2014). Additionally, in contrast to CHK2, CHK1 also localizes at the kinetochores and activates Aurora B by phosphorylation, but in late prometaphase, in the presence of unattached kinetochores. Thus, loss of CHK1 or CHK2 leads to an increased rate of chromosome missegregation and chromosomal instability (Santaguida et al., 2011, Petsalaki and Zachos, 2020)

Furthermore, presence of MRN is not only crucial in DNA damaged areas but also in mitotic spindle poles. During mitosis, MRN is localised at the spindle poles and interacts with MMAP (mitosis specific MRN-associated protein) through interaction of the C-terminal region of MRE11 protein. Depletion of MRN or MMAP blocks the interaction between PLK1 and KIF2A, which is important for regulation of microtubule polymerisation, and alters the mitotic spindle dynamics driving entry into anaphase with elevated rates of unaligned chromosomes (Xu et al., 2018).

Another gene that is crucial for the DNA damage response and proper function of anaphase and cytokinesis processes, is ATM. During mitosis, ATM is activated after phosphorylation of Aurora B at serine 1403. Then, ATM localises at the midzone in anaphase and at the midbody during cytokinesis, while it also phosphorylates BUB1, a kinetochore localised gene, essential for SAC activation. Loss of functional ATM promotes prolonged mitosis and elevated rates of lagging chromosomes (Yang et al., 2011, Petsalaki and Zachos, 2020). Similarly, more proteins essential for DNA damage response and repair, like ATR and BRCA2, are crucial during mitosis. ATR is important for correct chromosome segregation through CENP-F interactions, while BRCA2 is known to participate in SAC activation through association with BUBR1 and in cytokinesis completion, as its depletion is shown to both delay the membrane abscission and generate binucleated tetraploid cells (Kabeche et al., 2018, Choi et al., 2012, Mondal

et al., 2012).

1.3.1.4 Deregulation of the SWI/SNF complex as a path to chromosomal instability

In human cells, interphase DNA and its protein scaffold is folded in a structure named chromatin. Chromatin consists of nucleosomes, which contain 146 base pairs of DNA wrapped around histone molecules. Nucleosomes are linked with DNA and they are super coiled, generating a compact chromatin structure. The DNA inside the compact chromatin is inaccessible to DNA replication or transcription machineries. Thus, specific proteins are needed to unravel the DNA, in order of important cellular processes to initiate. These proteins are named chromatin remodellers and are separated in two categories: the covalent modifiers of the histones, such as methyltransferases and acetyltransferases, and the protein complexes that need energy from ATP hydrolysis to promote chromatin remodelling. ATP dependent chromatin remodellers are crucial for almost every essential DNA process and can be further categorised in four different families: switch/sucrose non-fermentable (SWI/SNF), imitation switch (ISWI), chromodomain helicase DNA-binding (CHD), and DNA helicase INO80. The SWI/SNF family is mutated in ~20% of human cancers, ranking it in the most frequently altered chromatin remodelling complex in cancer (Roberts and Orkin, 2004, Clapier et al., 2017, de Cubas and Rathmell, 2018).

In human, the SWI/SNF family contains three complexes: the BAF (or the canonical) complex, the PBAF complex, and the most recently discovered GBAF (or noncanonical BAF) complex. The BAF (BRG1-associated factors) complex includes the ARID1A (AT-rich interaction domain 1A) (BAF250a) or ARID1B (BAF250b) subunit. The PBAF (polybromo-associated BAF) complex contains the PBRM1 (polybromo 1) (BAF180), ARID2 (BAF200) and BRD7 (bromodomain-containing protein 7) subunits, while the GBAF consists of BRD9 and either GLTSCR1 (glioma tumour suppressor candidate region gene 1) or GLTSCR1L (GLTSCR1-like) subunits. BAF and PBAF share the same catalytic ATPase subunits, which can be either BRG1 (encoded by SMARCA4) or BRM (encoded by SMARCA2) and their amino-acid sequence is 75% identical.

However, more subunits are associated with the SWI/SNF complex, depending the specific process that takes place, as shown in Table 1.1 (Fukumoto et al., 2018, Wang et al., 2020, Mittal et al., 2020).

The exact functions of the SWI/SNF complex are not yet well understood, due to lack of information about the subunit organisation or assembly and their 3D structure. However, the BAF complex is recruited to enhancers, while PBAF is recruited primarily to promoters, and GBAF binds to CTCF (CCCTC binding factor) sites, which are important in maintaining DNA architecture. Moreover, mutations in the SWI/SNF complexes are linked to chromosomal instability and indirect tumourigenesis due to impairments in cell cycle checkpoints, DNA damage repair, DNA transcription or mitotic pathways (Wang et al., 2020, Roberts and Orkin, 2004, Mashtalir et al., 2018).

Previous studies have shown that RB interacts directly with BRG1 or BRM to inactivate the E2F transcription factor and promote cell cycle arrest. Lack of BRG1 and BRM lead to checkpoint inactivation and cell cycle progression from G1 to S and G2 phases (Roberts and Orkin, 2004). Furthermore, disruption of SWI/SNF complexes can increase the cell proliferation by deregulating transcription of some oncogenes, like MYC, a transcription regulator that its overexpression is linked with many human malignancies. However, it was recently found that MYC can also transcriptionally regulate some SWI/SNF subunits, generating a transcription regulatory loop that might contribute to the aggressiveness of MYC dependent cancers (Reisman et al., 2009, Santen et al., 2012, Srikanth et al., 2020).

The SWI/SNF chromatin remodellers are essential for recruitment of DNA damage repair pathways, as the latter cannot access the damaged area in the chromatin. Upon DNA damage, subunits of the SWI/SNF complexes, such as BRG1, bind to the promoters and transcriptionally activate ATM and ATR genes. Phosphorylated ATM can further activate itself as well as BRG1 and ATR, inducing the recruitment of more repair proteins in the damaged area. However, there are also subunits, like BAF180, that are recruited at the DNA damaged area, independently of ATM or ATR. In general, the PBAF complex is linked with activation of NHEJ pathway

by stimulating KU70/KU80 recruitment and activation of HR pathway, by promoting DNA end resection and/or RAD51 loading, via both BAF and PBAF complexes. Moreover, BRG1 protein can be recruited to the damaged area in a XPC-dependent manner and promotes recruitment of XPG and PCNA, facilitating DNA damage repair through the NER pathway, or it can interact with BRCA1 and FANCD2 for the repair of inter-strand crosslinks. Also, PBAF complex, through BRG1, promotes transcriptional repression in the area of damaged DNA. Mutation or deletion of SWI/SNF subunits, especially BRG1, may have a high impact in regulation of DNA damage pathways and promote cell cycle progression in the presence of unrepaired DNA, generating chromosome breakages and micronuclei formation (Ribeiro-Silva et al., 2019, Kwon et al., 2014, Brownlee et al., 2015, Sethy et al., 2018, Ribeiro-Silva et al., 2018).

The SWI/SNF complexes are also known to play a role in mitosis. The BAF180 (subunit, of PBAF complex) localises to the kinetochores of sister chromatids, maintaining their cohesion. Deletion of BAF180 promote disruption of chromatid cohesion and generates lagging chromosomes and micronuclei formation, leading to chromosomal instability. Similarly, loss of BRG1 function generates CIN cells with anaphase bridges, lagging chromosomes, micronuclei and it can also lead to mitotic catastrophe (Bourgo et al., 2009, Brownlee et al., 2015, Brownlee et al., 2014).

In summary, the chromatin remodelling complexes are crucial for unwrapping the condensed chromatin so that different machineries can access the DNA. The SWI/SNF chromatin remodelling complex is highly mutated in human cancers, and include three different complexes, however BAF and PBAF are the most well studied. BAF and PBAF contain subunits that are shared between the two complexes or unique in each. More studies are focused on BRG1, which is the ATP catalytic subunit in both complexes, and BAF180 that is binding to acetylated histones and it participates exclusively in the PBAF complex. Both are highly mutated in multiple cancers and are involved in important processes like DNA damage repair, transcription and mitosis. Synoptic information for the known function of BRG1 and BAF180, as well as of other BAF and PBAF subunits, involved in the same processes, is shown in Table 1.1. Furthermore, loss of individual

SWI/SNIF subunits does not necessary cause complete loss of DNA damage repair, transcription or chromatin cohesion pathways, thus the cells continue to survive. Nevertheless, SWI/SNF complex impairment promotes cell cycle progression and entry into mitosis even in the presence of unrepaired DNA and may also lead to chromatid cohesion dysfunctions during mitosis. As a result, lagging or missegregated chromosomes are generated leading to chromosomally unstable daughter cells with micronuclei (Brownlee et al., 2014, Brownlee et al., 2015).

Table 1.1: The SWI/SNF subunits, their function in DNA damage repair and chromatin cohesion, and the frequency of their alteration in tumours.

Protein	Gene	Complex	Function	Alteration in cancer %
BRG1	SMARCA4	BAF/PBAF	NHEJ, HR, repression of transcription after DNA damage, chromatid cohesion	Ovarian cancer (>10%), medulloblastoma (5-10%), melanoma (5-10%), small cell cancer of the ovary (100%)
BRM	SMARCA2	BAF	NHEJ	Rhabdoid tumor (60%); lung (4.8-10%), breast (15%), gastric (15%) and bladder (15%) cancers
BAF250B	ARID1B	BAF	NHEJ, promotes BRM association with damaged chromatin	Childhood neuroblastoma (7%), clear cell ovarian (>10%), gastric, colorectal and liver cancer (5-10%)
BAF200	ARID2	PBAF	Unclear	Melanoma (5-15%), lung and colorectal (5-10%) and liver (5-14%) cancer
BAF180	PBRM1	PBAF	sister chromatid cohesion, repression of transcription after DNA damage	Renal cancer (41%), epithelioid sarcoma (83%)
BRD7	BRD7	PBAF	Unclear	Breast cancer

BAF170	SMARCC2	BAF/PBAF	HR, NHEJ	Rarely mutated
BAF155	SMARCC1	BAF/PBAF	HR, NHEJ	Prostate cancer (30-31%)
BAF60A/B/C	SMARCD1/2/3	BAF/PBAF	NHEJ, promotes BRM association with damaged chromatin	Rarely mutated
BAF57	SMARCE1	BAF/PBAF	Unclear	Familial spinal meningiomas (45%)
BAF53A/B	ACTL6A/B	BAF/PBAF	Unclear	Rarely mutated
BAF47	SMARCB1	BAF/PBAF	NHEJ, promotes BRM association with damaged chromatin	Rhabdoid tumor (>98%), epithelioid sarcomas (>55%), familial schwannomatosis (30-45%)

1.3.1.5 Role of chromosomal instability in tumour evolution, patient prognosis and drug resistance

As a form of GIN, chromosomal instability, refers to the altered number or structure of chromosomes and drives tumour heterogeneity and evolution. CIN has been associated with both tumour initiation and tumour progression and it can change the chromosome defined genome context and therefore, the entire platform of gene interaction by altering the entire genomic topology and system architecture (Heng et al., 2013). Previous studies have shown that gain or loss, even of a single chromosome, may lead to overexpression of oncogenes (e.g. KRAS) or loss of tumour suppressors (ATM, CHK2, p53) that may interfere with DNA damage repair and checkpoint machineries, driving tumour initiation or increasing the rate of tumour growth and progression in multiple cancers. Notably, whole genome duplication (tetraploidization)

can be an intermediate state, present at the early stages of tumour evolution. Tetraploid cells are prone to chromosome missegregation and anaphase lagging chromosomes, generating, eventually, near diploid or near triploid karyotypes that promote tumour progression. Thus, CIN can initiate the malignant transformation of a cell, however it is not a bystander during cancer progression, but actively contributes to constant changes in the number or structure of chromosomes, providing the tumour with the necessary intratumour genetic variation for overcoming selection barriers. For example, whole exome sequencing of a breast cancer primary tumour and a later metastasis in the brain revealed that 90% of the whole chromosomal alterations were detected in both the primary tumour and the metastatic site. However, 80% of whole chromosome alterations found in the metastatic tumour and 60% of the corresponding xenograft model derived from the same primary tumour, overlap with the alterations found in the primary tumour. These results indicate that some alterations were pre-existing in subclones of the primary tumour and selected upon metastasis, while ongoing CIN fuelled further heterogeneity in the metastatic site (Ding et al., 2010). Moreover, in renal cancer, loss of 9p and 14q was highly enriched in metastasizing clones but not in the clones on the original site, indicating active selection (Turajilic et al., 2018). Thus, this altered chromosomal structures, provide the ability to specific clones to overcome the tumour microenvironment barrier and metastasise (Bakhoom and Compton, 2012, Bakhoom and Landau, 2017, Bolhaqueiro et al., 2019, Jing et al., 2018, Turajilic et al., 2018).

The impact of CIN in cancer prognosis has been investigated in multiple cancers, using various methods, such as FISH (fluorescence in situ hybridization), gene expression signatures for CIN, SNPs (single nucleotide polymorphisms) or single cell sequencing. In a pan-cancer study of more than 2,000 tumour samples, was shown that only moderate levels of CIN (between 25% and 75% of a tumour's genome) are linked with poor prognosis and decreased survival (Turajilic et al., 2019). Strikingly, it was shown that excessive levels of CIN, identified by FISH or expression of CIN signature genes, are linked with better prognosis in multiple cancer cohorts, such as ER-negative breast, ovarian and gastric (Roylance et al., 2011, Birbak et al., 2011). This non-linear

relationship between CIN levels and cancer patient prognosis indicates that CIN can generate an optimal genetic variation, advantageous for tumour evolution. However, according to this hypothesis, the levels of CIN should be high enough to drive the evolution process, but low enough not to cause cell death (Turajilic et al., 2019, McGrahan et al., 2012, Targa and Rancati, 2018, Lee et al., 2019).

This relationship between CIN and cancer prognosis, indicates that high CIN levels may be an important phenotype to target therapeutically. A potential mechanism to target CIN indirectly, is the inhibition of centrosome clustering in centrosome amplified cancer cells. Inhibition of bipolar mitosis can enforce the rate of multipolar divisions which can be lethal, due to extreme chromosome losses in the multiple daughter cells (Patel et al., 2018, McGranahan et al., 2012). Additionally, inactivation of SAC by inhibition of MPS1 or MAD2 increases the frequency of missegregated chromosomes, leading to excessive levels of CIN. This phenotype can be further promoted by combining SAC inhibitors with taxanes. In more detail, combination of SAC inhibitors (such as an MPS1 inhibitor) with docetaxel or paclitaxel, that promote spindle microtubule stabilisation and interfere with mitotic spindle assembly, drive cancer cells to excessive and lethal levels of CIN (Al-Ejeh et al., 2014, Faisal et al., 2017). Moreover, CIN can generate synthetic lethal interactions in cancer cells, by inducing gene dependencies that do not exist in normal cells, and which could be exploited therapeutically. For example, in breast cancer, BRCA1 and BRCA2 deficiency, by loss of the physiological wild type (WT) allele in heterozygous mutated cells, sensitizes cancer cells to PARP inhibitors. As described before, PARP and BRCA1/2 are important for DNA damage repair and their simultaneous inhibition increase the level of GIN, due to replication stress and increased damaged DNA that cannot be repaired, promoting cell death (Slade, 2020, Vargas-Rondón et al., 2018).

Interestingly, a recent study showed that different levels of CIN can have different effects in tumour initiation and progression. In mice that conditionally express in the intestine two separate mutations of MPS1 that cause moderate or severe CIN, adenoma formation was both more prominent and occurred earlier in mice with moderate CIN (12

weeks) than in mice with high CIN (8 months). When the same mutants were expressed in $Apc^{Min/+}$ mice that are predisposed to intestinal adenomas, moderate levels of CIN promoted tumour initiation in the entire intestinal track and the distal colon. High levels of CIN were also able to promote tumour initiation, however, not in the small intestine but only in the distal colon and strikingly, it was more severe than in moderate levels of CIN. These results indicate that different levels of CIN have different potentials to drive tumour initiation in distinct tissues, possibly due to the different tissue characteristics, such as cell proliferation rate or the immune landscape (Hoevenaar et al., 2020).

Moreover, several studies have shown that CIN is linked with poor cancer prognosis, due to increased tumour resistance to therapies. It has been demonstrated that chromosomally unstable colorectal cancer cells are more resistant to therapies (kinase inhibitors targeting signal transduction, cell cycle and trans-membrane receptor signalling pathways or 5-flouoruracil) than chromosomally stable cancer cells, due to the increased chromosomal heterogeneity and the subsequent adaptation (Lee et al., 2011). Additionally, microtubule-stabilizing (MTS) agents, such as taxanes, are broadly used in cancer treatment. In a previous study it was shown that taxanes efficiently promote cell death in cancer cells with low level of CIN (<15% of chromosomes displayed numerical heterogeneity from cell to cell) but not with high CIN (>40% of chromosomes exhibited numerical heterogeneity from cell to cell). It was suggested that cancer cells with high degree of CIN displayed increased expression of genes that are involved to their survival. These results also indicate that the cell karyotype and the tumour heterogeneity are important for acquisition of tumour resistance on specific therapies (Swanton et al., 2009). From a Darwinian perspective, drug treatment can be viewed as a selective pressure. CIN fuels tumour heterogeneity, increasing the possibility of resistant clones to pre-exist before the treatment. Nevertheless, many commonly used chemotherapeutic agents may promote excessive levels of CIN, which further generates genetic heterogeneity and the emergence of drug-resistant clones (McGranahan et al., 2012, Sansregret et al., 2018, Turajilic et al., 2019). Lastly, even targeted therapies that are based on oncogene addiction may not be effective in cancer cells with ongoing

chromosomal instability, as CIN can bypass the oncogene addiction after oncogene withdrawal by activating compensatory pathways and promote relapse. For example, in a previous study, more aggressive KRAS-driven lung tumours with increased degree of CIN were generated in mice by inducing tetracycline-driven overexpression of MAD2 and mutant KRAS, compared to the control mice models that overexpressed, either MAD2 or mutant KRAS alone . In the absence of tetracycline, tumour regression was observed in every mouse model, however, tumour relapse was detected only in the MAD2, KRAS mice models. The relapse was independent to the size but dependent to the intratumour heterogeneity of the primary tumour (Sottilo et al., 2010). Thus, targeting mechanisms that prevent CIN, like the SAC or centrosome clustering, driving CIN to excessive levels or understanding the mechanisms by which CIN is tolerated in cancer cells may lead to therapeutic approaches to improve patient prognosis, by reducing therapy resistance and promoting cancer cell death (Sansregret et al., 2018, Turajilic et al., 2019).

1.3.2 Summary

Chromosomal instability is a form of GIN that includes both numerical and structural chromosomal alterations. CIN can be caused by errors in mitosis, such as erroneous microtubule-kinetochore attachments or SAC abrogation. In addition, errors in DNA damage response and repair pathways or in chromatin remodelling complexes can be manifested during mitosis and generate chromosomally unstable cells. However, they can also indirectly, promote CIN by allowing cells with damaged DNA to progress into mitosis. Finally, CIN is a driver of tumour heterogeneity and a crucial process for tumour initiation, progression and resistance to cancer therapies. Thus, this study is focusing on targeting CIN induced by multiple causes, such as loss of function either of mitotic proteins (CENP-E), DNA damage response proteins (ATM), or disruption of chromatin remodelling complexes (through deletion of BRG1 or BAF180). Furthermore, our aim was the identification of synthetic lethal interactions either to the CIN phenotype in general or to the CIN phenotype induced by distinct pathways.

1.4 Aneuploidy

Aneuploidy refers to a phenotype in which a cell's set of chromosomes deviates from the euploid set (Figure 1.6) and is closely related to chromosomal instability (CIN) which describes a dynamic state in which cells frequently gain or lose chromosomes or chromosomal regions. Therefore, an aneuploid cell is not necessarily chromosomally unstable, but a cell characterised by CIN will give rise to aneuploid daughter cells. Thus, triploid or tetraploid cells are not necessarily considered aneuploid. Aneuploidy refers to chromosomal alterations that can be either numerical (whole chromosome gains or losses) or structural (gains, losses or translocations of chromosomal regions) (Sheltzer and Amon, 2011, Santaguida and Amon, 2015).

Aneuploidy was initially observed over a century ago, by the German zoologist Theodor Boveri. Boveri based his hypothesis on the observations by von Hansermann, of unbalanced divisions in different cancer types (Hansemann, 1890). In 1902, Boveri described abnormal mitotic divisions in sea urchin embryos (Boveri, 1902). In 1914, Boveri combined his observations with von Hansemann's findings and proposed a hypothesis of tumorigenesis, in which a tumour can arise from a single cell with an incorrect set of chromosomes (Boveri, 1914). However, aneuploidy as a term, was described for a first time by Gunnar Täckholm, in 1922. Täckholm investigated the karyotypes of meiotic cells of the first filial generation (F1) hybrids, generated from crosses between different species of roses (with seven chromosomes). He observed in a number of meiosis of the F1 hybrids: 'bivalent and univalent chromosomes are not a multiple of seven. In many instances this is also the case for their somatic karyotypes. Because it is necessary to coin a term for a chromosome number that is not a multiple of the base chromosome number, I will call this condition aneuploidy. Henceforth, aneuploidy refers to hyper and hypoploid chromosome numbers' (Täckholm, 1922, Holland and Cleveland, 2009, Sheltzer and Amon, 2011, Knusdon, 2001, Hardy and Zacharias, 2005, Santaguida and Amon, 2015).

Human cells, contain 23 pair of chromosomes in total, 22 of which are autosomes

and the 23rd pair consists of the sex chromosomes, known as X and Y. Aneuploidy is usually a lethal event in developmental stages and whole chromosome aneuploidy, gain or loss of even one chromosome, is the most common cause of miscarriages. For example, monosomy, loss of one chromosome, in autosomal chromosomes is lethal in embryonic cells, even in culture. The only known monosomy in humans that is not embryonically lethal, is loss of X chromosome and causes the Turner Syndrome, which generates infertile females with developmental issues (Bondy and Cheng, 2009, Biancotti et al., 2012). Trisomy, gain of one chromosome, is more common than monosomy, however it can be also lethal or cause developmental problems. Most common non embryonically lethal trisomy in humans, is in chromosome 21, which causes Down's syndrome. Females or males, with Down syndrome present developmental delays, mental disabilities and are in high risk of leukaemia predisposition. Moreover, trisomies of chromosomes 8 (Warkany syndrome), 13 (Patau syndrome), 18 (Edwards syndrome), 9, 16 or 22 have been observed, but in most cases they are lethal after the first months of birth. In sex chromosomes, trisomies are not as severe as in autosomes. The triple X (XXX) syndrome in female and XYY in male, generate no physiologically distinct adults, but they may present learning disabilities. However, males may suffer a potential trisomy in the sex chromosomes that causes the XXY or Klinefelter syndrome, resulting in distinct physiological alterations and infertility (Markov et al., 2007, Cereda and Carey, 2012, Wu et al., 2013, Kehinde et al., 2014, Beck et al., 2015, Rafique et al., 2019, Kim et al., 2013, Kompus et al., 2011).

Nevertheless, aneuploidy is very common phenotype in cancer with 90% of solid tumours and 50-60% of blood cancers being aneuploid. Whether aneuploidy is a cause or consequence in cancer and whether aneuploidy affects positively or negatively the cell fitness, are, still, active areas of research (Santaguida and Amon, 2015).

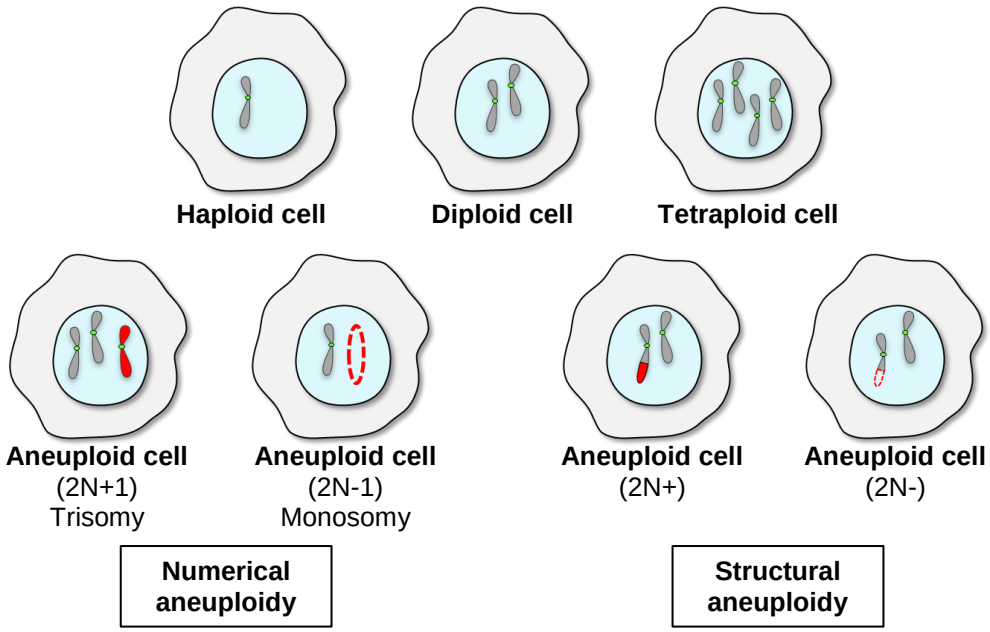

Figure 1.6: Numerical and structural aneuploidy illustrated in a post mitotic cell. One set of chromosomes is used for brevity. The haploid number of chromosomes is represented by N (23 in human cells).

1.4.1 Causes of numerical and structural aneuploidy

Similarly to CIN, aneuploidy can be caused by errors in mitosis or unrepaired breaks in the DNA. The main difference is that aneuploidy describes a stable chromosomal pattern within a cell. These are caused by transient errors, which when they persist over the course of multiple cell cycles, they cause CIN. Whole chromosome gains or losses (numerical aneuploidy) can arise through chromosome missegregation. As described previously, merotelic and syntelic kinetochore-microtubule attachments, unaligned chromosomes in the metaphase plate, defects in sister chromatid cohesion or SAC deregulation, may lead to whole chromosome missegregation (Orr et al., 2015, Barra and Fachinetti, 2018). Previous studies have shown that reduction in expression of CENP-E (responsible for chromosome alignment and interactions with SAC proteins) or MPS1 (core SAC component and role in chromosome alignment) promotes unaligned chromosomes and inactivation of SAC, leading to numerical aneuploidy through chromosome missegregation (Weaver et al., 2007, Gurden et al., 2015). Moreover, decrease or increase in MAD2 expression leads to aneuploidy through SAC inactivation or through SAC hyperactivation, respectively. The latter promotes MAD2 dependent

inhibition of separase activity, separation of the two sister chromatids and leads to prolonged mitosis. Eventually, aneuploid daughter cells are generated through chromosome missegregation (Weaver et al., 2007, Sotillo et al., 2007, Pellman, 2007).

Numerical aneuploidy may also arise through supernumerary centrosomes. Clustering of the supernumerary centrosomes at the opposite spindle poles increases the frequency of merotelic attachments and of whole chromosome missegregations (Raff and Basto, 2017, Orr et al., 2015, Levine et al., 2017). In the same context, Storchova and Pellman reviewed in 2004 the hypothesis that tetraploid cells with supernumerary centrosomes, may generate aneuploid progeny in subsequent divisions (Orr et al., 2015, Storchova and Pellman, 2004, Levine et al., 2017, Paim and FitzHarris, 2019).

Lastly, telomere dysfunction is a cause of numerical and structural aneuploidy. Loss of telomerase exposes the telomeres at the end of the chromosomes and NHEJ pathway is recruited at the area, which promotes telomeric fusion. As a result, dicentric chromosomes are formed that contain two centromeres and are prone to missegregation or breakage during anaphase and cytokinesis (Orr et al., 2015). In addition, structural aneuploidy can be induced by unrepaired DNA damage or breaks resulting in translocations or deletions/amplifications of chromosomal regions. Moreover, errors in DNA replication can cause acentric chromosomes during mitosis that further result to chromosome breakages and lagging chromosomes. DNA replication errors and DNA breaks may lead to chromothripsis in which a chromosome can be shuttered in many pieces. These pieces can be re-ligated by the DNA damage repair machineries but lead to translocations and deletions of chromosomal regions (Orr et al., 2015, Ly and Cleveland, 2017, Cortés-Ciriano et al., 2020).

The terms CIN and aneuploidy are commonly used interchangeably due to the similarities in their origin. However, CIN and aneuploidy are two distinct processes. CIN is a dynamic state that fuels the intratumour heterogeneity and can generate stable aneuploid subclones, which may undergo selection, resulting to tumour progression. Thus, mosaic aneuploidy, the presence of different subclones with stable but distinct chromosomal changes, can be a consequence of CIN. (Foijer, 2010, Schukken and

Foijer, 2018).

Moreover, mosaic aneuploidy may arise independently of CIN through karyotype divergence. Karyotype divergence refers to a population phenotype in which subclones of cells with distinct karyotypes, change over time. The level of divergence indicates the changes in the size or number of the subclones over time. Environmental perturbations, such as alterations in temperature, pH, nutrition deficiency or presence of chemotherapeutic or other drugs, can lead to karyotype divergence, which can be driven by selection or genetic drift, a stochastic process that changes subclone frequency. Although CIN has the potential to generate intratumour heterogeneity, the evolutionary dynamics in a heterogeneously aneuploid population can take place independently of the presence or absence of CIN (van Jaarsveld and Kops, 2016, Turajilic et al., 2019, Pavelka et al., 2010). Nevertheless, systemic aneuploidy in which the same chromosomal alterations exist in every somatic cell and gametes, can exist independently to CIN or karyotype divergence. For example, Down's, Edward's, Patau's, Klinefelter's or Turner's syndromes are some examples that have been described previously, in which systemic aneuploidy exists from the beginning of the development with no CIN or karyotype divergence getting involved (Foijer, 2010, Schukken and Foijer, 2018).

1.4.2 Consequences of aneuploidy in cell fitness and the aneuploid paradox

Abnormal number or structure of chromosomes can have a significant impact on cell physiology; it can promote cancer cell survival, but can also induce deleterious mutations and cellular stress, depending on the specific alterations in gene dosage that are produced. These impacts can be short- or long- termed after aneuploidisation. Immediately after the generation of an aneuploid cell, p53 is activated, resulting in G1 arrest or apoptosis (Santaquida and Amon, 2015). However, p53 is highly mutated in multiple cancers and most mutations occur in the DNA binding domain of the protein, resulting to inactivated function. For example, an analysis of more than 10,000 TCGA

patient samples from 32 cancer types showed that p53 is mutated in approximately 90% of ovarian and uterus cancers, 55% of pancreatic cancers, 50% of colorectal cancers and 30% of breast cancers. However, in some types of cancers, such as acute myeloid leukaemia and thyroid cancers, p53 is mutated up to 5%, or less (Donehower et al., 2019). The exact mechanism of p53 activation by aneuploidy is not yet understood, but previous studies have shown that p53 loss in tetraploid cells, impairs their ability to undergo centrosome clustering, driving cells to undergo multipolar divisions that result to highly aneuploid daughter cells. Additionally, in case of p53 loss, but not in WT p53 tetraploid cells, p38 is localised to centrosomes during metaphase and to the midbody during telophase and plays a role in mitotic progression. Inhibition of p38, in p53 deleted tetraploid cells, activates SAC and induces prolonged mitotic delay and increased frequency of multipolar divisions (Santaquida and Amon, 2015, Yi et al., 2011, Vitale et al., 2010).

Moreover, it has been suggested that aneuploidy induces cell cycle arrest in G1 or apoptosis, through p53 activation. One study suggested that DNA damage during cytokinesis activates p53, while another study proposed that chromosome missegregation induces expression of p53 independently of DNA damage during mitosis. Similarly, studies have shown that chromosome missegregation by SAC inactivation, induces p53 expression through p38 activation. Also, it has been shown that chromosome missegregation and the resulting aneuploidy increase the reactive oxygen species (ROS) in the cell and activate p53 in an ATM dependent manner. Thus, it was concluded that aneuploidy *per se* induces cell cycle arrest or apoptosis through p53 activation and that loss of p53 is responsible for the aneuploid cell propagation. Nevertheless, Soto et al., in 2017, generated random aneuploidies by SAC inactivation in p53 proficient and p53 deficient cells. They reported that p53 was not always activated in response to whole chromosome aneuploidy, arguing that aneuploidy *per se* inevitably activates p53. In contrast, they showed that only structural aneuploidies produced by segregation errors promote p53 activation and they can be tolerated only in p53 deficient cells. On the contrary, whole-chromosome imbalances can be tolerated by both p53

deficient and p53 proficient cells. They hypothesised that the p53 proficient cells tolerate a degree of aneuploidy, however, if it is above a threshold it generates cellular stress and activation of p53 pathway. Thus, high degree of aneuploidy may activate p53 through increased cellular stress, but not directly after chromosome missegregation. Additionally, loss of p53 cannot generate aneuploidy by itself but promotes cell cycle progression in the presence of both numerical and structural aneuploidies, however, the exact mechanisms are not yet understood (Santaguida and Amon, 2015, Thompson and Compton, 2010, Liu et al., 2016, Li et al., 2010, Soto et al., 2017).

Apart from p53, specific chromosomal gains have been linked with increased rate of cell proliferation or mitotic delay and apoptosis. For example, gain of chromosomes 1, 13, 16 or 19 or loss of chromosome 3 are linked with impaired proliferation. Gain of chromosomes 2, 5 or 9 cause no changes to cell proliferation rate compared to the diploid counterparts, while gain of chromosome 12 is linked with increased proliferation in almost every cell type, providing an advantage relative to diploid cells. These differences in cell proliferation may be caused by the function of the genes in the specific chromosomes that were affected. Some chromosomes may be enriched for proliferation-promoting genes, while others for genes that suppress proliferation (Ben-David and Amon, 2020, Gordon et al., 2012, Santaquida and Amon, 2015, Ben-David et al., 2014, Chunduri and Storchová, 2019).

Gains or losses of whole or parts of chromosomes are accompanied by changes both in the dosage of genes in those regions as well as genome-wide changes of gene expression. However, the cell can minimise the effects of aneuploidy through dosage compensation. It has been observed that some gene expression changes are shared between different aneuploid cells, independently of their specific numerical or structural aneuploidies. This gene expression signature is named APS (aneuploidy-associated protein signature) and is characterised by upregulation of proteins involved in oxidative, metabolic, proteotoxic and hypo-osmotic stress (Gordon et al., 2012, Santaguida and Amon, 2015, Tsai et al., 2019).

Human cells contain a complex regulatory network that maintains the cellular

protein homeostasis (proteostasis) and ensures that proteins are properly folded and in the right concentration. This network is composed of chaperones, which guarantee the proper folding of proteins and the ubiquitin proteasome pathways that ensure the degradation of misfolded or aberrant proteins. When this network is impaired, results to proteotoxic stress and impaired protein quality control that can further affect different pathways and cell functions. Numerical or structural aneuploidy can directly intervene to this network by gain of a single gene that may increase the efficiency of a cellular pathway. Altered gene dosage can also change the formation or function of stoichiometric sensitive complexes or promote promiscuous molecular interactions due to protein abundance. Loss of genes that encode for chaperones, such as HSP90, which is commonly lost in human cancers, or losses that result in an overwhelmed chaperone network may result in the accumulation of improperly folded proteins and cytotoxic aggregates. Additionally, increases in gene dosage can interfere with the proteasome function. For example, in diploid cells, the proteasome rapidly degrades overexpressed free subunits, such as histones and ribosomal proteins to ensure the proper formation of stoichiometric complexes. However, in an aneuploid cell, there are stoichiometric imbalances and misfolded proteins that are targeted through ubiquitination for proteasome degradation, resulting to severe stress of the proteasome and to proteins escaping degradation (Sheltzer and Amon, 2011, Chunduri and Storchová, 2019, Gordon et al., 2012, Santaguida and Amon, 2015).

Analysis of human aneuploid cells revealed alterations in metabolic processes such as upregulation of membrane metabolism and glycolysis (Chunduri and Storchová, 2019). Sphingolipids are a lipid family found in eukaryotic cell membranes that is essential for the membrane biology and cell signalling. In aneuploid cells, the levels of ceramides that belong to the family of sphingolipids and function as signalling molecules, are increased. Ceramides slow cell proliferation and further increase of their synthesis by either genetic or pharmacological causes, induces apoptosis in aneuploid cells (Ben-David and Amon, 2020, Tang et al., 2017, Hwang et al., 2017). Moreover, it has been observed that hypo-osmotic stress is a general outcome of the proteasome imbalance

and increases membrane stress in the aneuploid cells interfering with endocytosis of essential nutrients. Tsai et al. demonstrated a general dependency of aneuploidy on ubiquitin-mediated endocytic recycling of nutrient transporters, such as the ART1-NEDD4 pathway. ART1 is an arrestin-related trafficking adaptor that targets the NEDD4 E3 ubiquitin ligase to promote endocytosis of membrane amino-acid transporters and its disruption can target aneuploidy (Tsai et al., 2019). In addition, in the same study it was shown that in aneuploid cells there is glutamine abundance, which is in line with previous studies showing that high glutamine levels are essential for growth in cancer cells, a state known as glutamine addiction (Tsai et al., 2019, Zielinski et al., 2017). Lastly, aneuploid cells exhibit increased glucose uptake and secrete significantly more lactate during proliferation, even in the presence of oxygen, than the euploid cells, which is known as the Warburg effect (Zielinski et al., 2017, Torres et al., 2007, Williams et al., 2008).

Another consequence of aneuploidy is the generation of genomic instability. Aneuploid cells display high levels of DNA damage that arises from replication errors. In particular, they exhibit reduced expression of replication factors, such as MCM2-7 helicase that plays a role in replication licencing and replisome progression. It has been shown that high levels of replication stress is generated by protein imbalances, protein folding defects and proteotoxic stress. For example, inhibition of HSP90 chaperone reduces the expression of MCM2-7. Thus, aneuploidy can intervene in basic cell mechanisms through proteotoxic stress and can promote tumourigenesis and genomic instability (Santaguida and Amon, 2015, Sheltzer and Amon, 2011, Passerini et al., 2016).

Furthermore, while aneuploidy can be caused by chromosomal instability, it can also result in further chromosomal instability. Aneuploid cancer cells may display increased levels of chromosome missegregation in the form of lagging chromosomes during anaphase. Frequently, lagging chromosomes may become trapped and damaged during cytokinesis, at the cleavage farrow. The broken chromosomes induce the DNA damage response and repair pathways and the DNA damaged is repaired in the next G1

phase by the NHEJ repair pathway, which may result in chromosomal translocations and deletions. Moreover, lagging chromosomes may not incorporate in any of the reforming nuclei and can be excluded from both daughter cells. Alternatively, lagging chromosomes may form their own micronuclei, which are not fully functional. Into micronuclei, DNA replication proceeds slowly and results in replication stress and increased DNA damage, the repair of which generates extensive DNA rearrangements which are prone to chromothripsis. However, aneuploid cells may exhibit impaired DNA repair pathways which can further increase the frequency of unrepaired damaged chromosomes and micronuclei formation that are indicative of CIN (Sheltzer et al., 2011, Santaguida and Amon, 2015, Rutledge and Cimini, 2016). However, not every aneuploid cell induces segregation errors. For example, trisomy of chromosome 7 or 13 further promotes chromosome segregation errors, while trisomy of chromosome 18 or 21 does not affect chromosome segregation. Thus, aneuploidy can result to chromosomal instability but not in all settings (Schukken and Foijer, 2017, Passerini et al., 2016, van Jaarsveld and Kops, 2016, Nicholson et al., 2015).

1.4.2.1 The aneuploidy paradox

Naturally occurring or experimentally induced aneuploidy has been shown to be detrimental in untransformed primary cells during tissue development and it is mostly associated with reduced cell fitness. However, in cancer cells, aneuploidy can be tolerated better than in untransformed cells, as it has been observed that 90% of solid tumours and 50% of blood cancers are aneuploid. But aneuploidy can also introduce lethal consequences to the cells and inhibit tumour progression. Thus, the aneuploidy paradox arises: is aneuploidy beneficial or detrimental for cancer cells (Ben-David and Amon, 2020, Sheltzer and Amon, 2011)?

At present there is not a clear answer to this question. Gain or losses of whole or parts of chromosomes may result in gaining of oncogenes or losing of tumour suppressor genes, promoting tumour initiation and progression. Correspondingly, gain of tumour suppressor genes and loss of oncogenes will inhibit tumourigenesis. Moreover,

aneuploidy alters the transcription of many genes and interferes with many cellular processes such as proliferation, DNA replication or damage repair. Thus, when aneuploidy is induced in a diploid population, the protein imbalances may generate stress that becomes a disadvantage for the cancer cells. As a result, the aneuploid cells are outcompeted by the diploid population. However, cancer cells can promote dosage compensation and escape the stress induced by aneuploidy. For example, gains of chromosomes X or 4 can be dosage compensated and be tolerated by cancer cells, however, the exact mechanisms are unclear (Santaguida and Amon, 2015, Chunduri and Storchová, 2019, Holland and Cleveland, 2009, Gronroos and López-García, 2018, Sansregret and Swanton, 2017).

Aneuploid cells can promote genomic instability through chromosome missegregations or induced proteotoxic stress, which may result in high levels of replication stress, DNA damage and impaired DNA repair pathways. As discussed previously, genomic instability can promote or inhibit tumour initiation and progression, depending the cell type and the genetic background in which it arises. Thus, aneuploidy can promote or inhibit tumourigenesis depending the genetic or cellular alterations that may cause and the different cell type in which will arise. For example, heterozygous deletion of CENP-E gene promotes tumorigenesis in spleen and lung but not in liver tissue. By contrast, BUB1B or BUB3 heterozygous deletions do not promote tumourigenesis in mice, but tissue ageing, even in the presence of chromosome missegregations. Lastly, patients with Down's syndrome are prone to leukaemia, but they do not exhibit high risk of developing solid tumours (Chunduri and Storchová, 2019, Santaguida and Amon, 2015, Sheltzer and Amon, 2011).

1.4.3 Role of aneuploidy in cancer, patient prognosis and cancer therapies

During the past decades there has been a dispute about whether aneuploidy is a cause or a consequence of cancer that can promote tumour progression. However, the last years became clear that aneuploidy can be both a cause and a consequence of tumour initiation. Numerical or structural aneuploidy can directly cause tumourigenesis

through gain of oncogenes or loss of tumour suppressor genes. Moreover, aneuploidy can indirectly promote tumour initiation through induction of genomic instability or accumulation of mutations through unbalanced gene expression. An alternative hypothesis is that aneuploidy provide the cells with advantageous characteristics under specific conditions, such as a drug treatment, promoting their proliferation and survival, as in the case of karyotype divergence (Holland and Cleveland, 2009, Gordon et al., 2012, van Jaarsveld and Kops, 2016).

Aneuploidy plays a role also in tumour progression and evolution. Chromosomal instability fuels the intratumour heterogeneity through generation of mosaic aneuploid subclones. Positive selection, the evolutionary force for tumour progression will act on the aneuploid clones promoting the survival of the clones that are phenotypically advantageous within a given tumour-environmental context (Turajilic et al., 2019). Furthermore, as discussed previously, increased levels of CIN above a certain threshold may be lethal in cancer cells, similarly, stable aneuploidies with low or moderate numerical or structural alteration can be better tolerated by cancer cells (Chunduri and Storchová, 2019). Consequently, aneuploidy promotes adaptation of cancer cells in stressful conditions such as elevated temperature, drug treatments or the immune system, and promotes tumour progression (Turajilic et al., 2019, Chunduri and Storchová, 2019).

High degree of aneuploidy has been linked with poor patient prognosis in multiple cancer cases. A recent analysis of data from The Cancer Genome Atlas (TCGA) demonstrated that highly aneuploid tumours are associated with poor prognosis in 9 of 27 cancer types. In addition, the degree of aneuploidy is representative of later tumour stages (Vasudevan et al., 2020). A systematic meta-analysis of more than 7,000 patients with colorectal cancer indicates that later stage tumours were significantly more aneuploid than early stage tumours (Laubert et al., 2015). More studies have associated aneuploidy with poor patient prognosis in multiple cancers such as serous ovarian cancer, breast cancer and with progression from Barrett's oesophagus to oesophageal carcinoma (Ben-David and Amon, 2020, Hieronymos et al., 2018, Martinez et al., 2018).

Thus, aneuploidy can be used for predictive purposes to assess if a disease will progress to carcinoma. Nowadays, aneuploidy can be reliably detected through a variety of techniques, such as single-nucleotide polymorphism arrays (SNPs), comparative genomic hybridization arrays (CGH) and genome-wide DNA and RNA sequencing, many of which are already used in clinic (Ben-David and Amon, 2020, Das and Tan, 2013, van den Bos et al., 2018).

The ability to identify the degree and the genomic alterations in aneuploid cells arises the potential for targeting specific types of aneuploidy or pathways in cancer, therapeutically. There are three therapeutic approaches that have been proposed. The first is including targeting of specific chromosomal alterations, while the second involves driving aneuploidy above a threshold that cannot be tolerated from cancer cells. However, most cancer types contain mosaic aneuploidies, and as a result not all the tumour subclones may be sensitive to the same agent, therefore resistant subclones may pre-exist. The third approach is called ‘the evolution trap’ and is a combination of the latter two. It includes treatment with a therapeutic agent that reduces the karyotypic heterogeneity of a population into one with a predominant and predictable karyotypic feature, which can be targeted by a second therapeutic agent (Ben- David and Amon, 2019, Van Jaarsveld and Kops, 2016, Rodrigues-Ferreira and Nahmias, 2020, Chen et al., 2015).

Targeting specific chromosome alterations is useful in selectively targeting aneuploid cells. Previous studies have shown that loss of chromosome arm 8p promotes sensitivity to autophagy inhibitors, while gain of chromosome 12 sensitises the aneuploid pluripotent stem cells and germ cancer cells to replication inhibitors. In addition, loss of chromosome arm 2q in breast and hematopoietic cancers promotes sensitivity to splicing inhibitors and deletion of chromosome arm 5q in myelodysplastic syndromes sensitises the cells to lenalidomide, which is an approved drug (Ben- David and Amon, 2019, Ben-David et al., 2014, Paollela et al 2017, List et al., 2018).

In order to reduce a cancer cell’s tolerance to aneuploidy, targeting the cellular dependencies induced by aneuploidy itself, may also be important. As described

previously, aneuploidy results to proteotoxic, replication, metabolic, mitotic and hypo-osmotic stress in the cells. These cellular stresses can induce vulnerabilities in the aneuploid cells independently to specific chromosome alterations. For example, inhibition of USP10 deubiquitinase, important for proteostasis, sensitises aneuploid cells after chromosome missegregation. However, it has also been described that aneuploid cells are sensitive to heat shock protein 90 (HSP90) inhibitors (17-AAG) but not to proteasome inhibitors (Ben-David and Amon, 2020, Dodgson et al., 2016, Tang et al., 2011, Donnelly et al., 2014). Deregulation of sphingolipid metabolism might be another vulnerability in cancer cells, as increase of ceramides induces apoptosis in highly aneuploid colorectal cancer cells (Hwang et al., 2017). Moreover, due to increased hypo-osmotic stress in aneuploid cells, another therapeutic approach may be targeting the membrane amino-acid transporters (Tsai et al., 2019).

Similarly, mitotic stress can sensitise aneuploid cells to chemotherapy. Inhibition of MPS1 kinase, a SAC component, in combination with paclitaxel, induce abrogation of paclitaxel-induced mitotic delay resulting to gross chromosomal abnormalities and cell death (Faisal et al., 2017). This effect has been observed by the cancer drug target discovery lab, at ICR, and is currently the subject of a clinical study (NCT03328494). Furthermore, depletion of ATIP3, a microtubule-stabilizing protein, increases the sensitivity of breast patient-derived xenografts to taxane treatment. Combination of ATIP3 depletion with taxanes led to centrosome amplification, increased rate of multipolar division, high degree of aneuploidy and cell death (Rodrigues-Ferreira and Nahmias, 2020).

In conclusion, the consequences of aneuploidy and the aneuploidy paradox that arises, promote potential vulnerabilities in cancer cells that may be used therapeutically. Thus, understanding and targeting the mechanisms of tolerance to aneuploidy as well as using aneuploidy as an indicator for cancer prognosis can be essential in cancer treatment (Ben-David and Amon, 2020).

1.4.4 Summary

Aneuploidy is a state, in which a cell's set of chromosomes deviates from the euploid set, and can be categorised to numerical or structural aneuploidy, depending the chromosomal alteration. Numerical and structural aneuploidies can arise through errors in mitosis by incorrect microtubule-kinetochore attachments and centrosome amplification or through unrepaired DNA damage, CIN and karyotype divergence. Additionally, aneuploidy can provide cancer cells with either advantageous or disadvantageous characteristics, forming the aneuploidy paradox. Aneuploidy can reduce cell viability through loss of oncogenes or gain of tumour suppressor genes and increase of cellular stress. However, it can induce cancer cell survival and proliferation due to gains of oncogenes and loss of tumour suppressor genes or dosage compensation and the effects of genomic instability. Lastly, aneuploidy can be a cause or a consequence of tumorigenesis and can be used as an indicator for patient prognosis and prediction of the disease evolution. Taken together, understanding the mechanisms of aneuploidy tolerance may reveal vulnerabilities that can be exploited therapeutically. This research study is aiming to investigate aneuploidy, dependently or independently of specific stable chromosomal alterations, in cancer.

1.5 Cell fusion and mechanisms of DNA content reduction

Cell fusion has been described as the membrane merging of two cells into one, allowing the mixing of their cytoplasm and their luminal contents. As a result, cell fusion forms multinucleated cells and is a fundamental process for sex reproduction, development and may be involved in the origin of the first eukaryotic cell. However, it has been shown that cell fusion plays a role in diseases, such as in viral infections and cancer initiation, progression and therapy resistance (Bastida-Ruiz et al., 2016, Hernández and Podbilewicz, 2017).

1.5.1 Cell fusion in eukaryotic cell origin and organism development

The first theories for the origin of the eukaryotic cell initiated in the beginning of the 20th century but none was established until 1967, when Lynn Margulis published the 'On the origin of mitosing cells' presenting the theory of endosymbiosis. According to this theory, the membrane of an aerobic prokaryote (Archaea) was fused to the membrane of an anaerobic prokaryote (Bacteria), with the latter being incorporated to the former. A symbiotic relationship was established and through evolution, the aerobic bacterium gave rise to the mitochondrion (López-García et al., 2017). While this theory is widely accepted, it does not explain efficiently the origin of the nucleus and questions remain about the stage of eukaryogenesis, from which the mitochondria originated. Additionally, it is suggested that a third prokaryote (from the Archaea family) was involved in the endosymbiotic process, which gave rise to the eukaryotic nucleocytoplasm. Moreover, multiple serial endocytosis may have been occurred, with mitochondria being acquired in the chimeric host (López-García et al., 2017, Pittis and Gabaldón, 2016).

Furthermore, cell fusion is essential for the processes of reproduction and development in mammals. Fertilisation includes migration of the sperm along the female tract and fusion of the two gamete cells. Inability of fusion between the sperm and the oocyte results to infertility (Oren-Suissa and Podbilewicz, 2007). Post-fertilisation and during embryonic development, trophoblasts undergo fusion to generate the syncytium,

also known as the syncytiotrophoblast, that is essential for maternal-foetal interactions such as nutrient and hormone transfer, gas exchange and waste elimination. Disruption of trophoblast fusion results in placental malformation and pregnancy complications like preeclampsia and intrauterine growth restriction (Ogle et al., 2005, Ma et al., 2020). Skeletal muscle formation is another process in mammal, in which cell fusion plays a critical role. Mononucleated myoblast cells are aligned and undergo fusion and merging of their cytoplasmic components. Hundreds of fusions between these cells form a myofiber and bundles of contractile myofibers form the skeletal muscle. However, myoblast fusion is not essential only during embryogenesis, but also in regeneration of injured myofibers in adults (Zhang et al., 2017, Hindi et al., 2017). Additionally, bone development and tooth eruption are acquired through osteoclasts. Osteoclasts are huge multinucleated cells, which are formed after fusion between cells of the monocyte/macrophage lineage. Disruption of osteoclasts is linked with osteoporosis and periodontitis (Yahara et al., 2020, AlQranei et al., 2020).

1.5.2 Cell fusion in viral infections

Apart from role of cell fusion in development, cell fusion is also crucial in viral infections, as viruses can infect and enter a host cell by endocytosis or fusion. Examples of fusogenic viruses are the HIV, the SARS-CoV-2 and the HPV viruses (Xia et al., 2020, Oren-Suissa and Podbilewicz, 2007, Gao and Zheng, 2010). Moreover, cell fusion may explain the emergence of new viruses. In particular, it is suggested that HIV derived, when SIV entered the human cells after cell fusion of an infected African green monkey cell with a human cell. The nuclei between the two cells could have been remained distinct or got merged, resulting to heterokaryons or synkaryons, respectively. In the case of heterokaryon formation, the human cell provided to the virus a ‘human’ viral coat, enhancing the infection of more human cells. On the other hand, after synkaryon formation, chromosome translocations or mutations could have promoted generation of a new virus (Ogle et al., 2005). Inhibition of viral cell fusions is a research area that is attracting a lot of interest, especially due to the SARS-CoV-2 pandemic, as it may lead

to antiviral therapies (Xia et al., 2020).

1.5.3 Cell fusion in cancer

Cell fusion can be an essential event in cancer initiation, progression, metastasis and resistance to therapies, directly as well as indirectly, by cancer stem cell (CSC) generation, aneuploidisation and DNA content reduction mechanisms, which may follow cell fusion (Bastida-Ruiz et al., 2016, Zhou et al., 2015, Puig et al., 2008, Díaz-Carballo et al., 2018).

1.5.3.1 Generation of cancer stem cells by cell fusion

A cancer theory suggests that cancer stem cells (CSCs), or tumour initiating cells, are responsible for tumour initiation, progression and therapy resistance. CSCs are very similar to embryonic stem cells regarding their ability to proliferate indefinitely, to self-renew, to differentiate into different cell types, such as vascular endothelial cells, and to activate similar signalling pathways (Yang et al., 2020, Cao et al., 2020). There are two possible mechanisms by which CSCs can be generated: a) by stem cells that accumulate genetic abnormalities or b) by cell fusion of a stem cell with a differentiated cell or a cancer cell. In more detail, it has been shown that CSCs can be generated after fusion of hematopoietic stem cells with differentiated cells or after fusion of bone marrow-derived stem cells with epithelial cells and can initiate tumour formation through their high proliferation rate and their self-renewal ability (Bastida-Ruiz et al., 2016, Ratajczak et al., 2018, Lu and Kang, 2009). In breast cancer, fusion of adipose-derived stem cells with breast cancer cells generated CSCs with one nucleus (synkaryons). The fused cells were more aggressive and generated bigger tumours *in vivo* compared to the cancer cells alone (Chan et al., 2020). Additionally, fusion of human embryonic stem cells with human liver cancer cells generated CSCs which were highly tumorigenic and more resistant to doxorubicin compared to the unfused cancer cells (Wang et al., 2016). Further studies have shown that during chemotherapy or irradiation treatment, CSCs become quiescent and do not enter the cell cycle but retain the ability, and after the end

of the treatment, they re-enter the cell cycle (Chen et al., 2016).

Furthermore, in breast cancer, fusion of mesenchymal stem cells with breast cancer cells, *in vitro*, is increased under hypoxic conditions and the hybrid cells show three times more migratory capacity than the unfused breast cancer cells (Noubissi et al., 2015). Similarly, in another study, fused mesenchymal stem cells with breast cancer cells also showed increased invasion and migratory capability than the cancer cells alone (McArdle et al., 2016). In addition, a recent study also showed that fusion of breast cancer cells with mesenchymal stem cells demonstrates an additional pathway of epithelial to mesenchymal transition (EMT) by expression of mesenchymal genes from the one donor cell (Hass et al., 2019). The invasion and migratory capability of CSCs together with the increased proliferation rate and the self-renewal ability can facilitate tumour metastasis (Shiozawa et al., 2013, Bastida-Ruiz et al., 2016).

1.5.3.2 Cell fusion, a cause of multinucleation and a mechanism that drives genomic instability, aneuploidisation and DNA content reduction

Over a century ago, Aichel proposed the cell fusion theory for tumour progression, in which combination of extra chromosomes by cell fusion of two different cells can cause tumour formation (Aichel, 1911, Delespaul et al., 2019). Since then, more studies have been conducted suggesting that cell fusion can be a mechanism of tumour initiation through induction of genomic instability and aneuploidisation. In particular, it has been shown that fusion between untransformed epithelial cells, between fibroblasts or between cancer cells can generate hybrid cells with distinct nuclei (heterokaryons). However, cell culture of the fused cells demonstrated that at the beginning of mitosis, the nuclear membranes are disassembled, all the chromosomes are mixed and undergo mitosis. This process generates mononucleated cells with DNA from all the fused cells (synkaryons) and is known as heterokaryon to synkaryon transition (HST) (Zhou et al., 2015, Delespaul et al., 2019, Weiler and Dittmar, 2019, Dörnen et al., 2020). HST is associated with chromosome missegregation, small translocations and generation of genomic unstable and aneuploid cells that are able to

form tumours *in vivo*, in comparison to the unfused cells. Furthermore, the hybrid cells with abnormal chromosome number demonstrated an increased rate of DNA damage and double strand breaks, which do not lead to apoptosis but can be sustained in the cells and promote further genomic instability and aneuploidy (Zhou et al., 2015, Searles et al., 2018, Delespaul et al, 2019). Additionally, cell fusion can lead to tetraploidization. As previously discussed, tetraploid cells can generate chromosomally unstable or aneuploid daughter cells through chromosome missegregation, lagging chromosomes or multipolar divisions. Thus, cell fusion is a driver from a “diploid-to-tetraploid-to-aneuploid” state (Figure 1.7 A) (Storchova and Pellman, 2004, Ganem et al., 2007, Delespaul et al., 2019).

Fusion of two or more cells can generate a cell with distinct nuclei that are known as heterokaryons. As described before, the nuclei can undergo mitosis simultaneously and form synkaryons, cells with one nucleus that allows re-sorting and recombination of the DNA. However, the nuclei can be kept distinct, sustaining the heterokaryon phenotype, and can function independently of each other (Figure 1.7 A) (Ogle et al., 2005). Fusion of breast cancer cells with endothelial cells can generate both heterokaryons and synkaryons and both types of cells remained viable and able to undergo mitosis (Mortensen et al., 2004). The fate of synkaryons and the generation of genomic unstable or aneuploid cells is better understood. However, less is known about the fate of heterokaryons that retain distinct nuclei.

In recent years, much attention has been focused on polyploid giant cancer cells (PGCCs), large mononucleated or multinucleated cancer cells, mostly generated under hypoxic conditions or after chemotherapy or irradiation treatment. PGCCs are a model for both heterokaryons and synkaryons and it is proposed that they contain stem cell-like-abilities, are highly tumorigenic, chemo-/radio-resistant and contribute to tumour maintenance and recurrence (Bastida-Ruiz et al., 2016, Fei et al., 2019, Qu et al., 2013).

However, the mechanism by which they are generated is still disputed, though it may be via cell fusion. It has been shown that treatment of colon, breast or ovarian cancer cells with cobalt chloride (CoCl2), a hypoxia inducer, generates PGCCs, 10-20%

of which are due to cell fusion (Lopez-Sánchez et al., 2014, Zhang et al., 2014, Fei et al., 2019, Yart et al., 2020). In addition, chemotherapy (paclitaxel, doxorubicin, cisplatin or epirubicin) or irradiation treatment in breast cancer or melanoma cells can promote PGCCs formation through endoreplication, cell fusion, nuclear budding or nuclear fission (Chen et al., 2019, Niu et al., 2016, Searles et al., 2018, Puig et al., 2008, Yan et al., 2015, Xuan et al, 2018, Sandaram et al., 2004).

The fate of the nuclei in a PGCC derived by either cell fusion or endoreplication and nuclear budding is not well understood, and various fates have been observed (Figute 1.7.B). Some of the nuclei in the fused giant cells may undergo abortive mitosis generating micronuclei in the cytoplasm. Others, can undergo atypical, asymmetric, bipolar or multipolar mitosis, producing daughter cells that either die or undergo subsequent fusion, while a subpopulation of cells can survive as multinucleated cells with no changes (Puig et al., 2008). Moreover, in 2004 and 2006, Sundaram and Rajaraman, respectively, showed that PGCCs can generate mononuclear aneuploid cells by karyokinesis via nuclear budding, while the mother cell dies. This process was named neosis (Sundaram et al., 2004, Rajaraman et al., 2006). It was also suggested that after chemotherapeutic treatments, the PGCCs that undergo neosis, present a senescent phenotype (Rajaraman et al., 2006). However, a more recent study of ovarian tumours post-chemotherapy, showed that the PGCCs observed are neither senescent nor apoptotic and they are able to undergo cytokinesis and divide as a whole system. In the same study, nuclei of the PGCCs could be ejected from the initial giant cells, giving rise to cells that were able to enter other neighbour cells (Díaz-Carballo et al., 2018).

Another mechanism for PGCCs formation is entosis. Entosis characterises the engulfment of one cell from another, generating the ‘cell-in-cell’ or ‘bird-eye’ structure (Figure 1.7 C). The main difference with cell fusion is that in entosis the cell membranes remain separated and the cytoplasmic contents are not merged. The engulfed cell can be killed and digested in order for the host cell to gain energy and nutrients. Alternatively, the internalised cell can be released and undergo mitosis or remain alive and undergo cell division inside the host cell, with the daughter cells remaining in the host cell and

generating a complex multinucleated cell, or subsequently getting released. Moreover, the host cell often attempts to undergo mitosis, while the internalised cell remains in its cytoplasm, which may lead to multinucleation and PGCCs formation through obstruction of cytokinesis (Figure 1.7 C). In most cases of entosis, however, tetraploid cells arise that may form multipolar spindles in the next mitosis leading to chromosomal instability or aneuploidisation (Balvan et al., 2015, Durgan and Florey, 2018, Overholtzer et al., 2007, Janssen and Medema, 2012). Experiments in human bronchial epithelial cells revealed that after Paclitaxel treatment, the frequency of entosis appeared to be increased and may lead to reduced treatment sensitivity (Durgan et al., 2017).

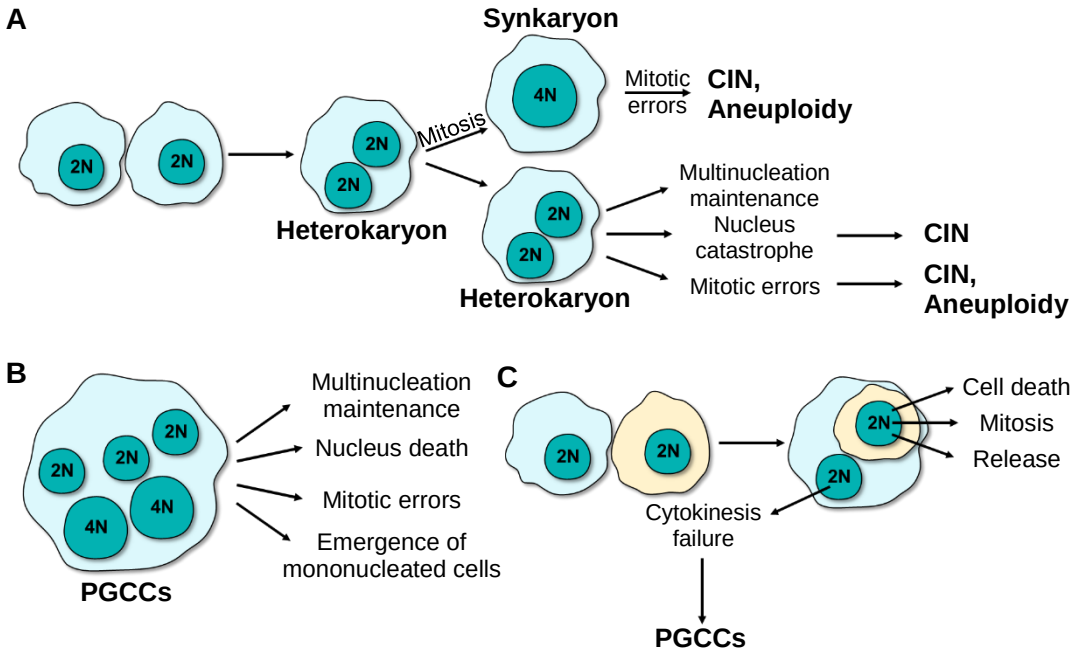

Figure 1.7: Cell fusion in cancer. (A) Generation of heterokaryons and synkaryons by cancer cell fusion and the fate of the fused cells if they do not undergo apoptosis. (**B)** PGCC formation by cell fusion and their possible fate if they escape apoptosis. **(C)** Entosis and the fate of the host and entotic cells. The haploid number of chromosomes is represented by N (23 in human cells).

1.5.3.3 Cell fusion increases genetic heterogeneity and resistance to therapy

Fusion between cancer cells or between cancer cells and somatic cells within the tumour microenvironment can generate genetic diversity and enhance tumour formation, progression or resistance to therapy and tumour relapse. As mentioned previously, cell fusion can generate genomically unstable or aneuploid hybrids through HST that are

able to form tumours, enabled by the increased genetic heterogeneity that is created (Zhou et al., 2015). Indeed, injection of mice with melanoma cells, containing a reporter gene, generated tumours, in which cancer cells were fused with cells from the microenvironment, mostly macrophages. Karyotype analysis in an *in vivo* derived clone generated by a hybrid cell, revealed high heterogeneity between the cells, in the number of chromosomes, ranging between 21 and 105 chromosomes (Searles, et al., 2018). In agreement with these findings, co-cultures of prostate cancer cells and rat neural stem cells generated hybrid cells and each co-culture generated clones with high phenotypic heterogeneity in morphology, proliferation rate and migration ability (Yin et al., 2020). Thus, cell fusion contributes to tumour formation and progression by increasing the degree of heterogeneity though genomic instability and aneuploidy (Searles, et al., 2018, Zhou et al., 2015).

Cell fusion between cancer cells and the surrounding stem cells, increases the cellular heterogeneity generating cells with stem cell-like properties, such as self-renewal that can promote tumour initiation or metastasis in an EMT-like manner (Chan et al., 2020, Noubissi et al., 2015, Hass et al., 2019). An additional study has shown, *in vivo* and *in vitro*, that fusion of murine colon cancer or melanoma cells with macrophages generates hybrids with different chromosomal number that retain both epithelial and mesenchymal characteristics. Isolation of hybrid cells from primary tumours revealed high intratumour heterogeneity and differential growth properties. Notably, the hybrid cells were highly tumorigenic, displaying shorter doubling time, with increased metastatic potential, and they were also present in the blood as circulating tumour cells, demonstrating the acquisition of properties required for trafficking to metastatic sites (Gast et al., 2018). Thus, cell fusion can be a direct mechanism of increasing tumour heterogeneity through generation of hybrids between cancer cells and cells of the microenvironment, facilitating the acquisition of novel and diverse phenotypes, which may aid tumour initiation and progression (Gast et al., 2018, Mirzayans and Murray, 2020).

As described previously, heterogeneity derived by genomic instability can be

essential in tumour initiation and progression, while positive selection, the evolutionary force, is acting on aneuploid and genetically diverse clones (Turajilic et al., 2019). Moreover, it has been mentioned the impact of heterogeneity in poor patient prognosis and therapy resistance, through the cellular genetic diversity that is generated. Cell fusion can be an alternative mechanism that generates heterogeneity in the tumour though induction of genomic instability and aneuploidy or generation of hybrids from cells of different origin (Mirzayans and Murray, 2020). However, there is a hypothesis suggesting that cell fusion may be a direct mechanism of chemotherapy or irradiation resistance. It has been shown that chemotherapy or irradiation treatment increases the events of fusions and the generation of PGCCs. In more detail, in a breast cancer xenograft study, the percentage of fused cells in the tumour was increased from 6% to 12%, after treatment with epirubicin (Yan et al., 2016). Moreover, examination of ovarian tumours from five patients pre- and post-cisplatin treatment demonstrated striking increase in the number and size of PGCCs post-chemotherapy (Zhang et al., 2014). Similarly, studies in prostate, breast, colon and brain cancer have shown resistance of PGCCs to chemotherapy and radiation treatment (Amend et al., 2019, Mittal et al., 2017, Sirois et al., 2019, Fei et al., 2019, Zhang et al., 2016, Kaur et al., 2015). Strikingly, post-treatment, small mononucleated cells can appear around the resistant PGCCs which are also resistant to the initial treatment (Sirois et al., 2019, Puig et al., 2008, Fei et al., 2019). Thus, chemotherapeutic drugs or irradiation appears to promote the formation of PGCCs, which, can then generate mononucleated cells resistant to the initial treatment. However, the detailed mechanisms by which the resistant mononucleated cells are generated is still unclear (Fei et al., 2019).

1.5.4 The model and possible mechanisms of cell fusion in human cells

A model of cell fusion has been proposed that includes three steps, which are named as hallmarks of cell-cell fusion. Initially, the membranes of the two future fused cells are positioned in close proximity (approximately 100 Å or 10 nm). Then, the membrane bending is initiating and the outer membranes come into contact. At the site

of contact, reduction of the hydration repulsion forms a fusion stalk, the first step of cell fusion, in which the outer lipid leaflets are mixed. The stalk is progressed and leads to the second hallmark, a hemifusion diagram, where the inner membranes are still separate. Finally, the inner leaflets are fused and the fusion pore is formed and expanded, mixing the cytoplasm of the two cells. The formation and expansion of the fusion pore is the last step of cell-cell fusion and is essential for the completion of the fusion event (Figure 1.8) (Oren-Suissa and Podbilewicz, 2010, Gerbaud and Pidoux, 2015, Bastida-Ruiz et al., 2016, Brukman et al., 2019, Hernández and Podbilewicz, 2017).

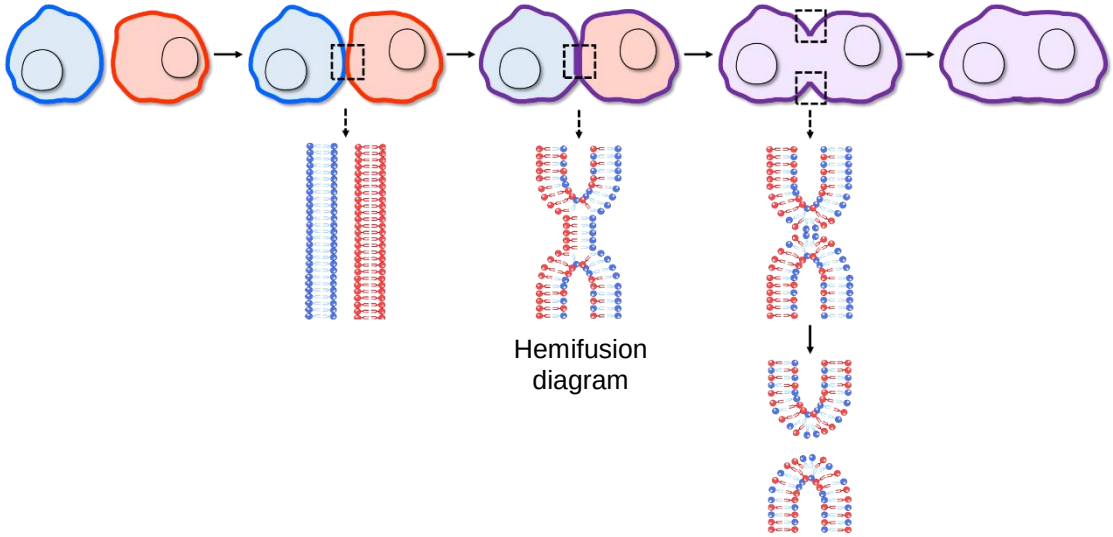

Figure 1.8: The model of cell fusion. The two future fused cells are positioned closely and the outer cell membranes come in contact, start to bend and the stalk is generated. Stalk progression forms the hemifusion diagram, in which the inner phospholipid membranes are still separate, and finally, the fusion pore is formed, the cytoplasmic materials are mixed and the two cells are fused.

However, the exact mechanisms or necessary proteins for cell fusion, are still unclear. In some fusion events, proteins essential for membrane fusion (fusion proteins or fusogens) need to be expressed in both fusion partners, while in other cases, their expression is required only in in one of the two cell membranes. However, it is difficult to distinguish fusogens involved in the actual fusion stage from proteins that are expressed before or after the fusion event. Thus, a panel of characteristics has been described that the fusion proteins need to accommodate in order to be categorised as bona fide fusogens. These characteristics include that a) the protein is necessary for

fusion, b) the protein needs to be expressed in the cell membrane at the moment of the fusion and c) the protein is sufficient to fuse membranes that normally do not (Brukman et al., 2019, Hernández and Podbilewicz, 2017).

The first *bona fid*e fusogens have been identified in recent years, including syncytin in the mammalian placenta. Syncytins are envelop proteins, derived from retroviruses and are essential for the fusion of trophoblasts and generation of the syncytiotrophoblast during pregnancy (Brukman et al., 2019). However, syncytins are likely also important in mediating the fusion between cancer cells and endothelial cells. In particular, expression of syncytin-1 is increased in Oral Squamous Cell Carcinoma, breast or prostate cancer as well as its receptor ASCT2 (Alanine, Serine, Cysteine Transporter 2) (Bjerregaar et al., 2006, Yan et al., 2017, Uygur et al., 2019). Moreover, it has been shown that increase in TNF-α (Tumour Necrosis Factor- α) promotes the up-regulation of syncytin-1 and ASCT2 through activation of Wnt/β-catenin signaling pathway (Yan et al., 2017). Lastly, elevated expression of syncytin-1 has also been found in PGCCs, suggesting that syncytin may be essential for cell fusion in cancer (Fei et al., 2019).

SNARE (soluble N-ethylmaleimide–sensitive factor attachment protein receptor) complex is another fusogen that has been identified in humans. This complex can promote cell fusion by forming bundles of α-helixes in the membrane and inducing ‘zippering’, the approach of the membranes followed by hemifusion, completing the merging of the two cells (Bastida-Ruiz et al., 2016, Oren-Suissa and Podbilewicz, 2007, Hernandez et al., 2012). However, SNAREs are normally face in the cytoplasm and they need to flip in order to promote cell-cell fusion. Flipped SNAREs are present in the membrane of fibroblasts but whether they are responsible for cancer cell fusion is still unclear (Hu et al., 2003, Giraudo et al., 2005, Chen and Olson, 2005).

Further fusogen-independent fusion mechanisms have been proposed. For example, fusion of breast cancer cells with mesenchymal stem cells is induced in the presence of apoptotic cells upon normal or hypoxic conditions (Noubissi et al., 2015). Similarly, in myoblasts it has been shown that apoptotic cells produce phospatidylserine

on their surface which is recognized by receptors on the surface of the healthy cells. However, mechanistically, the apoptotic cells are not fused with the healthy myoblasts but they promote a contact signalling to induce fusion of the neighbouring healthy cells. Phospatidylserine receptor BAI1 was identified upstream of ELMO and forms a trimeric complex with ELMO and Dock 180, which function together as a guanine nucleotide exchange factor for the small GTPase Rac. Activation of Rac pathway modulates the cytoskeleton and generates new actin filaments. This chemical signal recruits MyoII to the area of the fusion as it can sense mechanical strains in the actin network and promotes cortical tension which is necessary for cell fusion (Hochreiter-Hufford et al., 2013, Noubissi and Ogle, 2016). Similarly, inactivation of caspase-2/-3 or -9 reduces the frequency of cell fusion in myoblasts further suggesting the theory that apoptotic cells induce cell fusion events (Dehkordi et al., 2020). Lastly, it has been shown that the actin cytoskeleton is necessary for fusion between embryonic stem cells and inhibition of actin polymerisation by cytochalasin D can significantly reduce cell fusion events (Sottile et al., 2016). Additionally, inhibition of ROCK-actin/myosin pathway with a ROCK inhibitor (Y-27632) reduces the events of cell fusion but also of entosis, *in vitro*, in mouse embryonic stem cells or human epithelial cells, and *in vivo*, in mouse uterine luminal epithelial cells during early stages of pregnancy (Durgan et al., 2017, Li et al., 2015).

1.5.5 Summary

Cell fusion defines the membrane merging of two cells into one, allowing the mixing of their cytoplasmic contents. It is a fundamental process for sex reproduction, development, viral infections and cancer initiation, progression and therapy resistance. A model of hemifusion is proposed for cells fusion, but the exact mechanisms or *bona fide* fusogen proteins are still unclear. However, fusogens as syncytin-1 and mechanisms dependent to apoptosis and actin cytoskeleton have been proposed. After cell fusion, the two separate nuclei can be fused in turn and form synkaryons, which in most cases are genomically unstable or aneuploid, fuelling the genetic heterogeneity. Alternatively, the nuclei in the fused cells can remain distinct and function independently.

Moreover, cell fusion can generate PGCCs, which are highly resistant and can promote tumour reoccurrence after treatment by ejection of mononucleated cells that are also resistant to the initial treatment. In this study we will be focused on the mechanism of cancer cell fusion induction after chemotherapy treatment and the fate of the fused cells.

1.6 Project aims

Chromosomal instability (CIN), aneuploidy and cell fusion are distinct phenotypes involving complex mechanisms which can increase tumour heterogeneity, either by acting independently of each other or intermingling. The generated intratumour heterogeneity guarantees the genetic variation in which positive selection acts for phenotypically advantageous cells to overcome selection barriers and drive tumour initiation, progression or resistance to cancer treatments (Figure 1.9). CIN and aneuploidy can alter cell's physiology by gaining of oncogenes, loss of tumour suppressor genes or increased metabolic and proteotoxic stress. However, they can also generate gene dependencies that did not exist previously and can be used therapeutically.

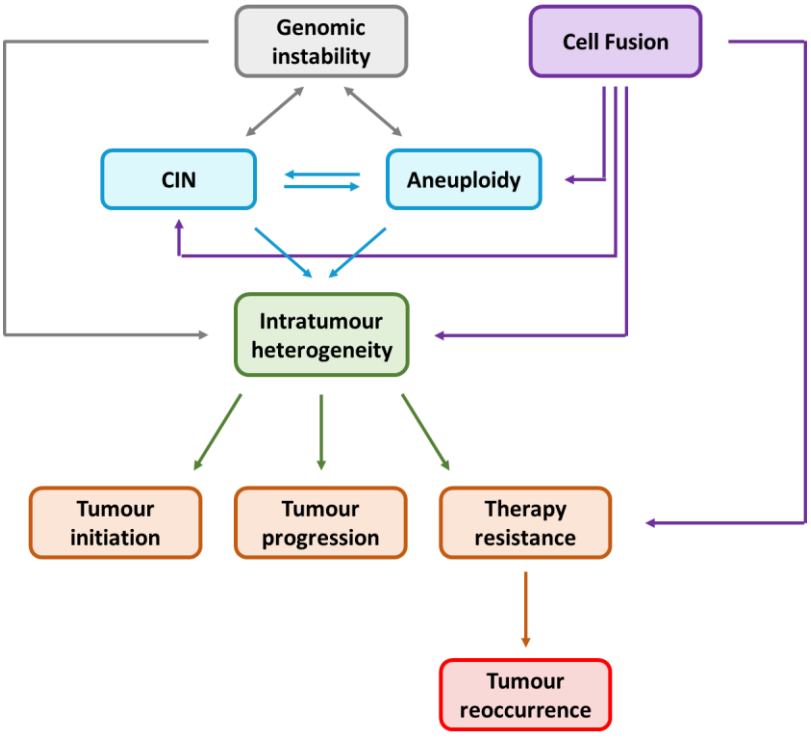

Figure 1.9: Schematic illustration of GIN, CIN, aneuploidy and cell fusion and their impact in cancer. Two possible mechanisms of CIN and aneuploidy generation are genomic instability and cell fusion. However, both CIN and aneuploidy may lead to each other. CIN and cell fusion are drivers of genetic heterogeneity, while positive selection will act on aneuploid clones, promoting the survival of phenotypically advantageous clones, within a given tumour-environmental context. In line with Darwinian evolution, the transformed cells with advantageous characteristics will outcompete the rest and grow into the main cell population promoting tumour initiation, progression or therapy resistance, which will lead to tumour reoccurrence. Cell fusion can directly promote therapy resistance and tumour reoccurrence through multinucleation or generation of mononucleated cells.

It has been observed that chemotherapy treatment, although induces massive cell death, a small fraction of cancer cells escape death leading to tumour relapse. One of the chemotherapy-induced effects is cell fusion, which can directly result to therapy resistance and tumour relapse via the formation of distinct phenotypes including multinucleated polyploid giant cells and mononucleated cells through distinct mechanisms (Figure 1.9).

Thus, the goals of this project are two-fold: a) to identify novel targets in aneuploidy and CIN, dependent or independent of specific chromosome or gene dependencies and b) to investigate the mechanism by which cell fusion drives tumour relapse after chemotherapy treatment to identify new approaches of targeting resistance.

The aims of this study are:

I. To identify potential targets in CIN
    1. Generation of CIN models through errors in mitosis and DNA damage response
    2. Confirm CIN induction
    3. Identify potential hits by screening the CIN models, using the CRISPR/Cas9 system and a custom sgRNA library
    4. Confirm and validate the candidate hits in different CIN models

II. To identify potential targets in aneuploidy
    1. Generation of aneuploid clones through errors in mitosis
    2. Characterisation of aneuploid clones
    3. Identify potential hits by screening the aneuploid clones, using the CRISPR/Cas9 system and a custom sgRNA library
    4. Confirm and validate the candidate hits in the aneuploid models

III. To investigate and target the mechanisms by which cell fusion contributes to cancer cell recovery after chemotherapy treatment

1. Investigate the mechanism of cell fusion
2. Identify the events by which cell fusion drives cell recovery
3. Identify new targets of cell recovery of chemotherapy treated breast cancer cells using a small molecule compound library screening
4. Confirm the candidate hits in cell models

Chapter 2 - Materials & Methods

2.1 Materials

Table 2.1: List of general materials, reagents, kits, enzymes and chemicals.

Materials, reagents, kits and chemicals	Supplier / Code	Storage
Acetic Acid	ThermoFisher / 10304980	RT
Blasticidine S hydrochloride	Sigma Aldrich by Merck / 15205	-20°C
bromophenol-blue powder	Sigma Aldrich by Merck / B0126	RT
CellCarrier-96 Ultra Microplates, black, sterile, 96-well with lid	Perkin Elmer / 6055300	RT
Cell culture 24 well plate	Nunc by ThermoFisher / 142475	RT
Cell culture microplate, 384 well, F-bottom, clear, sterile with lid	Greiner / 781182	RT
Cell culture microplate, 384 well, F-bottom, white, sterile, no lids	Greiner / 781073	RT
CellTiter-Glo Luminescent Cell Viability Assay	Promega / G7570	-20°C
Cotton Buds	ICR / LK0379	RT
Countess automated cell-counter slides	Invitrogen, by ThermoFisher / C10283	RT
CryoTube Vials	ThermoFisher / 363401	RT
Crystal violet	Sigma Aldrich by Merck / C0775-25G	RT
DharmaFECT 2 Transfection Reagent 0.75 ml	Horizon / T-2002-02	4°C
Dithiothreitol DTT	Sigma Aldrich by Merck / D9779	4°C
DNeasy Blood & Tissue Kit (250)	Qiagen / 69506	RT
Doxycycline	Sigma Aldrich by Merck / D9891	-20°C

Dulbecco's Modified Eagle's Medium (DMEM)	Gibco by ThermoFisher / 41965-039	4°C
Dimethyl sulfoxide (DMSO)	Sigma Aldrich by Merck / D8779	RT
Echo Qualified 384-Well Polypropylene Microplate 2.0 (384PP 2.0)	Labcyte / PP-0200	RT
Ethanol	VWR / 101077Y	RT
Falcon Cell Culture 5- layer Multi Flasks	Corning by ThermoFisher / 353144	RT
FACS tubes (5ml)	Fisher Scientific / 10100151	RT
Foetal bovine serum (FBS)	Gibco by ThermoFisher / 10106-169	-20°C
Fetal bovine serum (FBS), Tetracycline Free	PAN-Biotech / P30-3602	-20°C
Glycerol 99+%	Fisher Scientific / 10579570	RT
High-Capacity cDNA Reverse Transcription Kit	Applied Biosystems by Fisher scientific / 4368814	-20°C
Hoechst 33342	ThermoFisher / H3570	4°C
µ-Ibidi 96 well plate	ThermoFisher/ 50305829	RT
Isopropanol	Fisher Scientific, BP2618-212	RT
Lipofectamine 2000 Transfection Reagent	Invitrogen by ThermoFisher / 11668027	4°C
Lid, ultra-low profile, clear, 127/85mm, sterile	Greiner / 691161	RT
L-glutamine 240 mM	LSS / 06	-20°C
MES 20X	Novex/ NP0002	RT
Methanol ≥99.8%	VWR / 20847.307	RT
Milk powder	Marvel	RT
Novex Sharp Pre-stained Protein Standard	ThermoFisher / LC5800	-20°C
Nuclease-free water	Ambion / AM9937	RT
NuPAGE 4 to 12%, Bis-Tris, 1.0 mm, 15-well	ThermoFisher / NP0323PK2	4°C

OptiMEM reduced serum medium	Gibco by ThermoFisher / 31985	4°C
Parafilm	Sigma Aldrich by Merck / P7793	RT
Paraformaldehyde	Sigma Aldrich by Merck / 15812-7	RT
Penicillin/Streptomycin	LSS / 37	4°C
Phosphate-buffered saline (PBS)	LSS / 08	4°C
Polyvinylidene fluoride (PVDF) membrane	Merck / 05317	RT
Ponceau S	Sigma Aldrich by Merck / P7170	RT
Potassium chloride (KCl) 1M	LSS / 65	4°C
Propidium iodide solution 1.0 mg/ml in water	Sigma Aldrich by Merck / P4864	4°C
Puromycin	Sigma Aldrich by Merck / 540222	-20°C
Qubit Assay Tubes	Invitrogen by ThermoFisher / Q32856	RT
Qubit dsDNA BR Assay Kit	Invitrogen by ThermoFisher / Q32853	4°C
Qubit protein	Invitrogen by ThermoFisher / Q33211	4°C
Ribonuclease A from bovine pancreas	Sigma-Aldrich by Merck / R4642	-20°C
RNeasy Mini Kit	Qiagen / 74104	RT
Roswell Park Memorial Institute (RPMI) 1640 medium	Gibco by ThermoFisher / 21875091	4°C
Sodium dodecyl sulfate (SDS)	Sigma-Aldrich by Merck / 436143	RT
Senescence Cells Staining Kit	Sigma-Aldrich by Merck / CS0030-1KT	Staining solution at 4°C, rest at -20°C
SuperFrost Plus Adhesion slides	ThermoFisher / 10149870	RT
SYBR Green PCR Master Mix 1.5ml	Applied Biosystems by ThermoFisher / 4309155	-20°C
Tris Buffered Saline (TBS) 10X	LSS / 86	4°C
Tissue culture plastics	BD Biosciences, Falcon (unless otherwise stated)	RT

Transfer Buffer	LSS / 81	4°C
Transwell 24-well plate with 8.0µm porepolycarbonate membrane cell culture inserts	Corning by Merck / CLS3422	RT
Triton X-100	Sigma Aldrich by Merck / T9284	RT
Trypan Blue 0.4%	Invitrogen, by ThermoFisher / T10282	RT
Trypsin / Versene	LSS / 16	-20°C
Tween-20	Sigma Aldrich by Merck / P1754	RT
Ultra-filtered (UF) water	LSS / 21	4°C
VECTASHIELD Antifade Mounting Medium with DAPI	ThermoFisher / H-200	4°C
Whatman paper	ThermoFisher / 88615	RT
4’,6-diamidino-2-phenylindole (DAPI)	Invitrogen / D1306	4°C
β-mercaptoethanol	Sigma Aldrich by Merck / M7154	RT

Table 2.2: List of general solutions and recipes.

Solution	Recipe
Cell culture media	500ml DMEM/RPMI, 10% FBS (50ml), 1% L-Glutamine (5ml) and 0.5% Pen/Strep (2.5ml)
CellTiter-Glo reagent solution	CellTiter-Glo buffer and CellTiter-Glo substrate were mixed and stored at -20°C. Before use, 60% of CellTiter-Glo mix was added in 40% cell culture media
Crystal violet solution 0.5%	0.5% crystal violet plus 25%l Methanol in H2O
Freezing solution for human cancer cell lines	10% DMSO in FBS
Milk solution 2.5%	2.5% powder milk in TBS-T
MES buffer 5%	5% MES 20X plus 95% dH2O
Paraformaldehyde 4%	4% weight/volume paraformaldehyde powder in PBS dissolved at 50°C on a heated stirrer.
PBS	10g/l NaCl, 0,25g/l KCl, 1.437g/l Na2HPO4, 0.25g/l KH2PO4 in UF H2O. pH adjusted to 7.2 with HCl
Penicillin/Streptomycin (Pen/Strep) 200 X solution	12 g/l Benzylpenicillin and 20 g/l Streptomycin sulfate in dH2O
TBS-T	500ml TBS plus 0.125ml Tween-20
Transfer Buffer	200ml/l methanol, 3.03g/l Tris, 14.40g/l Glycine in UF H2O pH adjusted to 8.2
Tris Buffered Saline (TBS) 10X	30.27g/l Tris base, 84.16g/l NaCl in UF H2O, pH adjusted to 7.5 with HCl. Used at 1X concentration
Trypsin 0.05% in Versene 0.02%	8g/l NaCl, 0.2g/l KCl, 1.15 g/l Na2HPO4, 1g/l DGlucose, 0.2g/l KH2PO4, 0.2g/l EDTA, 3g/l Tris, 1.5ml/l Phenol red 1%, 0.5g/l Trypsin Difco 1:250, 0.1g/l Streptomycin sulphate, 0.06g/l
Ultra-filtered (UF) water	17 Mega Ohms filtered water
5x Sample Buffer	2% SDS, 10% glycerol, 80 mM Tris pH 6.8,100 mM DTT, 2% β -mercaptoethanol plus traces of bromophenol-blue powder

Table 2.3: List of drugs and inhibitors.

Drugs / inhibitors	Supplier / Code	Storage
CCT289346 (or BOS-172722)	ICR produced (or Boston Pharmaceuticals)	-20°C
Colcemid	Gibco by ThermoFisher / 15212-012	4°C
GSK923295	Selleckchem / S7090	-20°C
CCT241106	ICR produced	-20°C
KU60019	Tocris / 4176	-20°C
Monastrol	Tocris / 1305	-20°C
Nocodazol	Sigma Aldrich by Merck / M1404	-20°C
Paclitaxel	Sigma Aldrich by Merck / T7191	-20°C
Crenolanib	Selleckchem / S2730	-20°C
BCI-121	Sigma Aldrich by Merck / SML1817-5MG	-20°C
GSK626616	Tocris / 6638	-20°C
RK-33	Selleckchem / S8246	-20°C
GSK2879552	Selleckchem / S7796	-20°C
BAY6035	Tocris / 6561	-20°C
(R)-PFI 2 Hydrochloride	Tocris / 4892	-20°C
(S)-PFI 2 Hydrochloride	Tocris / 5400	-20°C

Table 2.4: List of primary antibodies.

Antibodies	Species of Origin	Application	Working dilution	Supplier / Code
BRG1	Mouse	WB	1:500	Santa Cruz / 17796
BAF180	Rabbit	WB	1:100	Novus / NBP2-55731
Cas9	Rabbit	WB	1:1000	Abcam / ab191468
Cas9	Mouse	IF	1:1000	Abcam / ab18938
PRIM1	Rat	WB	1:750	Cell Signaling / 4725
TEX14	Rabbit	WB	1:500	Novus / NBP2-20605
HELQ	Rabbit	WB	1:500	Cell Signaling / 19436
AuroraA	Mouse	IF	1:1000	Abcam / ab13824
pHH3	Rabbit	IF	1:500	Abcam / ab47297
α-tubulin	Mouse	WB	1:3000	Merck / TS168
α-tubulin	Rabbit	WB	1:3000	Abcam / 18251
GFP	Mouse	IF	1:1000	Abcam / ab1218

Table 2.5: List of secondary fluorescent antibodies.

Antibodies	Species of Origin	Application	Working dilution	Supplier / Code
anti-Mouse IgG (H+L) Cross-Adsorbed Secondary Antibody, Alexa Fluor 488	goat	IF	1:3000	Thermo Fisher scientific / A11001
anti-Mouse IgG (H+L) Cross-Adsorbed Secondary Antibody, Alexa Fluor 555	goat	IF	1:3000	Thermo Fisher scientific / A21422
anti-Rabbit IgG (H+L) Cross-Adsorbed Secondary Antibody, Alexa Fluor 488	goat	IF	1:3000	Thermo Fisher scientific / A1108
anti-Rabbit IgG (H+L) Highly Cross-Adsorbed Secondary Antibody, Alexa Fluor 555	goat	IF	1:3000	Thermo Fisher scientific / A21429
IRDye® 680RD anti-Rabbit IgG Secondary Antibody	donkey	WB	1:3000	LI-COR / 926-68073
IRDye® 680RD anti-Mouse IgG Secondary Antibody	goat	WB	1:3000	LI-COR / 925-68070
IRDye® 800RD anti-Rabbit IgG Secondary Antibody	donkey	WB	1:3000	LI-COR / 925-32213
IRDye® 800RD anti-Mouse IgG Secondary Antibody	goat	WB	1:3000	LI-COR / 926-32210
IRDye® 800RD anti-Rat IgG Secondary Antibody	goat	WB	1:3000	LI-COR / 926-32219
IRDye® 680RD anti-Rat IgG Secondary Antibody	goat	WB	1:3000	LI-COR / 926-68076

Table 2.6: List of SYBR green primers.

Gene symbol	Species	Sequence (5'- 3')
IL-1α	Human	F: GGTTGAGTTTAAGCCAATCCA R: TGCTGACCTAGGCTTGATGA
IL-1β	Human	F: CTGTCCTGCGTGTTGAAAGA R: TTGGGTAATTTTTGGGATCTACA
IL-6	Human	F: CCAGGAGCCCAGCTATGAACT R: CCCAGGGAGAAGGCAACTG
IL-7	Human	F: CTCCAGTTGCGGTCATCATG R: GAGGAAGTCCAAAGATATACCTAAAAGAA
IL-8	Human	F: CTCTTGGCAGCCTTCCTGATT R: TTAGCACTCCTTGGCAAAACTG
CXCL1/ GRO1	Human	F: CCCACTGCGCCCAAAC R: CAGGATTGAGGCAAGCTTTCC
CXCL2/ GRO2	Human	F: AACTGCGCTGCCAGTGCT R: CCCATTCTTGAGTGTGGCTA
CCL5	Human	F: TCTGCGCTCCTGCATCTG R: GGGCAATGTAGGCAAAGCA
CSF2	Human	F: CAGTAGAAGTCATCTCAGAAATGTTTGA R: GCTCCAGGCGGGTCTGTAG
MMP3	Human	F: TGATGAACAATGGACAAAGGATACA R: TTTCATGAGCAGCAACGAGAA
SDF1	Human	F: CACTCCAAACTGTGCCCTTCA R: CAATGCACACTTGTCTGTTGTTGT
ANKRD1	Human	F: AGTAGAGGAACTGGTCACTGG R: TGGGCTAGAAGTGTCTTCAGAT
TNF-α	Human	F: GCTGCACTTTGGAGTGATCG R: TCACTCGGGGTTCGAGAAGA
TNF-β	Human	F: GAGGCCAAGCCCTGGTATG R: CGGGCCGATTGATCTCAGC
β-Actin	Human	F: GAGTCCGGCCCCTCCAT R: GCAACTAAGTCATAGTCCGCCTAGA
PRIM1 pair1	Human	F: ATGGAGACGTTTGACCCCAC R:CTCCACCGTAGTTGAGCCAG
PRIM1 pair2	Human	F: CAGGTCGCATATCTGTGCCTAT R:ATGGCATCCAATTCACGGCA
HELQ	Human	F: GGAAAAACCCTCGTGGCTGA R:TCATGTGCAACTTTTCTTGGAC
TEX14	Human	F: CCCAGAAAGGAGCAACC R:TGGGACTCGAGGTACTGTAAGA

Table 2.7: List of lentivirus particles.

Lentivirus particles	Supplier / Code	Storage
Edit-R CRISPRa Lentiviral hCMV-Blast-dCas9-VPR Particles	Horizon / VCAS11918	-80°C
Edit-R lentiviral sgRNA library	Horizon / custom made	-80°C
LentiBrit Histone H2B-GFP Lentiviral Biosensor	Millipore / 1710229	-80°C
H2BmCherry Lentiviral particles	Provided by Prof Andrew Tutt	-80°C
LentiBrit Histone H2B-RFP Lentiviral Biosensor	Millipore / 1710228	-80°C

Table 2.8: List of oligos for short interfering RNA (siRNA).

Gene Symbol	Number allocated	Sequence (5'- 3')	Code	Storage
SMYD3	1	CAAGGAUGCUGAUAUGCUA	D-013737-01	-80°C
SMYD3	2	GGAAGUUGGUGUUGGCCUA	D-013737-02	-80°C
SMYD3	3	GCCAAAUACUGUAGUGCUA	D-013737-03	-80°C
SMYD3	4	CAACAUCAGAGCAUCCUAA	D-013737-04	-80°C
BLM	1	GAGCACAUCUGUAAAUUAA	D-007287-01	-80°C
BLM	2	GAGAAACUCACUUCAAUAA	D-007287-03	-80°C
BLM	3	CAGGAUGGCUGUCAGGUUA	D-007287-04	-80°C
BLM	4	CUAAAUCUGUGGAGGGUUA	D-007287-05	-80°C
DDX3X	1	GCAAAUACUUGGUGUUAGA	D-006874-01	-80°C
DDX3X	2	ACAUUGAGCUUACUCGUUA	D-006874-02	-80°C
DDX3X	3	CUAUAUUCCUCCUCAUUUA	D-006874-04	-80°C
DDX3X	4	GGUAUUAGCACCAACGAGA	D-006874-17	-80°C
EIF4A3	1	GAAAGCGGCUGCUCAAAGA	D-020762-01	-80°C
EIF4A3	2	GAACGUUGCUGAUCUUAUC	D-020762-02	-80°C
EIF4A3	3	GGUGAAACGUGAUGAAUUG	D-020762-03	-80°C
EIF4A3	4	ACUAUGAUCUCCCUAAUAA	D-020762-04	-80°C
KDM1A	1	UGAAUUAGCUGAAACACAA	D-009223-01	-80°C
KDM1A	2	GACAAGCUGUUCCUAAAGA	D-009223-02	-80°C
KDM1A	3	GUAAAGCCACCCAGAGAUA	D-009223-03	-80°C
KDM1A	4	CUAUAAAGCUCCAAUACUG	D-009223-04	-80°C
KMT2D	1	GCAAAUCGCUAGCAUCAUU	D-004828-01	-80°C
KMT2D	2	GAAAGAAGCUGCGGAAGGA	D-004828-02	-80°C
KMT2D	3	GCAGAUACCUUGUUUAGCA	D-004828-03	-80°C
KMT2D	4	CAUCAAAUCCGACAUCGUU	D-004828-05	-80°C
MEF2C	1	GCACCGACAUGGACAAAGU	D-009455-01	-80°C
MEF2C	2	GAACCUGUUUCUCCUCCUA	D-009455-02	-80°C
MEF2C	3	CAACAGCAACACCUACAUA	D-009455-03	-80°C
MEF2C	4	GGAUAUCCAUCAGCCAUUU	D-009455-04	-80°C
DYRK3	1	CAGAAGCUCUACACAUAUA	D-004731-01	-80°C

DYRK3	2	GCACACCAAUUGACAUAUG	D-004731-02	-80°C
DYRK3	3	GAAAGGGUGUGAUGACUAC	D-004731-03	-80°C
DYRK3	4	CCAUCUAGCUUAUCGAUAU	D-004731-04	-80°C
RUNX1	1	GACAUCGGCAGAAACUAGA	D-003926-01	-80°C
RUNX1	2	CACCGCAAGUCGCCACCUA	D-003926-03	-80°C
RUNX1	3	CAAAUUGAAAUGACGGUAU	D-003926-18	-80°C
RUNX1	4	GGCGAUAGGUCUCACGCAA	D-003926-19	-80°C
SETD1A	1	GGAAAGAGCCAUCGGAAAU	D-022793-01	-80°C
SETD1A	2	GACAACAACGAAUGAAAUA	D-022793-02	-80°C
SETD1A	3	CAACGACUCAAAGUAUAUA	D-022793-03	-80°C
SETD1A	4	GCGAUUCGUCUUCCAAAUG	D-022793-04	-80°C
SMARCA1	1	GAAGAAACCAGUACGUGUA	D-011392-01	-80°C
SMARCA1	2	CAACGAGAAUGGUAUACAA	D-011392-02	-80°C
SMARCA1	3	CGAAGGAUCAGUAUCAAGA	D-011392-03	-80°C
SMARCA1	4	ACUAACCGCUUGCUCCUAA	D-011392-04	-80°C
SMARCA4	1	GAAAGGAGCUGCCCGAGUA	D-010431-01	-80°C
SMARCA4	2	CCAAGGAUUUCAAGGAAUA	D-010431-02	-80°C
SMARCA4	3	GAAAGUGGCUCAGAAGAAG	D-010431-03	-80°C
SMARCA4	4	AGACAGCCCUCAAUGCUAA	D-010431-04	-80°C
SRCAP	1	GGAAAUUGCUGCCCUCGUA	D-004830-01	-80°C
SRCAP	2	GCCCAAACCUGUCUUGUAA	D-004830-02	-80°C
SRCAP	3	GAACAGGUCUCCAGCAGAU	D-004830-03	-80°C
SRCAP	4	CCACUUGGCUUGUGAGAAA	D-004830-04	-80°C
TDP2	1	GCAAGAGGCUCCAGAGUCA	D-017578-01	-80°C
TDP2	2	GCCAAGAGAUUAUUCCUUU	D-017578-02	-80°C
TDP2	3	UCUAAGGGAUCGAGAGGUU	D-017578-03	-80°C
TDP2	4	CAGAAGAGGGACACAUUAU	D-017578-04	-80°C
TNIK	1	UAAGCGAGCUCAAAGGUUA	D-004542-03	-80°C
TNIK	2	GAACAUACGGGCAAGUUUA	D-004542-04	-80°C
TNIK	3	GCACAAGCCUCUGCUAGUU	D-004542-07	-80°C
TNIK	4	GGUCAAAGAUUAAAGGUUA	D-004542-09	-80°C
XRCC6	1	GAAGGAGGUUGCAGCAUUG	D-005084-02	-80°C
XRCC6	2	GGCCCAAGGUGGAGUAUUC	D-005084-05	-80°C
XRCC6	3	GAAGAUGAGUUGACACCUU	D-005084-06	-80°C
XRCC6	4	ACAGAGAUAUCAUCAGCAU	D-005084-07	-80°C
ATRX	1	GCUAAGAGCUCUAUAAUUU	D-006524-01	-80°C
ATRX	2	GCAAAGAACUUCAUCUAAA	D-006524-02	-80°C
ATRX	3	GAGGAAACCUUCAAUUGUA	D-006524-03	-80°C
ATRX	4	GCAGAGAAAUUCCUAAAGA	D-006524-04	-80°C
CHD4	1	CCAAGGACCUGAAUGAUGA	D-009774-01	-80°C
CHD4	2	CAAAGGUGCUGCUGAUGUA	D-009774-02	-80°C
CHD4	3	GAAAGAGGCAUCUGUGAAA	D-009774-03	-80°C
CHD4	4	GAUGAUAUCCUCAAAUUUG	D-009774-04	-80°C
CTPS1	1	GUUAGAAGAUCAUCCCUUU	D-006644-02	-80°C
CTPS1	2	AGAGAUGGCUGACAGAUAU	D-006644-03	-80°C
CTPS1	3	GAACCUCAAGUGUGUGUUA	D-006644-04	-80°C
CTPS1	4	CCAGAAUAGUGUUCGGGAA	D-006644-17	-80°C
HELZ	1	GGAAAUAGAACGCAUCAAA	D-021180-01	-80°C

HELZ	2	CAGCACACCUUGUUAAAUC	D-021180-02	-80°C
HELZ	3	GAUAUCACGUGGAAGACUU	D-021180-03	-80°C
HELZ	4	CUACAGAAGAUCUCGAAUA	D-021180-04	-80°C
HELQ	1	GAAGAGGUCCAAUAUAAUU	D-015379-01	-80°C
HELQ	2	AAUGUGAGGUGAUUAAGAA	D-015379-03	-80°C
HELQ	3	GGUAGAAGAGUUACUAAGA	D-015379-04	-80°C
HELQ	4	GUUUGAAGAUUGCAACGAA	D-015379-17	-80°C
REV1	1	GAAUAUGGCAUUUGACUUU	D-008234-01	-80°C
REV1	2	GAAAUACUGUACUGAUCUA	D-008234-02	-80°C
REV1	3	GAAAUGUGCUGCCUCUGUU	D-008234-03	-80°C
REV1	4	GAGAAGAGCAGCACUGAUU	D-008234-04	-80°C
SETD2	1	GAGAGGUACUCGAUCAUAA	D-012448-01	-80°C
SETD2	2	GCUCAGAGUUAACGUUUGA	D-012448-02	-80°C
SETD2	3	GAAACCGUCUCCAGUCUGU	D-012448-03	-80°C
SETD2	4	GGAGACAUUUGUAUGAGGA	D-012448-04	-80°C
ARID1A	1	GCAACGACAUGAUUCCUAU	D-017263-01	-80°C
ARID1A	2	GAAUAGGGCCUGAGGGAAA	D-017263-02	-80°C
ARID1A	3	AGAUGUGGGUGGACCGUUA	D-017263-03	-80°C
ARID1A	4	UAGUAUGGCUGGCAUGAUC	D-017263-04	-80°C
USP10	1	CCAUAAAGAUUGCAGAGUU	D-006062-05	-80°C
USP10	2	CAAACAAGAGGUUGAGAUA	D-006062-06	-80°C
USP10	3	CCACAUAUAUUUACAGACU	D-006062-08	-80°C
USP10	4	GAGUUGCACACCACGGAAA	D-006062-21	-80°C
XRCC1	1	GGAAUGAUGGCUCAGCUUU	D-009394-02	-80°C
XRCC1	2	CCCGAUGGAUCUACAGUUG	D-009394-03	-80°C
XRCC1	3	GAACACGGACAGUGAGGAA	D-009394-04	-80°C
XRCC1	4	CAACCGCGUUCGCAUGUUU	D-009394-05	-80°C
FZD6	1	GGACAAGGAUAUAAGUUUC	D-005505-01	-80°C
FZD6	2	CACCAAACAUUGAAACUUU	D-005505-03	-80°C
FZD6	3	GCUUGAAUGUGACAGAUUA	D-005505-04	-80°C
FZD6	4	CCUUAAAUCAUGUUCGACA	D-005505-17	-80°C
KAT6A	1	GAACAGCUAUCGAAUGACA	D-019849-01	-80°C
KAT6A	2	GGAGUUGAGUGUUAAAGAU	D-019849-02	-80°C
KAT6A	3	GCGCUAUACUAAUCCAAUA	D-019849-03	-80°C
KAT6A	4	AGAUGUAGAUCCAGAAUGU	D-019849-04	-80°C
CDK12	1	GAAAGAAGACAAACAGAAA	D-004031-01	-80°C
CDK12	2	GAACUGAUCAGCCGACUUU	D-004031-02	-80°C
CDK12	3	GCACAGUUAUCAAACCUUU	D-004031-04	-80°C
CDK12	4	UAACACAUCUAAACACAGA	D-004031-06	-80°C
RSPO1	1	GAAGUCAACGGCUGCCUCA	D-018179-01	-80°C
RSPO1	2	AUGAACAAGUGCAUCAAAU	D-018179-03	-80°C
RSPO1	3	AGCCAUAACUUCUGCACCA	D-018179-04	-80°C
RSPO1	4	GUGAGGGUUUGGCGAGGUA	D-018179-17	-80°C
TLK2	1	GAAAUGAUCUGGACUUCUA	D-005389-01	-80°C
TLK2	2	CCAAAGAUCUCAAAUAAAG	D-005389-03	-80°C
TLK2	3	GCAUGGAGCUAACAUCACA	D-005389-04	-80°C
TLK2	4	GGGAAGAGAUAGAAAGACA	D-005389-05	-80°C
SPINT2	1	GAAGACCACUCCAGCGAUA	D-010216-01	-80°C

SPINT2	2	GCAAUAACUUCAUCUAUGG	D-010216-02	-80°C
SPINT2	3	CCUGCCAGCUGUUUGUGUA	D-010216-05	-80°C
SPINT2	4	CAGCAGGAAUGCAGCGGAU	D-010216-18	-80°C
FANCM	1	GUACUGCACUUGAGAAUUU	D-021955-01	-80°C
FANCM	2	CAAACCAUGUUCACAAUUA	D-021955-02	-80°C
FANCM	3	CAACAGUGGUGAAUAGUAA	D-021955-03	-80°C
FANCM	4	GAACAAGAUUCCUCAUUAC	D-021955-04	-80°C
HFM1	1	UCAAGGAACUAUAGCAAUA	D-021627-01	-80°C
HFM1	2	GCAAAUGUGUUUACAGCAA	D-021627-03	-80°C
HFM1	3	UGCCAUGGUUGAAUAUUAA	D-021627-04	-80°C
HFM1	4	GUUCAUAAUUGUUCGGAUU	D-021627-17	-80°C
MCM7	1	GGAAAUAUCCCUCGUAGUA	D-003278-05	-80°C
MCM7	2	GGAGAGAACACAAGGAUUG	D-003278-08	-80°C
MCM7	3	UGUCAUACAUUGAUCGACU	D-003278-21	-80°C
MCM7	4	GAGACAAUGACCUACGGUU	D-003278-22	-80°C
MDN1	1	GAAAUUUGAUGGACUUUGA	D-009786-03	-80°C
MDN1	2	GGAGAUAUAUCCCGAGCUA	D-009786-17	-80°C
MDN1	3	GGACAUUAAAGUACCGAUA	D-009786-18	-80°C
MDN1	4	CUACAAUAGAUGAGACGUA	D-009786-19	-80°C
BUD31	1	GAAAGUGGAAUCUCUGUGG	D-018665-01	-80°C
BUD31	2	CUACAUCUUCGACCUCUUU	D-018665-02	-80°C
BUD31	3	GCGGAAAGCCAUCAGCAGA	D-018665-03	-80°C
BUD31	4	CAGAACCGCAUGAGGGAAA	D-018665-04	-80°C
PES1	1	CAACGAAGGUGAUGGUGAU	D-009542-01	-80°C
PES1	2	GAAGGAAGGAGAUUACGUU	D-009542-02	-80°C
PES1	3	CCUUGAAGCUGGAGGAUAA	D-009542-03	-80°C
PES1	4	GAGCUUGGCUGACUUUAGG	D-009542-04	-80°C
SMURF2	1	GAUGAGAACACUCCAAUUA	D-007194-01	-80°C
SMURF2	2	GACCAUACCUUCUGUGUUG	D-007194-02	-80°C
SMURF2	3	CAAAGUGGAAUCAGCAUUA	D-007194-03	-80°C
SMURF2	4	GAACAACACAAUUUACAGA	D-007194-04	-80°C
TEX14	1	GAAGAGGACUUUGAAGGAA	D-005386-03	-80°C
TEX14	2	GCACUUAGAAGAACAAGAA	D-005386-04	-80°C
TEX14	3	UAAAGAUGAUGGAAAGGUA	D-005386-05	-80°C
TEX14	4	GCAGCGAGUUAUUGAGUAU	D-005386-06	-80°C
TRIB1	1	GUACAUCGACUCAGAAAUA	D-003633-01	-80°C
TRIB1	2	GGAGGACAGUGACAUUAGU	D-003633-03	-80°C
TRIB1	3	CGGAAAGGCUGCGGACGUU	D-003633-05	-80°C
TRIB1	4	GAACCCAGCUUAGACUAGA	D-003633-06	-80°C
XRCC5	1	GGAAGAAGCCAUUAAGUUU	D-010491-01	-80°C
XRCC5	2	GAAGUGAUAUAGUUCCUUU	D-010491-02	-80°C
XRCC5	3	GAUGAUAUCUUUAGAAGGU	D-010491-03	-80°C
XRCC5	4	GCUCAUAAAUCACAUCGAA	D-010491-04	-80°C
PRIM1	1	GAUGUGAGGAGAUGUUGUA	D-020200-01	-80°C
PRIM1	2	CAUACAAGAUUGAUAUAGG	D-020200-02	-80°C
PRIM1	3	CGCAGUAUAUUCUCACAGA	D-020200-04	-80°C
PRIM1	4	UGACAAUGGCCAUACGCAU	D-020200-18	-80°C
RAD18	1	CAUAUUAGAUGAACUGGUA	D-004591-01	-80°C

RAD18	2	GCAGGUUAAUGGAUAAUUU	D-004591-02	-80°C
RAD18	3	GAUAAUAUGACCUCAGUAA	D-004591-03	-80°C
RAD18	4	GCAGUUUGCUUUAGAGUCA	D-004591-04	-80°C
UBA2	1	GGACUGGGCUGAAGUACAA	D-005248-01	-80°C
UBA2	2	GGAAGAAGAUGCUGAUCAA	D-005248-02	-80°C
UBA2	3	GAACAAUCCUAAUAUCUUC	D-005248-03	-80°C
UBA2	4	UAACAGAGCUGCCCGAAAC	D-005248-04	-80°C
UBE2T	1	CCUGCGAGCUCAAAUAUUA	D-004898-01	-80°C
UBE2T	2	AGGAAGAGAUGCUUGAUAA	D-004898-02	-80°C
UBE2T	3	AGAGAGAGCUGCACAUGUU	D-004898-03	-80°C
UBE2T	4	GAAGUUAUCAUUCCUGAGA	D-004898-04	-80°C
WRN	1	GAAGAGAUCUGUUCAAGUU	D-010378-01	-80°C
WRN	2	GAAAUAAAGUGGAACGAAA	D-010378-02	-80°C
WRN	3	GAACAUGAACUCCAAAUUU	D-010378-03	-80°C
WRN	4	UGACAGAUGUUGCCAAUAA	D-010378-04	-80°C
ATP23	1	UAACAAGACUUAUGCAAGA	D-015098-01	-80°C
ATP23	2	UGAAGACGCUGGAGACAAA	D-015098-02	-80°C
ATP23	3	GAAUAUCAGCAAAGAAGUA	D-015098-03	-80°C
ATP23	4	AACCAGAAGUGCCAGCUUA	D-015098-04	-80°C

Table 2.9: List of cell lines.

Cell line	Description	Origin
DLD1 (2N)	Human colorectal carcinoma cell line	ATCC
DLD1 (4N)	Human colorectal carcinoma cell line	K. Drosopoulos
HCC1143	Human triple negative breast cancer cell line	ATCC
HCT116	Human colorectal carcinoma cell line	Prof. J. Downs lab
HCT116BRG1$^{-/-}$	Human colorectal carcinoma BRG1 KO cell line	Prof. J. Downs lab
HCT116p53$^{-/-}$	Human colorectal carcinoma p53 KO cell line	P. Wolkenstein
U2OS	Human osteosarcoma cell line	Prof. J. Downs lab
U2OSBAF180$^{-/-}$	Human osteosarcoma BAF180 KO cell line	Prof. J. Downs lab

HCT116p53$^{-/-}$ H2B GFP	HCT 116p53$^{-/-}$ with stable expression of H2B GFP	M. Mandelia
HCT116p53$^{-/-}$ H2B mcherry	HCT 116p53$^{-/-}$ with stable expression of H2B mcherry	M. Mandelia
HCC1143 H2B GFP	HCC1143 with stable expression of H2B GFP	M. Mandelia
HCC1143 H2B RFP	HCC1143 with stable expression of H2B RFP	M. Mandelia
HCT116 Cas9	HCT 116 with stable dox inducible Cas9	M. Mandelia
HCT116p53$^{-/-}$ Cas9	HCT 116p53$^{-/-}$ with stable dox inducible Cas9	M. Mandelia
HCT116BRG1$^{-/-}$ Cas9	HCT 116BRG1$^{-/-}$ with stable dox inducible Cas9	M. Mandelia
U2OS Cas9	U2OS with stable dox inducible Cas9	M. Mandelia
U2OSBAF180$^{-/-}$ Cas9	U2OSBAF180$^{-/-}$ with stable dox inducible Cas9	M. Mandelia
DLD1 (2N) Cas9	DLD1 (2N) with stable dox inducible Cas9	M. Mandelia
DLD1 (4N) Cas9	DLD1 (4N) with stable dox inducible Cas9	M. Mandelia
HCT116p53$^{-/-}$ aneuploid clones	HCT 116p53$^{-/-}$ stable aneuploid cells	M. Mandelia
DLD1 aneuploid clones	DLD1 stable aneuploid cells	M. Mandelia
CAL51	Human breast carcinoma cell line	ATCC
SKOV3	Human ovarian serous cystadenocarcinoma cell line	ATCC
IGROV1	Human ovarian cancer cell line	ATCC
MDA-MB-231	Human breast cancer cell line	ATCC
PATU8988S	Human liver metastasis of a primary pancreatic adenocarcinoma cell line	ATCC

2.2 Methods

2.2.1 Cell culture

All adherent cell lines, apart from HCC1143, were cultured in DMEM based cell culture media, while HCC1143 cell line was cultured in RPMI based cell culture media (Table 2.2). Cells were cultured in the appropriate size of flasks, in humidified incubators at 37°C and 5-10% CO_2, and were grown up to 80-90% confluence, after which they were passaged at the desired dilution every 2-4 days.

To passage cells, the existing media was removed by aspiration and cells were washed, once, with a sufficient volume of PBS to cover the flask, prior to adding a covering volume of trypsin / versene solution (for example: 1ml / T25cm^2, 2ml / T75 cm^2, 5ml / T175cm^2 or 25ml / 5-layer tissue culture flask), with short incubation at 37°C. Once the cells were fully detached, the trypsin solution was neutralised by addition of fresh culture medium, the cell suspension was diluted at the desired fraction in fresh culture medium and re-plated into a new culture flask or plate. For all cell culture based experiments described below, cells in suspension were stained with 0.4% Trypan Blue and counted using a Countess automated cell counter system.

To maintain stocks of adherent cell lines, cells were frozen and stored in -80°C or liquid nitrogen. Initially, cells were detached as described above. Once resuspended in fresh culture medium, the cell suspension was centrifuged at 1,500 rpm for 5 minutes. The resulting cell pellet was resuspended in cell freezing medium and 1 ml was transferred to CryoTube vials. Vials were frozen at -20°C for 3 hours and then transferred at -80°C for short term storage or for 3 days, after which they were transferred to liquid nitrogen for long term storage.

2.2.2 Generation of aneuploid clones

In order to generate aneuploid cancer cells, the HCT116p53$^{-/-}$ and DLD1 (2N and 4N) were treated with drugs to induce mitotic errors in the cells. After the treatments, cells were single cell sorted, depending on their DNA content as was indicated by

Hoechst cell cycle profiling. Clones were propagated and characterised by cytogenetic assays.

2.2.2.1 Cell treatments for induction of mitotic errors and single cell FACS sorting

Mitotic errors were generated by seeding an appropriate number of cells in T175 cm^2 culture flasks and after 24 hours, treating them with 100 ng/ml Nocodazole overnight (approximately for 16 hours). Mitotic shake off was followed and the mitotic cells were centrifuged at 1,500 rpm for 5 min. After washes with fresh media, the cell pellets were resuspended in media with 50 nM GSK923295, or 2 nM Taxol, or 40 μM Monastrol and incubated at 37^{o}C. 2 hours after the treatment, 150 nM of MPS1 inhibitor was added to the cells for 2 hours, without removing the initial treatments, after which the cells were centrifuged at 1,500 rpm for 5 minutes, washed with growth medium and cultured for 24hours. The next day, the cells were split again and prepared for FACS sorting. The trypsinized cells were centrifuged at 1,500 rpm for 5 minutes and the pellet was resuspended in media with Hoechst in 1:2,000 dilution. 500,000 cells were transferred into FACS tubes and were incubated for 30 minutes at 37^{o}C. Single cells with DNA content between diploidy (2N) and tetraploidy (4N) were sorted and cultured in 96 well plates with 200 μl of fresh media. After 10 days in culture, the media was replaced and the cells were left to grow for another 10 days.

2.2.2.2 Characterisation of aneuploid clones by FACS cell cycle profile

Characterisation of the generated clones was conducted, initially, by analysing the cell cycle profile by FACS. Cells were passaged as described before and the next day, they were trypsinized again, counted and 800,000 cells were centrifuged at 1,500 rpm for 5 minutes and resuspended in 1 ml PBS. The cells were fixed by dropwise addition of 10ml cold (-20^{o}C) 70% Ethanol in PBS, under slow speed vortexing. Samples were stored at -20^{o}C overnight. The next day, the cells were centrifuged at 1,500 rpm for 5 minutes, washed with 10 ml PBS and centrifuged again at the same conditions. The cell pellets were resuspended in 1 ml of PBS with 30 μg/ml PI and 100 μg/ml of

RNAse A. The samples were incubated at 37°C for 30 minutes and analysed using the LSR II Flow cytometer (BD).

2.2.2.3 Characterisation of aneuploid clones by metaphase spreads

3million cells were seeded in a T75cm^2 culture flask. The next day, 0.1μg/ml of Colcemid was added to the cells for 90 minutes at 37°C and the mitotic cells were collected by mitotic shake off. The cells were centrifuged at 1,500 rpm for 5 minutes and the cell pellets were resuspended in 6ml of 0.56% KCl for 10 minutes at room temperature. 300μl Fixative of 3:1 Methanol-Acetic acid solution were added at the samples, which were then centrifuged at 1,500 rpm for 5 minutes and the cell pellets were resuspended in 8 ml of fixative at -20°C for 20 minutes. After centrifugation at 1,500 rpm for 5 minutes, the supernatant was discarded and the cell pellet was diluted gently in 1 ml fixative and stored at -20°C until the day of use. Then, from a height of 20 cm, 3 drops of fixed cells were thrown to a microscopy slide and left 45 minutes at room temperature to dry. Finally, 2 drops of mounting medium with DAPI were added over the dried cells and covered by coverslips, which were sealed with clear nail polish. The slides were then imaged by confocal microscopy or stored at 4°C for further use.

2.2.2.4 DNA extraction and characterisation of aneuploid clones by CGH or SNPs

Genomic DNA was extracted by using the QIAGEN DNeasy Blood and Tissue kit, according to manufacturer's protocol (Qiagen, Quick-Start Protocol DNeasy Blood & Tissue Kit). However, for increasing the final amount of the DNA yield, the DNA was extracted in warm 100 μl extraction buffer, with no EDTA, and that step was repeated twice. The amount of DNA was measured by Nanodrop 800 or Qubit dsDNA BR Assay Kit, according to manufacturer's protocol (ThermoFisher, Q32853). The DNA samples were stored at -20°C until they were sent for Comparative Genomic Hybridization (CGH) (to Eurofins Genomics) or Single Nucleotide Polymorphisms (SNPs) (to Barts Institute) and were analysed by Oxford Gene Technology.

2.2.3 Induction of chromosomal instability

In order to induce chromosomal instability, HCT116, HCT116p53$^{-/-}$ and DLD1 cells were treated continuously during the experiments with 20 nM CENP-E inhibitor GSK923295 or 1 μM ATM inhibitor KU60019 or 1 μM CHK1/CHK2 inhibitor CCT241106. GSK923295 and KU60019 or CCT241106 promote chromosomal instability through increased chromosome missegregation or micronuclei formation, respectively, which were identified by immunofluorescence.

2.2.4 Viability assay

Viability assays were performed in white 96- or 384-well plates over a 5 or 6-day incubation period. 1,500 or 500 cells were plated in 96- or 384-well plates, respectively, on day 0, in growth medium with/without drugs or inhibitors and viability was measured after 5 or 6 days. The number of viable cells in each well was determined by the addition of CellTiter-Glo Luminescent reagent, which quantifies the presence of ATP in a sample, providing a measure of viable cells in the form of a chemi-luminescent signal. For each well, media was aspirated and 100 μl of 60% CellTiter-Glo Reagent and 40% of complete growth medium mix, was added in 96-wells (or 80μl in 384-wells). The plate was placed immediately on a bench top plate shaker (Heidolph), covered with foil, as CellTiter-Glo is light-sensitive, and shaken for 15 seconds, at 750 rpm, in RT. The covered plate was then left to stand for 20 minutes. Before measuring the ATP levels, the plate was shaken again briefly. Luminescence of each sample was measured using the VictorTM X5 Multilabel Reader and the GraphPad software was used to analyse the data.

2.2.5 Senescence associated β-galactosidase staining

Cells were seeded into two different 6 well plates at an appropriate density depending of the addition or not of Paclitaxel and cultured for three days. Then, the cells in one of the two 6-well plates were washed with PBS and released in fresh growth medium with no drug, for three more days. In the second plate, growth medium was removed and cells were washed once with PBS, then fixed for 6-7 minutes with 1.5 ml /

well of 1X fixating solution, followed by three washes with PBS and addition of 1.5 ml staining mixture containing X-Gal, according to senescence cells histochemical staining kit protocol. Fixed cells were incubated in the staining mixture at 37°C in a non-humidified incubator at atmospheric CO_2 concentration and plates were sealed using Parafilm to prevent evaporation. After ~16 hours, the cells were imaged at 10X magnification with EVOS. For long term storage 2 ml of a 70% glycerol solution was added to the wells, the plates were sealed with Parafilm and stored at 4^{o}C. The same protocol was repeated for the first plate after the end of the release.

2.2.6 Small molecule screening

HCC1143 cells were treated with 7.5 nM Paclitaxel for three days and 100 cells were seeded in 384-wells in 80 µl of fresh media. On top, the 604 small molecule library was added by ECHO 550, in a final concentration of 100 nM. Two technical repeats of each drug was included in the screen and as control, 128 wells with cells treated with Paclitaxel but released in media were used. The cells were imaged the next day by CeligoS and every week for a total of 2 weeks. The confluence of the cells was analysed by CeligoS software, measuring the area (in cm^2) of the wells that are covered by cells.

To identify which of the small molecules were hits in the screening, initially, the average of all the confluence values in the control was estimated. To continue, the ratio of the confluence value for each drug relative to the average control value was calculated. Then, the difference between the normalised value of each small molecule and the control was calculated. The average of the difference values between the two technical repeats for each small molecule was calculated and the standard deviation (STDEV) value of all average final values was estimated. As hits were considered the drugs that their average value was 3 times higher than the STDEV value of all the drugs in the library.

2.2.6.1 Cell recovery after simultaneous or sequential treatment with Paclitaxel and Crenolanib

800.000 cells were seeded in T25 cm^2 flasks in cell culture media with Paclitaxel alone or in combination with Crenolanib and incubated in 37^oC for 3 days. Then, the cells were washed with fresh media and 1,000 cells were plated in 384-well plates with or without the presence of Crenolanib. After 24 hours, images of the wells were taken by CeligoS and the percentage of confluence/well was analysed by CeligoS software, through measuring the area that the cells were covering in each well. Every 7 days for a period of 3 weeks, images were taken and the percentage of confluence was measured by CeligoS software and the GraphPad software was used to analyse the data.

2.2.7 Clonogenic assay

Clonogenic assays were performed in 24-well plates over 12-15 days of incubation, depending the cells line growth rate. Appropriate number of cells were seeded in the wells, depending to the growth rate of each cell line. Following the 15 days incubation, the formed colonies were fixed with methanol for 15 minutes and were stained with 0.5% crystal violet for another 15 minutes. Then, the plates were washed with water and after drying, they were scanned and analysed with Cell Profiler.

2.2.8 Migration assay

The ability of cells, treated with Paclitaxel, to attract untreated cells and promote cell fusion was tested by migration assay. 1 x10^6 cells were seeded in a T25 cm^2 flask and treated with Paclitaxel for three days. Moreover, 200,000 cells with no treatment, but the same volume of media, were seeded in another T25cm^2 flask. After three days in culture, the cells in both flasks were washed with PBS and fresh growth medium was added for three more days. Then, from both flasks, with treated or untreated cells, the growth media were removed and filtered with a 40 μm cell filter. 600 μl of the filtered media was placed in the bottom of a 24-well transwell plate and 100 μl of 25,000 untreated cells in fresh growth medium were added on the insert of the 24-transwell plate

that includes a 8.0μm porepolycarbonate membrane at the bottom. The cells were cultured for 5 hours and the inserts were transferred in another transwell plate filled with iced-cold methanol. 15 min later, the inserts were placed in wells filled with PBS and the non-migrated cells on the top of the membrane were removed carefully with a cotton bud. Lastly, the inserts were placed in wells filled with Dapi, diluted 1:10,000 in PBS, for 30 minutes and then, were transferred in wells with PBS, where three images/ sample were taken with a 4X lens at EVOS fluorescent microscope. The migrated cells were measured by ImageJ and the analysis was made by GraphPad Prism.

2.2.9 Immunofluorescence assay

Immunofluorescence was used to detect the presence and localisation of specific proteins in the cells. Depending the experiment, appropriate number of cells were plated in in 96- or 384-well plates with cell culture medium with or without a drug or inhibitor. At the last day of each experiment, cells were fixed by aspirating the media and adding the appropriate volume to cover the surface of the wells of ice-cold (-20^{o}C) methanol for 15 minutes. The methanol was then removed and the cells were washed once with 100 μl of PBS. Primary antibodies were diluted in 1.5% FBS/ PBS blocking solution and 80 μl or 40 μl was pipetted into the 96- or 484 well plate, respectively, and incubated overnight at 4°C. Following the incubation, the primary antibodies were aspirated and the cells were washed twice with PBS prior the addition of secondary antibody and Dapi (1:10,000 dilution), diluted in 1.5% FBS/PBS for 60-90 min, RT, in the dark. After the second antibody incubation, cells were washed twice with PBS and stored at 4°C, in the dark, until images were taken by fluorescence microscopy.

2.2.10 Protein manipulation

2.2.10.1 Protein extraction

Cells seeded in 6-well plates were collected and prepared for analysis by lysis in 5X Sample buffer using the back off a 200 μl pipette tip. Samples were placed immediately on ice, sonicated for 10-12 sec, in amplitude 6, in Soniprep-150, to sheer

genomic DNA. Then, the DNA was boiled (5 min, 95°C) and vortexed briefly. Samples were then centrifuged for 1 min and the protein levels were quantified by the Qubit protein kit, according to manufacturer's protocol, prior to loading onto an SDS-PAGE acrylamide gel. Alternatively, after sonication, the samples were stored at -80^{o}C, until further use.

2.2.10.2 SDS-polyacrylamide gel electrophoresis (SDS-PAGE)

SDS-polyacrylamide gel electrophoresis was performed to separate proteins according to their molecular weight. Small proteins migrate faster moving to the bottom of the gel, while large proteins remain at the top. Samples were separated using NuPAGE 4-12% Bis-Tris 1.0 mm, 15-well gels. Gels were clamped into a Novex Mini running tank (Invitrogen) and the tank was filled with MES buffer and 18 µl of protein sample was loaded into the gel's wells. In addition, 5 µl of Novex Sharp Standard ladder mixed to 13µl of MES buffer and the mix was loaded in one of the wells. Samples were run at 90V for 10 min followed by 130V in ice for 120-180 min.

2.2.10.3 Immunoblotting assay

Immunoblotting was used to identify the presence of specific proteins in a sample that had been separated by SDS-PAGE electrophoresis. Initially, proteins were transferred from the gel to a low fluorescence PVDF membrane, which was activated by incubation in 100% methanol for 5 min, through a Mini Protein 3 electrophoretic transfer cell (Bio Rad). 4 pieces of Whatman paper and a PVDF membrane were then equilibrated in transfer buffer for 5min. The gel was carefully removed from the electrophoresis cast and the top (stacking gel) and bottom were cut before being placed in transfer buffer for 5min. The transfer apparatus was assembled as follows: the open clamp was placed in the transfer buffer tray and a sponge was put on top. 2 pieces of Whatman paper were placed on the sponge before the gel was carefully positioned on top. The equilibrated membrane was placed onto the gel and 2 more pieces of Whatman paper and a sponge were placed on top. The stack was gently compressed by rolling

over a falcon tube to remove air bubbles. The cassette was then secured and placed in a transfer tank with the gel orientated to the cathode. The tank was filled with transfer buffer and run at 100V for 85 min.

To determine if proteins transferred well and check the running of the gel, the membrane was stained with PonceauS for 2-3 min and rinsed in water before visualising the transferred proteins. The membrane was de-stained with 3 washes in H_2O and incubation in TBS-T for 5-15 min at RT with gentle rocking.

Membranes were blocked for 30 min in 2.5% milk in TBS-T prior to incubation with primary antibody diluted in 1.25% blocking solution at 4°C, overnight with gentle rocking. Membranes were washed three times for 5 min in TBS-T on a gyro-rocker (Stuart Scientific) to remove excess primary antibody. Membranes were then incubated in secondary antibody, diluted in 1.25% blocking solution for 1hr in RT, with gently rocking. Secondary antibodies were used at concentration of 1:3000. The membranes were washed two times in TBS-T and once in TBS on a gyro-rocker. The secondary antibodies used were fluorescent and the signals were captured by LI-COR ODYSSEY FC and were analysed by Image Studio Lite.

2.2.11 Reverse lentivirus transduction and generation of stable H2B-GFP/RFP/mCherry or inducible Cas9 cell lines

For each cell line, the functional titer (fT), which is expressed in transforming units/ml (tu/ml), was identified by plating cells with serial dilutions of viral particles with a known reference titer (rT, in HEK 293 cells) that contain constructs driving the expression of non-targeting siRNA controls and GFP (SP-001000-01, Dharmacon). 25 µl of serially diluted viral particles in growth medium were placed in a black 96-well plate and 50 µl of 2,000 cells in growth medium with 5% FBS were plated in the 96-well plate. The next day, 100 µl growth medium with 16% FBS was added on the cells to raise the FBS concentration to 10% at the cells. A day later, an immunofluorescent assay was conducted; the cells were fixed in ice-cold methanol and stained with an anti-GFP primary antibody. The fraction of cells that were fluorescent positive (FP) for GFP was

determined by imaging with Operetta HCS system and analysed by Harmony software. Then, the functional titer for each cell line was calculated by the following formula in excel: fT = rT*((FP*CP)/(rT/vol)).

H2B GFP/ RFP or mCherry cells were generated by reverse transduction as described above and the multiplicity of infection (MOI) of 1 (100% of the cells infected), according to the functional titer. Two days after the transduction the growth medium was replaced by fresh with no viral particles and three days later the fluorescent positive cells were isolated by FACS sorting. The sorted cells were cultured for one week and the positive cells were isolated again by FACS sorting. The same process was repeated for a third time to ensure that all of the cells in the cultured population were positive for the appropriate H2B fluorescence.

Cas9 inducible cells were generated using Inducible Lentiviral hEF1a-Blast-Cas9 Nuclease Particles (Dharmacon by Horizon-VCAS11227). 100,000 cells were generated by reverse transduction as described above and the multiplicity of infection (MOI) of 0.25 (25% of the cells infected), according to the functional titer. The lentivirus vector expresses the Cas9 gene under the expression of hEF1a promoter and it is containing a blasticidin resistant marker (Figure 2.1). Thus, the cells continued to be cultured in growth media with 10% FBS tetracycline free and 15 µg/ml blasticidin (as was identified from viability assays). After 12 days in culture, the concentration of blasticidin was reduced to 5 µg/ml.

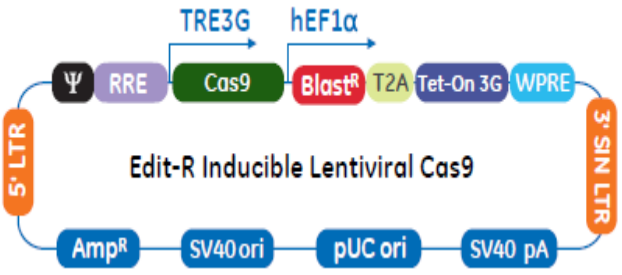

Figure 2.1: Schematic map of the Edit-R Inducible lentiviral Cas9 vector. hEF1α: Human elongation factor-1 alpha which drives the constitutive expression of the blasticidin resistance gene and the Tet-On 3G transactivator. TRE3G: an optimised inducible RNA polymerase II promoter which, upon doxycycline treatment, is activated by Tet-On 3G transactivator (figure was adapted by Dharmacon/Horizon).

2.2.12 CRISPR Cas9 loss of function screening

For CRISPR screening, we used a high titer (>1.25x109 tu/ml) custom Dharmacon Edit-R pooled lentiviral sgRNA screening library. This library is based on a two-vector system that utilizes a lentiviral vector for inducible Cas9 expression and a gene-specific lentiviral vector for constitutive expression of sgRNA. A blasticidin resistance gene is included in the inducible Cas9 lentiviral vector and a puromycin resistance gene in the sgRNA lentiviral vector which they provide the infected cells with resistance to each antibiotic (Figures 2.1 and 2.2). Therefore, we followed the mixed population workflow of the Edit-R sgRNA system (Figure 2.3).

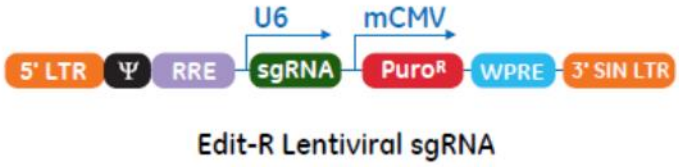

Figure 2.2: Schematic map of the Edit-R Lentiviral sgRNA vector. The Edit-R Lentiviral sgRNA vector provides the gene-specific sgRNA required to direct Cas9 nuclease activity and is expressed under the control of the human U6 promoter. It also expresses the puromycin resistance gene (PuroR) driven by the mouse CMV promoter allowing for rapid selection of cells with integrated sgRNA (figure was adapted by Dharmacon/Horizon).

The library targets 200 genes, using 10 sgRNAs per gene. The first half of the library includes sgRNAs against genes that have been selected by literature search. In particular, recent literature was surveyed to select targets that have been confirmed as aneuploidy or CIN hits in studies that used cellular models to identify synthetic lethal interactions and gene addictions (Table 2.10). The second half of the library consists of sgRNAs against genes that have emerged from recent publications on Breast and Pancreatic TCGA mutation data or they are involved in DNA damage response/repair pathways, metabolic pathways, cancer stem cell signalling and chromosomal instability (Table 2.10). Moreover, the custom lentiviral sgRNA library contains 200 target genes and 5 positive controls (CDK1, DYNC1H1, MAD2L1, PLK1, POLR2B), each one of which is represented by 10 unique sgRNAs. In addition, the library contains 30 individual non-targeting sgRNAs, which bring the total number of sgRNA constructs in the library to 2080. As recommended by Dharmacon and according to the literature, we aimed for a

minimum 400 to 500-fold coverage of the sgRNA library in the transduced cells. This means that each individual sgRNA will integrate in at least 400-500 cells, allowing selection of hits with increased confidence in the downstream analysis. In addition, taking into account the functional titer for each cell line, we aimed to transduce 20-30% of the population in order to ensure that each transduced cell contains a single sgRNA. According to these aims, we transduced $5x10^6$ cells for each cell line with an MOI of 0.25. Two days after the transduction the cells were selected by 1μg/ml puromycin, as was identified from viability assays.

For the screening of the library, $5x10^6$ cells were seeded in a T75 cm^2 flask, in which the appropriate amount of virus for each cell line, was initially added. By the same time, $5x10^6$ cells were seeded, but no virus was added. As described before, the Dharmacon sgRNA vector expresses a puromycin resistance gene (PuroR), which allows for rapid selection of cells with integrated sgRNA. From viability experiments, the appropriate concentration of puromycin was estimated to 1μg/ml. After 5 days of selection with puromycin, $5x10^6$ cells were frozen and DNA was extracted from $8x10^6$ cells by using the Qiagen DNeasy Blood and Tissue Kit. Additionally, $5x10^6$ cells were seeded into a 5-layer flask and 1μg/ml doxycycline was added for 4 days, in order to produce the maximum percentage of Cas9 (concentration was estimated by immunofluorescence and immunoblotting experiments). Following the induction of CAS9 for 4 days, the cells were cultured for 17 more days always in growth media with puromycin, in order to prevent the generation of clones with no intergraded sgRNA. At the end of the screening, cells were frozen again and DNA was extracted, as previously.

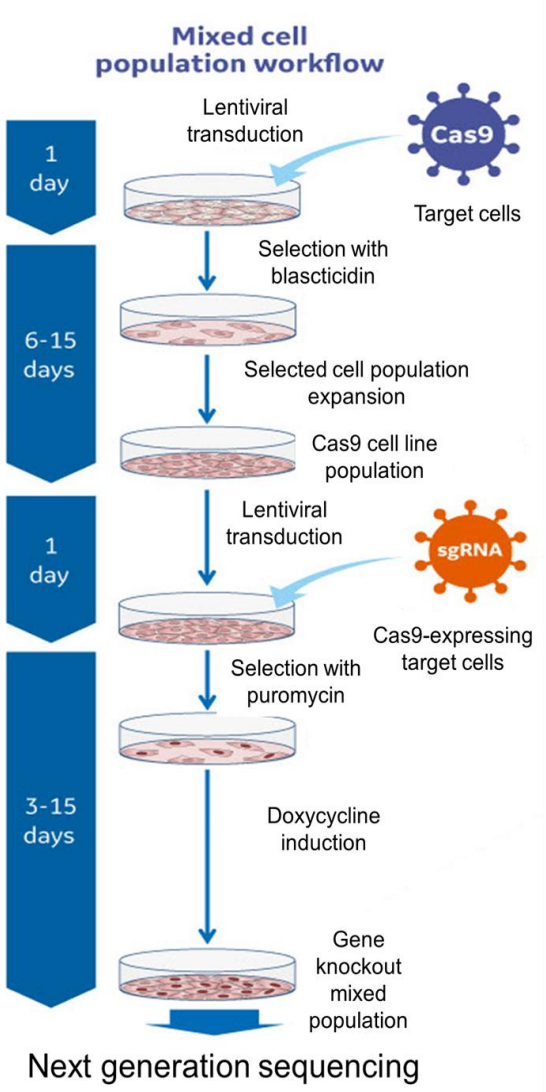

Figure 2.3: Gene knockout workflows using the Edit-R Inducible Lentiviral Cas9 with sgRNA system. Gene editing with Edit-R Inducible Lentiviral Cas9 and sgRNA can be done by induction of Cas9 expression with doxycycline in a mixed cell population approach (left side) which is used here or using isolated clonal cells lines (right side) when a defined genotype is required on each step for the phenotypic analysis (figure was adapted from Dharmacon/Horizon library manual).

2.2.12.1 CRISPR-Cas9 screening analysis and hit selection

Due to technical issues during the PCR amplification, before the sequencing of the samples, there is a large variation in the number of the sgRNAs between individual samples (0 – 10,000) and in some of them, most of the counts are close to 0. Thus, samples with average sgRNA count close to 0 were excluded from the analysis. The endpoint samples were normalised to the ratio of the averages of all the baseline and the endpoint samples. However, there was a large difference in the abundance of the different sgRNA constructs in the library, thus an additional normalisation step was

needed and each sgRNA count was normalised to the original abundance (counts per million) in the library. Finally, the depth value for each sgRNA was calculated by subtracting the baseline value from the corresponding endpoint value and the median absolute deviation relative to all sgRNA depth values in the same cell line was estimated. As hits were considered sgRNAs with depth value higher than 2.5 times the median absolute deviation number. In addition, in order to identify strong outliers (individual sgRNA constructs) that might merit further investigation, an additional hit list was generated by subtracting the strongest individual sgRNA per gene in the endpoint of the isogenic cell lines, from the strongest individual sgRNA per gene in the endpoint of the parental cell lines.

Table 2.10: List of genes included in the library used for the CRISPR-Cas9 loss of function screening.

Confirmed genes from literature					Genes involved in pathways of interest				
ACVR1B	EMC2	MSX2	PLA2G6	TEX14	ABCA13	DDX23	HELQ	PIP4K2B	SIRT3
AGL	FANCL	MUSK	PRIM1	THOC1	ADCY8	DDX39B	HELZ	PLB1	SMARCA1
AKR1C3	FOXN3	MUT	PTP4A3	TIE1	AICDA	DDX3X	HERC1	POLD3	SMARCA4
ANKRD46	FZD6	NCSTN	PTPN14	TNIK	ALDH1A3	DDX42	HERC2	POLR2E	SMC3
APOBEC3A	GAK	NDRG1	RBM38	TRIB1	APOBEC1	DDX46	HFM1	PRKD1	SMURF2
ASNS	GNB4	NEIL1	REV1	TRRAP	APOBEC2	DDX5	IKBKE	PRMT6	SMYD1
BOK	HCK	NRBP1	RIPK2	TXK	APOBEC3B	DHX15	KAT5	PTK6	SMYD3
BUD31	HECTD3	NUAK1	RIPK3	UBA2	ARID1A	DHX16	KDM1A	RAD18	SOAT1
CASK	HNRNPR	NUAK2	RNF31	UBA52	ASCC3	DHX35	KMT2D	RELN	SRCAP
CDK12	HSD17B4	NUP62	SBK2	UBE2I	ATRX	DHX38	MACF1	RFWD2	ST6GAL2
CECR2	ING4	PCBD1	SCD	UBE2T	BIRC6	DHX58	MAGI2	RNF213	STK19
COPS3	IRS2	PES1	SCYL1	USP33	BLM	DHX8	MAP2K3	ROR2	STK33
COPS4	KAT6A	PFKFB3	SDC4	USP39	CAMK1G	DHX9	MDN1	RSPO1	STK38L
COX20	KMT2C	PFKFB4	SEC61G	VPS45	CDA	DICER1	MDH2	RUNX1	TDP2
CSNK1E	LGR5	PFKP	SGK2	VRK1	CHD4	EIF2AK2	MEF2C	RYK	TLK2
CTPS1	LHX2	PHKG1	SPINT2	WRN	CHD6	EIF4A3	MOV10	SDHA	TRPM7
DLAT	LTK	PI4KA	SRPK2	XRCC1	CHD8	FANCM	MPP3	SDHB	UBR4
DLX3	MAP2K4	PI4KB	STRADA	XRCC5	COL4A3BP	FLAD1	MVK	SETD1A	USP10
DYRK3	MAP2K6	PIK3R3	SULT1A2	XRCC6	DDX17	GALNT2	NLK	SETD2	USP11
EFNB3	MCM7	PKN1	SUV39H1	XRCC6BP1	DDX20	HECTD4	PIF1	SFPQ	USP34

2.2.13 Knockdown of genes by siRNA

siRNA gene silencing was performed by using DharmaFECT2 or Lipofectamime 2000 transfection reagent and reverse transfection of siRNA with a final concentration of 20 nM (Table 2.11). The transfection reagent was gently mixed with OptiMEM medium and incubated for 5 min in RT. The appropriate volume of OptiMEM/Transfection reagent was added in the wells and the appropriate volume of siRNA was added on top and the mixture was incubated for 25 min in RT. Then, appropriate amount of cells were added in the wells, in growth media with no antibiotic overnight. The next day, the medium was removed and fresh growth medium was added. After 24 more hours, the cells were used for subsequent experiments.

Table 2.11: Volumes of siRNA/Transfection reagent/OptiMEM transfection mix.

Plate	1μM siRNA (μl)	OptiMEM (μl)	Transfection reagent (μl)	Cell number
384-well	0.2	9.95	0.05	500
96-well	2	17.805	0.195	10,000
24-well	26	272.75	1.25	1,000

2.2.14 siRNA loss of function screening

The protocol for the siRNA screening was adjusted from the siRNA screening protocol from the gene function team, at ICR, using DharmaFECT2 transfection reagent via reverse transfection of 20 nM siRNA in 384-well plates (Table 2.11). The siRNA library used is against 48 genes, including 4 siRNAs/ gene, as well as a negative siRNA control, which does not affect the cell viability and a positive siRNA control, which promotes cell death (Table 2.12). 5μM of each siRNA were transferred in a 384PP-well plate and stored at -80oC until used. 5 μl OptiMEM were added in a 384-white well plate by multidrop and 200 nl of siRNA were added by ECHO 550 in each well. DharmaFECT2 was gently mixed with OptiMEM and incubated for 5 min in RT. 5μl of OptiMEM/ DharmaFECT2 was transferred in each well and the mixture of OptiMEM/

DharmaFECT2/siRNA was incubated for 25min in RT. Then, in 40μl of growth media with no antibiotic but in presence of the inhibitors, where needed, 400 or 500 cells depending their growth rate, were added in each well and were incubated overnight. The next day, the media was replaced with fresh and the cells were incubated for 5 more days. The last day, the viability of the cells was determined by CellTiter-Glo Luminescent reagent as was described in section 2.2.4.

Table 2.12: List of genes included in the siRNA library.

Genes in the siRNA library							
ARID1A	CHD4	FZD6	KMT2D	RAD18	SMARCA1	TDP2	UBE2T
ATP23	CTPS1	HELQ	MCM7	REV1	SMARCA4	TEX14	USP10
ATRX	DDX3X	HELZ	MDN1	RSPO1	SMURF2	TLK2	WRN
BLM	DYRK3	HFM1	MEF2C	RUNX1	SMYD3	TNIK	XRCC1
BUD31	EIF4A3	KAT6A	PES1	SETD1A	SPINT2	TRIB1	XRCC5
CDK12	FANCM	KDM1A	PRIM1	SETD2	SRCAP	UBA2	XRCC6

2.2.14.1 siRNA screening analysis and hit selection

During the siRNA screening, each cell line was screened in 384-well plates and in each plate 16 wells of positive and 16 wells of negative siRNA controls were included. Additionally, two technical repeats for each cell line were included in each biological repeat of the siRNA screening. Initially, the average of the 16 luminescence values of the negative control in each plate was calculated and the luminescence value for each siRNA was normalised to the average value/plate. Then, the difference between the normalised values of each siRNA between the parental and the isogenic cells was calculated. The average of the difference values between the two technical repeats for each siRNA was calculated and the standard deviation (STDEV) value of all average final values was estimated. As hits were considered the siRNAs that their average value

was 1.5 times the STDEV value of all the siRNAs.

2.2.15 RNA extraction, cDNA synthesis and Real Time PCR

Depending the experiment, or the existence of treatment, appropriate number of cells were seeded in a 6-well plate so that the day of cell lysis, the cells were 90% confluent in the 6-well plate. Lysis of the cells was performed by RLT buffer from the Qiagen RNeasy Mini kit. The same kit was used for RNA extraction, according to manufacturer's instructions and the RNA was eluted in nuclease-free water and was quantified on NanoDrop 8000 Spectrophotometer. Then, cDNAs were synthesized using high-capacity cDNA reverse transcription kit, according to manufacturer's instructions. 0.5 μg of RNA was diluted in RNase-free water to a total volume of 10 μl. 10 μl of master mix was prepared and added to each RNA sample (Table 2.13). The samples were incubated at 25^{o}C for 10 min, followed by 120 min at 37^{o}C, 5 min at 85^{o}C and lastly were maintained at 4^{o}C. The cDNA samples were diluted 1:5 in RNase-free water and placed in an ECHO 384PP-well plate and stored at -20^{o}C.

Analysis of the gene expression was performed by Real-Time Polymerase Chain Reaction (RT-PCR). The forward and the reverse primer for a reference gene were equally mixed and diluted 1/50 in RNase-free water. A PCR mix was prepared as it is indicated in table 2.14. 5 μl of PCR mix were transfer in 384 PCR plates and 80 nl of cDNA were transferred by ECHO 550. The real-time PCR was performed by using the Quant Studio 6 Flexi RT-PCR machine (Life Technologies). The real-time PCR run for 40 cycles of amplification and at the end, the relative mRNA levels for each gene were calculated after normalization to β-ACTIN mRNA values using the ΔCt method.

Table 2.13: Master mix for cDNA synthesis.

Reagent	Volume/Sample (µl)
10X RT buffer	2
25X dNTP mix (100mM)	0.8
10X RT random primers	2
MultiScribe reverse transcriptase	1
Nuclease-free water	4.2
Total / reaction	**10**

Table 2.14: Real-time PCR mix for gene expression analysis.

Reagent	Volume/well (µl)
SYBR Green	0.5
Primers (1/50)	0.5
Nuclease-free water	2
Total / reaction	**5**

2.2.16 Microscopy

2.2.16.1 Time-lapse microscopy

Time-lapse microscopy was used to follow the fate of cells during or after drug treatments. Appropriate number of cells, with fluorescent nuclei, was seeded in 96-well Ibidi plates. Drug treatments were added or removed 3 hours before the time-lapse initiation and the fate of the cells was followed for 3 days, by using a 20X lens of Zeiss3i widefield microscope. 10 or 8 positions/well were captured in two different focal planes in order to achieve visualization of mitosis. Furthermore, H2B mCherry/ RFP/ GFP tagged cells were captured with phase contrast in addition to the corresponding fluorescent channels. Analysis of the videos was made with Slidebook 6 software.

2.2.16.2 Cell Imaging

Cell Imaging was performed in order to observe micronuclei formation, chromosome missegregation, expression of specific proteins, confluence, cell fusion or to count the chromosome number, with or without drug treatments. Appropriate number of cells was seeded in 96 well plates (black or transparent, depending the existence of fluorescence or not, respectively). Alive or fixed cells were imaged with Operetta, ImageExpress, CeligoS or EVOS in phase contrast or in the appropriate fluorescent channels. Quantification of chromosome number after metaphase spreads, was conducted by confocal microscopy. Analysis of the images was performed initially through MetaExpress, Harmony Software or CeligoS (for imaged derived from ImageExpress, Operetta or CeligoS, respectively) and then through Photoshop software (independently to the source of the images).

Chapter 3 - Targeting CIN in cancer

3.1 Introduction

Chromosomal instability is a type of genomic instability in which the chromosome number or structure is constantly changing. The main causes of CIN are errors in the mitotic machinery, in DNA damage response pathways, or impaired chromatin remodelling. In more detail, correct chromosome alignment and kinetochore microtubule attachments are essential for proper chromosome segregation and chromosomal stability (She et al., 2020). As described in chapter 1, the CENP-E inhibitor GSK923295 promotes errors in chromosome alignment. Treatment of cervical and colorectal cancer cells with GSK923295 induced high levels of chromosome missegregation and mitotic delay through activation of SAC, while increased concentrations of the inhibitor promoted apoptosis. However, when used in lower concentrations, GSK923295 generated missegregated chromosomes, the cells were arrested in mitosis but at the end were able to divide, possibly through SAC exhaustion (Bennett et al., 2015).

Impaired sister chromatid cohesion can also be a cause of chromosomal instability. Cohesion of sister chromatids is necessary in mitosis until the initiation of anaphase in order to avoid premature segregation and CIN (Sajesh et al., 2013). Interestingly, the SWI/SNF chromatin remodelling complex is important for sister chromatin cohesion and loss of BAF180 or BRG1 has been shown to promote anaphase bridges, lagging chromosomes and micronuclei formation (Bourgo et al., 2009, Brownlee et al., 2015, Brownlee et al., 2014). The SWI/SNF complex also plays a significant role in DNA damage response and repair. It has been shown that BRG1 binds to the promoters and transcriptionally activates ATM and ATR that are essential genes for DNA damage repair initiation. Also, subunits of the SWI/SNF complex interact or enable the recruitment of DNA damage repair proteins such as the KU70/KU80 complex, Rad52,

PCNA or BRCA1, as discussed in section 1.3.1.4. Defects in the SWI/SNF complex are linked with unrepaired DNA, chromosome breaks and micronuclei formation (Ribeiro-Silva et al., 2019, Kwon et al., 2014, Brownlee et al., 2015, Sethy et al., 2018, Ribeiro-Silva et al., 2018).

Loss of function in genes of DNA damage response have been linked to chromosomal instability and disease. For example, Ataxia-telangiectasia (A-T), caused by loss of ATM, is a genomic instability syndrome, an autosomal recessive condition in which patients have increased risk of developing epithelial malignancies (Ahmet and Rahman et al., 2006, Shiloh et al., 2003). ATM function is essential for response to DSBs and initiation of DNA damage repair through the homologous recombination repair pathway. Moreover, ATM phosphorylates and activates CHK2, which promotes proteasome degradation of CDC25C and G1/S cell cycle arrest. Thus, loss of ATM induces errors in DNA damage repair and progression of cell cycle even in the presence of unrepaired DNA, promoting chromosomal rearrangements, dicentric chromosomes and micronuclei formation (Drosos et al., 2017, Marechal and Zou, 2013). Similarly to ATM, ATR is also recruited in response of DSBs or SSBs and further promotes repair of the damaged DNA. Moreover, ATR promotes intra-S and G2/M cell cycle arrest in the presence of DNA damage by CHK1 and WEE1 activation. Loss of ATR promotes entry to mitosis even in the presence of damaged DNA, formation of micronuclei and chromosomal instability (Jardim et al., 2009, Wilhelm et al., 2020).

Chromosomal alterations can initiate tumour growth through gain of oncogenes or loss of tumour suppressor genes. CIN is also present during tumour progression, contributing to the intratumour genetic variations allowing the tumour to overcome selection barriers and metastasise (Bakhoom and Compton, 2012, Bakhoom and Landau, 2017, Bolhaqueiro et al., 2019, Jing et al., 2018). Moderate levels of CIN are linked with poor prognosis and tumour progression, however excessive CIN levels are associated with better prognosis as it cannot be tolerated by cancer cells and promotes cell death. Low expression of CENP-E induces CIN and promotes tumour growth in mice, however, CENP-E loss in different genetic contexts with ongoing instability

diminishes the tumour growth *in vivo* through excessive levels of chromosomal instability (Weaver et al., 2007, Turajilic et al., 2019, McGrahan et al., 2012).

The relationship of CIN degree with cancer prognosis can hypothetically be exploited therapeutically by driving chromosomal instability to excessive levels that reduce cancer cell fitness. Moreover, CIN may enable the discovery of novel synthetic lethal interactions in cancer cells, by inducing gene dependencies that do not exist normally. Thus, in order to identify potential targets in CIN, dependent or independent to specific gene interactions, chromosomal unstable cancer cellular models were generated and screened with a custom sgRNA library.

3.2 Results

3.2.1 Generation of chromosomally unstable cellular models

Chromosomal instability, as discussed in chapter 1, can be generated through defects in multiple pathways. In order to identify potential gene targets against CIN, different CIN models were generated by inhibiting CENP-E, ATM, CHK1 or CHK2. Initially, the sensitivity of HCT116p53$^{-/-}$ and DLD1 cells to the CENP-E inhibitor GSK923295, the ATM inhibitor KU60019 or the CHK1/CHK2 inhibitor CCT241106 was investigated. Growth inhibition of the cells in response to different concentrations of the inhibitors for six days were measured by CellTiter-Glo and the half maximal inhibitory concentrations (IC_{50}) were calculated. For the HCT116p53$^{-/-}$ cells, the IC_{50}s of GSK923295, KU60019 and CCT241106 were 0.196 μM, 1.52 μM and 1.78 μM, respectively. Correspondingly, for DLD1 cells the IC_{50} of GSK923295 compound was 0.45 μM, of KU60019 to 3.02 μM and of CCT241106 to 2.47 μM (Figure 3.1 A-D).

Three concentrations for each compound were selected that did not induce more than 80% reduction in cell viability. Specifically, in HCT116p53$^{-/-}$ cells, concentrations of 7.5 nM, 15 nM and 30 nM for GSK923295 and 0.625 μM, 1.25 μM and 2.5 μM for KU60019 and CCT241106 were selected to confirm the induction of CIN. CENP-E

inhibition promotes chromosome missegregation, thus the percentage of missaligned chromosomes was identified by looking for missegregated chromosomes by immunofluorescence. HCT116p53$^{-/-}$ cells were treated with the three different concentrations of the GSK923295 for 72 hours. Following the treatment, the cells were fixed and stained for phosphorylated histone H3 (pHH3), which stains the mitotic DNA, and with Aurora A, to visualise the mitotic spindle. Compared to the DMSO control, 30 nM of GSK923295 induced more than 15% increase of mitotic cells with chromosome missegregation errors (Figure 3.2 A).

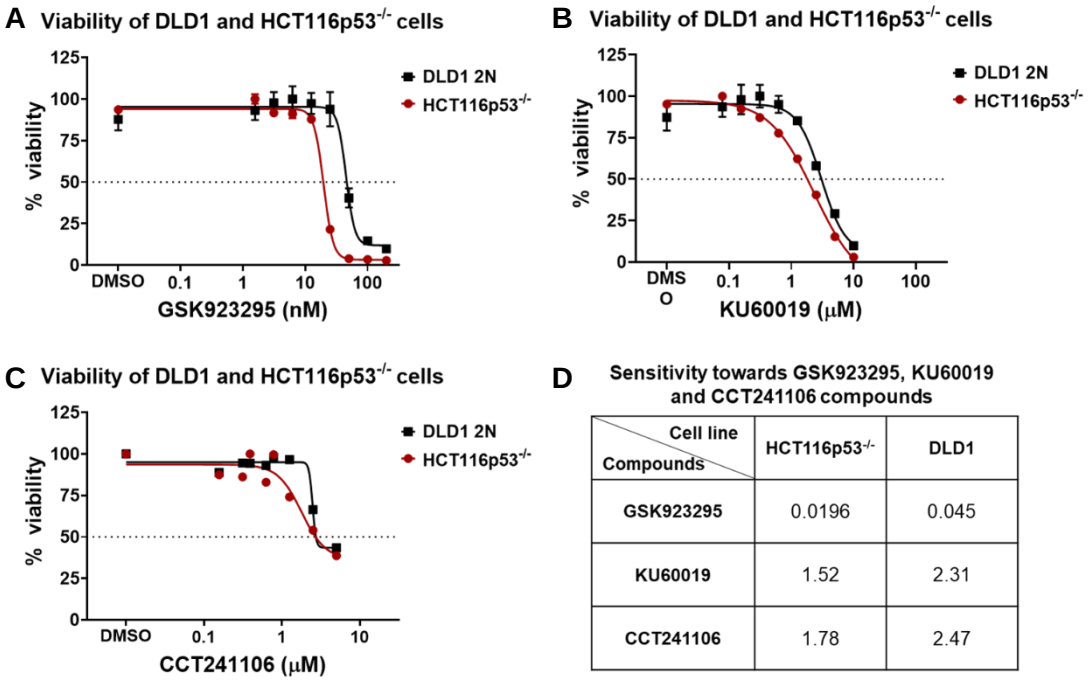

Cell line / Compounds	HCT116p53$^{-/-}$	DLD1
GSK923295	0.0196	0.045
KU60019	1.52	2.31
CCT241106	1.78	2.47

Figure 3.1: Sensitivity of HCT116p53$^{-/-}$ and DLD1 cells to GSK923295, KU60019 and CCT241106. (A) 6-day growth inhibition assay with GSK923295 with highest concentration of 150nM followed by 7 1/2 serial dilutions. **(B)** 6-day growth inhibition assay with KU60019 with highest concentration of 10 μM followed by 7 1/2 serial dilutions and **(C)** 6-day growth inhibition assay with CCT241106 with highest concentration of 5 μM followed by 7 1/2 serial dilutions. **(D)** Estimated IC_{50} values in μM, after dose response of GSK923295, KU60019 and CCT241106 compounds for 6 days that were presented in A, B and C.

Inhibition of ATM or CHK1 and CHK2 promotes chromosome breaks that can lead to micronuclei formation in the following cell cycle, thus the percentage of micronuclei that were induced after ATM or CHEK1,CHK2 inhibition was identified. HCT116p53$^{-/-}$ cells were treated with 0.625 μM, 1.25 μM and 2.5 μM of KU60019 or CCT241106 for 72 hours, fixed and the nuclei were stained with Dapi. Increasing

concentrations of KU60019, increased the percentage of micronuclei that were formed in the cells peaking at 20% more miconuclei after treatment with 2.5 μM, compared to the DMSO control (Figure 4.2 B). Similarly to KU60019, CCT241106 also increased the formation of micronuclei in a dose dependent manner and peaking at 25% more, at 1.25 μM compared to approximately 5% in the DMSO control. Treatment with 2.5 μM of CCT241106 showed increased percentage of micronuclei, albeit to a lesser extent, possibly due to promoting excessive CIN levels and cell death (Figure 3.2 C).

The growth inhibition data, combined with the chromosome missegragation and micronuclei formation experiments enabled us to identify conditions in which the cells can still grow, albeit more slowly than their untreated counterparts, while presenting CIN. Thus, for the experiments that followed, the cells were always pre-treated for three days with 20nM GSK923295, 1 μM KU60019 or 1 μM CCT241106 in order to induce CIN and the compounds were not removed until the end of the experiments.

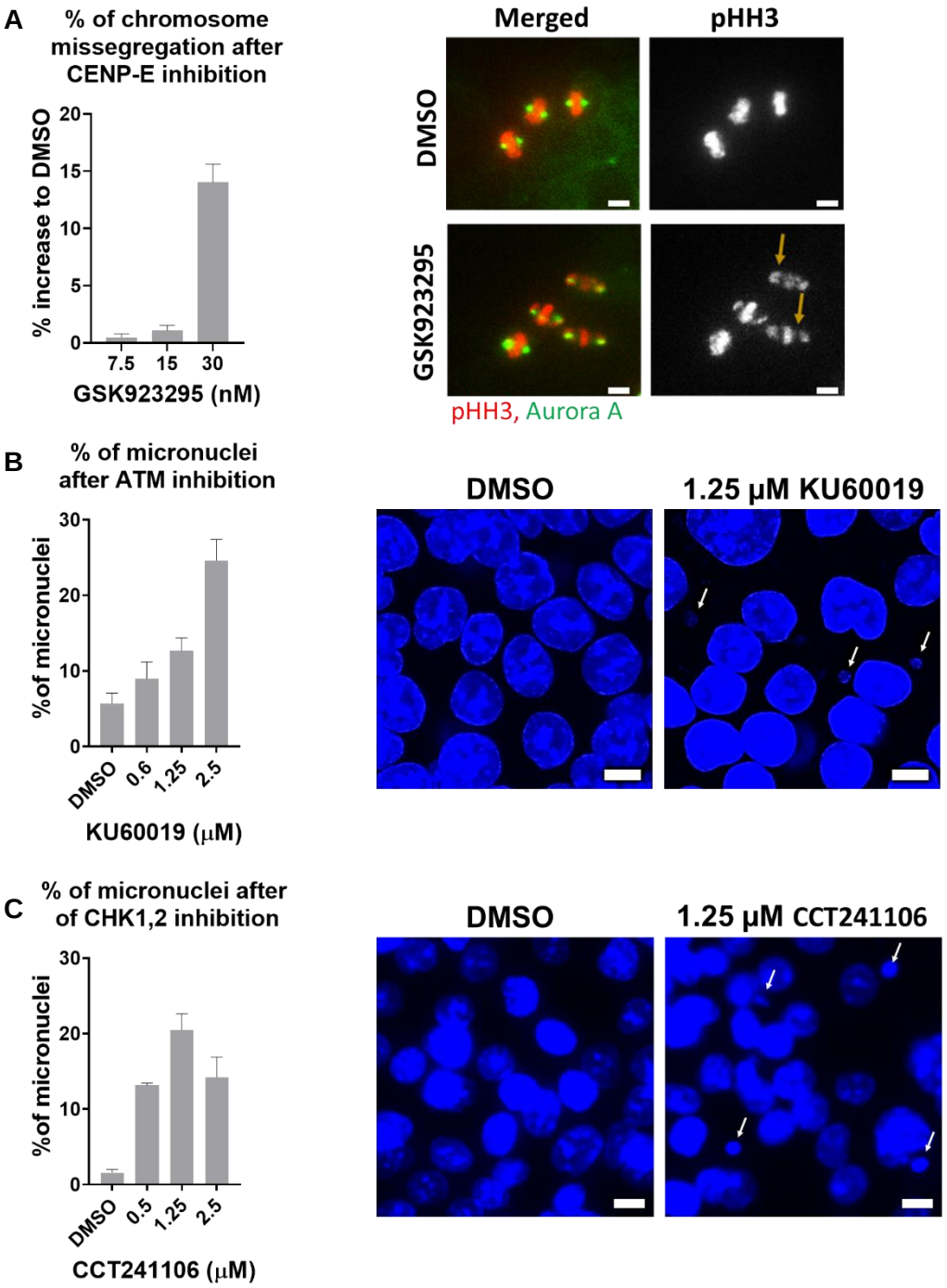

Figure 3.2: Induction of CIN in HCT116p53$^{-/-}$ cells after treatment with GSK923295, KU60019 and CCT241106 compounds. (A) Percentage of increase of mitotic cells with chromosome missegregation after treatment with 7.5 nM, 15 nM and 30 nM of GSK923295 for 72 hours. Red illustrates the pHH3 staining and green the AuroraA and the arrows indicate examples of chromosome missegregation. Imaged and analysed by ImageXpress. **(B)** Percentage of micronuclei formation after treatment with 0.625 nM, 1.25 μM and 2.5 μM of KU60019 for 72 hours. Blue illustrates the staining of the nuclei with Dapi and the arrows indicate examples of micronuclei. **(C)** Percentage of micronuclei formation after treatment with 0.625 nM, 1.25 μM and 2.5 μM of CCT241106 for 72 hours. Blue illustrates the staining of the nuclei with Dapi and the arrows indicate examples of micronuclei. Scale bar at 10 μm. Error bars illustrate SEM between the number of micronuclei in three different replicates from one experiment. 1000 cells / condition were counted.

3.2.2 Hit identification to target CIN

To identify potential targets in CIN, a CRISPR/Cas9 loss of function screening was conducted. CIN was induced by CENP-E, ATM or CHK1/CHK2 inhibition in HCT116p53$^{-/-}$ and DLD1 cells and the generated CIN models as well as the chromosomally stable parental cell lines were screened, for 21 days, with a custom sgRNA library, against 200 genes. These genes are involved in pathways of DNA damage response/repair, metabolism, DNA replication and chromosomal instability and have been identified as potential hits in aneuploidy or CIN or have emerged from recent publications on Breast and Pancreatic TCGA mutation data (Table 2.10). The screening aims to identify genes that selectively kill cells that present CIN features either regardless of the driver of CIN or due to the inhibition of a subset of the CIN-drivers that were selected for these CIN models. In order to expand the panel of CIN models, an extra CIN model generated by impaired function of SWI/SNF complex was used. U2OSBAF180$^{-/-}$ and HCT116BRG1$^{-/-}$ isogenic cell lines were provided by Professor Jessica Down's lab and were further included in the loss of function CRISPR/Cas9 screen.

3.2.2.1 Targeting CIN by CRISPR/Cas9 loss of function screening

Stable HCT116p53$^{-/-}$Cas9, DLD1Cas9 cells and stable U2OSCas9 and HCT116Cas9 cells as well as Cas9-expressing BAF180$^{-/-}$ and BRG1$^{-/-}$ isogenic cell lines were generated. In line with the workflow given by Dharmacon, which was presented in figure 2.3, the cells were transduced with the Edit-R inducible Cas9 lentivirus. This system allows the generation of stable cell lines that express Cas9 in response to doxycycline, while, at the same time, conferring resistance to blasticidin (BlastR) (Figure 2.1). Similarly, the sgRNA vector expresses a puromycin resistance gene (PuroR), which allows for rapid selection of cells with integrated sgRNA (Figure 2.2). However, the Edit-R Lentiviral Cas9 expression and sgRNA expression vectors do not contain a fluorescent reporter. Therefore, SMARTvector non-targeting control lentiviral particles, containing a green fluorescent protein (GFP) reporter gene, were used for optimization of transduction conditions. Notably, the SMARTvector has a known reference titer from which the

functional titer in the cell lines of interest was estimated. In order to estimate the relative transduction efficiency, the cells were transduced with different concentrations of the SMARTvector lentiviral particles in growth media with reduced FBS (4%). Media with increased FBS to reach a final of 10% was added on the next day and after 24 hours the percentage of GFP positive cells was quantified by immunofluorescence. Increasing the concentration of the viral particles increased the percentage of Cas9 positive cells, reaching approximately 50% for HCT116p53$^{-/-}$ cells, 32% for DLD1, 35% for HCT116 and 52% for U2OS in the maximum concentration of the viral particles used (Figure 3.3).

In parallel, the HCT116p53$^{-/-}$, DLD1 cell lines and the U2OS, HCT116 cells and their isogenic counterparts were assayed for their sensitivity to different concentrations of the antibiotics blasticidin and puromycin to identify the optimal concentrations for selection of the Cas9 and sgRNA transduced cells. The highest concentrations tested were 15 μg/ml and 5 μg/ml for blasticidin and puromycin, respectively (Figure 3.4 A and B). Based on the CellTiter-Glo viability assay, 15 μg/ml of blasticidin and 1 μg/ml of puromycin were selected, as at these concentration, a 100% reduction in the viability of untransduced cells was achieved. In addition, the appropriate concentration of doxycycline was identified using viability assays in order to estimate the degree of toxicity of the antibiotic in untransduced cells. A maximum concentration of 10 μg/ml of doxycycline was tested, however this concentration induced toxicity to the cells. Thus, a concentration of 1 μg/ml was pre-selected as it was the highest concentration of doxycycline that did not induce toxicity (Figure 3.4 C).

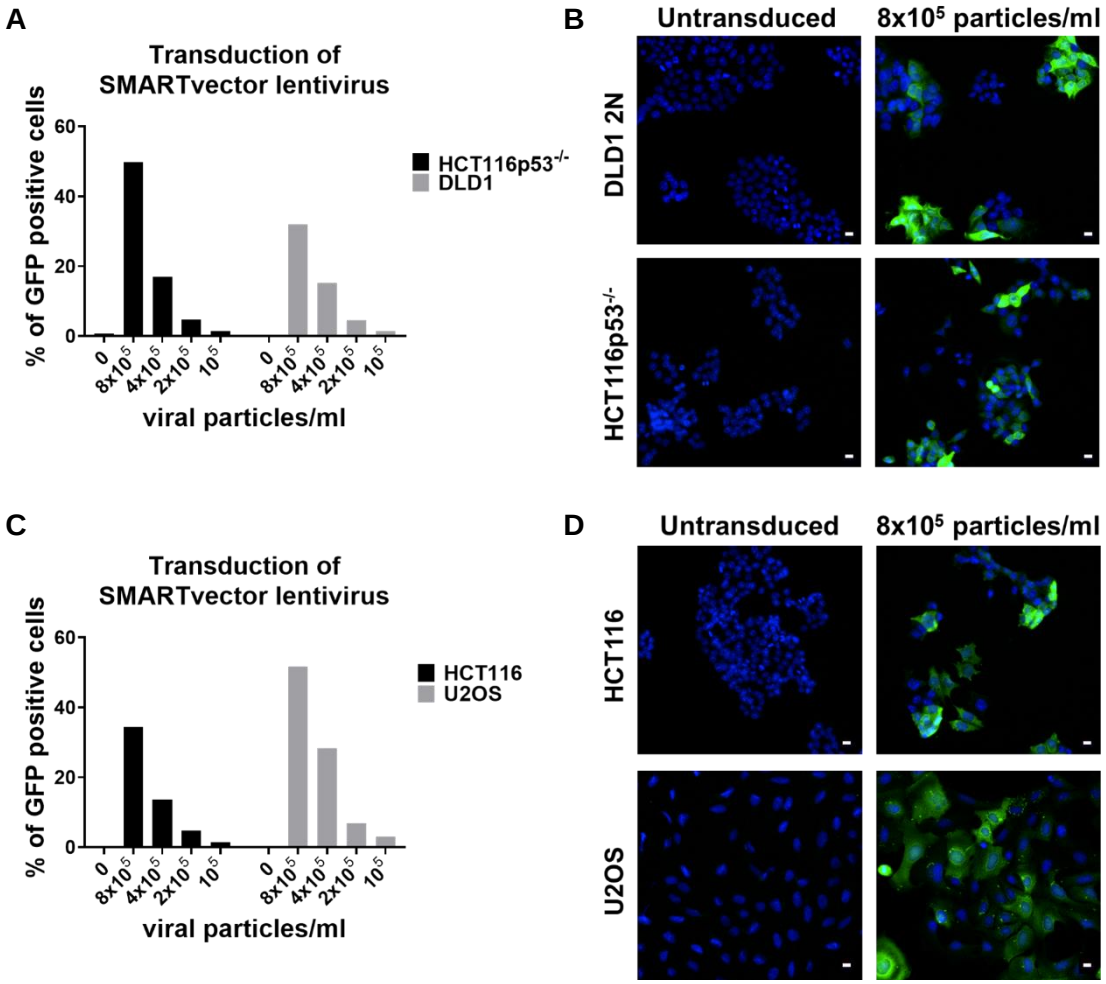

Figure 3.3: Percentage of GFP positive cells in the parental cell lines. (A) Percentage of GFP positive HCT116p53$^{-/-}$ and DLD1 cells in four different concentrations of viral particles calculated through GFP expression from Operetta High Content microscope. **(B)** Illustration of viral infectivity of HCT116p53$^{-/-}$ and DLD1 cells in the highest concentration of particles compared to the non-transduced cells. **(C)** Percentage of GFP positive HCT116 and U2OS cells in four different concentrations of viral particles calculated through GFP expression analysis. **(D)** Illustration of viral infectivity of HCT116 and U2OS cells in the highest concentration of particles compared to the non-transduced cells. Images were taken with Operetta and analysed with Harmony Software. The nuclei are stained with Dapi (blue) and GFP with GFP antibody (green). Scale bat at 10µm.

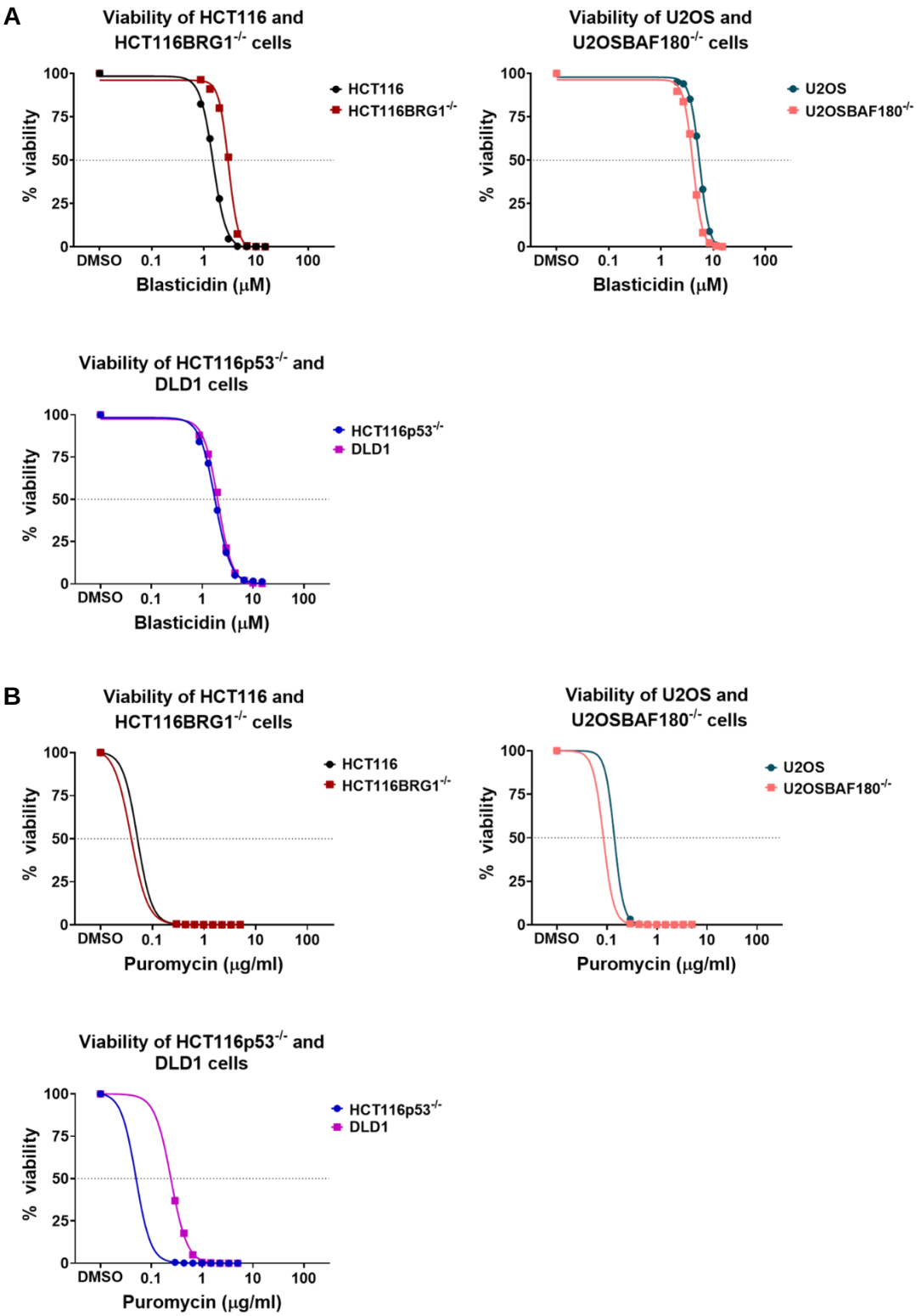

Figure 3.4: Sensitivity of untransduced HCT116p53$^{-/-}$, DLD1 and HCT116, U2OS and their isogenic cell lines to antibiotics. Figure continues at the next page.

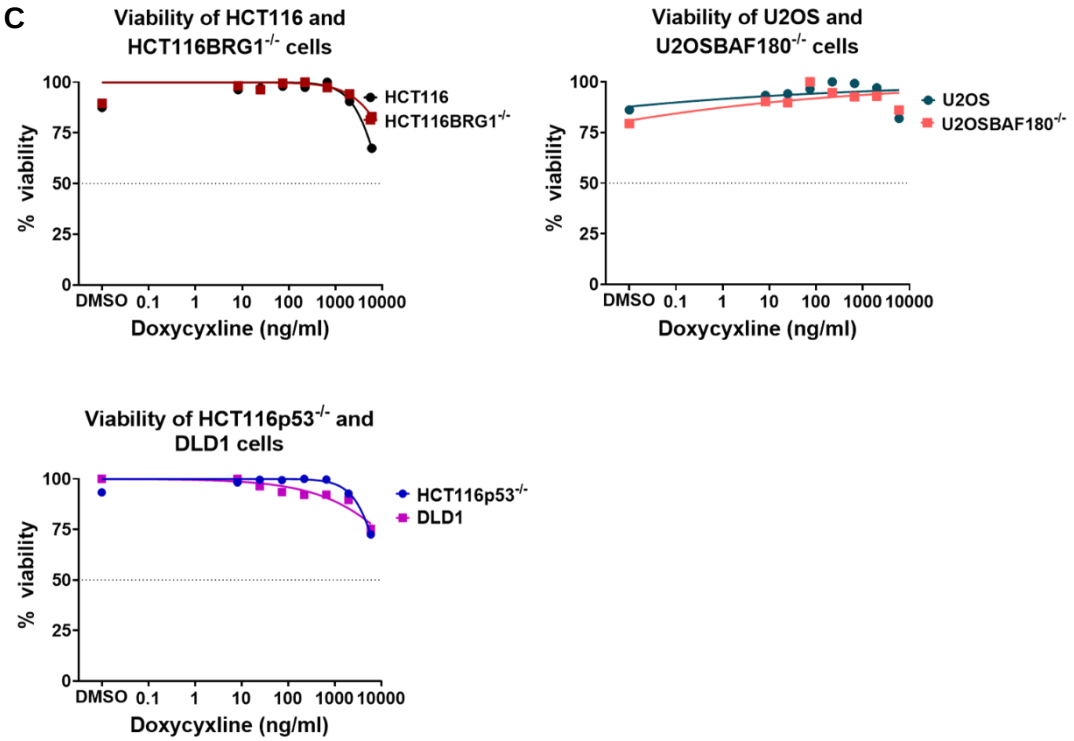

Figure 3.4: Sensitivity of untransduced HCT116p53$^{-/-}$, DLD1 and HCT116, U2OS and their isogenic cell lines to antibiotics. (A) Sensitivity of cells to blasticidin treatment with a highest concentration of 15 µg/ml followed by 7 1/1.5 serial dilutions. **(B)** Sensitivity of cells to puromycin treatment with a highest concentration of 5 µg/ml followed by 7 1/1.5 serial dilutions. **(C)**Sensitivity of cells to doxycycline treatment with a highest concentration of 10 µg/ml followed by 7 1/10 serial dilutions.

Following the estimation of the functional titter and the appropriate concentrations of the antibiotics, the CRISPR/Cas9 inducible cell lines were generated by reverse transduction. Two days after the transduction, 15 µg/ml of blasticidin was added for the selection of the Cas9 infected cells. Selection with blasticidin continued for approximately 7 days, until no growing cells could be detected in the untransduced controls and was subsequently reduced to 5 µg/ml. During this period the infected cells where split as necessary.

Induction of Ca9 by doxycycline was confirmed by immunofluorescence and immunoblotting. Initially, the percentage of Cas9 positive cells was identified by immunofluorescence in response to six different concentrations of doxycycline with a maximum of 2 µg/ml. Antibody staining for Cas9 indicated that approximately 0.074 µg/ml of doxycycline can induce the maximum amount of Cas9 positive cells. However the percentage of Cas9 positive cells for HCT116p53$^{-/-}$, HCT116 and HCT116BRG1$^{-/-}$

was 55%, 60% or 40%, respectively (Figure 3.5 A). Thus, the cells were transduced for a second time and after doxycycline addition, the percentage of cas9 positive cells was identified by immunofluorescence. Second transduction with the Cas9 virus increased the percentage of Cas9 positive cells to approximately 85% for HCT116p53$^{-/-}$, DLD1 and HCT116 cells and 75% for the HCT116BRG1$^{-/-}$ cells (Figure 3.5 B). Additionally, Cas9 expression was confirmed by immunoblotting after 96 hours of treatment with 0.1 μg/ml and 1 μg/ml of doxycycline. Treatment of untransduced cells with 1 μg/ml doxycycline and infected cells with no doxycycline, demonstrated no induction of Cas9, while infected cells with either 0.1 μg/ml or 1 μg/ml doxycycline produced a strong signal (Figure 3.5 C). Thus, a total of 0.1 μg/ml of doxycycline was selected in order to promote Cas9 expression, as it was the lowest doxycycline concentration that ensures the highest Cas9 expression without toxicity.

The stable Cas9 cell lines were transduced with the sgRNA library and the cells with the integrated sgRNAs were selected with 1 μg/ml puromycin. Untransduced Cas9 cells were used as control and the puromycin selection lasted for approximately 5 days, until no cell population was growing in the untaransduced control (Figures 3.6 and 3.7). Following selection with puromycin, the HCT116 and U2OS parental cells, as well as their isogenic CIN models were separated in two groups. In the first group, DNA was extracted, named as baseline, while in the second, 100ng/ml of doxycycline was added for 4 days and after 16 days of culturing and splitting as needed, DNA was extracted, named as endpoint DNA. A minimum of 10 million cells was preserved after each split in order to maintain the required coverage of the sgRNAs within the cell population.

The HCT116p53$^{-/-}$Cas9 and DLD1Cas9 cell lines were transduced with the sgRNA libraries, selected with puromycin and then separated in four distinct groups. In order to induce CIN, the cells in the first group were treated with 20 nM of GSK923295, in the second group with 1 μM KU60019, while in the third group with 1 μM CCT241106. In the last group none of the inhibitors was added, thus the cells remained chromosomally stable. Three days after the treatments, each group of cells was subdivided in two categories. In the first, the baseline DNA was extracted, while in the

second, the treatments with the inhibitors continued, but also doxycycline was added for 4 days to induce Cas9 expression. Following 16 days of culture with the inhibitors to continiously generate errors and CIN, the endpoint DNA was extracted. This time period was selected in order to ensure that the effect of each gene deletion in cell viability will be visible. All the DNA samples were sent to Horizon for next generation sequencing (NGS).

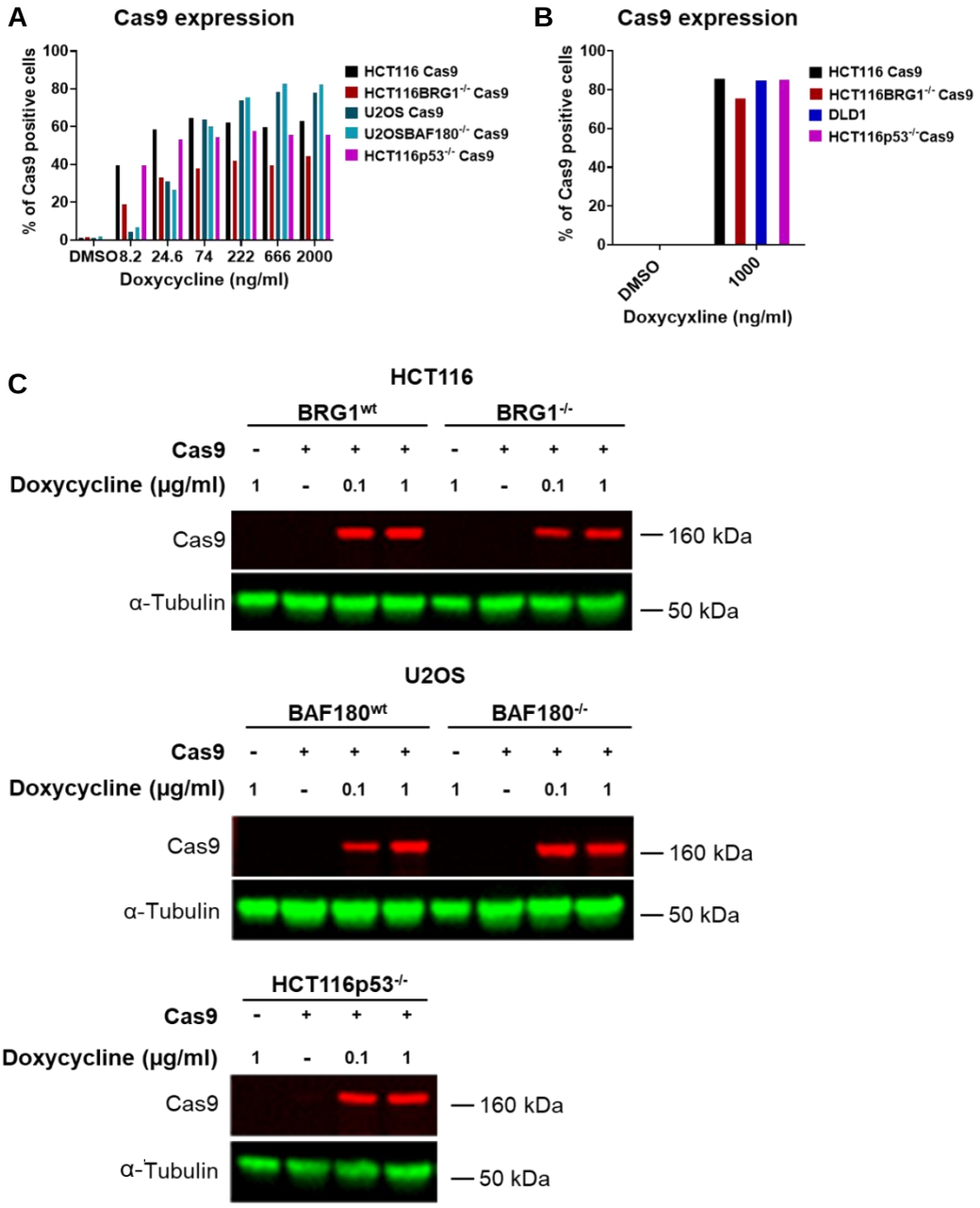

Figure 3.5: Cas9 expression after induction by doxycycline. (A) Percentage of Cas9 positive HCT116p53$^{-/-}$, HCT116, U2OS and BRG1$^{-/-}$ and BAF180$^{-/-}$ isogenic cell lines by immunofluorescence, after treatment with six different concentrations of doxycycline for 72 hours. **(B)** Final percentage of Cas9 positive HCT116p53$^{-/-}$, DLD1, HCT116 and HCT116BRG1$^{-/-}$ cell lines by immunofluorescence, after second viral infection and treatment with 1 μg/ml doxycycline for 72 hours. **(C)** Western blot illustration of uninfected and infected cells with no doxycycline addition or after the treatment with 0.1 μg/ml or 1 μg/ml doxycycline.

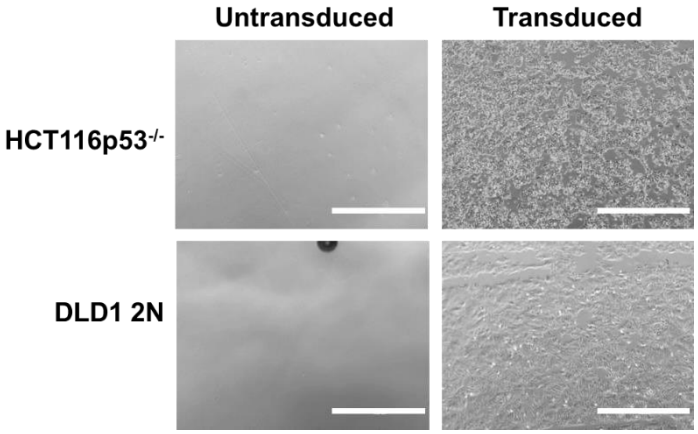

Figure 3.6: Viral transduction of HCT116p53$^{-/-}$ and DLD1 parental cell lines with the Edit-R sgRNA lentivirus and selection with puromycin. Selection was made with 1 µg/ ml puromycin. Photographs were taken by 4x lens of EVOS FL microscope 4 days after initial treatment with puromycin. Scale bar at 100 µm.

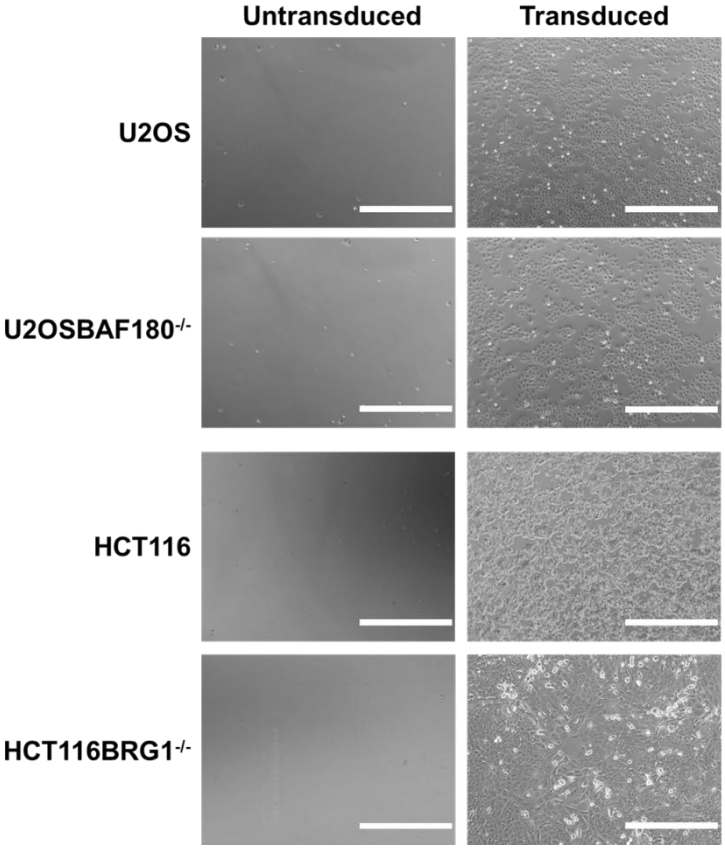

Figure 3.7 Selection of transduced HCT116 and U2OS cell lines with the Edit-R sgRNA lentivirus. Selection was made with 1 µg/ml puromycin for 5 days. Photographs were taken by 4x lens of EVOS FL microscope. Scale bar at 100 µm.

3.2.2.2 Hit identification in CIN by CRISPR/Cas9 loss of function screening

Prior to performing next generation sequencing, the quality of the samples was investigated by the outsourced company. Nevertheless, due to technical limitations, the majority of the DNA samples did not pass the PCR quality control and the products were not visible after PCR amplification. The list of the samples that failed the quality control included the baseline samples from the parental HCT116, HCT116p53$^{-/-}$ cells and the CIN HCT116p53$^{-/-}$ cells treated with KU60019 and the endpoint sample of U2OSBAF180$^{-/-}$ cells (Figure 3.8). However, the parental DLD1 cell line and the CIN models generated after treatment with KU60019, GSK923295 or CCT241106 compounds passed the quality control and the results from the NGS were further analysed to identify hits in CIN.

For each cell line, normalised counts from the baseline were subtracted from normalised counts from the endpoint, in order to identify sgRNAs that were selectively depleted in the endpoints of the models of interest. In the library, 10 different sgRNAs for PLK1 were included and used as positive control, while 30 non-targeting sgRNAs that were also present, were used as negative control. The PLK1 sgRNAs were mainly depleted in the endpoint samples, but the non-targeting sgRNAs were the majority of the sgRNAs that were enriched in the endpoint sample relatively to the baseline, likely due to the library enrichment for potential targets (Figure 3.9). Similarly, NGS counts for sgRNAs of potential targets are expected to be decreased in the endpoints of the CIN models compared to the baselines but not in the parental cell lines. Thus, in the DLD1 CIN models, as hits were considered sgRNAs that were depleted in the endpoints of the samples but not in the endpoint of the parental DLD1 parental cell line. However, because the baseline of the parental HCT116 cell line did not pass the quality control, the HCT116BRG1$^{-/-}$ sample was compared with the DLD1 parental cell line. Moreover, hits in the U2OSBAF180$^{-/-}$ cell line could not be identified as the endpoint sample did not pass the quality control (Figure 3.8). A large number of potential hits were identified due to the technical limitations of the screen and the lack of an appropriate control cell line in the BRG1$^{-/-}$ model. Thus, we prioritised hits that have been previously shown to be

associated to the gene of interest for each individual model. For example, in the CENP-E inhibited model we prioritised TEX14, FANCM and MCM7 (Figure 3.10 A). Additionally, because ATM, CHK1 and CHK2 belong in the DNA damage response, and ATM and CHK2 are highly associated, we clustered these proteins and we prioritised hits as PRIM1, WRN, MCM7 or RAD18 that are known to be associated with our models (Figure 3.10 B). Similarly, for SWI/SNF model, we prioritised hits that are associated with BRG1 (SMARCA4) and BAF180 (PBRM1) proteins, such as SMARCA1, KAT6A or KMT2D, in order to continue with the hit confirmation (Figure 3.10 C).

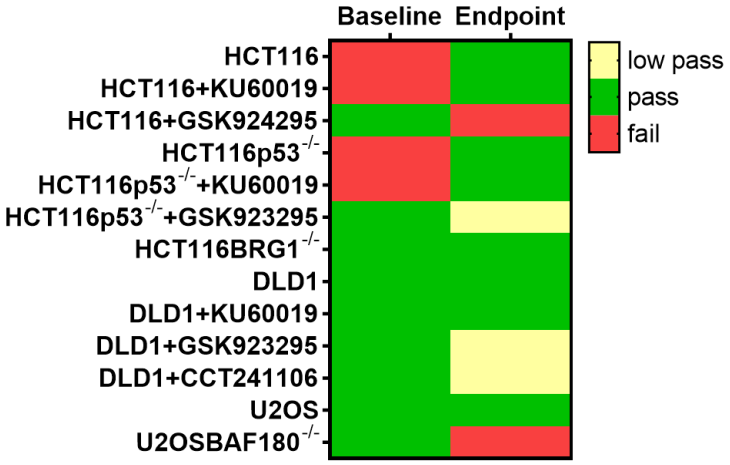

Figure 3.8: Status of samples after the quality control. Pass demonstrates that the amplified PCR product was able to be identified in the sample, low pass that the product could be roughly identified, while fail represent the samples, in which the products could not be identified after PCR amplification.

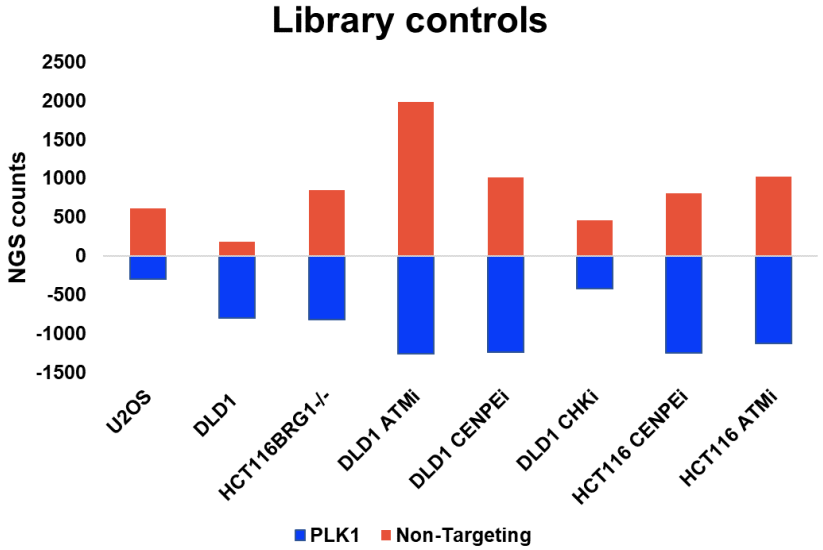

Figure 3.9: Normalised NGS counts of positive and negative controls in the library. The average normalised NGS counts for the PLK1 and the non-targeting sgRNAs in the baseline samples were subtracted from the corresponding counts in the endpoint samples.

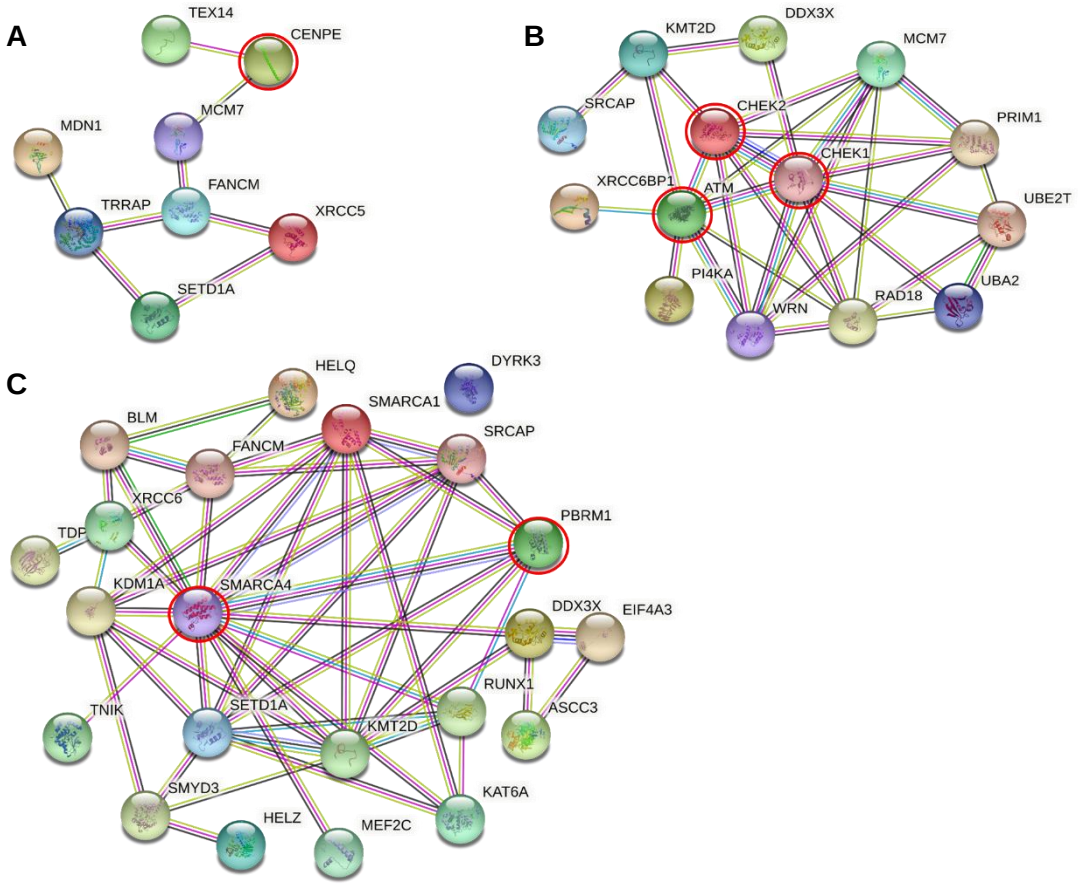

Figure 3.10: Interaction networks of potential hits with the genes of interest. (A) Hits associated with CENP-E. **(B)** Hits associated with ATM, CHK1 and CHK2 and **(C)** hits associated with BRG1 (SMARCA4) and BAF180 (PBRM1). The red circles illustrate the proteins of interest and were included as "bait" to identify interacting proteins from the hit list. SMARCA4: BRG1. PBRM1: BAF180.

3.2.3 Hit confirmation in CIN

Confirmation of the hits that were identified in the CRISPR/Cas9 loss of function screening was performed by three different approaches. Initially, all the CIN models were screened with a custom siRNA library, containing four different siRNAs for each gene that was identified as a potential hit from the CRISPR/Cas9 screening. This approach enabled a fast, high-throughput initial confirmation of the hits, in order to eliminate any false positive hits that might have emerged due to the technical issues generated in the PCR library preparation step or subsequent NGS analysis, which due to these limitations was only run once (N=1). Secondly, viability assays were performed using either existing selective small molecule inhibitors if available, or sets of four siRNAs towards the hits.

The latter underwent an additional confirmation by colony formation assays, using individually each of the four siRNAs per hit.

3.2.3.1 Hit confirmation by siRNA screening

To confirm the hits identified from the CRISPR/Cas9 loss of function screening, the CIN models were screened against a custom siRNA library that included negative, non-targeting control as well as a positive control (siRNA toxic) to confirm efficient transfection of the siRNAs. DLD1 cells were pre-treated for three days with 20 nM of GSK923295, 1 µM of KU60019 or 1 µM of CCT241106 in order to induce CIN and together with the HCT116BRG1$^{-/-}$, the U2OSBAF180$^{-/-}$ and the corresponding untreated or parental cells, they were screened against the siRNA library at a final siRNA concentration of 20 nM. The viability of the cells was measured five days after the siRNA transfection by CellTiter-Glo.

For each CIN model, each siRNA was present in duplicate, except for the siRNA control and the siRNA toxic (referred here as siRNAtox) that had 16 replicas each. Moreover each screening was performed in triplicate. Initially, for each cell line, the average of raw luminescence values for the siRNAcontrols was calculated and, in order to estimate growth inhibition, luminescence values from each siRNA were subtracted from the average luminescence value of the siRNA control replicates. Then, the average growth inhibition from each siRNA duplicate value was calculated and the difference between siRNAs in parental cells and in each corresponding CIN model was estimated. For each CIN cell line, the average of the three biological repeats was calculated. Values above 0 indicate that the siRNA reduces the viability of CIN cells compared to the parental cells, while values below 0 indicates that the siRNA enhances the CIN cells to outgrowth the parental. Then, the standard deviation of the differences for each model was claculated across all siRNAs. In this analysis, we consider as hits the siRNAs that produced differences that were higher than 1.5 the standard deviations (Figure 3.11).

Using this hit selection criteria, 2 siRNAs against each of DDX3X, REV1, DYRK3 or HFM1 appeared to be selective towards HCT116BRG1$^{-/-}$ cells relative to the parental

cell line. In addition, 3 siRNAs against PRIM1 selectively reduced the viability of DLD1 CIN cells, induced by treatment of CHK1 and CHK2 inhibitor CCT241106 (Figure 3.11). However, in the majority of the hits, the differences of all the siRNAs or three of the four siRNA, were above 0, indicating a trend of sensitivity (but less than 1.5-fold the standard deviation threshold) towards the CIN models, when compared to the parental cell lines. For example, in HCT116BRG1$^{-/-}$ cells, the hits DDX3X, REV1, KAT6A or HFM1 contained at least three siRNAs each that showed selectivity towards the BRG1$^{-/-}$ cells (Figure 3.12). Aditionally, the same results were obsered for hits in CIN cells induced by treatment of KU60019, CCT241106 or GSK923295 (Figures 3.13, 3.14 and 3.15).

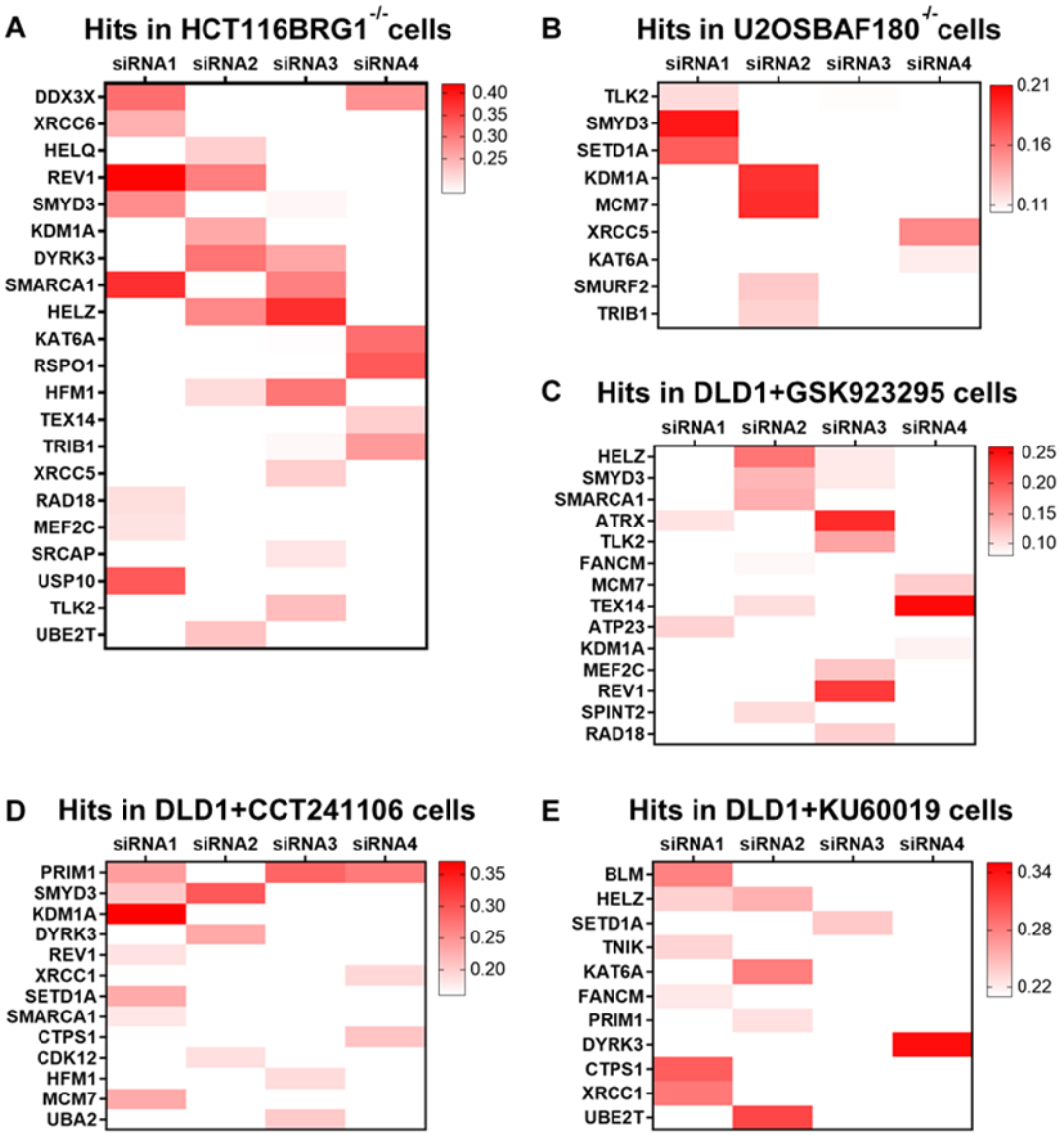

Figure 3.11: Hit confirmation by siRNA screening in the CIN models. (A-E) Heatmap of growth inhibition relative to control cells for each siRNA in HCT116BRG1$^{-/-}$ cells, in U2OSBAF180$^{-/-}$ cells and in DLD1 cells continuously treated with 20 nM GSK923295 (CENP-E inhibitor) or 1 µM CTT241106 (CHK1/CHK2 inhibitor) or 1 µM KU60019 (ATM inhibitor). The red gradient illustrates

the hierarchy of the siRNA differences that were higher than 1.5 STDEV of all the siRNA values in each model. Mean from three biological replicates is shown.

In the second BAF180$^{-/-}$ model, a small group of hits were identified but only one siRNA in each group demonstrated high selectivity towards BAF180$^{-/-}$ cells and that obesrvation was confirmed as shown in Figures 3.11 B and 3.16. To further investigate these results, the expression of BAF180 in the U2OS was tested by immunobloting. We noticed that BAF180 was reduced only by 50% in the isogenic cells compared to the parental (Figure 3.17 A). Thus, residual expression of BAF180 in the BAF180$^{-/-}$ model, may be responsible for the reduced selectivity towards this model and further confirmation of the hits in the SWI/SNF models continued only in the BRG1$^{-/-}$ cells as the knockout of the protein was confirmed by immunoblotting (Figure 3.17 B). Only the final confirmed hits in the BRG1$^{-/-}$ cells, were further investigated in the BAF180$^{-/-}$ cells.

Interestingly, hits that were selective towards specific drivers of CIN were observed. ATRX, TEX14, ATP23 and SPINT2 were hits in CIN cells induced by CENP-E inhibition using the GSK923295 compound. In the CIN model generated by ATM inhibition, using the KU60019 compound, BLM and TNIK were identified as selective hits, while CDK12 and UBA2 presented selectivity towards the model generated after CHK1 and CHK2 inhibition with the CCT241106 compound. DDX3X, XRCC6 and HELQ were sellective in the SWI/SNF model, generated by BRG1 deletion, and TRIB1 was the only selective hit for BRG1 and BAF180 deleted cells. Additionally, ATM and CHK1,CHK2 are involved in the same DNA damage response pathways and as expected, PRIM1 and CTPS1 were identified as hits in both models (Figure 3.18).

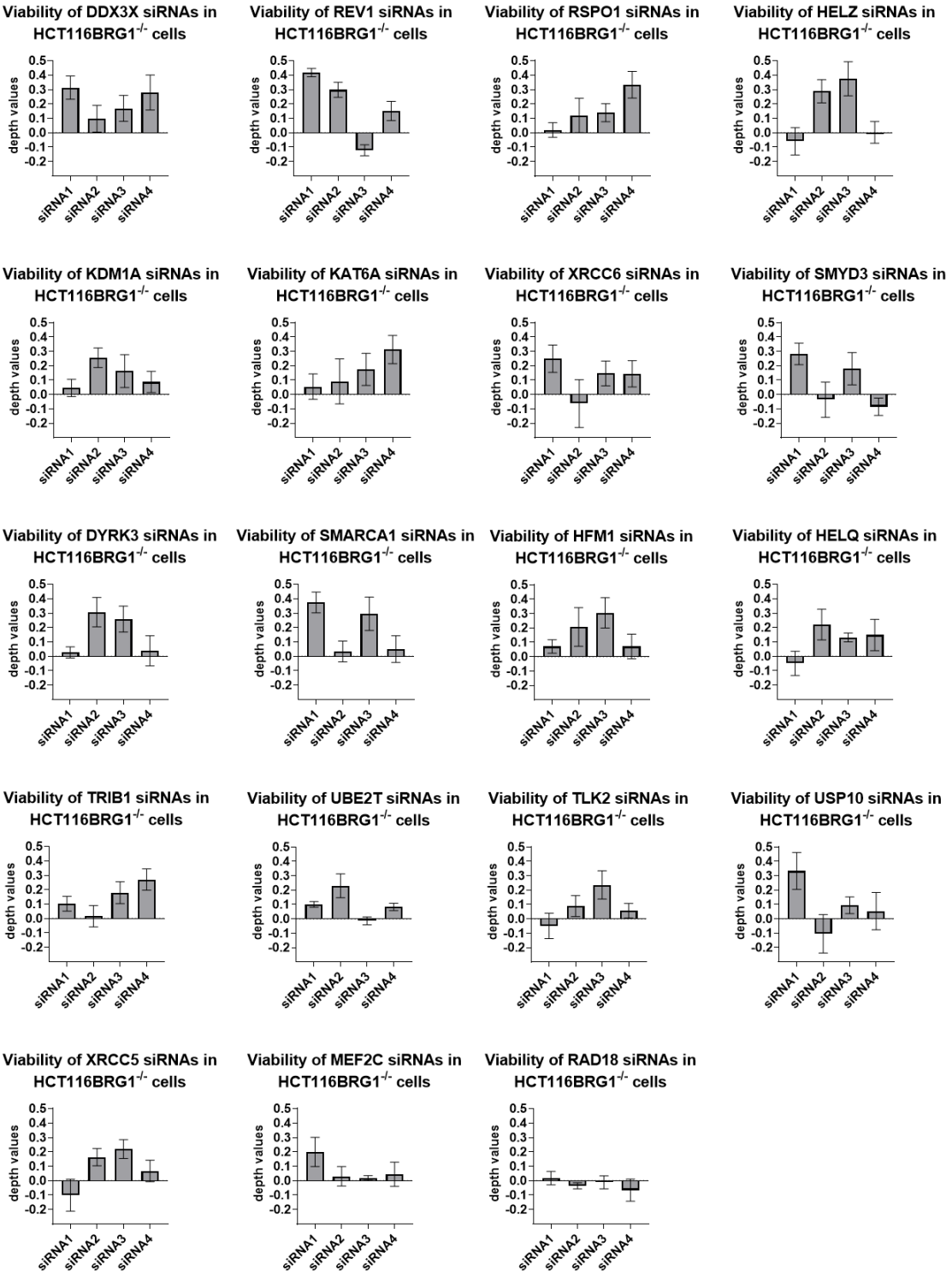

Figure 3.12: Confirmed hits in HCT116BRG1$^{-/-}$ by siRNA screen. Plots represent growth relative to control cells for each siRNA per gene. A value > 0 demonstrates sensitivity of the siRNA towards the BRG1$^{-/-}$ cells, while a value < 0 shows the outgrowth of the SWI/SNF impaired cells compared to the parental cells. Bars indicate SEM from three biological replicates.

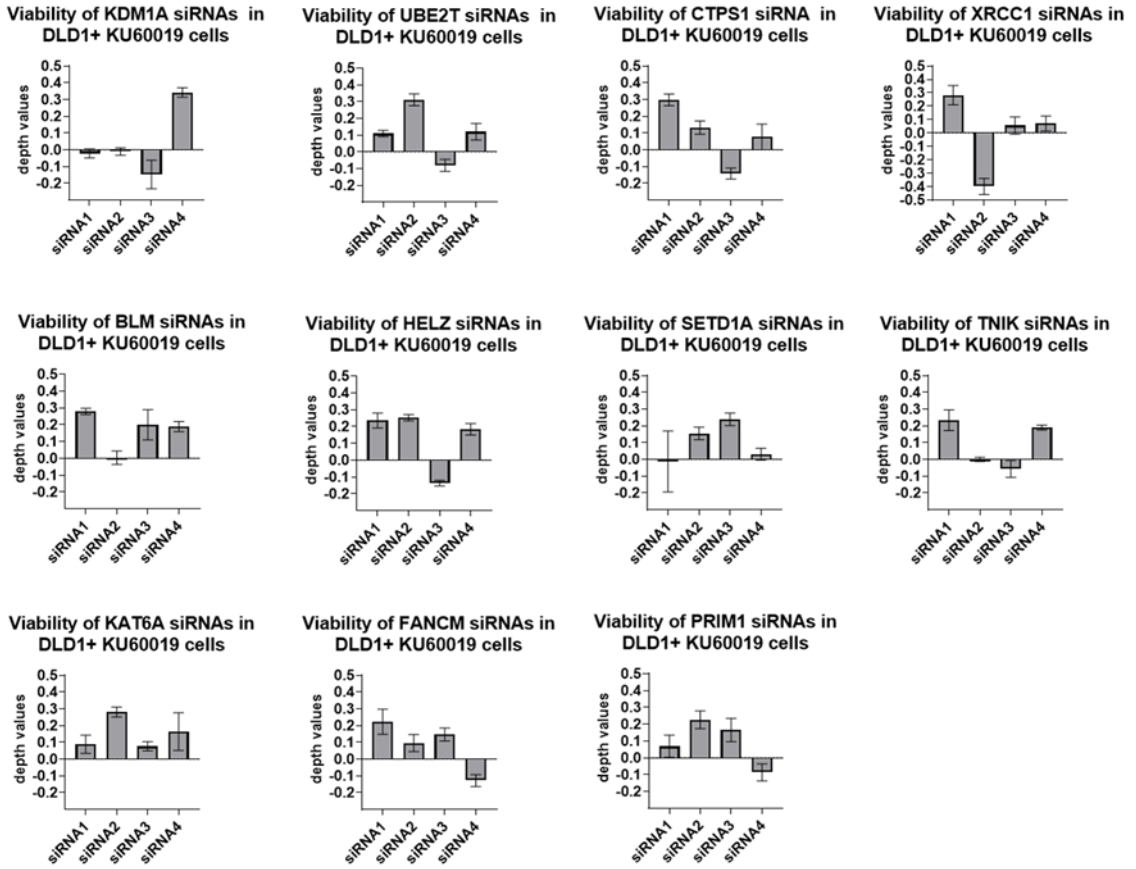

Figure 3.13: Confirmed hits in DLD1+KU60019 cells by siRNA screen. Plots represent growth inhibition relative to control cells for each siRNA per gene. A value > 0 demonstrates sensitivity of the siRNA towards the CIN cells, while a value < 0 shows outgrowth of the CIN cells compared to the parental cells. KU60019: ATM inhibitor. Error bars indicate SEM of three biological replicates.

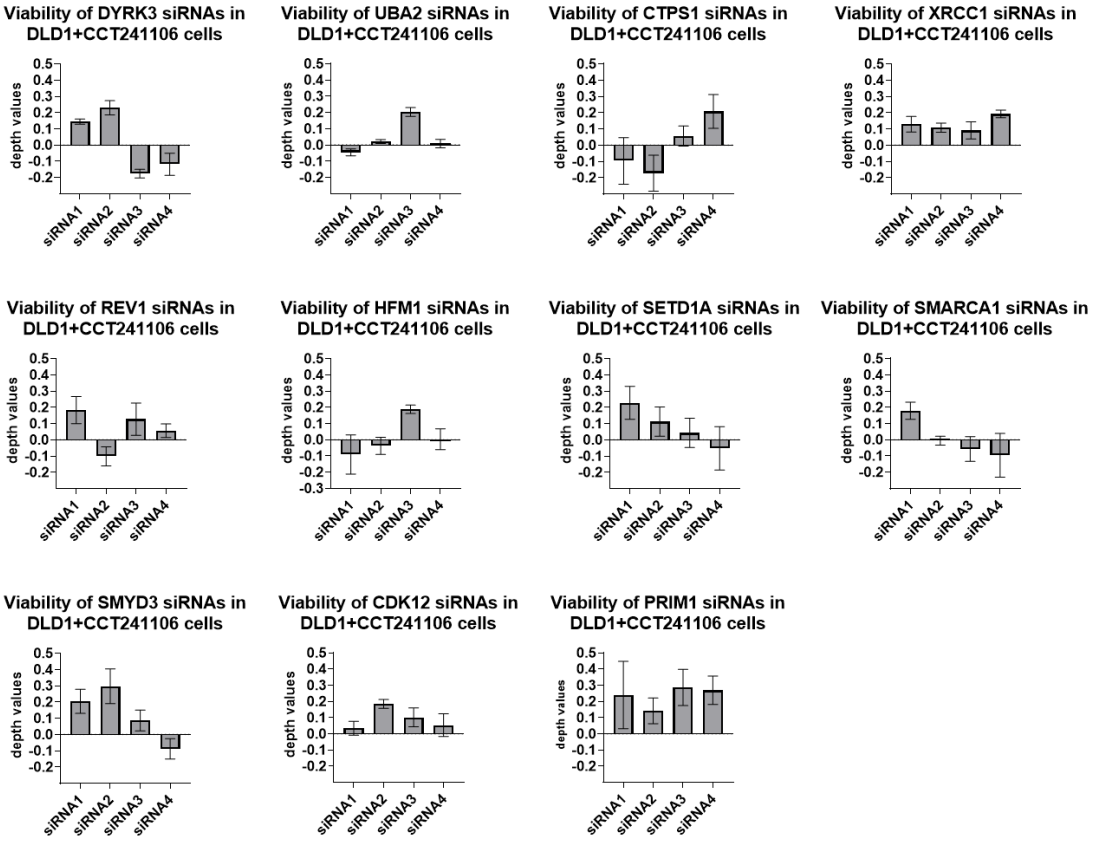

Figure 3.14: Confirmed hits in DLD1+ CCT241106 cells by siRNA screen. Plots represent growth inhibition relative to control cells for each siRNA per gene. A value > 0 demonstrates sensitivity of the siRNA towards CIN cells, while a value < 0 shows outgrowth of the CIN cells compared to the parental cells. CCT241106: CHK1 and CHK2 inhibitor. Error bars indicate SEM from three biological replicates.

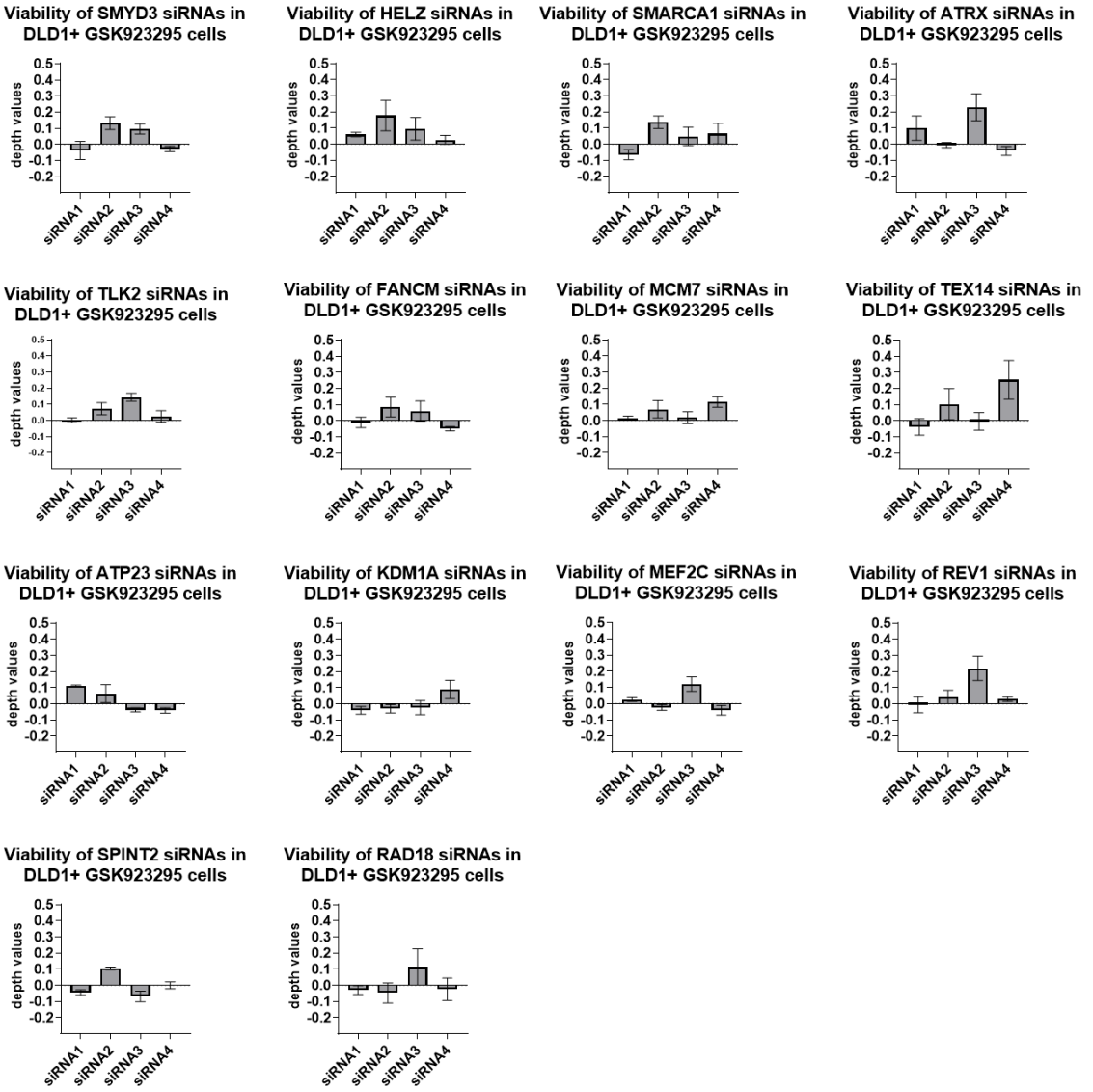

Figure 3.15: Confirmed hits in DLD1+GSK923295 cells by siRNA screen. Plots represent growth inhibition relative to control cells for each siRNA per gene. A value > 0 demonstrates sensitivity of the siRNA towards CIN cells, while a value < 0 shows outgrowth of the CIN cells compared to the parental cells. GSK923295: CENP-E inhibitor. Error bars indicate SEM from three biological replicates.

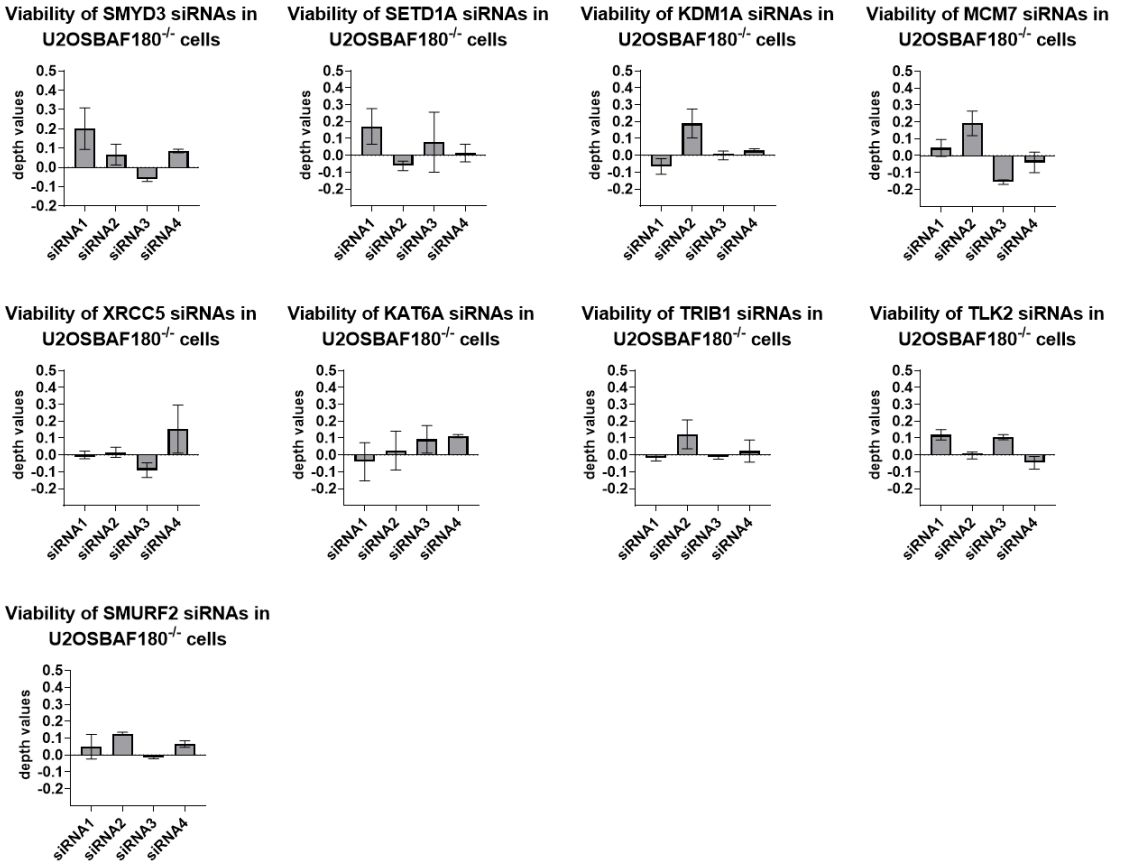

Figure 3.16: Confirmed hits in U2OSBAF180$^{-/-}$ by siRNA screen. Plots represent growth inhibition relative to control cells for each siRNA per gene. A value > 0 demonstrates sensitivity of the siRNA towards BAF180-/- cells, while a value < 0 shows outgrowth of the SWI/SNF impaired cells compared to the parental cells. Error bars indicate SEM from three biological replicates.

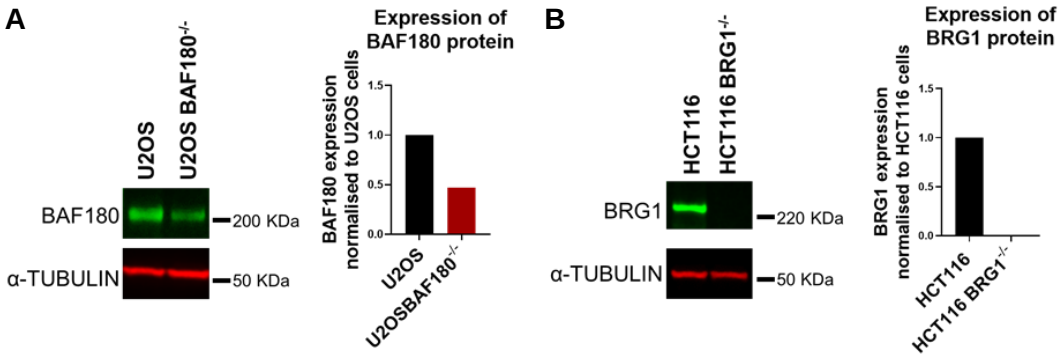

Figure 3.17: Expression of BRG1 and BAF180 proteins. (A) Quantification of BAF180 expression (right) in U2OS cells by immunoblotting (left). **(B)** Quantification of BRG1 expression (right) in HCT116 cells by immunoblotting (left).

Interestingly, a number of hits were identified in multiple CIN models, as shown in Figure 3.18. For example, SMYD3, REV1, SMARCA1 and KDM1A were hits in the SWI/SNF isogenic models and the CIN induced cells after CENP-E or CHK1,CHK2 inhibition (with GSK93295 and CCT241106, respectively). Similarly, SETD1A was identified as a hit in the models with impaired SWI/SNF complex and with ATM and CHK1,CHK2 inhibition (Figure 3.18). To identify if there is a certain pathway or biological process that shows tendency to sensitise chromosomally unstable cells, the connectivity of the genes that were confirmed as hits from the siRNA screen in at least three of the five CIN models was further investigated (Figure 3.19). The majority of these hits were connected to each other, but interestingly, SETD1A interacts with half of the common hits identified in the CIN models. These interactions indicate that SETD1A may be essential for CIN tolerance in cancer cells. However, only one siRNA for the majority of these hits, including SETD1A, showed significant difference between the viability of the CIN models and their corresponding parental cell lines. Thus, further confirmation for these hits continued by chemical inhibition, when available.

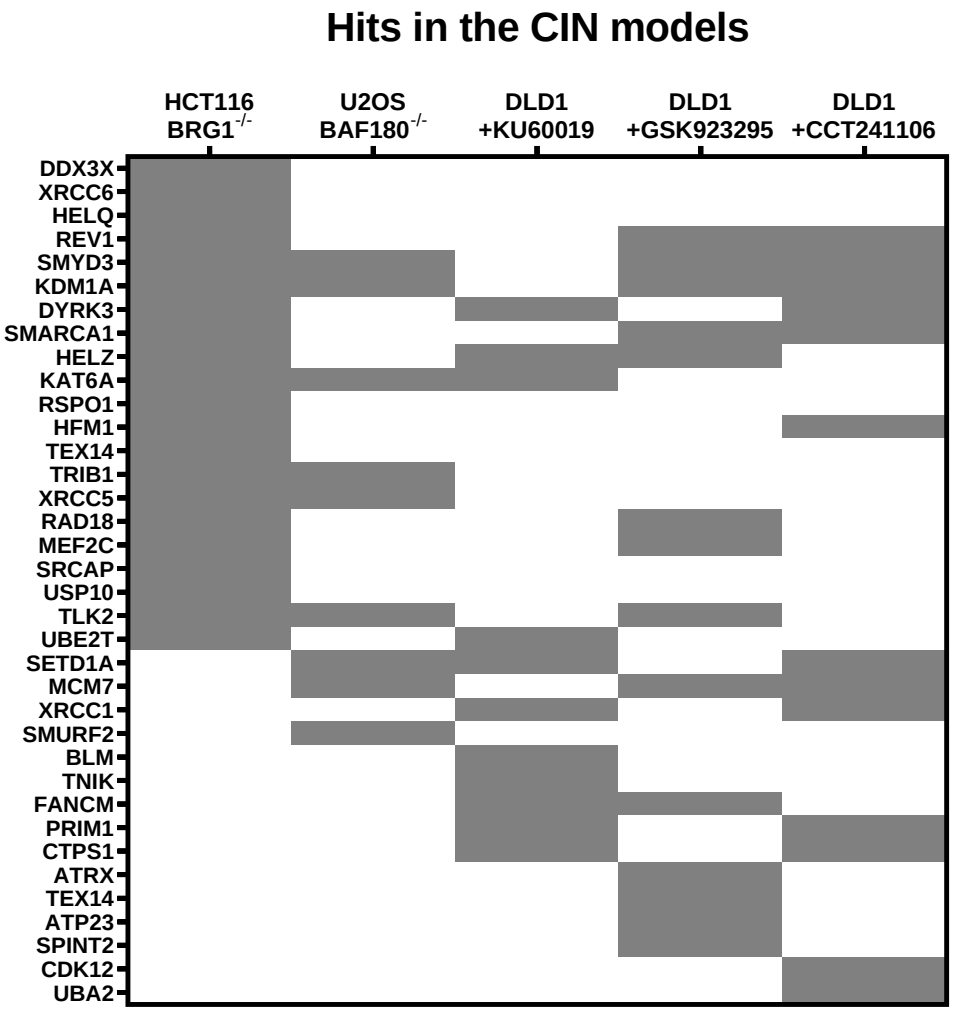

Figure 3.18: Hits in the different CIN models. Illustration of the hits in the siRNA screen, in five different CIN models. KU60019: ATM inhibitor, GSK923295: CENP-E inhibitor and CCT241106: CHK1 and CHK2 inhibitor.

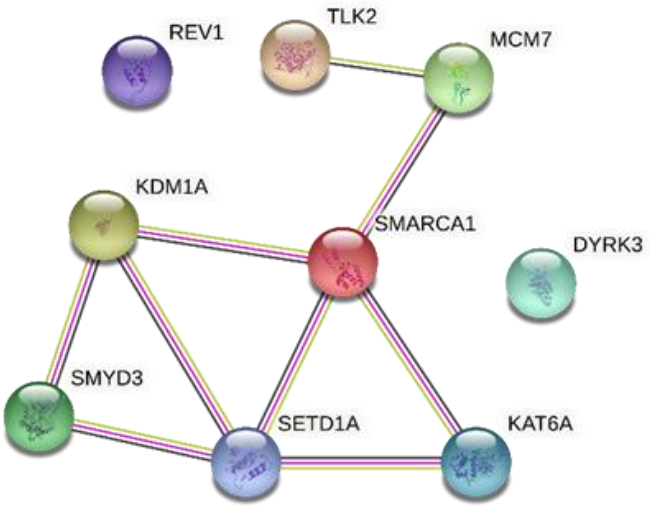

Figure 3.19: Interaction network of the most common hits in the CIN models. Connections of the proteins for the genes that were confirmed as hits from the siRNA screen in at least three of the five CIN models.

3.2.3.2 Hit confirmation by chemical compounds

Following the siRNA screen, in order to further confirm selectivity of potential targets towards the CIN models, small molecule inhibitors were used when available. The effect of each compound in the CIN cells was investigated by measuring the cell viability with CellTiter-Glo, after 10 days of dose response for each inhibitor.

In particular, WM1119 was used as a selective KAT6A inhibitor, GSK626616 was used as DYRK inhibitor, RK-33 for DDX3, BAY6035 and BCI-121 for SMYD3 and GSK2879552-2HCl for KDM1A. Additionally, (R)-PFI 2 hydrochloride was used as a potential SETD1A inhibitor, however it is known to inhibit at least 19 methyltransferases, some of which belong to the same family of SETD1A, and no selective inhibitor for SETD1A exists so far. Only compounds with at least half the IC_{50} concentration in the CIN cells compared to the parental cell lines, were considered to show selectivity towards the CIN models.

From the siRNA screen, KAT6A was confirmed as a hit in the SWI/SNF models and the CIN induced cells by ATM inhibition. However, the compound showed no selectivity towards these models but a trend towards CENP-E inhibition (Table 3.1). DYRK3 selectivity towards BRG1 deleted and ATM inhibited cells was evidenced with the GSK626616 compound, a DYRK1/2/3 inhibitor. GSK626616 reduced the IC_{50} concentration of the $BRG1^{-/-}$ cells by half and even more in the ATM inhibited cells, without affecting the parental cell lines or the rest of the CIN models (Table 3.2 and Figure 3.20 A). Interestingly, the DDX3X inhibitor RK-33 also showed selectivity only towards the $BRG1^{-/-}$ cells, supporting the results from the siRNA screen (Table 3.3 and Figure 3.20 B).

Table 3.1: Sensitivity of CIN models towards WM1119.
Estimated IC_{50} values after dose response of the KAT6A inhibitor for 10 days. Highest concentration of 100 µM was used, followed by 7 1/2 serial dilutions. Mean of the IC_{50} replicates is demonstrated when available. N refers to the number of biological replicates.

	Cell model	IC_{50}(µM)	N
WM1119	DLD1	62.59	2
	DLD1+GSK923295	34.69	2
	DLD1+KU60019	85.32	2
	DLD1+CCT241106	78.34	2
	HCT116	>100	2
	HCT116BRG1$^{-/-}$	78.59	2
	U2OS	85.03	1
	U2OSBAF180$^{-/-}$	50.67	1

.

Two separate inhibitors, BAY6035 and BCI-121, were used to chemically inhibit SMYD3. SMYD3 was identified as hit in SWI/SNF impaired models and when CENP-E or CHK1 and CHK2 were inhibited, inducing CIN. Nevertheless, BCI-121 sensitised only the cells in which CENP-E was inhibited, while BAY6035 showed selectivity towards CENP-E and ATM inhibition. Neither of the compounds demonstrated selectivity towards the SWI/SNF models, or the CHK1, CHK2 inhibited cells (Table 3.4 and Figure 3.20 C). Moreover, the KDM1A inhibitor GSK2879552-2HCl was used to confirm sensitivity of SWI/SNF impaired cells, and CENP-E or CHK1, CHK2 inhibited cells. However, high concentrations of GSK2879552-2HCl were needed in order to observe any sensitivity. All the CIN models demonstrated sensitivity to the KDM1A inhibitor, when compared to their corresponding parental cell lines (Table 3.5 and Figure 3.20 D).

Table 3.2: Sensitivity of CIN models towards GSK626616.
Estimated IC50 values after dose response of the DYRK inhibitor for 10 days. Highest concentration of 20 μM was used, followed by 7 1/2 serial dilutions. N refers to the number of biological replicates.

	Cell model	IC_{50}(μM)	N
GSK626616	DLD1	5.294	1
	DLD1+GSK923295	3.707	1
	DLD1+KU60019	1.147	1
	DLD1+CCT241106	3.423	1
	HCT116	6.345	1
	HCT116BRG1$^{-/-}$	3.186	1
	U2OS	6.018	1
	U2OSBAF180$^{-/-}$	5.717	1

In addition, (R)-PFI 2 hydrochloride was used as a potential SETD1A inhibitor, as it inhibits SETD7 and other proteins of the same SET-domain family. Therefore, it was expected to be selective towards BAF180 impaired cells and the ATM and CHK1, CHK2 inhibited CIN cells. However, (R)-PFI 2 hydrochloride only showed selectivity towards the BRG1 deleted and the CENP-E or ATM inhibited cells (Table 3.6). Further confirmation was performed using the (S)-PFI 2 hydrochloride compound, which is a 500- fold less active enantiomer of (R)-PFI 2 hydrochloride, and is used as a negative control. Viability experiments with dose response of the (S)-PFI 2 hydrochloride compound also demonstrated sensitivity to CENP-E and ATM inhibited cells but not to the BRG1 deleted cells (Table 3.6 and Figure 3.20 E). Thus, (R)-PFI 2 hydrochloride effect is selective only towards BRG1$^{-/-}$ cells. These results indicate SETD7 as a potential target for BRG1 deleted cells, however, more experiments are needed in order to confirm the exact methyltransferase.

Table 3.3: Sensitivity of CIN models towards RK-33.
Estimated IC_{50} values after dose response of the DDX3 inhibitor for 10 days. Highest concentration of 20 µM was used, followed by 7 1/2 serial dilutions. N refers to the number of biological replicates.

	Cell model	IC50(µM)	N
RK-33	DLD1	1.076	1
	DLD1+GSK923295	1.351	1
	DLD1+KU60019	1.284	1
	DLD1+CCT241106	2.004	1
	HCT116	2.741	1
	HCT116BRG1$^{-/-}$	1.442	1
	U2OS	2.484	1
	U2OSBAF180$^{-/-}$	2.974	1

Table 3.4: Sensitivity of CIN models towards BAY6035 and BCI-121.
Estimated IC_{50} values after dose response of the two SMYD3 inhibitors for 10 days. Highest concentration of BAY6034 used was 100 µM was used, while for BCI-121 was 400 µM, followed by 7 1/2 serial dilutions in each. N refers to the number of biological replicates and the mean or the mean ± STDEV of the IC_{50} replicates is shown, when available.

	Cell model	IC_{50}(µM)	N
BAY6035	DLD1	77.91 ± 11.46	3
	DLD1+GSK923295	8.108	2
	DLD1+KU60019	13.58	2
	DLD1+CCT241106	69.78 ± 3.96	3
	HCT116	56.80	1
	HCT116BRG1$^{-/-}$	>100	1
	U2OS	30.85	1
	U2OSBAF180$^{-/-}$	89.27	1
BCI-121	DLD1	109.4	1
	DLD1+GSK923295	53.30	1
	DLD1+KU60019	88.10	1
	HCT116	86.80	1
	HCT116BRG1$^{-/-}$	120.3	1
	U2OS	102.8	1
	U2OSBAF180$^{-/-}$	83.22	1

Table 3.5: Sensitivity of CIN models towards GSK2879552-2HCl.
Estimated IC_{50} values after dose response of the KDM1A inhibitor for 10 days. Highest concentration of 200 µM was used, followed by 7 1/2 serial dilutions. N refers to the number of biological replicates.

	Cell model	IC_{50}(µM)	N
GSK2879552-2HCl	DLD1	>200	1
	DLD1+GSK923295	115.6	1
	DLD1+KU60019	154.9	1
	DLD1+CCT241106	147.2	1
	HCT116	>200	1
	HCT116BRG1$^{-/-}$	94.63	1
	U2OS	> 200	1
	U2OSBAF180$^{-/-}$	142.2	1

Table 3.6: Sensitivity of CIN models towards (R)-PFI-2HCl and (S)-PFI-2HCl.
Estimated IC_{50} values after dose response of (R)-PFI-2HCl and (S)-PFI-2HCl for 10 days. Highest concentration for both compounds used was 100 µM, followed by 7 1/2 serial dilutions in each. N refers to the number of biological replicates and the mean ± STDEV of the IC_{50} replicates is shown, when available.

	Cell model	IC_{50}(µM)	N
(R)-PFI-2HCl	DLD1	32.92 ± 3.24	3
	DLD1+GSK923295	3.61 ± 2.97	3
	DLD1+KU60019	9.44 ± 3.17	3
	DLD1+CCT241106	21.12 ± 6.33	3
	HCT116	31.98 ± 2.83	3
	HCT116BRG1$^{-/-}$	12.2 ± 2.5	1
	U2OS	16.17	1
	U2OSBAF180$^{-/-}$	19.39	1
(S)-PFI-2HCl	DLD1	40.34 ± 4.15	3
	DLD1+GSK923295	2.23 ± 0.85	3
	DLD1+KU60019	13.28 ± 5.2	3
	DLD1+CCT241106	NA	0
	HCT116	41.56 ± 9.80	3
	HCT116BRG1$^{-/-}$	34.59 ± 7.9	3
	U2OS	12.18	1
	U2OSBAF180$^{-/-}$	14.94	1

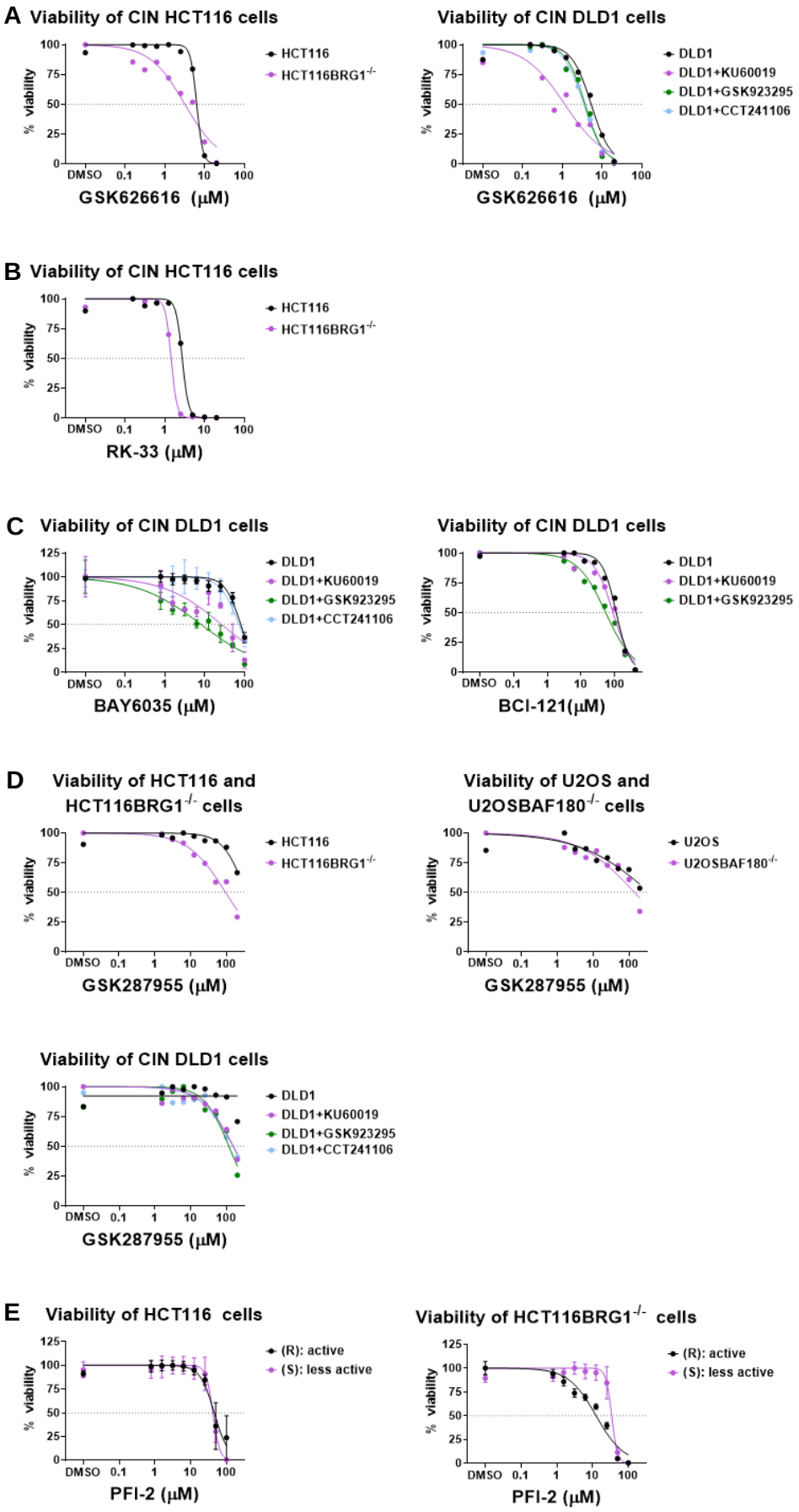

Figure 3.20: Sensitivity of CIN models towards chemical inhibition of distinct hits. 10-day growth inhibition assay in the indicated models with **(A)** DYRK inhibitor GSK626616, **(B)** DDX3X inhibitor RK-33 **(C)** SMYD inhibitors BAY6035 and BCI-121, **(D)** KDM1A inhibitor GSK287955,

(E) (R)-PFI-2HCl methyltransferase inhibitor and 500-fold less active (S)-PFI-2HCl. Error bars, when applicable, demonstrate the range of two biological repeats or the SEM of three biological replicates.

3.2.3.3 Hit confirmation by clonogenic assays

In parallel with the hit confirmation by chemical inhibition, in order to investigate the effect of longer term knock-down of the hits identified by the siRNA screen, a 14-day clonogenic assay was performed. In this assay, at the endpoint the cells were fixed, stained with crystal violet and the plates were scanned and analysed by CellProfiler. In every experiment a non-targeting siRNA and a siRNA toxic (referred as siRNAtox) were used as negative and positive controls, respectively. In addition, in order to initiate validation of the hits, we used a panel of cell lines that were available in the lab and were selected by the presence of likely deleterious mutations in the genes of interest. Interestingly, interrogation of the CCLE database for deleterious mutations in the SWI/SNF complex revealed that parental HCT116 cells, contain deleterious mutations in several subunits of the SWI/SNF complex (Table 3.7), including mutations in the ATPase domain of BRG1 (Bartlett et al., 2011, Oike et al., 2013).

Table 3.7: Mutations of interest in the coding sequence, in the panel of cancer cell lines used.
Mutations were extracted from Cancer Cell Encyclopedia.

Cell Line	Gene	Protein	Type of mutation
CAL51	ARID1A	BAF250	Frame shift deletion
	ARID1A	BAF250	Nonsense
	ARID1B	BAF250B	Frame shift insertion
	CHK1	CHK1	Frame shift deletion
SKOV3	SMARCC1	BAF155	Frame shift deletion
	ARID1A	BAF250	Nonsense
	CENP-E	CENP-E	Frame shift insertion
IGROV1	ARID1B	BAF250B	In frame insertion
	ARID1A	BAF250	Frame shift insertion
	ARID1A	BAF250	Frame shift deletion
	ARID4B	ARID4B	Nonsense
	SMARCA4	BRG1	In frame deletion
	CHK1	CHK1	Frame shift deletion
MDA-MB-231	-	-	-
DLD1	-	-	-
PATU8988S	CHK1	CHK1	Frame shift deletion
HCT116	SMARCA4	BRG1	Frame shift insertion
	ARID3C	BRIGHT-Like	Frame shift deletion
	ARID5A	MRF1	Frame shift deletion
	ARID3B	DRIL2	In frame deletion
	CENP-E	CENP-E	Frame shift insertion

For the two SWI/SNF impaired models, strong hits for which no compound existed, were prioritised. Additionally, because the U2OSBAF180$^{-/-}$ cells express BAF180, as shown in figure 3.17 A, the viability of the cells after gene silencing was initially investigated in the HCT116BRG1$^{-/-}$ cells and only the confirmed hits were further investigated in the BAF180$^{-/-}$ cells.

Overall, the majority of the siRNAs, independent of the gene tested, inhibited the ability of the BRG1$^{-/-}$ cells to form colonies compared to the siRNA control. However, many siRNAs supressed or significantly reduced the viability of the parental cells as well. For example, all four siRNAs used for RSPO1, XRCC6, SRCAP and TEX14 reduced the viability of the parental cell line and therefore did not show selectivity towards BRG1$^{-/-}$ cells in this assay (Figure 3.21). Thus, we focused on genes, such as HELQ, KAT6A, REV1, HFM1 and TRIB1, that showed minimal growth inhibition in the parental cells but significantly reduced the colonies in BRG1 deleted cells (Figure 3.21). Analysis of the experiments showed that at least two siRNAs against HELQ, KAT6A and HFM1 showed some selectivity towards the target cells relative to the parental (Figure 3.22). Therefore, clonogenic experiments were performed in the BAF180 deleted cells after gene silencing of each of these three genes. In addition, the effect of the siRNAs for TRIB1 was also investigated in BAF180$^{-/-}$ cells as the siRNAs 1, 2 and 4 reduced the viability of BRG1 deleted cells compared to the parental (Figure 3.22). Nevertheless, three out of four siRNAs for TRIB1, killed also the parental U2OS cells. For the HFM1, although the siRNAs were significantly affecting the parental cells, they clearly reduced even further the colonies of the BAF180 deleted cells. Importantly, two out of four siRNAs (2 and 4) for HELQ and for KAT6A (2 and 4), significantly inhibited the formation of colonies in the BAF180 deleted cells (Figure 3.23 and 3.24).

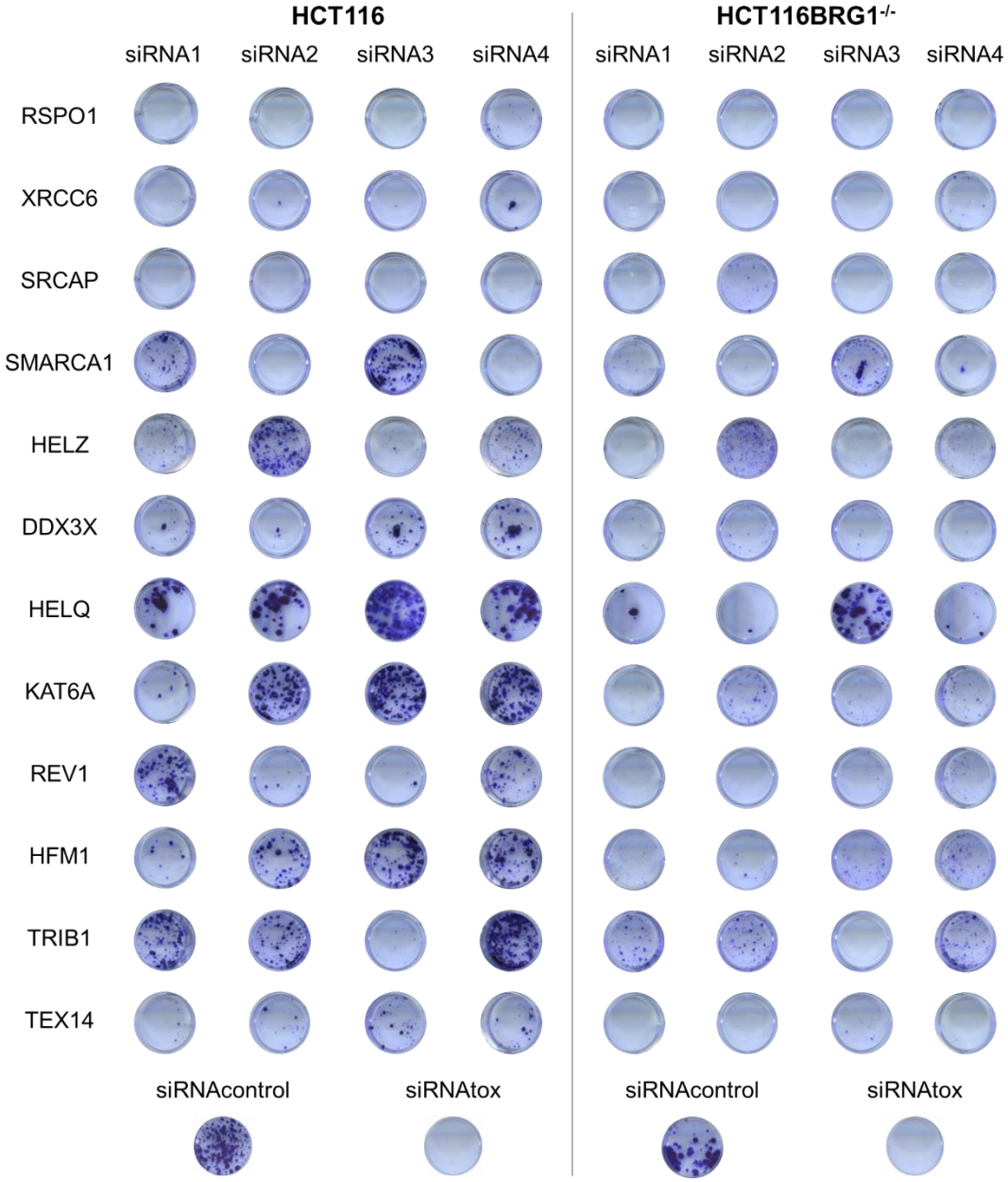

Figure 3.21: Colony formation in HCT116 and HCT116BRG1$^{-/-}$ cells after gene silencing for each potential hit. Illustration of colonies formed in a period of 14 days, after fixation and staining with crystal violet. Four different siRNAs per gene were used separately in order to investigate their effect in cell viability. Representative images are shown.

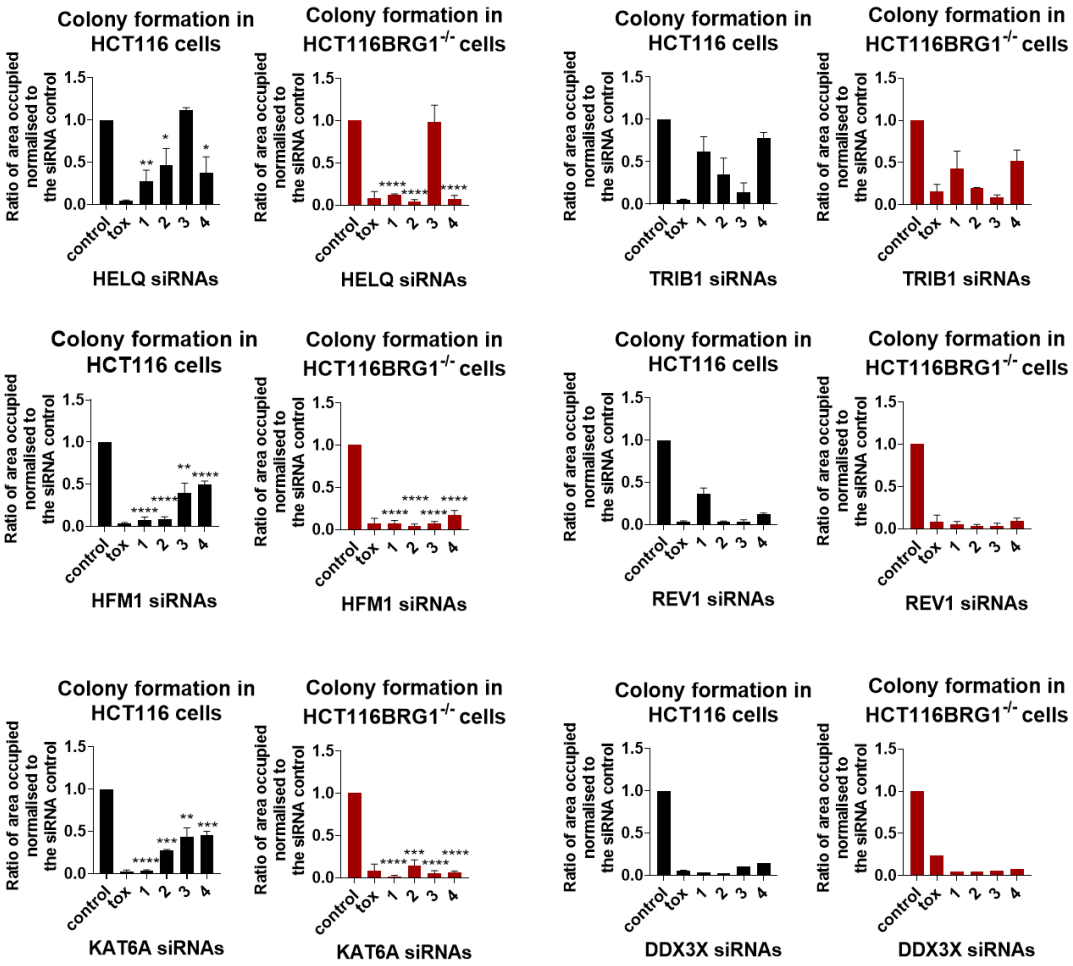

Figure 3.22: Analysis of colony formation in HCT116 and HCT116BRG1$^{-/-}$ cells after gene silencing. Analysis of colonies formed in a period of 14 days after siRNA transfection, by CellProfiller. The mean and the range of two biological replicates are shown, when available, and in case of three replicates, the mean and SEM are demonstrated and t test analysis was performed, comparing each sample to siRNA control.

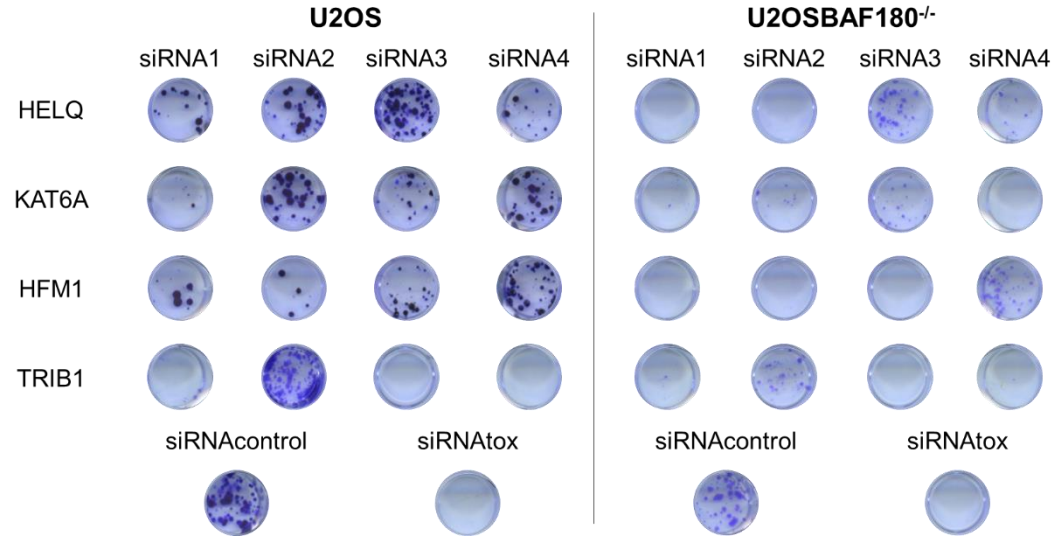

Figure 3.23: Colony formation in U2OS and U2OSBAF180$^{-/-}$ cells after gene silencing for each potential hit. Representative images of colonies formed after a period of 14 days following transfection with indicated siRNAs.

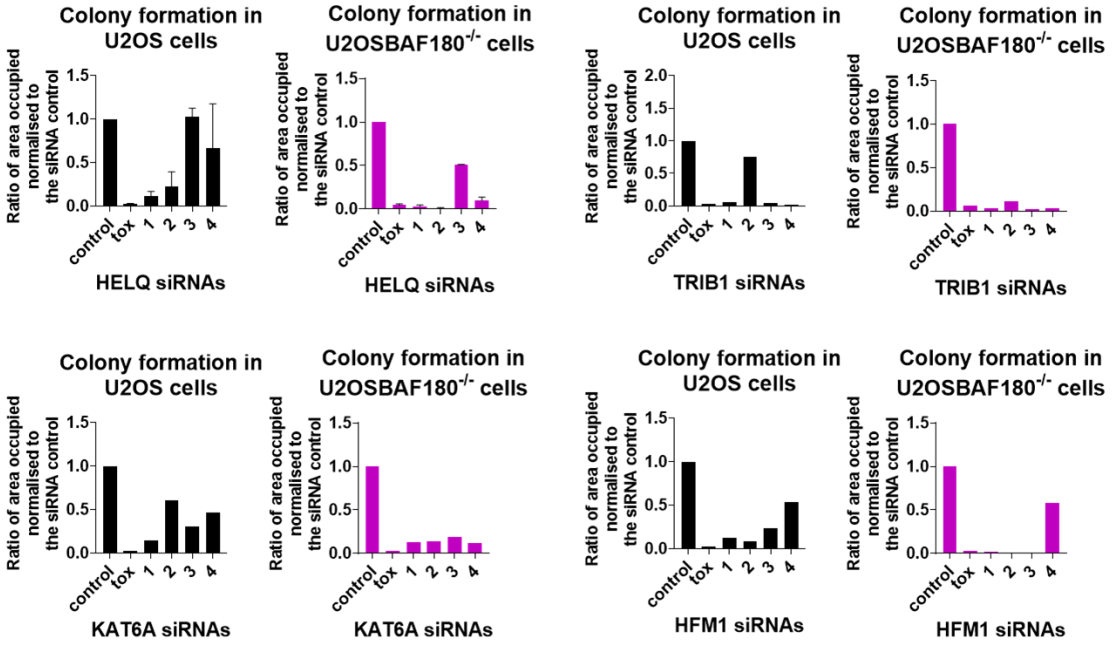

Figure 3.24: Analysis of colony formation in U2OS and U2OSBAF180$^{-/-}$ cells after gene silencing. Analysis of colonies formed in a period of 14 days after siRNA transfection, by CellProfiller. All the samples where compared to the siRNA control of each cell line. The mean and the range of two biological replicates are shown, when available.

Chemical inhibition of KAT6A with WM1119 selective compound did not show selectivity towards SWI/SNF impaired models, thus further hit confirmation was prioritised only for HELQ. Confirmation of the HELQ protein knockdown was performed by immunoblotting, three days after the transfection in the parental and SWI/SNF impaired isogenic cell lines. All of the four siRNAs used reduced the protein expression in both HCT116 and U2OS cells as well as in their SWI/SNF impaired isogenic models (Figure 3.25). However, we observed that HELQ siRNA 3 reduces the expression of the protein but does not affect the viability of either the parental or the SWI/SNF impaired models. These results indicate that HELQ siRNA 3 may generate an off-target effect that rescues the phenotype. To further investigate HELQ as a potential target, we used cancer cell lines that contain deleterious mutations in subunits of the SWI/SNF complex (IGROV1, CAL51), (Table 3.7). Knockdown of HELQ in the breast and ovarian cancer cell lines CAL51 and IGROV1, respectively, which contain multiple mutations in genes of the SWI/SNF complex, reduced the ability of the cells to form colonies (Table 3.7 and Figure 3.26). HELQ knock-down in response to siRNAs was also confirmed in these cell lines by immunoblotting (Figure 3.27). In contrast, HELQ knock-down in DLD1 cells that

do not contain any deleterious mutations in the SWI/SNF complex does not reduce the viability of the cells with or without treatment with the inhibitors used to induce CIN (KU60019, GSK923295 or CCT241106) (Figure 3.26). Moreover, reduction of the HELQ protein in the DLD1 untreated cells was observed with all of the four siRNAs by immunoblotting (Figure 3.27 D). Similarly to DLD1, HELQ knock-down did not reduced the viability of MDA-MB-231 and PATU8988S cancer cells that do not contain known deleterious mutations in the SWI/SNF subunits (Table 3.7 and Figure 3.26). These results demonstrate HELQ as a potential target in SWI/SNF impaired complex, however, further experiments would be needed for target validation.

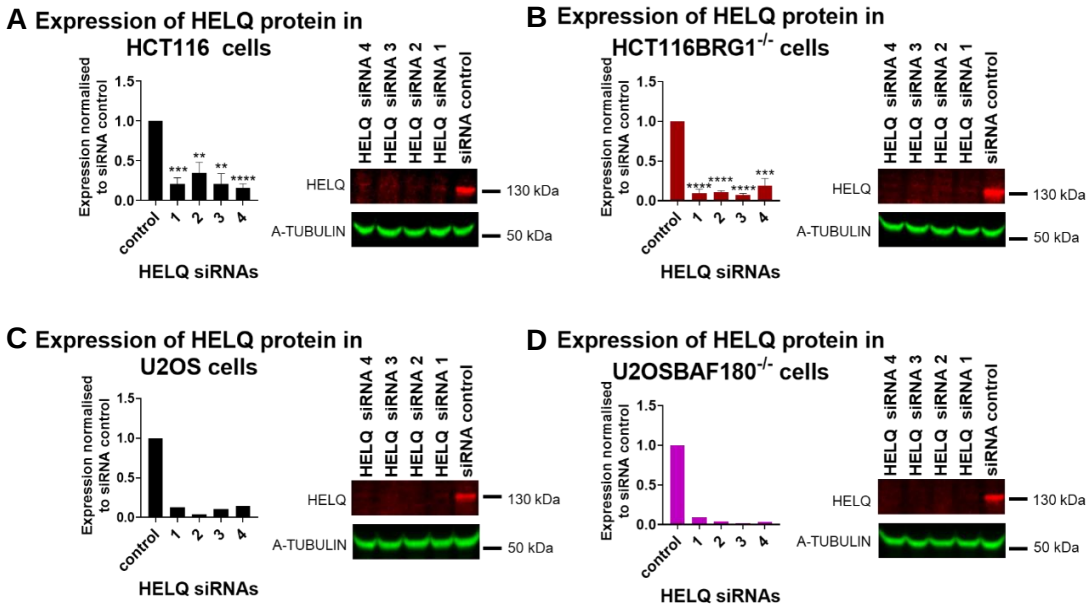

Figure 3.25: HELQ protein expression after siRNA gene silencing. Quantification (left) of HELQ protein expression by immunoblotting (right) in **(A)** HCT116 cells, **(B)** HCT116BRG1$^{-/-}$ cells, **(C)** U2OS cells and **(D)** U2OSBAF180$^{-/-}$ cells. Fluorescent secondary antibodies were used and the membrane imaging and analysis were performed with Image Studio Lite. When three biological replicates were available, bars indicate SEM, and additional t test analysis was performed, comparing each sample to siRNA control.

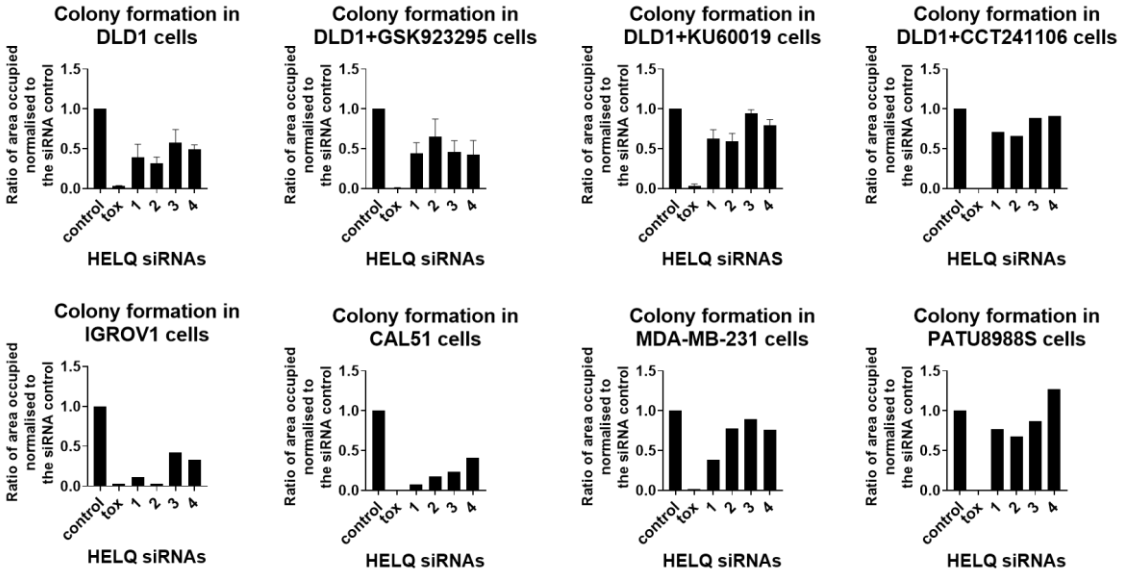

Figure 3.26: Analysis of colony formation after HELQ gene silencing. Analysis of colonies formed in a period of 14 days after siRNA transfection, by CellProfiller. All the samples where compared to the siRNA control of each cell line. The mean and the range of two biological replicates are shown, when available.

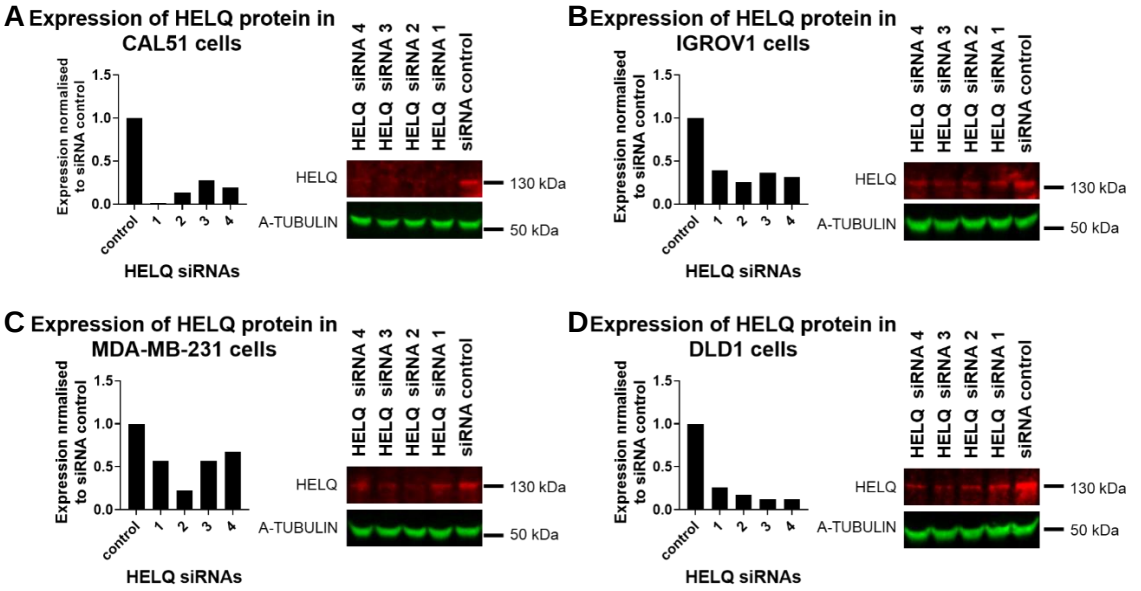

Figure 3.27. HELQ protein expression after siRNA gene silencing. Quantification (left) of HELQ protein expression by immunoblotting (right) in **(A)** CAL51 cells, **(B)** IGROV1 cells, **(C)** MDA-MB-231 cells and **(D)** DLD1 cells. Fluorescent secondary antibodies were used and the membrane imaging and analysis were performed with Image Studio Lite.

Similarly to the SWI/SNF impaired models, hits that were identified in CIN cells, induced by inhibition of CENP-E with GSK923295, of ATM with KU60019 or CHK1 and CHK2 with CCT241106, were also further investigated. The same approach was followed and DLD1 cells were treated for 3 days with each of the inhibitors, in order to

induce CIN, prior the transfection with four different siRNAs for each hit. The effect in cell viability was identified by the ability of the cells to form colonies after 14 days in culture.

As expected from the siRNA screen, strong hits for each model could be confirmed by clonogenic assays in almost all the CIN models. In particular, siRNA 3 for REV1 and siRNAs 1 and 3 for ATRX sensitised the cells treated with the CENP-E inhibitor. Additionally, knockdown of hits such as RAD18, SMYD3 or HELZ reduced the viability of the parental cells but did not completely kill the CIN cells (Figures 3.28 and 3.29). Similar was the effect of FANCM knockdown, which was initially investigated in the ATM inhibited cells as directed by the siRNA screen. However, when tested in the DLD1 CIN models, FANCM knockdown demonstrated no selectivity towards any of the CIN models (Figures 3.28 - 3.33). It is possible that FANCM knockdown does not persist over the length of the clonogenic assay or that there is a narrow window of selectivity towards CIN cells that is evidently only in shorter viability experiments. In contrast to FANCM, KAT6A knockdown reduced the viability of CHEK1, CHK2 inhibited cells but showed selectivity mainly towards CENP-E and ATM inhibited cells (Figures 3.29, 3.31 and 3.33).

Interestingly, all four siRNAs for TEX14 significantly reduced the viability in the cells treated with the GSK923295 compound (Figures 3.11, 3.28 and 3.29). Thus, it was investigated if TEX14 knockdown is also lethal in the CIN models generated by ATM or CHK1, CHK2 inhibition. However, selectivity was shown only towards CIN model induced by CENP-E inhibition (Figures 3.29, 3.31, 3.33). In parallel, PRIM1 was confirmed as a selective hit in CHK1 and CHK2 inhibited cells but not in the rest CIN models (Figures 3.29, 3.31, 3.33). The rest of the siRNAs tested in the ATM and CHK1/CHK2 inhibited cells either killed the parental cells, such as MCM7, or they did not reduce significantly the ability of the CIN cells to form colonies, for example TLK2 (Figures 3.30 - 3.33). Thus, further confirmation continued to investigate synthetic lethality of TEX14 knockdown towards CENP-E inhibition and PRIM1 knockdown towards CHK1 and CHK2 inhibition.

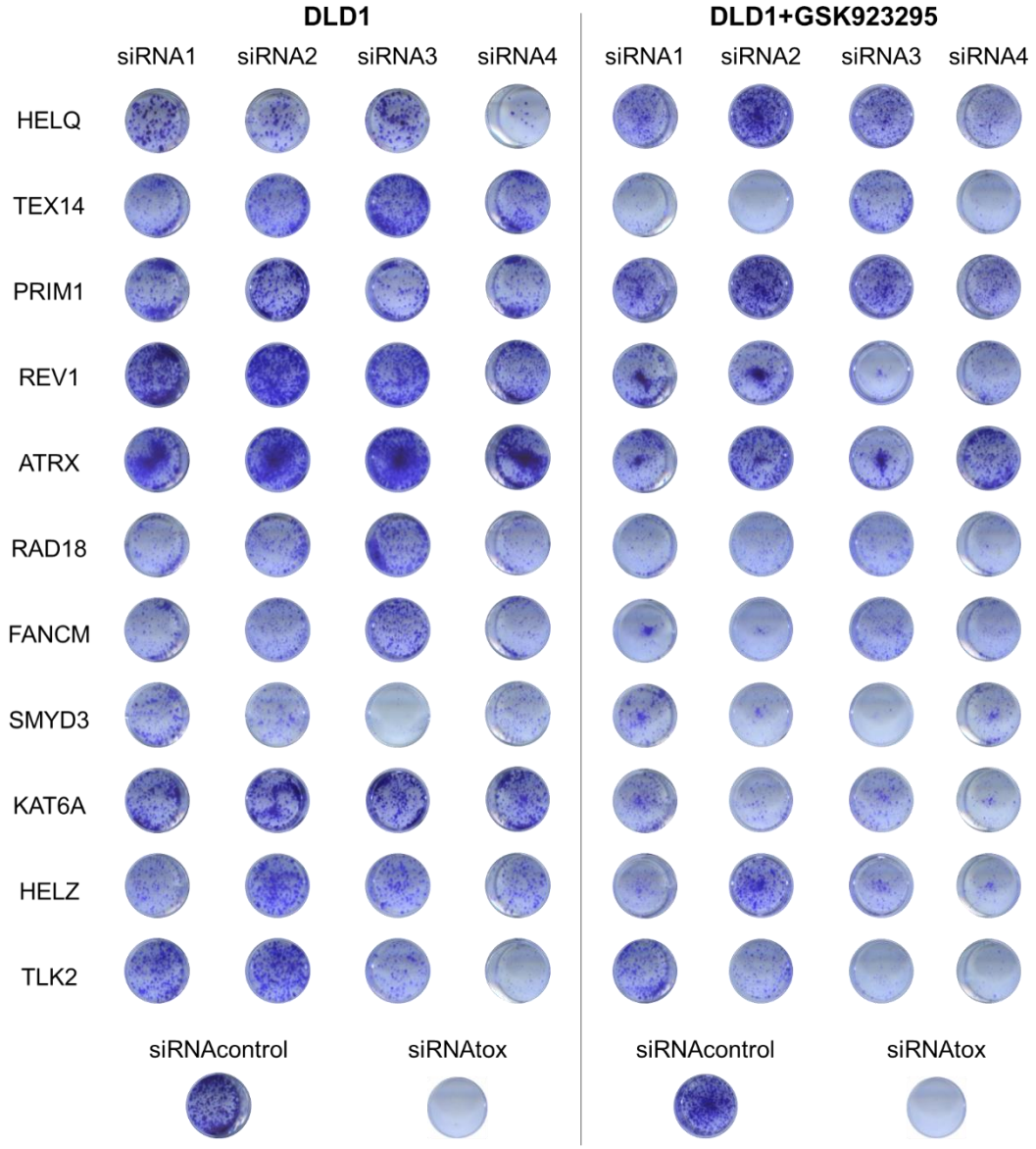

Figure 3.28: Colony formation assay in DLD1 cells treated with GSK923295 compound after gene silencing for each potential hit. Representative images of colonies formed after a period of 14 days following transfection with indicated siRNAs.

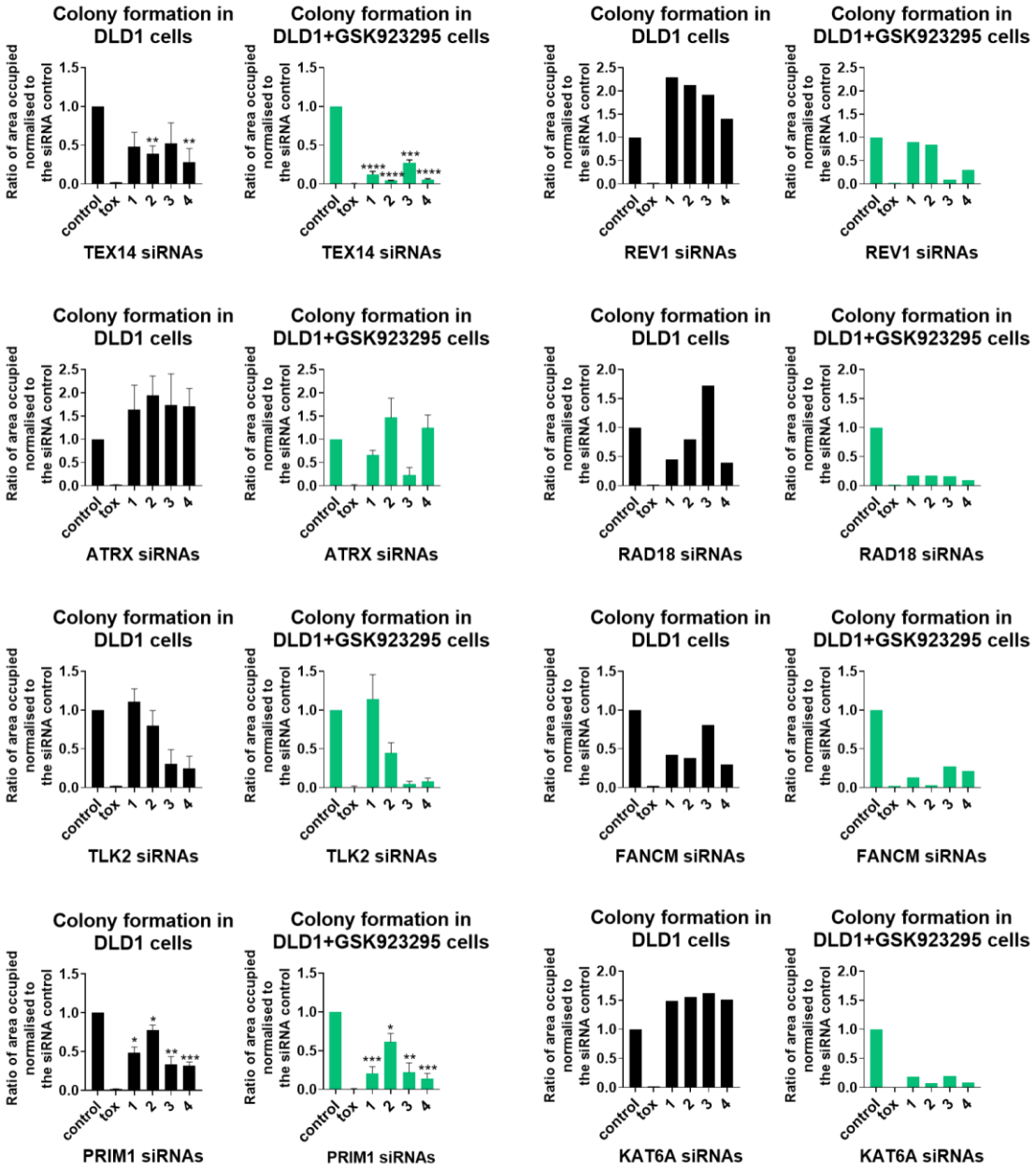

Figure 3.29: Analysis of colony formation in DLD1 cells treated with GSK923295 compound after gene silencing. Analysis of colonies formed in a period of 14 days after siRNA transfection, by CellProfiller. All the samples where compared to the siRNA control of each cell line. The mean and the range of two biological replicates are shown, when available, and in case of three replicates, the mean and SEM are demonstrated and t test analysis was performed, comparing each sample to siRNA control.

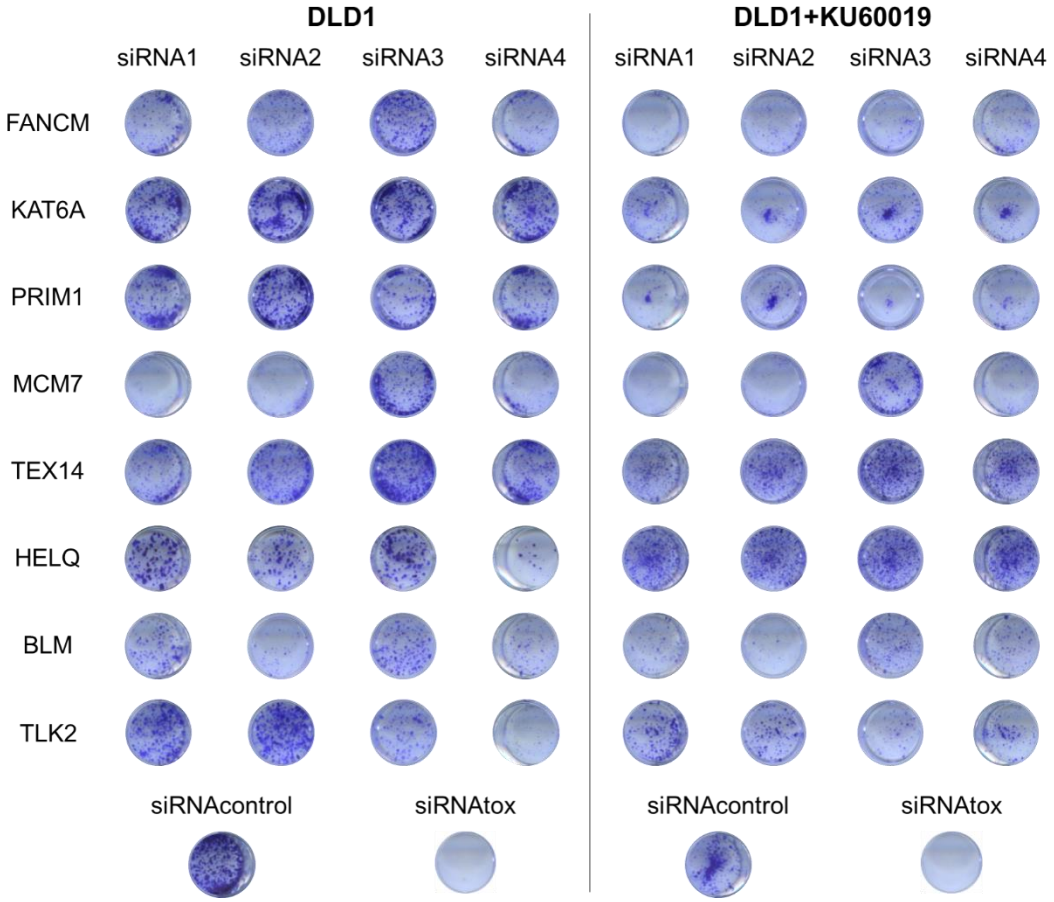

Figure 3.30: Colony formation in DLD1 cells treated with KU60019 compound after gene silencing for each potential hit. Representative images of colonies formed after a period of 14 days following transfection with indicated siRNAs.

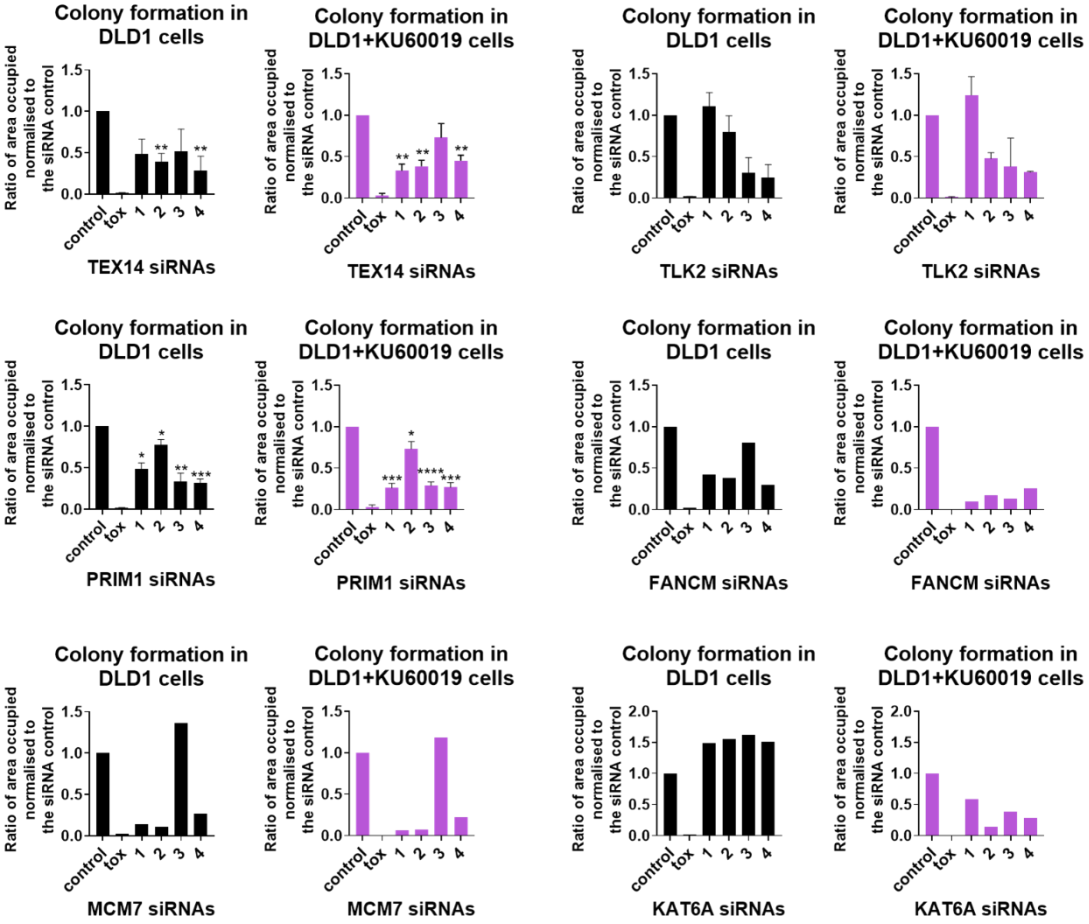

Figure 3.31: Analysis of colony formation in DLD1 cells treated with KU60019 compound after gene silencing. Analysis of colonies formed in a period of 14 days after siRNA transfection, by CellProfiller. All the samples where compared to the siRNA control of each cell line. The mean and the range of two biological replicates are shown, when available, and in case of three replicates, the mean and SEM are demonstrated and t test analysis was performed, comparing each sample to siRNA control.

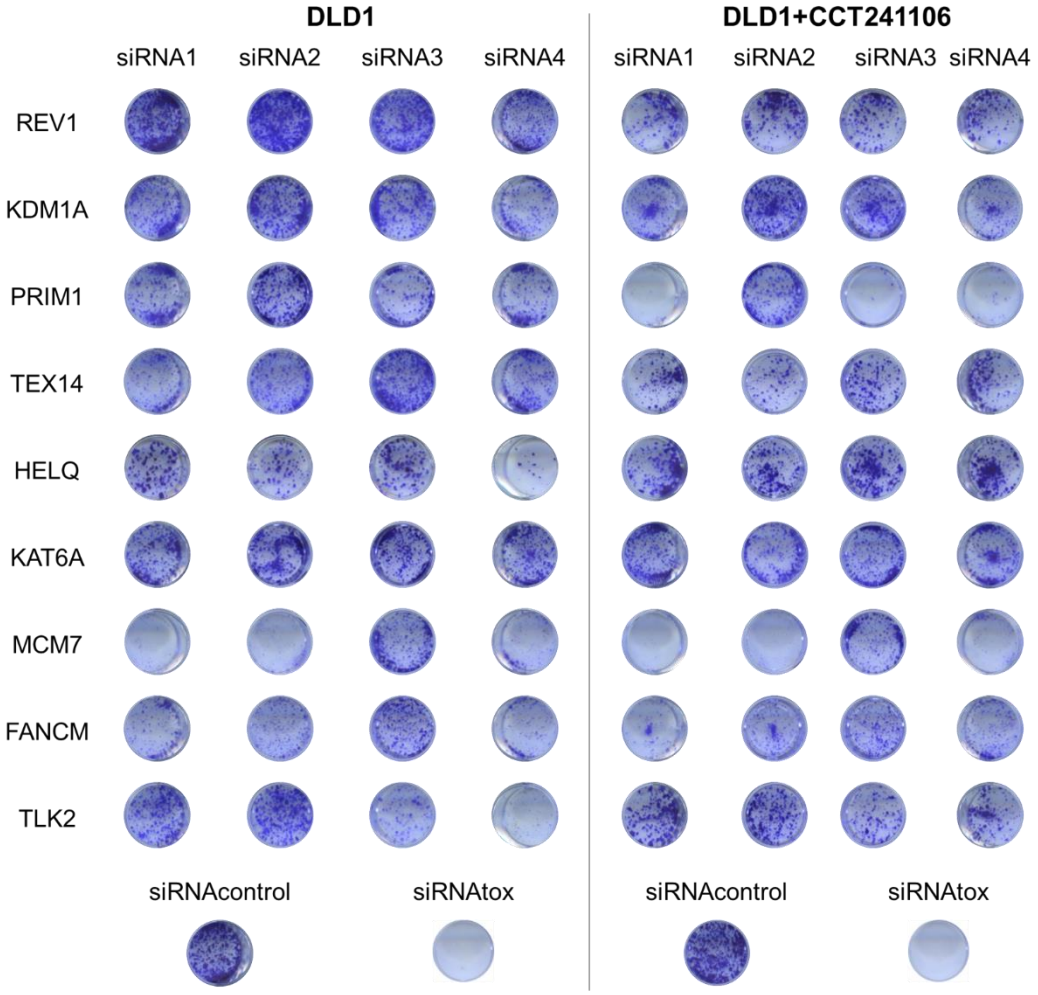

Figure 3.32: Colony formation in DLD1 cells treated with CCT241106 compound after gene silencing for each potential hit. Representative images of colonies formed after a period of 14 days following transfection with indicated siRNAs.

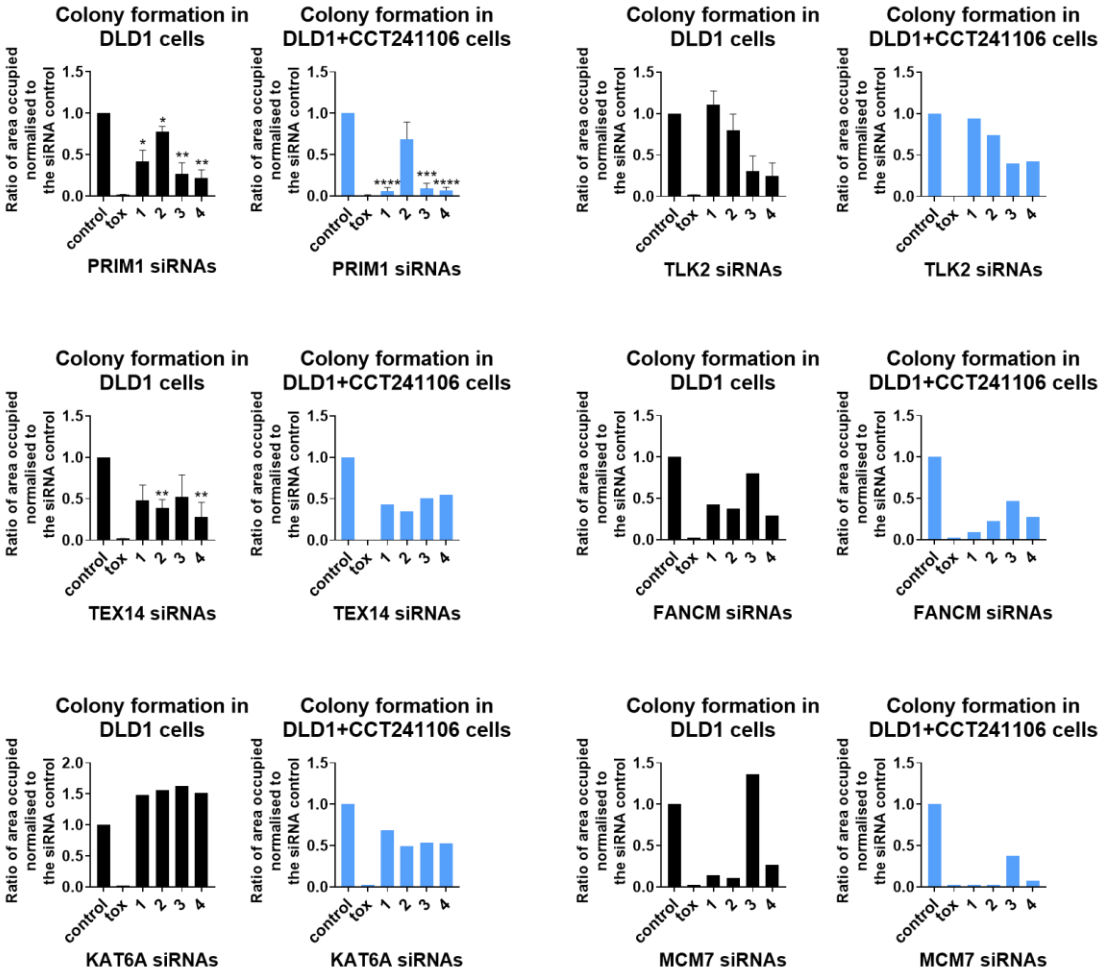

Figure 3.33: Analysis of colony formation in DLD1 cells treated with CCT241106 compound after gene silencing. Analysis of colonies formed in a period of 14 days after siRNA transfection, by CellProfiller. All the samples where compared to the siRNA control of each cell line. The mean and the range of two biological replicates are shown, when available, and in case of three replicates, the mean and SEM are demonstrated and t test analysis was performed, comparing each sample to siRNA control.

Confirmation of TEX14 and PRIM1 knockdown by four different siRNAs was initially investigated by immunoblotting. None of the siRNAs against TEX14 reduced significantly the bands of the protein, likely indicating a non-specificity of the antibody towards this protein. However, real-time PCR with primers for TEX14 demonstrated reduction in TEX14 gene expression in three of the four siRNA used (Figure 3.34 A and C). In contrast, PRIM1 antibody showed reduction in PRIM1 protein expression after knockdown with three out of four siRNAs, which is in agreement with the clonogenic assay that showed selective growth inhibition with the siRNA 1,3 and 4 that induced knock-down of PRIM1 but not with siRNA 2 (Figure 4.34 B). These results were further

confirmed by real-time PCR, using two separate primers specific for PRIM1 (Figure 3.34 D).

Furthermore, selectivity of TEX14 towards CENP-E was confirmed in additional cancer cell lines. The ovarian cancer cell line SKOV3 and the colorectal HCT116 contain a frame shift insertion each in CENP-E and nockdown of TEX14 with four different siRNAs promoted cell death in these two cell lines but it did not reduce significantly the viability of the breast cancer cell line CAL51 that does not contain any mutations in the CENP-E gene (Table 3.7 and Figure 3.35 A). However, atempts to confirm reduction of TEX14 by immunoblotting in those cancer cell lines also failed to demonstrate any change in the protein bands after gene silencing, possibly indicating non specificity of the antibody (Figure 3.35 B).

Similarly to TEX14, selectivity of PRIM1 towards CHK1 and CHK2 was further confirmed in a panel of cancer cell lines with mutations in the corresponding genes. Knockdown of PRIM1 in the breast cancer cell line CAL51 and ovarian cancer cell line IGROV1, both of which contain frame shift deletion of CHK1, induces cell death. Additionally, the HCT116 cell line does not contain a deleterious mutation in CHK1 or CHK2 genes but PRIM1 gene silencing also induced cell death (Table 3.7 and Figure 3.36 A). However, in PATU8988S cell line, derived from lung metastasis of a pancreatic tumour that contains a frame shift deletion in CHK1, PRIM1 knockdown reduced the ability of the cells to form colonies but not to the same extent as in CAL51, IGROV1 and HCT116 cancer cell lines (Table 3.7 and Figure 3.36 A). Moreover, when investigated in the ovarian cell line SCOV3 that do not contain any mutations in the CHK1 or CHK2 genes, we noticed that PRIM1 gene silencing induced cell death and the decreased expression levels of the protein were confirmed by immunoblotting (Figure 3.36). Importantly, all the cell lines tested contain multiple mutations in the SWI/SNF complex apart from PATU8988S. Thus, it is possible that PRIM1 is selective not only towards CHK1 and CHK2 inactivation but also towards impaired SWI/SNF complex in general. Nevertheless, more experiments are needed in order to confirm this hypothesis.

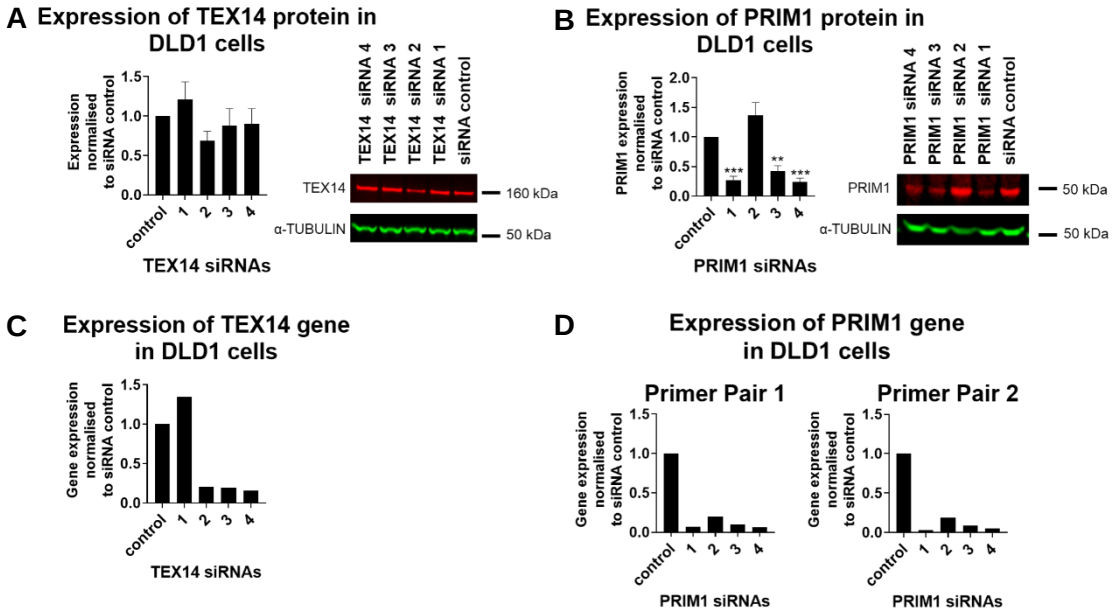

Figure 3.34. TEX14 and PRIM1 expression in DLD1 cells after siRNA gene silencing. (A and B) Illustration and quantification of TEX14 and PRIM1 protein expression by immunoblotting three days after the siRNA transfections. Fluorescent secondary antibodies were used and the membrane imaging and analysis were performed with Image Studio Lite. Mean and SEM of three biological repeats are demonstrated and t test analysis was performed, comparing each sample to siRNA control. **(C and D)** Quantification of TEX14 and PRIM1 gene expression by real-time PCR. RNA was extracted two days after transfection of the siRNAs and two distinct pairs of primers were used for PRIM1.

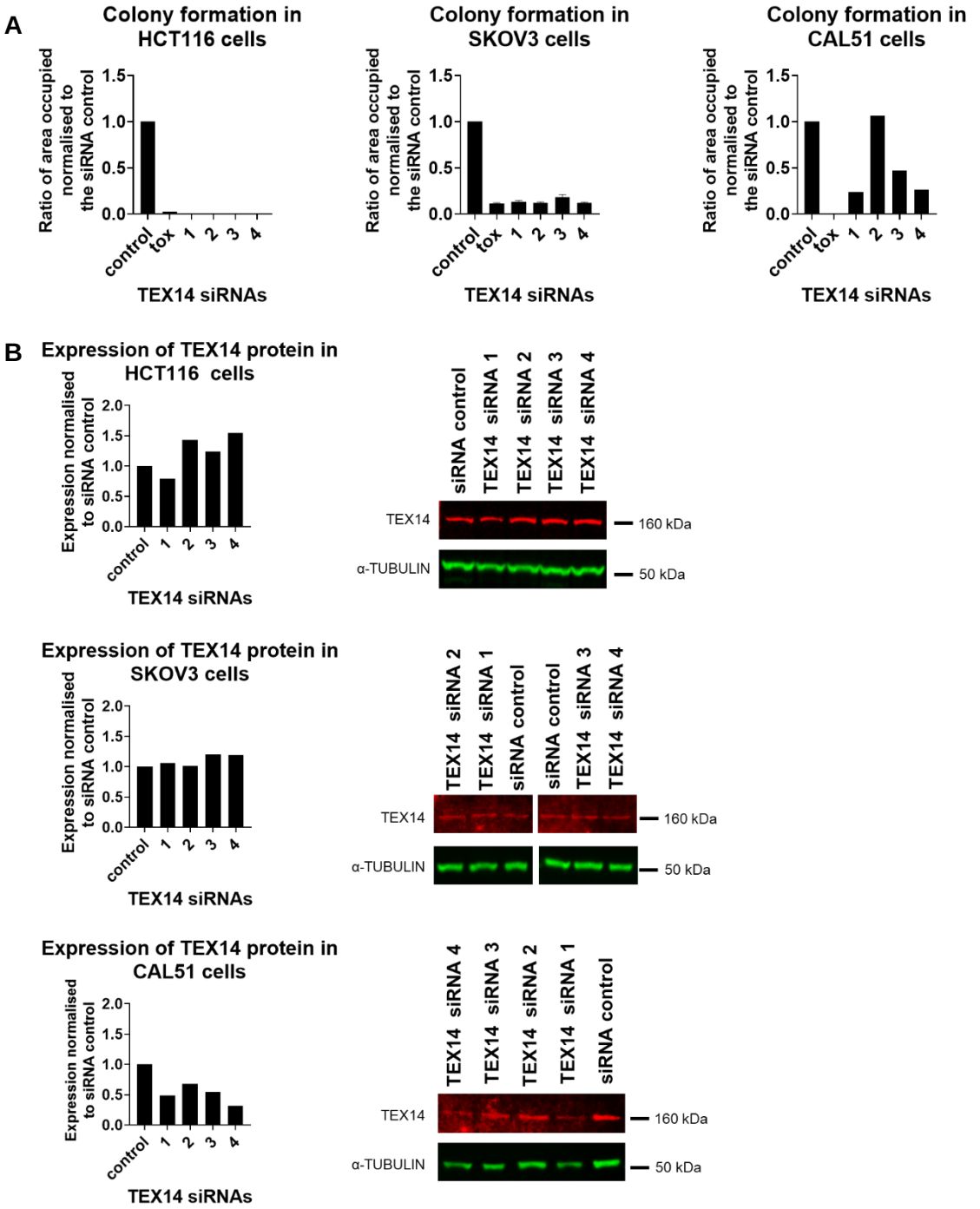

Figure 3.35: Selectivity of TEX14 towards CENP-E mutations. (A) Quantification of colony formation assay in SKOV3, HCT116 and CAL51 for a period of 14 days after siRNA transfection, by CellProfiller. All the samples where compared to the siRNA control of each cell line. **(B)** Illustration and quantification of TEX14 protein by immunoblotting in HCT116, SKOV3 and CAL51 cancer cell lines. Fluorescent secondary antibodies were used and the membrane imaging and analysis were performed with Image Studio Lite. The mean and the range of two biological replicates are shown, when available.

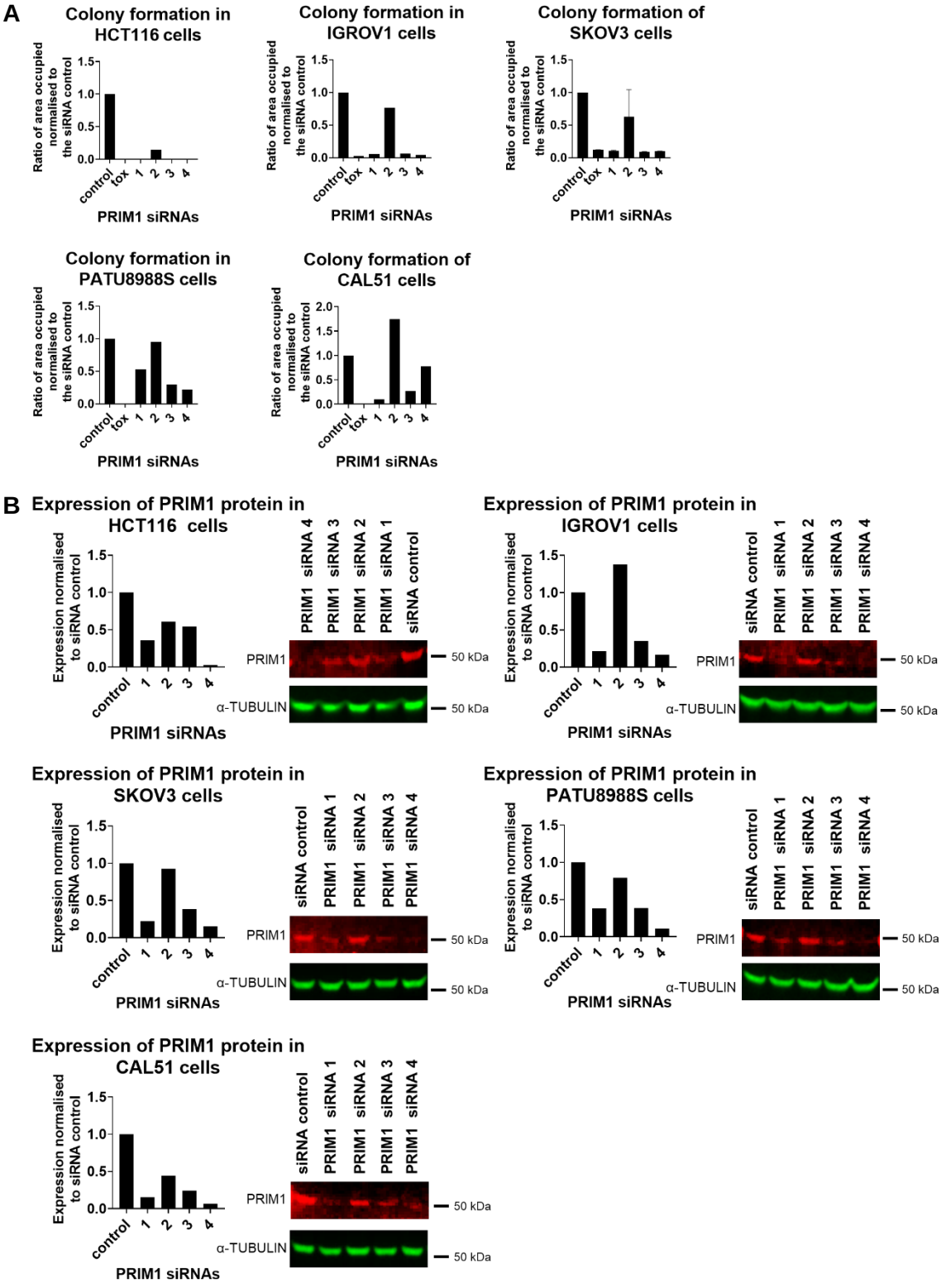

Figure 3.36: Selectivity of PRIM1 towards CHK1 and CHK2 mutations. Quantification of colony formation assay in HCT116, IGROV1, SKOV3, PATU8988S and CAL51 cancer cell lines for a period of 14 days after siRNA transfection, by CellProfiller. All the samples where compared to the siRNA control of each cell line. **(B)** Illustration and quantification of PRIM1 protein by immunoblotting in HCT116, IGROV1, SKOV3, PATU8988S and CAL51 cancer cell lines. Fluorescent secondary antibodies were used and the membrane imaging and analysis were performed with Image Studio Lite. The mean and the range of two biological replicates are demonstrated, when available.

3.3 Conclusions

The main focus of this part of the study was to identify targets in CIN, either linked to loss of function of a specific gene or independently of the driver of the CIN phenotype. Towards this aim, multiple CIN models were generated by promoting errors in mitosis with treatment of the CENP-E inhibitor GSK92395 or in DNA damage response by inhibiting ATM with the KU60019 compound or CHK1 and CHK2 with the CCT241106 inhibitor. Induction of CIN in HCT116p53$^{-/-}$ and DLD1 cells was confirmed by increase in the percentage of chromosome missegregations after treatment with GSK923295 or the presence of micronuclei after inhibition of ATM or CHEK1 and CHEK2 with KU60019 or CCT41106 treatment, respectively. In order to continuously generate errors and induce CIN in the cells, the treatments with the compounds remained until the end of each experiment. Furthermore, a SWI/SNF impaired model was used, which included two isogenic cell lines with deletion in BRG1 or BAF180, provided by Prof Jessica Down's lab, at ICR.

To identify new targets in CIN, all the models were screened against a custom sgRNA library, containing 200 genes that are involved in DNA damage repair, spliceosome and ubiquitin machinery, metabolism or genes that are associated in the literature with aneuploidy and CIN. Due to technical limitations with the quality control in some of the samples, the models that were involved in the same pathways were clustered and hits that were associated with the proteins of interest were prioritised. Moreover, in order to confirm the identified hits, the CIN models were screened against a custom siRNA library, containing four different siRNAs for each potential identified hit in the initial sgRNA screen.

The verified hits by the siRNA screen were further confirmed by investigating the effect of their chemical inhibition, when a selective small molecule inhibitor was available, and/or by gene silencing in viability assays of the CIN models. From the compounds tested, only the selectivity of SETD7 inhibition with (R)-PFI-2HCl towards BRG1 deletion could be confirmed with its enantiomer compound, (S)-PFI-2HCl. SETD7

is a monomethytransferase that triggers the transcriptional activation of genes involved in cell cycle progression, such as CYCLIN E or E2F, or in DNA damage repair, as PARP1 (Batista and Helguero, 2018). BRG1 is also involved in the transcriptional activation of genes involved in cell cycle progression or DNA damage response/ repair machineries (like CDK2, CDK4 or ATR) (Sobczak et al., 2020, Sobczak et al., 2019). Thus, deletion of both SETD7 and BRG1 might lead to transcriptional repression of genes essential for cell viability. However, further experiments would be needed in order to confirm that sensitivity of BRG1 deleted cells to (R)-PFI-2HCl is specific to SETD7 inhibition and not due to any of the other methyltransferases that the compound can inhibit.

Furthermore, clonogenic assays after gene silencing with four different siRNAs for each hit in the CIN models and in cell lines that carry the respective mutations in the genes of interest, confirmed selectivity of HELQ towards SWI/SNF complex, TEX14 towards CENP-E inhibition and PRIM1 towards CHK1 and CHK2 inhibition. Interestingly, reduction in colony formation after transfection with PRIM1 siRNAs in cancer cell lines with SWI/SNF mutations, indicates possible selectivity of PRIM1 towards the SWI/SNF complex. Nevertheless, the majority of the siRNAs investigated promoted a degree of toxicity also in the parental cells, compared to the non-targeting siRNA control. This toxicity may be induced because the cancer cells contain multiple mutations in the pathways that we investigate. For example, the HCT116 cell line contain multiple mutations in the SWI/SNF complex. Thus, further experiments would be needed in order to validate the targets and investigate their therapeutic window, as well as to elucidate the molecular mechanisms by which their inactivation promote synthetic lethality in the different CIN models.

Interestingly, PRIM1 is involved in the generation of Okazaki fragments during DNA replication and its deletion may promote errors during DNA replication (Lee et al., 2018, Xu et al., 2016). When the CHK1/CHK2 are inactive or the SWI/SNF complex is impaired, which can supress the transcriptional activation of ATR and CHK1, the damaged DNA cannot be repaired and may progress through cell cycle, generating excessive degree of CIN (Sethy et al., 2018, Zhang et al., 2013). Moreover, TEX14

function is essential in mitosis for localisation of CENP-E and SAC at the unattached kinetochores (Mondal et al., 2012). Thus, TEX14 deletion in the absence of CENP-E may increase CIN through excessive errors in chromosome segregation, to a degree that cannot be tolerated by cancer cells. However, attempts to confirm reduction of TEX14 by immunoblotting failed to show any change in the protein band, which may be indicating non specificity of the antibody or an unstable protein. Additionally, because of the role of TEX14 in mitosis, the protein may be present only during mitosis and thus further experiments are needed in order to investigate TEX14 expression after cell synchronisation in mitosis. Finally, the expression of the genes that were confirmed as hits by the siRNA screening can be further verified by a real time PCR primer-library, investigating the expression of each gene after silencing with each one of the four corresponding siRNAs. The model of mechanism for each target will be discussed in more detail in the final discussion (chapter 6).

In summary, the data presented in this chapter demonstrate potential targets for inducing synthetic lethal interactions dependent to the genes that drive the CIN phenotype. However, the synthetic lethality between the majority of the potential targets and the genes of interest may be resulted through induction of excessive levels of CIN, detrimental to cancer cell's physiology.

Chapter 4 - Targeting aneuploidy in cancer

4.1 Introduction

Aneuploidy can be a cause of tumour initiation, progression and therapy resistance and is present in the majority of solid tumours (Ben-David and Amon, 2019, Turajilic et al., 2019). Induction of numerical or structural aneuploidy can occur directly by the generation of mitotic errors, such as chromosome missegregation that may arise by syntelic or merotelic attachments, a non- functional or weakened SAC that allows the transition from metaphase to anaphase even in the presence of unattached chromosomes, or the induction of tetraploidy, which serves as an intermediate between diploidy and aneuploidy (McGranahan et al., 2012, Simmonetti et al., 2019). A well-studied mechanism of chromosome missegregation is inhibition of CENP-E by the GSK923295 compound, which promotes prolonged mitotic delay and complete failure in chromosome alignment. Importantly, the effects of GSK923295 treatment are reversible and therefore, after its removal, the cells progress through mitosis, but with increased frequency of chromosome segregation errors (Bennett et al., 2015). As explained in chapter 1, CENP-E is a kinesin-7 motor protein that localizes at the kinetochore of mitotic chromosomes and is crucial for chromosome alignment at the metaphase plate, through plus-end microtubule elongation, and interactions with SAC proteins, like BUBR1 that is a core SAC component (Weaver et al., 2007, Chen and Hancock, 2015, Ohashi et al., 2015). Similarly, Eg5 is a plus-ended directed kinesin-5 that is localised on centrosomes, in the beginning of prophase, and is important for the duplicated centrosomes movement to the opposite poles of the cells, through bundling and sliding of parallel and antiparallel microtubules (Chen and Hancock, 2015, Maliga et al., 2002). Thus, inhibition of Eg5 by Monastrol, prevents the separation of duplicated chromosomes and the formation of bipolar spindles and leads to monopolar spindles, which are prone to chromosome

missegregation by syntelic microtubule-kinetochore attachments, lagging chromosomes, chromosome fragmentation or cytokinesis failure (Maliga et al., 2002, Worall et al., 2018, Ohashi et al., 2015). Additionally, knockdown of CENP-E or Eg5 in combination with BUBR1 knockdown promoted lagging chromosomes and micronuclei formation or multipolar spindles, cytokinesis failure and polyploidy, respectively (Ohashi et al., 2015).

An additional antimitotic drug that is linked to aneuploidy, is Paclitaxel. Paclitaxel (or Taxol) is a chemotherapeutic agent that is used as a standard-of-care treatment in multiple cancers and specifically for ovarian cancer, since 1992, and breast cancer, since 1994. Taxol is a microtubule-targeting agent that binds to microtubules, on β-tubulin, and stabilises them, interfering with microtubules dynamic to attach to kinetochores and promotes mitotic arrest through SAC activation, that usually leads to cell death (Cermak et al., 2020). However, long-term and repeated treatment of Taxol drives drug resistance in cancer cells. Notable, human non-transformed or breast cancers cells, resistant to Taxol, were in their majority aneuploid, containing an abnormal microtubule network, promoting chromosome missegregations through multipolar division (Bouchet et al., 2007, Zasadil et al., 2014). Abrogation of paclitaxel-induced SAC, for example, by an MPS1 inhibitor, promoted rapid exit from mitosis with the majority of cells containing unaligned chromosomes, massive chromosome missegregation and cell death (Gurden et al., 2015).

Aneuploidy may be detrimental or advantageous in cell's physiology, introducing the aneuploidy paradox. This paradox may be the result of specific chromosome gains or losses, the generated cellular stress or the dosage compensation that can minimise the above consequences (Santaguida and Amon, 2015). Therefore, aneuploidy can have a profound impact in the cell physiology beyond the loss/gains of specific genes, which provides an opportunity to identify novel targets in aneuploidy, either in a gene-agnostic way or by synthetic lethal interactions due to specific gains/losses of chromosomes.

A second aim of this project is to identify potential targets in aneuploidy,

dependent or independent to specific chromosome gain or loss, using the CRISPR/Cas9 system and custom sgRNA libraries. Moreover, there is a dispute for the role of p53 in aneuploid cells. Thompson and Compton in 2010, suggested that chromosome missegregation events induce p53-dependent apoptosis, while in 2017, Sotto et al., argued that low degree of whole chromosome missegregations can be tolerated in p53 proficient cells, but structural aneuploidies are prohibited. Thus, we focused on targeting aneuploidy independently of p53 function.

In order to generate aneuploid cell models, mitotic errors were induced in euploid parental cell lines, with deleted or non-functional p53, to increase the aneuploid population. The generated potential aneuploid clones were propagated after single cell sorting and characterized by multiple methods, including CGH and SNPs microarrays, before proceeding with a CRISPR/Cas9 loss of function screening.

4.2 Results

4.2.1 Generation and characterisation of aneuploid clones

In order to isolate aneuploid clones with different number of chromosomes from the pseudo-diploid HCT116p53$^{-/-}$ cells and the diploid or the tetraploid DLD1 cells, a single cell sorting approach was utilized. Cancer cell lines, in which the major cell population has diploid or tetraploid DNA content, contain minor subpopulations with chromosome gains or losses that can be isolated by fluorescence-activated cell sorting (FACS) sorting, according to Hoechst cell cycle profile. Therefore, a multiple-fold approach was followed, presented in Figure 4.1, either by isolating naturally occurring aneuploid cells or by promoting mitotic errors in order to enrich our cells with aneuploid subpopulations.

Our rationale is based on the following approach: in the Hoechst cell cycle profile of a diploid cell line, the G2/M phase of a minor subpopulation of cells, with chromosome gains, would be distinct from the G2/M phase of the main diploid population and

therefore; could be isolated by FACS. In contrast, the G1 and S phases of a subpopulation of cells with chromosome gains would be intertwined with the G1 and S phases of the major diploid population (Figure 4.2 A). Similarly, in a tetraploid cell line, a minor subpopulation of cells with chromosome losses could be easily separated from the subG1 phase of the main tetraploid population (Figure 4.2.B). Consequently, in diploid HCT116p53$^{-/-}$ and DLD1 cells, single cell sorting was performed in cells with DNA content higher than G2/M, whereas, in tetraploid DLD1 cells, single cell sorting was performed in cells with DNA content lower than G1 (Figure 4.2 A and B).

Thus, initially, single HCT116p53$^{-/-}$ and DLD1 cells with DNA content higher than diploid G2 were sorted in 96-well plates to isolate naturally occurring transiently tetraploid cells that could potentially break down into aneuploid cells. Using an additional approach, HCT116p53$^{-/-}$, DLD1 2N (diploid) or DLD1 4N (tetraploid) were treated with the microtubule depolymerisation agent nocodazole (100 ng/ml), to enrich the mitotic cells in the cell population and allow their isolation by mitotic shake-off (Figure 4.1). Then, the cells were separated in three groups in the presence of compounds that are known to induce chromosome missegregation. The first group of cells was released in the CENP-E inhibitor GSK923295 to promote chromosome missegregation by unaligned chromosomes and incorrect microtubule-kinetochore attachments. The second group was released in Paclitaxel, to stabilize microtubules and, thus, prevent chromosome movement during mitosis, while the third group was released in the Eg5 inhibitor, Monastrol, for induction of monopolar mitotic spindles. The release from nocodazole, in the presence of these compounds, allows the mitotic spindle to reform, but the spindle assembly checkpoint (SAC) remains active due to induction of chromosome missegregation. Therefore, during the induction of mitotic errors, the MPS1 inhibitor CCT289346 was used, in order to abrogate SAC and enforce mitotic exit in the presence of unaligned chromosomes. It has been shown that MPS1 kinase activity is necessary for SAC-dependent metaphase arrest in the presence of unaligned and missegregated chromosomes (Figure 4.1). A day after the treatments, potential aneuploid single cells were sorted using the same rationale that was described previously (Figure 4.2 C and

D). The DNA content of the propagated clones generated by single cells before or after the treatments was initially tested by Propidium Iodide (PI) cell cycle profile, metaphase spreads and CGH or SNP arrays (Figure 4.1 and 4.2).

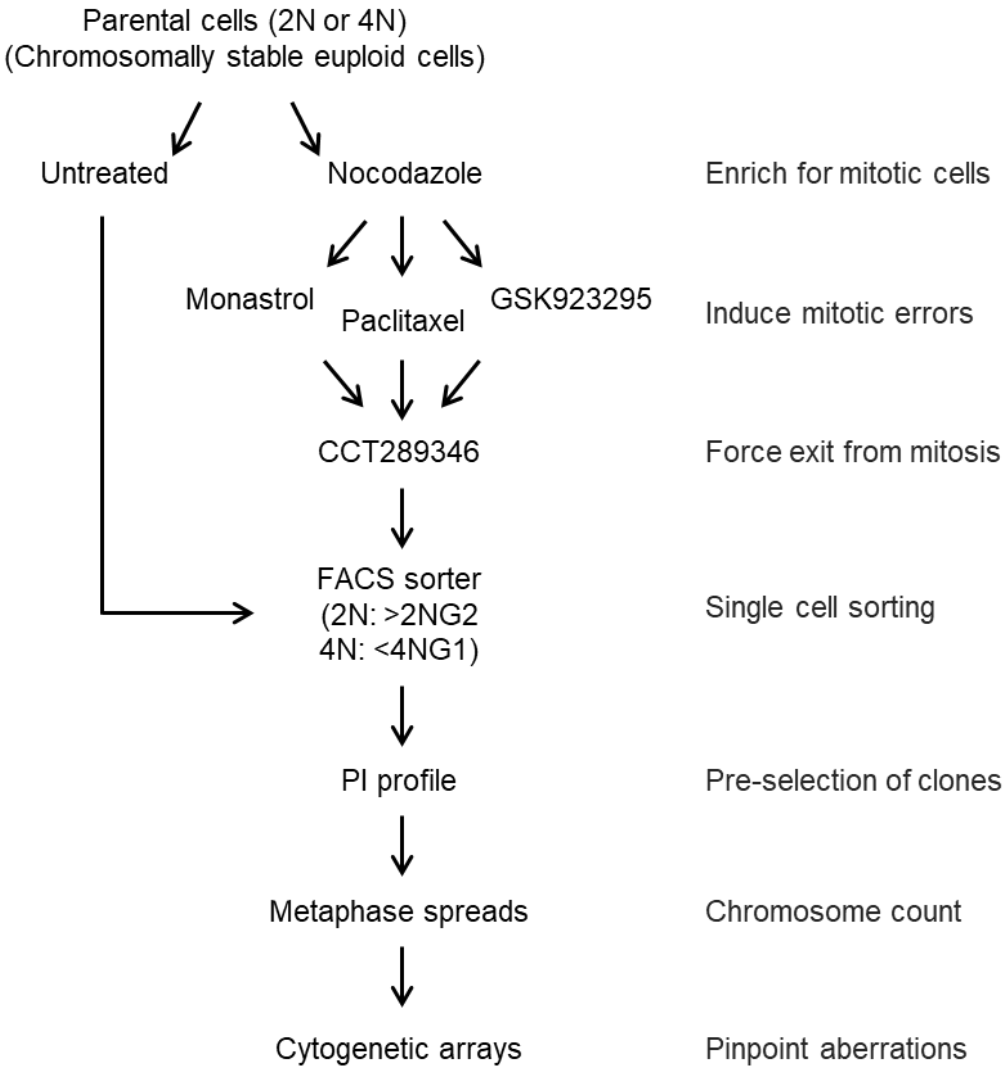

Figure 4.1: Workflow of generation and characterisation of aneuploid clones. Potential aneuploid single cells that pre-exist in chromosomal stable euploid cell lines were isolated by sorting. Moreover, chromosomal stable cells were treated with mitotic drugs to enrich the mitotic cells in the population and introduce mitotic errors in the cells. Then, the cells were released in an MPS1 inhibitor to force exit from mitosis and the possible aneuploid cells were isolated by single cell sorting and were further characterised.

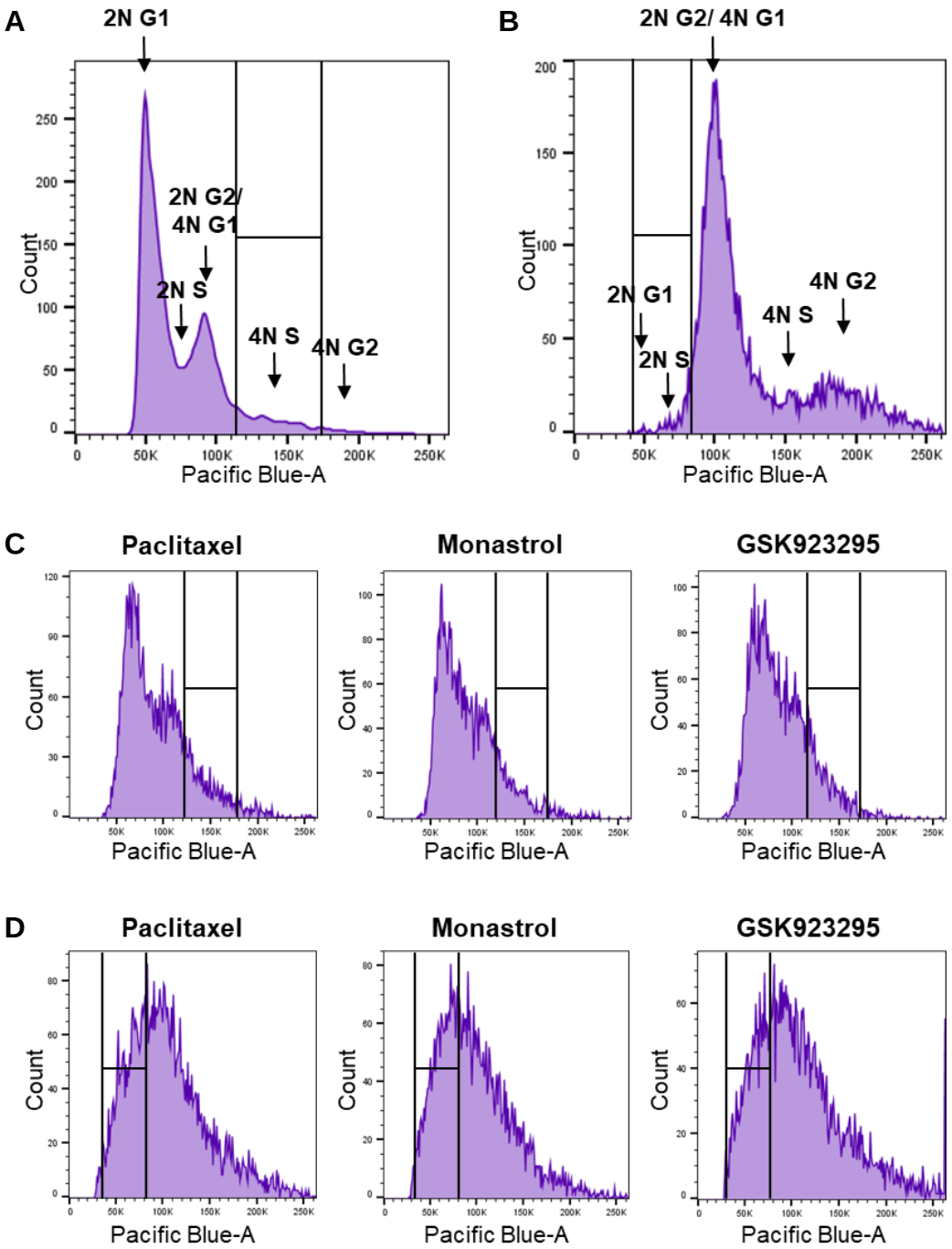

Figure 4.2: Isolation of potential aneuploid single cells through FACS sorting. (A) Illustration of the Hoechst cell cycle profile of diploid HCT116p53$^{-/-}$ cells with tetraploid or aneuploid subpopulations. Diploid G2 and tetraploid G1 phases are intertwined into a single peak**. (B)** Illustration of the Hoechst cell cycle profile of tetraploid DLD1 cells with diploid or aneuploid subpopulations. (**C)** Hoechst cell cycle profile of diploid HCT116p53$^{-/-}$ cells after treatment with Nocodazole, Paclitaxel/ Monastrol/ GSK923295 and MPS1 inhibitor. (**D)** Hoechst cell cycle profile of tetraploid DLD1 cells after treatment with Nocodazole, Paclitaxel/ Monastrol/ GSK923295 and MPS1 inhibitor. The gate in each graph illustrates the cell population, from which single cells were isolated.

4.2.1.1 Characterisation of aneuploid clones by FACS and metaphase spreads

Following propagation of the generated clones, for approximately 1 month, their DNA content was initially characterized by PI FACS cell cycle profile. The majority of clones derived from DLD1 diploid or tetraploid cells generated cell populations with tetraploid or near-tetraploid DNA content (Figure 4.3 A). In contrast, the pseudodiploid HCT116 p53 deficient cells generated both clones with near-diploid DNA content and stable tetraploid clones (Figure 4.3 B). However, unstable tetraploid clones were also generated, which transitioned to a newly formed diploid phenotype during continued culture (Figure 4.4). During this transition, additional potentially aneuploid single cells were isolated by FACS sorter, through isolation of cells with DNA content between diploidy and tetraploidy (Figure 4.5). The DNA content of the generated clones was also characterised by PI cell cycle profile. The majority of clones demonstrated similar PI cell cycle profile to the final transitioned diploid phenotype of the parental cell population (Figure 4.6). Of note, subclones with tetraploid or near tetraploid DNA content were also generated and remained stable even after weeks of continued culture, while the parental clone transitioned to a diploid DNA content. For example, all the clones generated by single cells during the transition of clone UN16, demonstrated a stable near tetraploid DNA content in contrast to the final diploid DNA content of the parental clone (Figure 4.6).

Moreover, in order to generate clones with more pronounced chromosomal alterations, near tetraploid or tetraploid HCT116p53$^{-/-}$ and DLD1 clones, which were generated after single cell sorting of cells treated with anti-mitotic drugs, were treated again with the same drugs following the workflow that was described in section 4.2.1. Similarly, possible aneuploid single cells were sorted and the DNA content of the generated clones was initially tested by PI cell cycle profile (Figure 4.7 A-B). Interestingly, second treatment of the cells and single cell isolation, generated clones with DNA content almost similar to the parental clones. Only small deviations were able to be identified by FACS, shifting the cell cycle profile slightly towards sub diploid or hyper diploid DNA content, indicating small chromosomal losses or gains, respectively

(Figure 4.7 C).

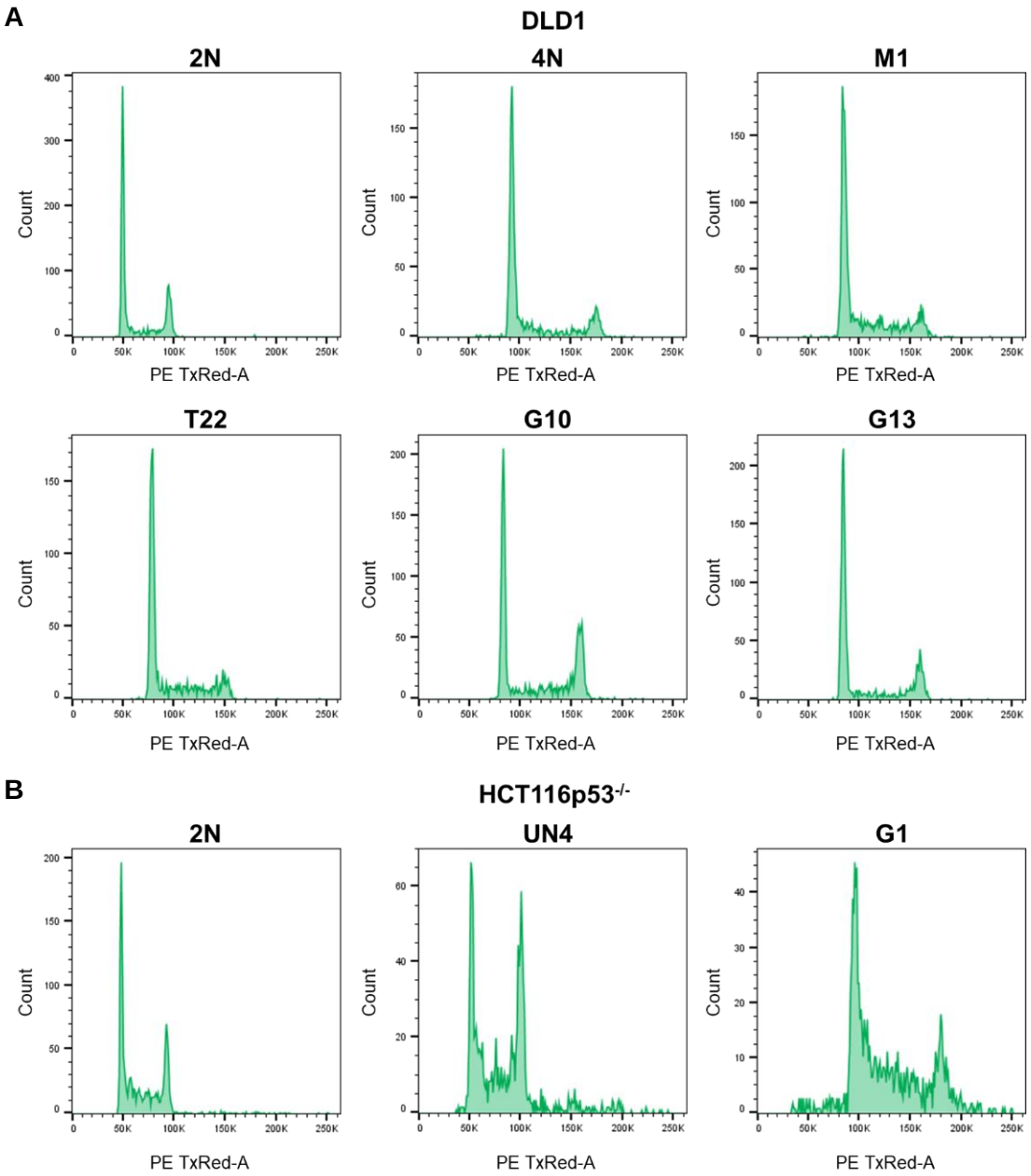

Figure 4.3: Characterisation of potential aneuploid clones by FACS. (A) Illustration of the PI cell cycle profile of diploid (2N), tetraploid (4N) DLD1 cells and generated tetraploid or near tetraploid DLD1 clones. **(B)** Illustration of the PI cell cycle profile of pseudodiploid HCT116p53$^{-/-}$ cells and the generation of near diploid (UN4) or near tetraploid clones (G1).

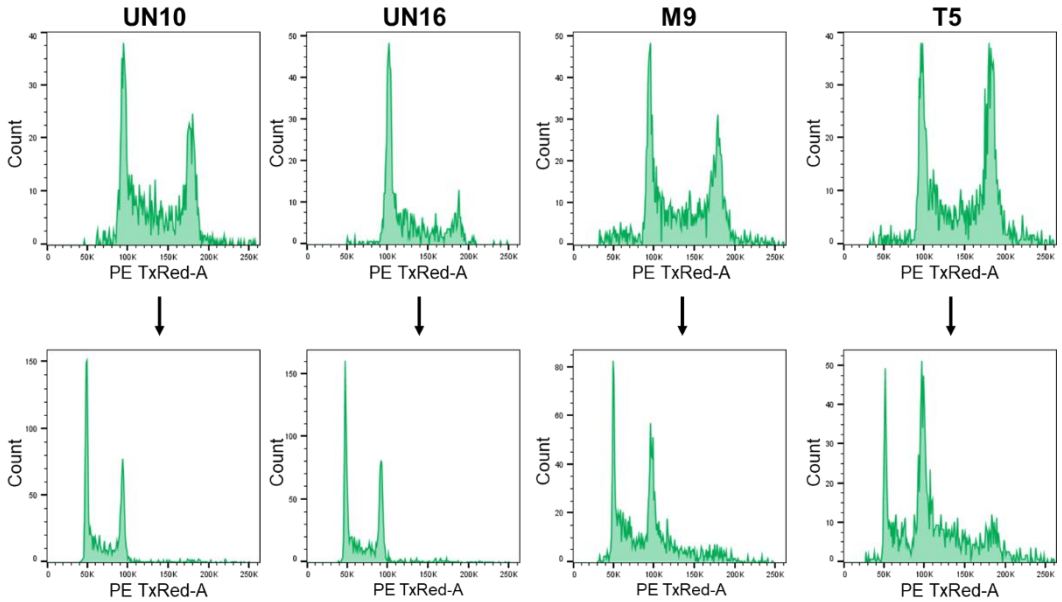

Figure 4.4: Transition of unstable HCT116p53$^{-/-}$ from tetraploidy to diploidy. (A) Demonstration of the PI cell cycle profile by FACS, of tetraploid (or near tetraploid) HCT116p53$^{-/-}$ cells before and after their transition to a diploid (or near diploid) phenotype.

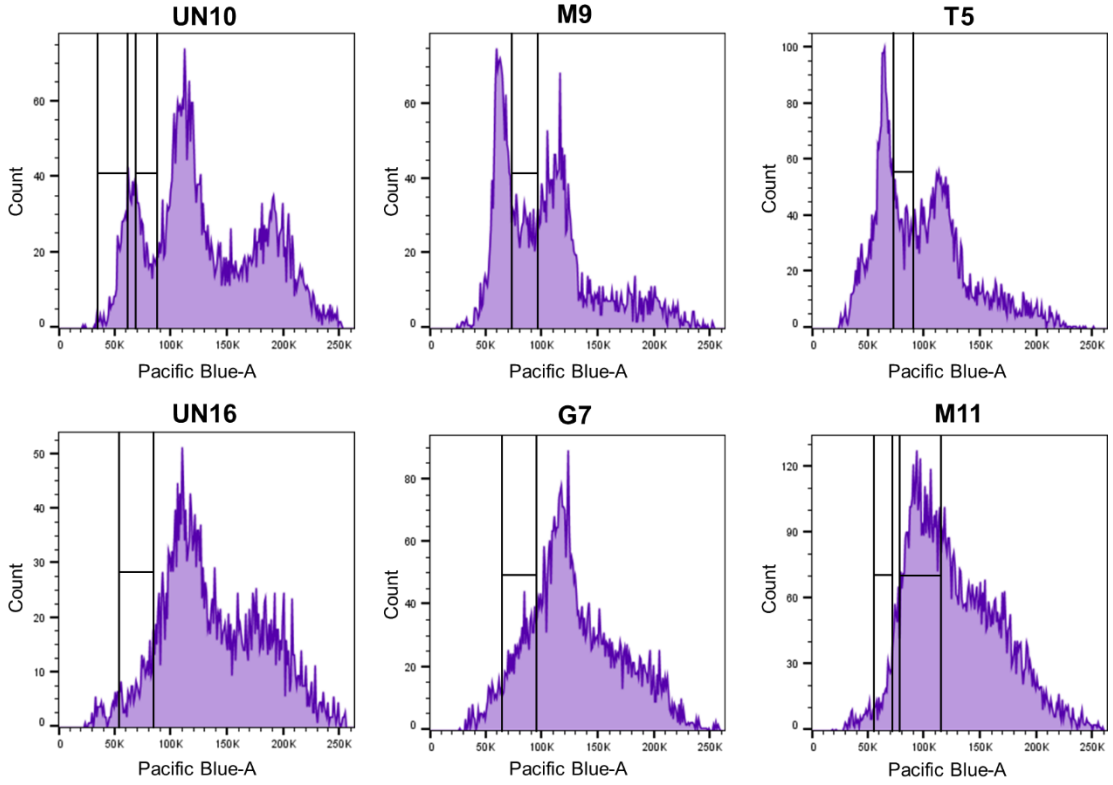

Figure 4.5: Isolation of potential aneuploid HCT116p53$^{-/-}$ cells during the transition of the cell population from tetraploidy to diploidy. Single HCT116p53$^{-/-}$ cells were isolated by FACS sorter. Depending the Hoechst cell cycle profile, the gates were placed in order to isolate single possible aneuploid cells with DNA content ranging between diploidy and tetraploidy.

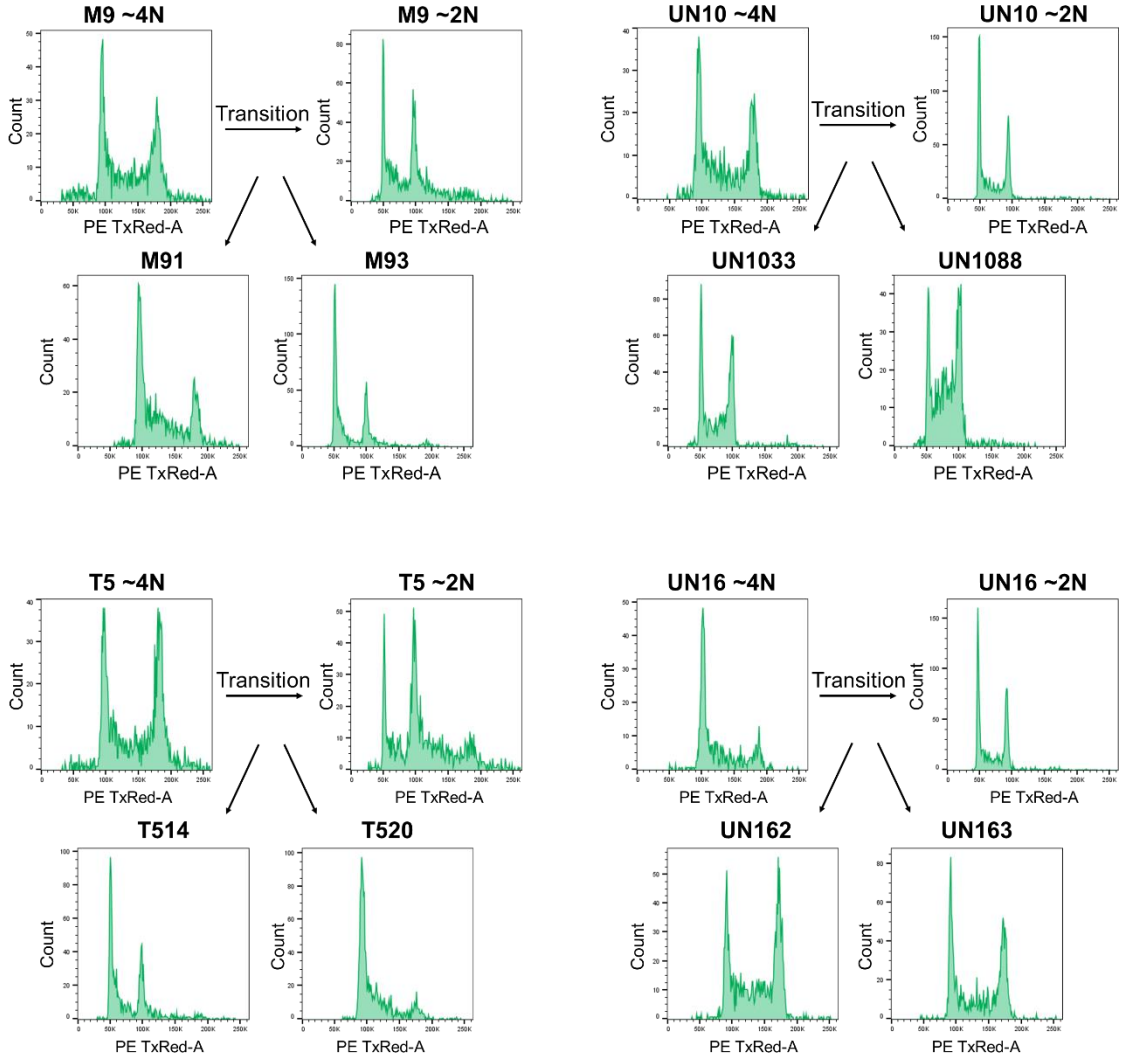

Figure 4.6: Propidium iodide cell cycle profile of HCT116p53$^{-/-}$ clones that transitioned from a near tetraploid to a near diploid cell cycle profile and clones that were generated during the transition. During the transition of near tetraploid clones to diploid, clones were generated by single cell sorting and their DNA content was characterised by PI cell cycle profile. And FACS. For each group, the original and the final clone after the transition are shown, as well as the cell cycle profile of the clones generated by single cell sorting from the transitioning cell population.

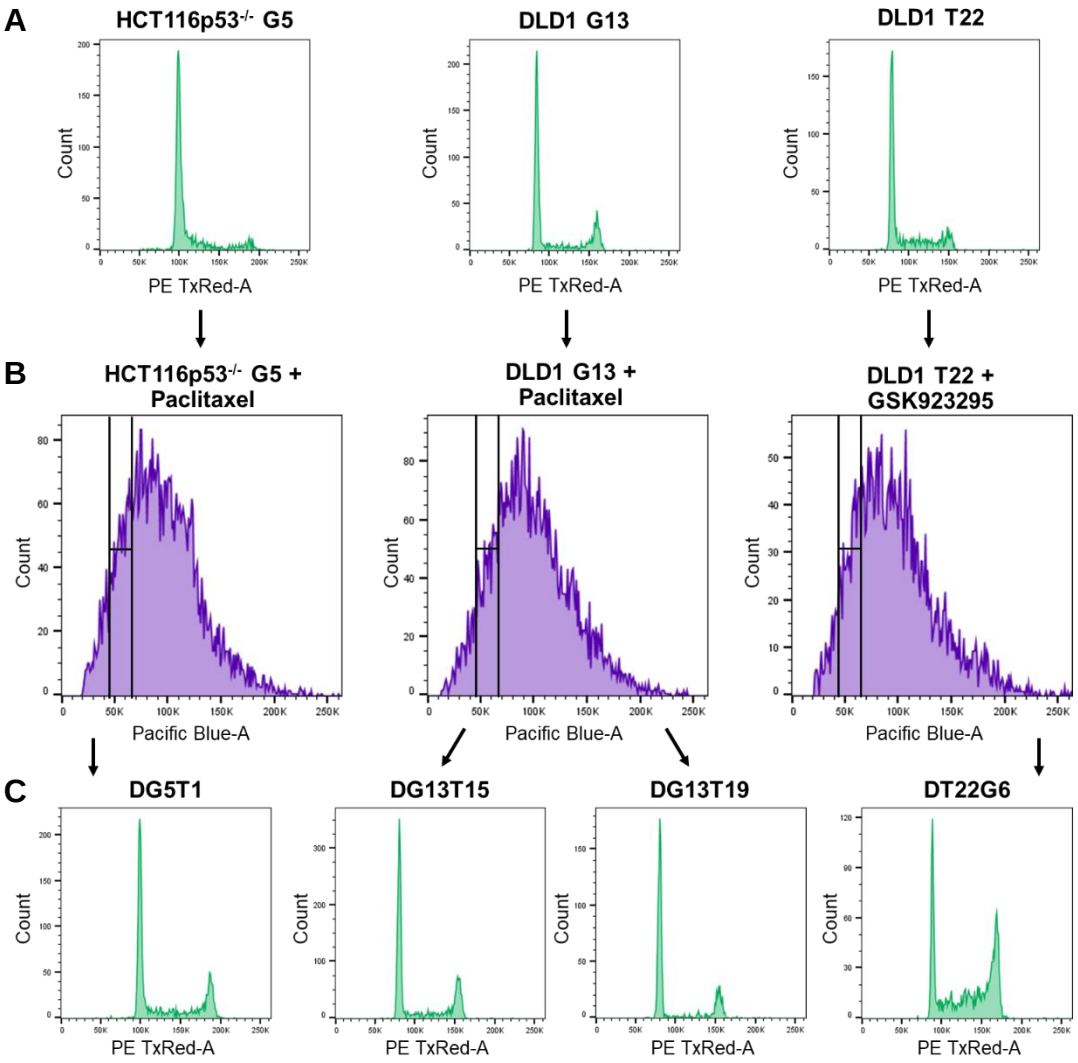

Figure 4.7: Second treatment of near tetraploid clones with anti-mitotic compounds, single cell isolation and clone propagation. (A) Near tetraploid HCT116p53$^{-/-}$ and DLD1 clones were treated with Paclitaxel or the CENPE inhibitor GSK923295 in order to generate cells with high level of chromosomal alterations. **(B)** Single aneuploid cells were sorted by FACS sorter, before the G1 phase of the near tetraploid parental clone. **(C)** The cell cycle profile of the propagated clones was characterised by FACS.

A number of clones, which appeared to shift mostly from pure diploid or tetraploid DNA content by PI cell cycle profile, were further characterized by metaphase spreads to count the exact number of chromosomes. Additionally, the transition of HCT116p53$^{-/-}$ clones from a near tetraploid to a near diploid phenotype was confirmed by chromosome count. For example, the HCT116p53$^{-/-}$ clone UN10 contained initially 86 chromosomes, but after its transition, its chromosomes were reduced to 45. Similarly, clone UN16 reduced it chromosome number from 82 to 45 (Figure 4.8 A). Moreover, slight shifting of the PI cell cycle profile of the clones in comparison to the parental cell cycle profile is

due to small changes in the chromosome number and not through technical errors (Figure 4.8 B). For example, the cell cycle profile of the clone UN1033 that was generated by single cell sorting of the transitioning clone UN10, is slightly shifted to the right compared to the cell cycle profiled of the transitioned ~2N UN10 clone or the parental HCT116p53$^{-/-}$ cell line. This slight shift can be explained by the extra chromosome that clone UN1033 contains in comparison to clone UN10 or the parental cell line, demonstrating the sensitivity of FACS PI cell cycle profile as a technique for DNA content characterisation.

4.2.1.2 Characterisation of selected aneuploid clones by CGH and SNP microarrays

A group of clones identified by FACS PI profiling and metaphase spreads as likely to be aneuploid were further characterised by Comparative Genomic Hybridization (CGH) or Single Nucleotide Polymorphisms (SNPs) microarrays, to verify their aneuploid phenotype and to identify their exact chromosomal alterations. Genomic DNA (gDNA) from the parental cells and the potential aneuploid clones was extracted and sent for CGH or SNPs microarrays. In CGH array, gDNA of possible aneuploid clones was hybridized against the DNA extracted from the HCT116p53$^{-/-}$ parental cells (originally isolated from a male patient), while the gDNA from these cells was hybridized against normal male gDNA. In SNPs genotyping, gDNA of possible aneuploid clones and the parental cells was hybridised against approximately 300,000 probes that can measure nucleotide polymorphisms and copy number variations.

Analysis of the arrays demonstrated both structural aneuploidies and whole chromosome alterations in the HCT116p53$^{-/-}$ clones compared to the parental cell lines (Fig. 4.9 A). Surprisingly, clone UN10, which was originally tetraploid and transitioned to a diploid DNA content while in culture, was slightly differentiated to the diploid parental cell line. Apart from very small alterations, clone UN10 contained a small deletion in chromosome 2 and a gain in chromosome 10, in addition to the gain or losses that are present in the parental HCT116p53$^{-/-}$ cells (Figure 4.9 A and 4.10 A). These alterations were present in all of the clones derived by single cell sorting during the transition of

clone UN10 (clones UN1033, UN1034, UN1037 and UN1088). However, all of the UN10 derived clones also contain extra chromosomal gains or losses with clone UN1088 contain a large gain of almost all the chromosome 14 (Figure 4.9 A and 4.10 A). Similarly, the clones UN16, G7 and T5, which also transitioned from a tetraploid DNA content to a diploid one, didn't demonstrate any major gains or losses in comparison with the diploid parental set of chromosomes apart from small differences (Figure 4.9 A). Of note, clone UN41 demonstrated gain of chromosome 21 compared to the diploid parent cells, while clone G1 exhibited structural losses of chromosomes 6 and 13, in comparison to the tetraploid parental cells (Figure 4.9 A and 4.10 A). Overall, excluding small chromosomal gains or losses, some HCT116p53$^{-/-}$ clones contained almost complete gain of chromosome 14 or 21 and large deletions of chromosome 6 and 13. Common chromosomal gains or losses were not identified between the HCT116p53$^{-/-}$ aneuploid clones, however chromosomes 2, 4, 16 and X were keen on obtaining short gains or losses (Fig. 4.9 A).

Characterisation by SNP microarray of DLD1 clones, generated by single cell isolation after induction of mitotic errors in tetraploid DLD1 parental cells, demonstrated only structural aneuploidies. Interestingly, all of the DLD1 clones presented mainly structural losses in chromosome 3 and a trend to demonstrate structural losses in chromosomes 2 and 21 but structural gains in chromosome 4 (Figure 4.9 B). Nevertheless, each DLD1 clone showed additional structural gains or losses that were distinct among the different clones. For example, clone G13T15 contained short structural gains in multiple chromosomes, while clone M1P1 contained gains in parts of chromosomes1, 3 and 17 but losses in chromosomes 8, 4 and 14 (Figure 4.9 B and 4.10 B). In order to target aneuploidy independently to the specific gains or losses, 10 clones with different degrees of aneuploidy, representing the majority of the generated aneuploid clones, were selected for further studies (Figure 4.11).

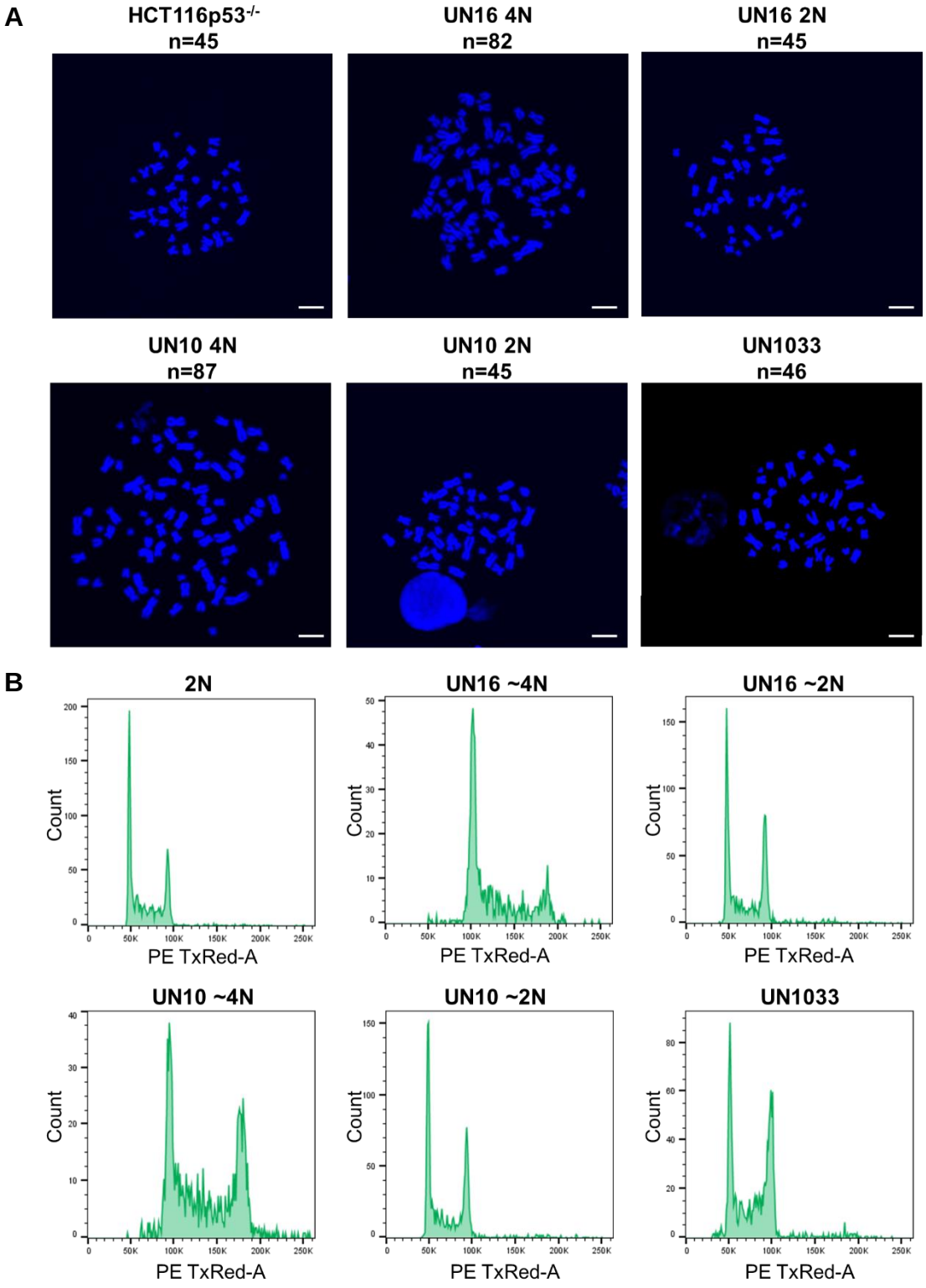

Figure 4.8: Characterisation of generated HCT116p53$^{-/-}$ by metaphase spreads and FACS. **(A)** Metaphase spreads of clones before and after their transition from a tetraploid to a diploid DNA content as well as UN1033 that was isolated during the transition of ~4N UN10 clone to a ~2N DNA content. **(B)** Propidium iodide cell cycle profile by FACS of the clones shown in (A); Scale bar= 10 µm, N=23 chromosomes and n= number of chromosomes.

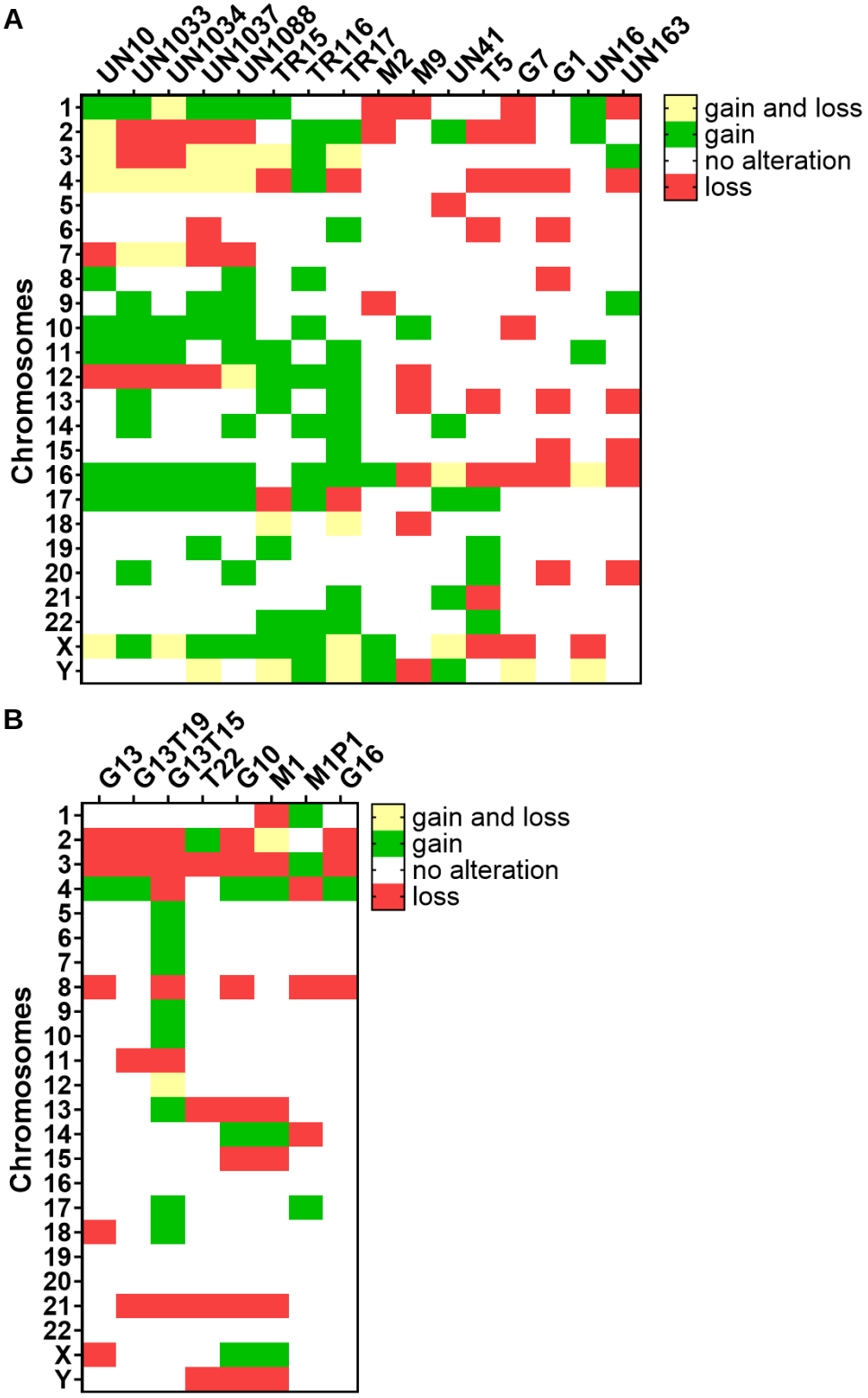

Figure 4.9: Characterisation of HCT116p53$^{-/-}$ and DLD1 clones by CGH or SNP arrays. (A) Chromosomal alterations of HCT116p53$^{-/-}$ clones, compared to the parental cells, by CGH or SNP arrays. **(B)** Chromosomal alterations of DLD1 clones, compared to the parental cells, by SNP arrays.

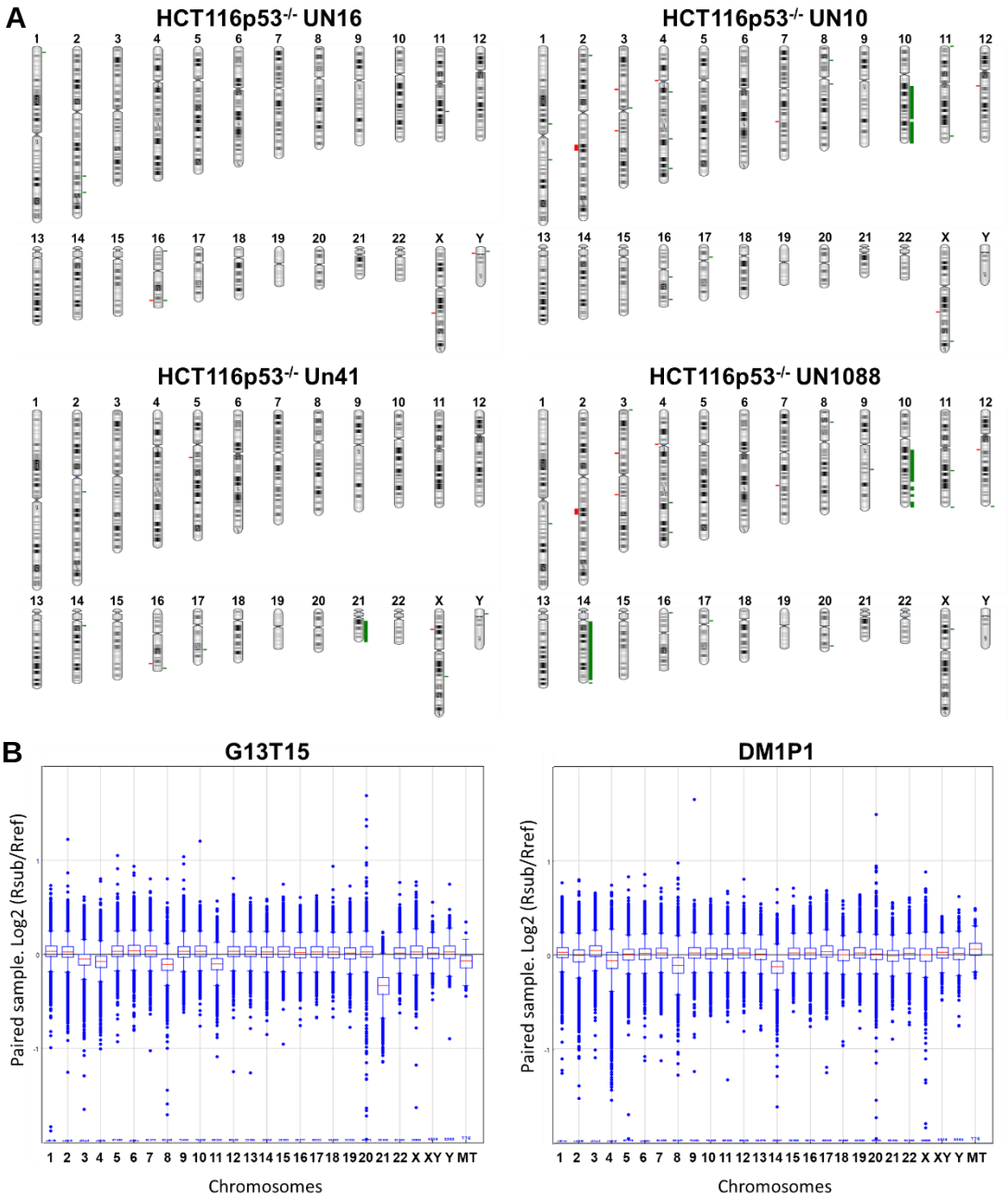

Figure 4.10: Genome wide aberrations of HCT116p53$^{-/-}$ and DLD1 clones, characterised by CGH or SNP arrays, compared to the parental cells. (A) Genome wide profile of four HCT116p53$^{-/-}$ clones characterised by CGH to the diploid parental cells. **(B)** Genome wide profile of two DLD1 clones characterised by SNPs and compared to the parental tetraploid cells. Each dot corresponds to a single SNP and the mean of the normalised SNP values is demonstrated by a red line.

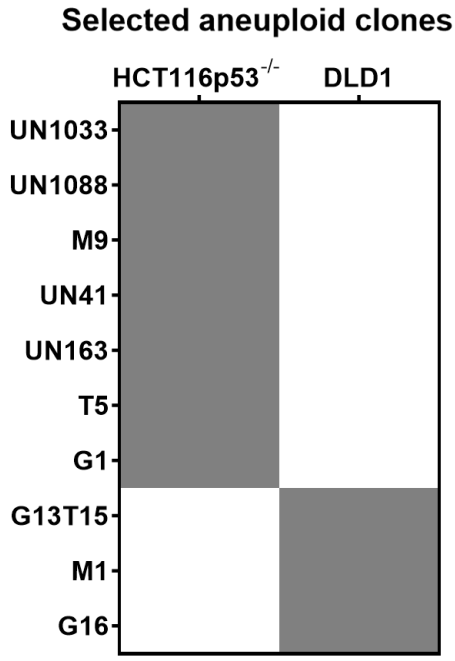

Figure 4.11: Clone selection. A total of 10 HCT116p53$^{-/-}$ and DLD1 clones with different degrees of aneuploidy were selected for further studies.

4.2.2 Targeting aneuploidy by a CRISPR/Cas9 loss of function screening

To identify potential targets in aneuploidy, a CRISPR/Cas9 loss of function screening was conducted in the selected aneuploid clones. The selected group of aneuploid clones with representative structural and numerical aneuploidies were screened, against the same custom sgRNA library that was used to identify potential hits in CIN (chapter 3).

Stable HCT116p53$^{-/-}$Cas9 and DLD1Cas9 cells were generated as presented in section 3.2.2.1. Additionally, knowing the transduction efficiency of the parental cell lines, HCT116p53$^{-/-}$ and DLD1 aneuploid clones were transduced with the Edit-R inducible Cas9 lentivirus by reverse transduction. Based to the sensitivity of the parental cells to blasticidine, presented in figure 3.4 A, the transduced aneuploid clones were selected by addition of 15 µg/ml for a period of 7 days. Selection with blasticidin continued until no growing cells could be detected in the untransduced controls and was subsequently reduced to 5 µg/ml. During this period the infected cells where split as necessary.

Induction of Cas9 in the puromycin selected HCT116p53$^{-/-}$Cas9 aneuploid clones was investigated by immunofluorescence, in response to six different concentrations of

doxycycline with a highest of 2 μg/ml, for 72 hours. Uninfected HCT116p53$^{-/-}$ cells were used as negative control and tetracycline-free FBS was used to avoid expression of Cas9 without addition of doxycycline. Nevertheless, some of the generated HCT116p53$^{-/-}$Cas9 aneuploid clones contained less than 60% of Cas9 positive cells, which was the lowest acceptable percentage (Figure 4.12 A). Thus, these Cas9 cell lines were re-infected with the Cas9 virus, by reverse transduction. A second Cas9 transduction increased the percentage of Cas9 positive cells to more than 70% in all of the clones, after addition of doxycycline. The final percentage of Cas9 positive cells in all the HCT116p53$^{-/-}$Cas9 aneuploid clones was between 73% and 93%, as shown in figure 4.12 B.

Similarly, cas9 expression was investigated by immunofluorescence in the generated DLD1Cas9 aneuploid cells, after doxycycline addition. In contrast to the HCT116p53$^{-/-}$Cas9 aneuploid clones, all the DLD1Cas9 clones were containing more than 70% of Cas9 positive cells, apart from clone G16, which contained ~60% (Figure 4.12 C). Thus, second Cas9 infection was not necessary in the DLD1 clones. Finally, the use of tetracycline-free FBS did not induce Cas9 expression, when doxycycline was not added to the cells (Figure 4.12 A - C).

Moreover, during the investigation of the percentage of Cas9 positive cells in the HCT116p53$^{-/-}$Cas9 aneuploid clones, after the first Cas9 infection, it was observed that all of the samples reached the maximum percentage of Cas9 positive cells after the addition of 74 ng/ml of doxycycline (Figure 4.12 A). In combination with the immunoblotting results for HCT116p53$^{-/-}$ presented in figure 3.5 C, a concentration of 100 ng/ml of doxycycline was selected for induction of Cas9.

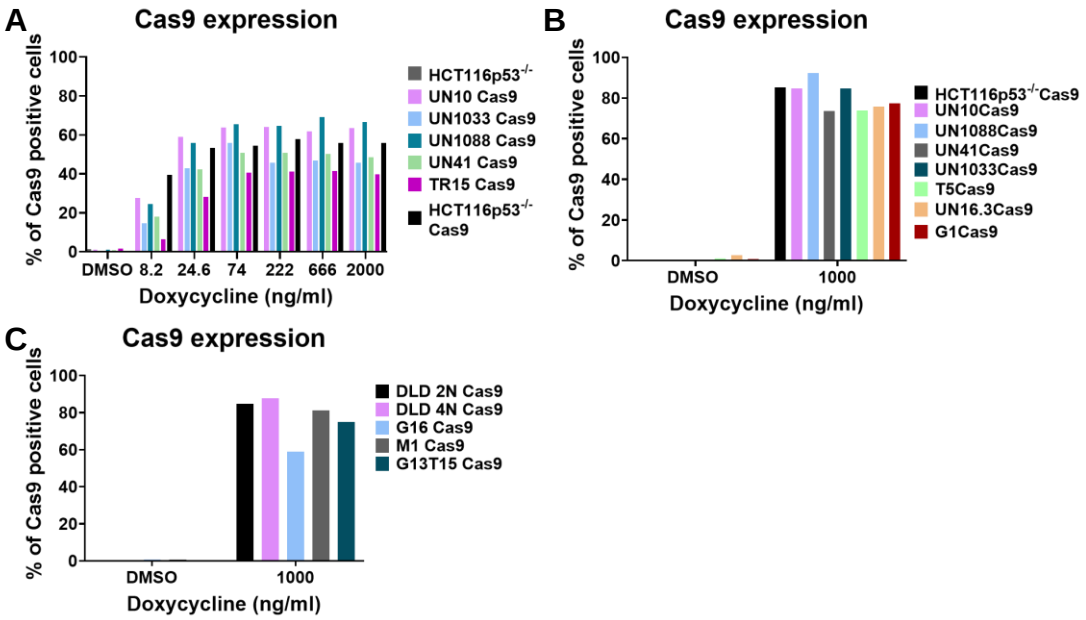

Figure 4.12: Cas9 expression after induction by doxycycline. (A) Percentage of Cas9 positive HCT116p53$^{-/-}$ cell lines by immunofluorescence, after treatment with doxycycline with a highest concentration of 2000 ng/ml, followed by six 1/3 serial dilutions for 72 hours. **(B)** Percentage of Cas9 positive cells in the final HCT116p53$^{-/-}$ clones by immunofluorescence, after treatment with 1 µg/ml of doxycycline for 72 hours. **(C)** Percentage of Cas9 positive cells in DLD1 clones by immunofluorescence, after treatment with 1 µg/ml of doxycycline for 72 hours.

Following the generation of stable Cas9 aneuploid clones and confirmation of Cas9 expression only after doxycycline addition, the Cas9 aneuploid clones were cultured in tetracycline-free FBS and each clone was transduced with the sgRNA library. The transduced cells were selected by addition of 1 µg/ml Puromycin, as was indicated from the sensitivity of the parental cells to the antibiotic, shown in figure 3.4 B. The cells were cultured in puromycin for approximately 5 days or until no cells were left growing in the transduced control aneuploid clones (Appendices figure 7.1).

The selected sgRNA transduced clones were kept in culture to grow for 2-3 more days and the cells were separated in two groups. In the first group, DNA was extracted named as baseline DNA, while in the second group, 100 ng/ml of Doxycycline was added for 96 hours in order to induce Cas9. The cells were kept in culture for 16 more days and at the end of this period, DNA was extracted and named as endpoint DNA. All the DNA samples (baseline and endpoint) for each cell line were sent for next generation sequencing (NGS) to Horizon.

Nevertheless, as in the samples from the screening of the CIN models, through technical limitations, the vast majority of the DNA samples did not pass the quality control and the products were not visible after PCR amplification. Unfortunately, the list of the samples that failed the quality control included the baseline sample from the parental HCT116p53$^{-/-}$ cells and baseline or endpoint samples from almost every clone (Figure 4.13). For this reason, no hits were able to be identified in the aneuploid clones and we focused on confirming the hits that were identified in the CIN part of the study (chapter 3).

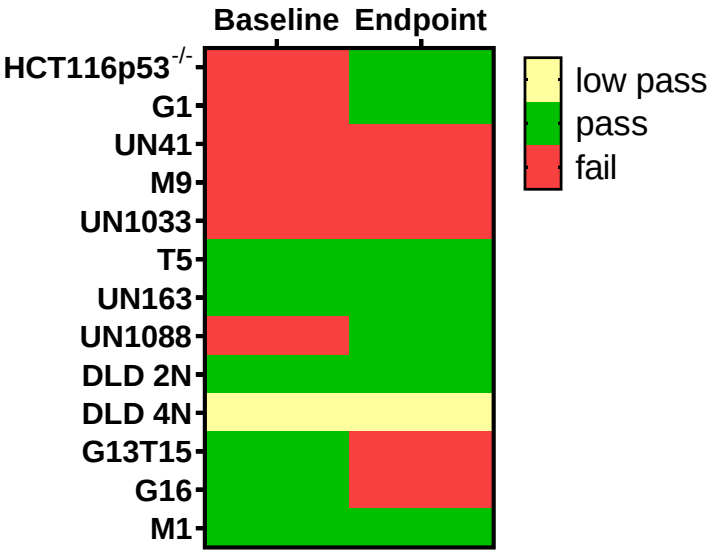

Figure 4.13: Status of samples after the quality control. PCR amplification was performed by PCR amplification in all of the samples, before the next generation sequencing. Pass demonstrates that the amplified PCR product was able to be identified, low pass that the product could be roughly identified, while fail represent the products could not be identified after PCR amplification.

4.3 Conclusions

The aim of this part of the study was to identify potential hits to aneuploidy dependent or independent of specific chromosomal gains or losses. Therefore, aneuploid clones were generated, initially, by single cell isolation of the naturally occurring aneuploid cells in the population of chromosomally stable euploid HCT116p53$^{-/-}$ and DLD1 cell lines. Using an additional approach, aneuploid population was induced

in parental cell lines by the induction of mitotic errors using chemical inhibition of CENP-E, Eg5 or paclitaxel treatment followed by MPS1 inhibition. Aneuploid cells were isolated by single cell sorting and the propagated clones were further characterised by PI cell cycle profile, metaphase spreads and CGH or SNPs microarrays. Interestingly, the majority of the generated clones contained near diploid or near tetraploid DNA content and some HCT116p53$^{-/-}$ clones were observed to transition from a near diploid to a near tetraploid DNA content. Further single cell isolation of the transitioning cells or second treatment of the near tetraploid clones failed to generate clones with high chromosomal alterations. These results indicate that high levels of aneuploidy cannot be tolerated in cancer cells.

Characterisation of possible aneuploid clones by CGH or SNP arrays confirmed the presence of small chromosomal alterations in the clones. All of the generated clones contained structural aneuploidies, however in some HCT116p53$^{-/-}$ clones, large chromosomal gains were observed, almost duplicating the chromosomes 14 or 21. No specific chromosomal alterations were able to be identified, nevertheless, chromosomes 2 and 4 were commonly presenting structural gains or losses in both HCT116p53$^{-/-}$ and DLD1 clones. HCT116p53$^{-/-}$ clones also demonstrated a trend to obtain alterations in chromosomes 16 and X, while DLD1 clones in chromosomes 3 and 21. For the purposes of this project, clones with different chromosomal alterations were selected to proceed with the CRISPR/Cas9 loss of function screening of two custom sgRNA libraries.

The CRISPR/Cas9 protocol, given by Dharmacon/Horizon, was followed and every step was optimised. Moreover, the Cas9 expression was confirmed by immunofluorescence and immunoblotting, only in the presence of doxycycline, as it was expected and addition of selection antibiotic only allowed the survival of the cells that were transduced with the sgRNA library. Nevertheless, most of the DNA samples, including some from the parental cell lines, failed to pass the quality control, preventing us from identifying potential targets in aneuploidy. Thus, we focused on confirming the hits that were identified from the sgRNA screen of the CIN models. Moreover, it would be interesting to further investigate if the hits that were confirmed in the CIN part of this

study, also sensitize the aneuploid clones due to excessive degree of chromosomal alterations that cannot be tolerated by cancer cells. For example, it has been presented that deletion of TEX14, which in chapter 3 was shown to be synthetic lethal with CENP-E, weakens SAC, promoting chromosome missegregations and aneuploidy (Mondal et al., 2012). Induction of aneuploidy in an already aneuploid genetic background will increase the level of aneuploidy in the cell in a degree that may be not be tolerated by cancer cells.

Chapter 5 - Mechanisms of DNA content reduction in cancer

5.1 Introduction

Aneuploidy and chromosomal instability are most commonly associated with loss of function of tumour suppressors and gain of function in oncogenes that result in errors during mitosis or DNA synthesis or repair. However, recently, neosis and cell fusion, have emerged as additional mechanisms leading to CIN and aneuploidy. Neosis describes a special type of cell division in polyploid giant cancer cells (PGCCs) by karyokinesis via nuclear budding resulting in smaller mononuclear cells. PGCCs and neosis have been shown to be induced post-irradiation or post-chemotherapeutic treatment (Sundaram et al., 2004, Rajaraman et al., 2006). Cell fusion refers to the insertion of one cell in a second host cell. The invading cell can either share its cytoplasm with the host cell or the fused cells can retain their individual cytoplasms (Bastida-Ruiz et al., 2016, Durgan and Florey, 2018). The latter event is named entosis, however for the purposes of this study, both events will be referred as cell fusion. Previous studies have shown that cancer cells acquire the ability to fuse with cells of the microenvironment and in the presence of chemotherapy treatment the fusion events increase in frequency (Searles, et al., 2018, Yan et al., 2016). The hybrid cells demonstrate aneuploidy and have also been shown to obtain cancer stem-like properties and resistance to chemotherapy (Searles, et al., 2018, Yin et al., 2020).

Following the fusion event, the two nuclei may remain separate, as heterokaryons that can undergo mitotic divisions independently. The presence of a second cell in the cytoplasm may intervene with the structure of the mitotic cell and lead to an error prone mitotic division, generating chromosome missegregations or cytokinesis failure (Durgan and Florey, 2018). Moreover, the nuclei of the fused cells can merge forming one nucleus, named synkaryon that can undergo mitosis with multipolar

spindles generating chromosomal instability or aneuploidisation (Zhou et al., 2015, Janssen and Medema, 2012).

The fate of the cells generated by neosis or cell fusion is not well understood. Research studies are mainly focused on mononucleated cells that can emerge from PGCCs after chemotherapy treatment, which are able to proliferate and can be resistant to the initial treatment (Amend et al., 2019, Mittal et al., 2017). Nevertheless, the mechanism that triggers cell fusion or the emergence of mononucleated cells from multinucleated cells is not well understood.

During the generation of the aneuploid clones, as described in chapter 4, we observed that the majority of the clones generated contained similar DNA content to the parental cells or were able to reduce their DNA content during propagation. Thus, the aims of this part of the study are a) to identify the mechanisms by which cancer cells can change their chromosome number or generate mononucleated cells and b) to investigate potential approaches of targeting cell recovery after chemotherapy treatment. Therefore, we performed experiments using time-lapse microscopy to follow the fate of chemotherapy treated cells and a screening of cells post-chemotherapy using a small molecule library, to identify targets for cell recovery.

5.2 Results

5.2.1 Identification of events by which cells can change their DNA content

During the first part of this study, to identify targets in aneuploidy, we generated and propagated aneuploid clones by single cell isolation of either the naturally occurring aneuploid cells or the aneuploid cells generated after induction of mitotic errors in diploid cancer cell populations. However, during the cell cycle profile characterisation we observed that the majority of the generated clones contained similar DNA content to the parental cells. Even under a second treatment of these clones using antimitotic drugs, the DNA content of the newly generated clones was also similar to the parental cells

(Table 5.1). Interestingly, clones that were changing their DNA content from a near tetraploid to a near diploid were also observed, independent of the initial drug treatment to generate aneuploidy. This transition was confirmed by FACS PI cell cycle profiling and metaphase spreads, while CGH or SNPs microarrays showed only small differences compared to the parental diploid cells (Figure 4.4, 4.6, 4.8, 4.9 and 5.1).

Table 5.1: Final DNA content of generated clones.

Cell Line	DNA content				
	Total number of clones	Similar to the parental cells	Near diploid	Between diploid and tetraploid	Near tetraploid
HCT116p53$^{-/-}$ (2N,4N)	261	200	28	1	32
DLD1 (2N, 4N)	205	182	3	6	14

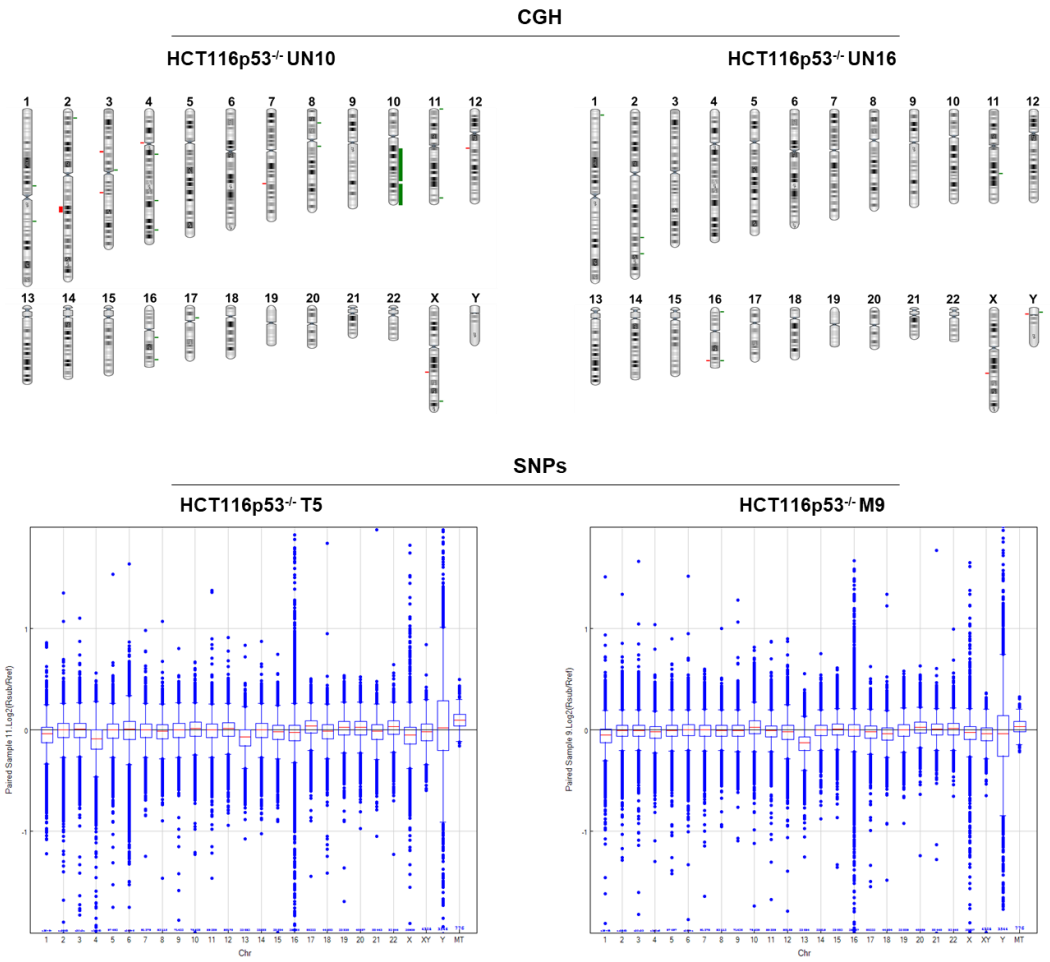

Figure 5.1: Differences in the genome wide profiles of clones transitioned to a diploid DNA content, compared to the diploid parental cells. Illustration of differences in the genome wide profile of HCT116p53$^{-/-}$ clones that transitioned from a near tetraploid to a near diploid DNA content as demonstrated by CGH or SNPs microarrays. In CGH analysis, red illustrates loss of

chromosomic regions, while green gain of regions. In SNPs analysis, each dot represents the different SNPs. Mean above 0 demonstrates chromosomal gains, while mean below 0 illustrates chromosomal losses.

To identify the events by which cancer cells can change their DNA content, H2B-mcherry and H2B-GFP HCT116p53$^{-/-}$ cells were generated. Equal number of H2B-mCherry and H2B-GFP cells were mixed and treated with 5nM of Paclitaxel for three days, as this was one of the drugs used initially to generate aneuploid clones and it is widely used in the clinic. The concentration of 5nM is considered clinically relevant and was selected based on the observation that even 6 days of dose response to Taxol, a small residual cell population remains (Figure 5.2 A). After Taxol treatment, cells were released to fresh media and the fate of the cells was investigated by time-lapse microscopy for 3 days.

As expected, Taxol treatment increased the number of multinucleated cells, due to microtubule stabilisation, causing cytokinesis failure or abortive mitosis. To summarise the distinct processes undergone by the cells after Taxol treatment, we observed: PGCCs and multinucleation generated by cell fusion. Importantly, the PGCCs contained green and red nuclei, indicating that cell fusion contributed to their generation (Figure 5.2 B and Appendices video 1). Fused cells underwent independent mitosis, in which only one of the two nuclei underwent mitosis (Figure 5.2 B and Appendices video 2). Moreover, we observed that often single cells exit the host cell, either by a mechanism that involves budding (neosis) or by a process we named “cell exodus” (Figure 5.2 B and Appendices videos 1 and 3). Finally, we observed fused cells in which one nucleus undergoes independent nucleus catastrophe and either was eliminated from the host cell or remained as a micronucleus (Figure 5.2 B and Appendices video 4). Of note, these events, at a much lower frequency, were observed in the control sample, however, treatment with Taxol increased their occurrence 2- to 3-fold, indicating that these processes may be the cause of the acquiring resistance to drugs (Figure 5.3).

Importantly, cells that underwent cell exodus (6 in DMSO and 29 in Taxol treated cells) were able to undergo mitosis (2 cells in DMSO and 3 cells in Taxol). In addition,

only in the Taxol treated cells, the cells that underwent cell exodus were able to become fused again (12 cells from the 29 cells in total). However, four of the exited cells in Taxol sample died or they moved out of the optical field and their fate couldn't be followed (10 cells in Taxol sample and 4 in the DMSO) (Figure 5.3).

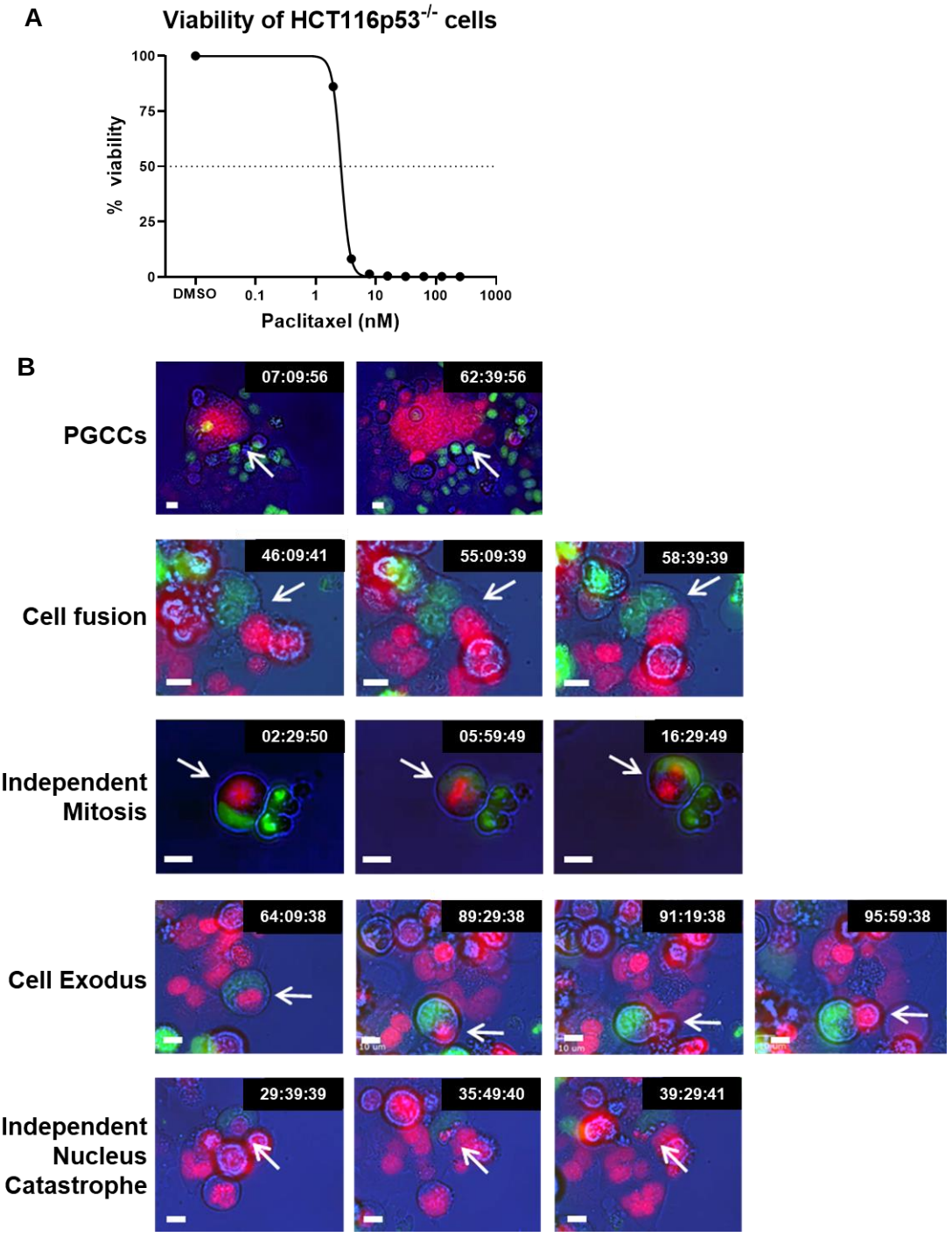

Figure 5.2: Events by which cancer cells can change their DNA content after Paclitaxel treatment. (A) Sensitivity to Paclitaxel with a maximum concentration of 250 nM followed by 7 1/2 serial dilutions. **(B)** Illustration of DNA content changing events induced by Paclitaxel treatment, during a three day time-lapse microscopy with Zeiss3i widefield microscope. Red demonstrated the H2B-RFP nuclei, green the H2B-GFP nuclei and blue the phase contrast. Scale bar at 10μm.

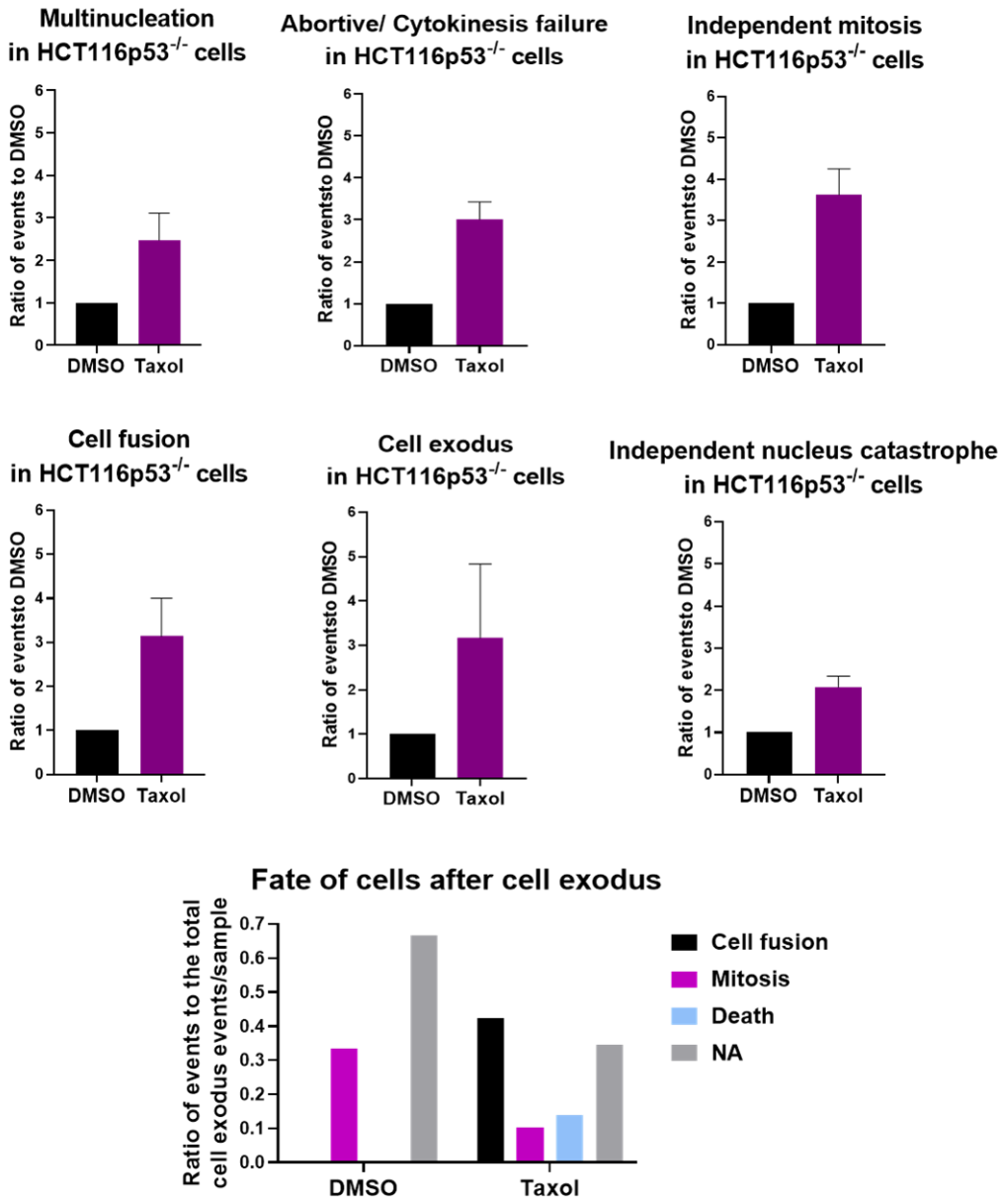

Figure 5.3: Increase of DNA content changing events after Paclitaxel treatment. Ratio of events observed after treatment with Taxol compared to the control sample. The fate of cells after cell exodus were compared to the total number of cell exodus event per sample. 10 positions per samples were imaged with Zeiss3i widefield microscope and the fate of at least 150 cells/sample was followed. Mean and range of two biological repeats are shown, where available.

5.2.1.1 Events of DNA content alteration in breast cancer cells

To exclude the possibility that the observed events are cell line specific, triple negative HCC1143 cells expressing either H2B-RFP or H2B-GFP were generated and analysed following the same approach. Equal number of cells with H2B-RFP or H2B-GFP were mixed and treated with three different concentrations of Paclitaxel for 3 days. Based on the sensitivity of HCC1143 cells to Taxol, the concentrations of 2 nM, 7.5 nM

and 30 nM were used to investigate if Taxol induces cell fusion in these cells and to characterise the remaining cells after high concentration of Taxol treatment (Figure 5.4 A). Thus, after Taxol treatment, the cells were fixed and imaged. Increasing the concentration of Taxol increased the number of multinucleated cells; approximately 60% of the remaining cells after 30nM of Taxol, being multinucleated. Furthermore, increasing Taxol concentration, increased the percentage of cell fusions, approximately 10% and 15% when the cells were treated with 7.5 nM and 30 nM Taxol, respectively. Nevertheless, only fusions between H2B-RFP and H2B-GFP cells were able to be identified, thus these percentages constitute only the 1/3 of the total fusions in each sample (Figure 5.4 B). These results indicate that treatment with Taxol induces cell fusion and the majority of the persistent cells after high concentrations of paclitaxel are multinucleated, with cell fusion significantly contributing to their generation.

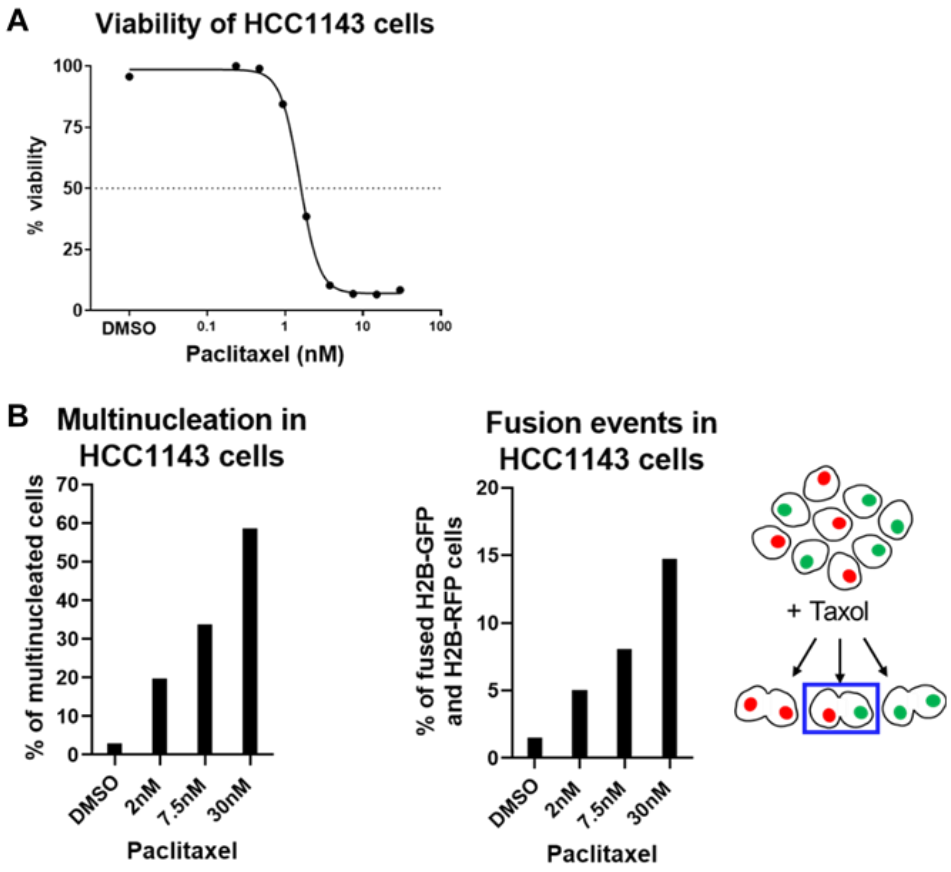

Figure 5.4: HCC1143 sensitivity to paclitaxel treatment and its effect to multinucleation and cell fusion. (A) 5-day growth inhibition assay in response to Paclitaxel. Highest concentration of 30 nM was used, followed by 7 1/2 serious dilutions. **(B)** Percentage of multinucleated and fused cells, three days after Taxol treatment. Images were taken with ImageExpress and the percentage was calculated after observation of 1000 cells per condition.

To investigate if additional DNA content changing events that were identified in HCT116p53$^{-/-}$ cells are also present during Taxol treatment in breast cancer cells, the fate of HCC1143 cells during Taxol treatment was followed by time-lapse. Equal number of H2B-RFP and H2B-GFP HCC1143 cells were mixed and treated with 7.5 nM Taxol. This concentration of paclitaxel was selected as it is the lowest concentration of the drug generating persistent fused cells that we could use as a model to study the cell fusion event as well as the events that follows it. Thus, when Taxol was added to the cells, their fate was followed for 3 days by time-lapse. All of the events that have been previously identified in HCT116p53$^{-/-}$ cells were also identified in HCC1143 cells (Figure 5.5 A). However, we noticed that during Taxol treatment, when cells undergo independent mitosis, the daughter cells can either remain in the original fused cell or exit, contributing to cell population recovery by cell exodus. Moreover, independent nucleus catastrophe is not as frequent as cell exodus (only 2 cells in the 26 that get fused in total, while 15 cells undergo cell exodus) and thus, for further experiments we focused in the events of cell fusion and cell exodus as a possible mechanism of cell population recovery after cell Taxol treatment (Figure 5.5 B).

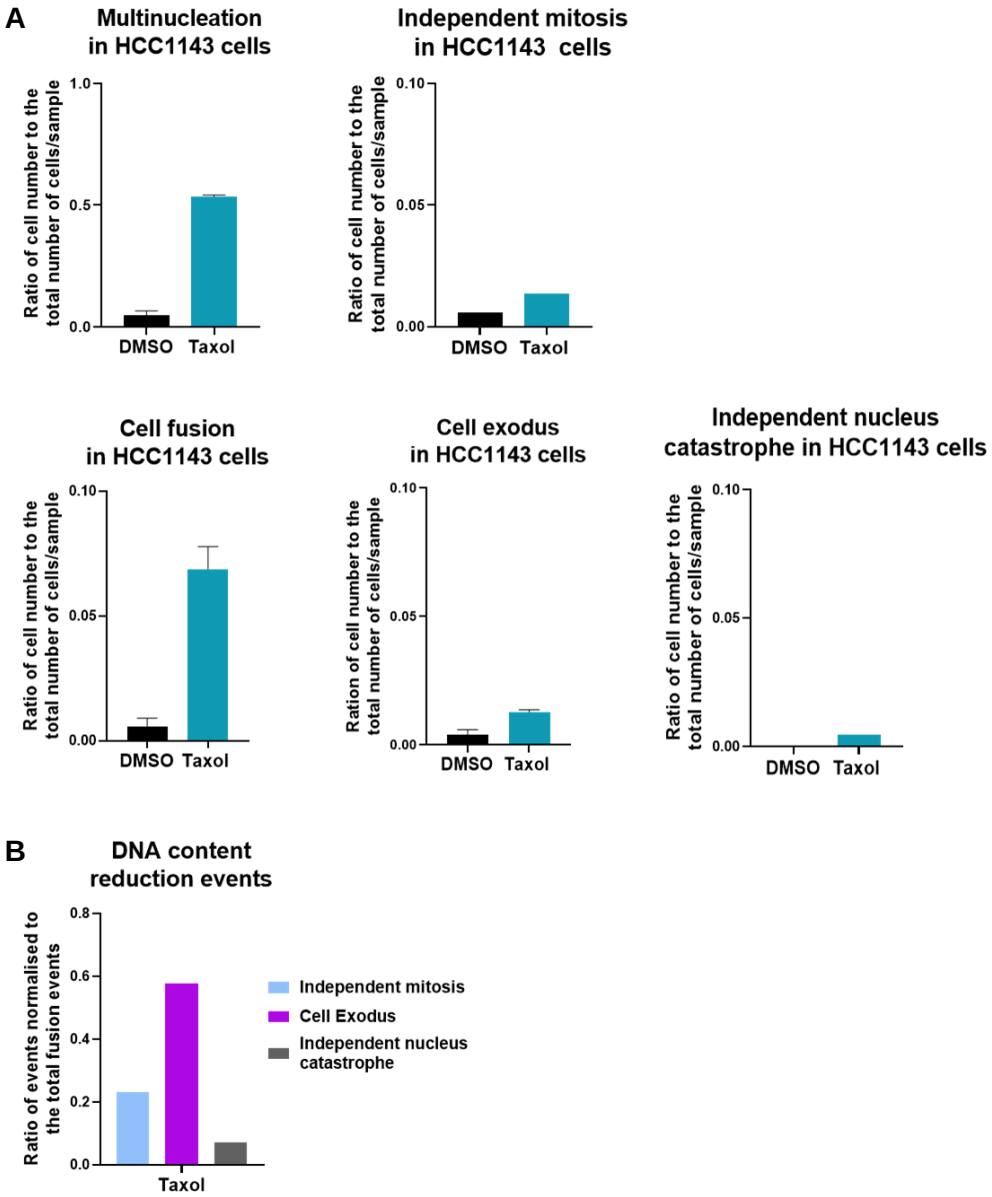

Figure 5.5: DNA content changing events during Taxol treatment in breast cancer cells. (A) Ratio of events observed after treatment with Taxol compared to the total number of cells per sample that were imaged. **(B)** Ratio of DNA content reduction events to the total number of fusions during Taxol treatment. 8 positions per samples were imaged with Zeiss3i widefield microscope and the fate of at least 150 cells/sample was followed. Mean and range of two biological repeats are shown, where available.

5.2.2 Paclitaxel enables cell fusion and induces cytokine expression

To investigate if treatment with Taxol is needed in order cell fusion to occur and to compare the number of fusion events during and after Taxol treatment, a time-lapse experiment was set up containing samples with ongoing Taxol treatment or released from treatment. Thus, H2B-GFP and H2B-RFP were mixed as previously and treated for 3 days with 7.5 nM of Taxol. The last day of the treatment, the cells were released in

media before the initiation of the time-lapse. In parallel, in mixed H2B-GFP and H2B-RFP cells, 7.5 nM Taxol was added before the time-lapse started and remained throughout the experiment. Mixed H2B-GFP and H2B-RFP with no paclitaxel treatment were used as control. In the period of 3 days that the time-lapse lasted, fusion events increased during Taxol treatment as well as after Taxol removal, compared to the control sample, however no significant differences were observed between the fusion events during and after the Taxol treatment (Figure 5.6 A). Thus, Taxol treatment enables cell fusion but continuous treatment is not required for cell fusion, indicating that Taxol, in the timeframes that we tested, drives the cells into a persistent state that enables cell fusion.

Then, we investigated if multinucleated cells, which is a known phenotype generated by Taxol treatment and also was observed in figures 5.3, 5.4 and 5.5 A, is enabling the fusion events. Thus, we investigated if during Taxol treatment at least one of the fusing cells is multinucleated. In the same time-lapse that was described above and in figure 5.6 A, we observed that from the fusions occurring during Taxol treatment, the number of the nuclei present in the fusing cells is not essential (Figure 5.6 B). However, in order to investigate whether Taxol treated cells, multinucleated or mononucleated, are attracting cells that then become fused, H2B-GFP HCC1143 cells were treated with 7.5 nM for 3 days and in the last day they were released in fresh media and untreated H2B-RFP cells were added on top. Time-lapse for a period of 3 days revealed that untreated cells enter Taxol treated host cells during fusion but not the other way around (Figure 5.6 C).

To confirm whether Taxol treated cells are attracting untreated cells, migration experiments were performed. Cells were treated with Paclitaxel for 3 days and were released for an additional 3 days in fresh media. Following release for 3 days, growth media from these cells was filtered and placed in the bottom of transwells. On top of the transwells, untreated cells in fresh media were seeded. The top part of the transwells is separated from the bottom with a 8.0μm porepolycarbonate membrane. The cells were allowed to migrate for 5 hours and then were fixed, stained with dapi and the bottom of the porepolycarbonate membrane was imaged. In the samples that released media from

Taxol treated cells was added, the untreated cells were migrating faster, indicating that Taxol treated cells attract other cells, possibly by expressing cytokines or chemokines (Figure 5.7).

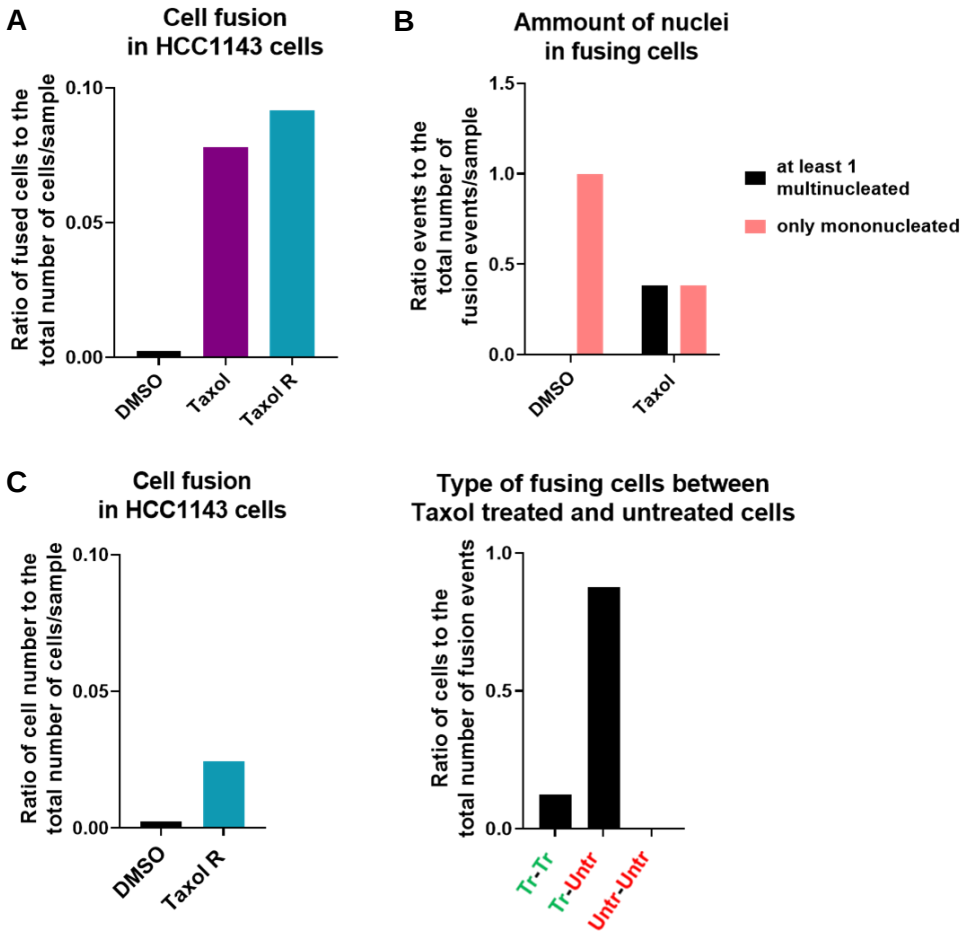

Figure 5.6: Cell fusion during and after Paclitaxel treatment. (A) Ratio of fusion events observed during (Taxol) and after the release (Taxol R) of 7.5 nM Taxol treatment to the total number of cells per sample that were imaged. **(B)** Number of nuclei in the fusing cells normalised to the total number of fusions during 7.5 nM Taxol treatment. **(C)** Total fusion events and types of fusing cells when H2B-GFP cells are pre-treated for 3 days with Taxol and released for 3 days in fresh media and untreated H2B-RFP cells. 8 positions per samples were imaged with Zeiss3i widefield microscope and the fate of at least 150 cells/sample was followed for 3 days.

To address the hypothesis that Taxol treated cells can attract other cells through cytokine and chemokine expression, we analysed the gene expression of a panel of 14 cytokines and chemokines, by real-time PCR. HCC1143 cells were treated with 7.5 nM of Taxol, then the third day of the treatment, RNA was extracted and cDNA was generated. β-Actin was used as an endogenous control and samples containing the primers but not cDNA were included as a negative control. The cycle threshold (CT)

value for each cytokine, which indicate the number of cycles needed for the fluorescent signal to cross the background level, was normalised to the β-Actin CT value per sample. Then, the ratio of gene expression for each cytokine during Taxol treatment to the corresponding gene expression of the DMSO control was identified. Taxol treatment increased the expression of the majority of cytokines and chemokines tested with the exception of SDF1, which was reduced. Higher gene expression, approximately 20 times higher than the control, was observed for IL-1β, IL-6, IL-8, CSF2 and CCL5 (Figure 5.8 A). However, when expression of the same cytokines was tested in cells treated for 3 days with 7.5 nM Taxol and released for 3 days in fresh media, we observed that IL-8 and GRO2 was increased almost 100 and 15 times, respectively, compared to the DMSO control sample. IL-6, CCL5 and TNFα gene expression levels remain similar during Taxol treatment and after its release, while the expression of the rest of the cytokines was slightly reduced after Taxol removal (Figure 5.8 B).

From the time-lapse experiment, we observed that cell fusion events do not change significantly after Paclitaxel removal (Figure 5.6 A). Thus, cytokines with increased expression during Paclitaxel treatment, which are reduced after the drug's release might not be implicated with cell fusion and the increase in their expression is a response to the drug treatment. Nevertheless, cytokines and chemokines such as IL-6, CCL5 or TNFα that remain highly expressed after Taxol removal may be important for cell fusion. It will be interesting to also investigate the effect of IL-8 and GRO2 chemokines in cell fusion as they are increased during Taxol treatment but after the drug's release their expression is even more upregulated.

Finally, it was investigated if cytokine expression is increased due to induction of senescence. Hence, β-gal expression was tested in cells either treated for 3 days with 7.5 nM Taxol or treated for 3 days with Taxol and released for 3 days in fresh media. As negative control we used HCC1143 cells with no Paclitaxel treatment and as a technical positive control for β-gal expression we used untreated but confluent HCC1143 cells. As illustrated in Figure 5.9, Paclitaxel treatment at the concentration and timeframes used

in this study, did not induce senescence. Thus, cytokine expression is not increased due to induction of senescence but by another mechanism.

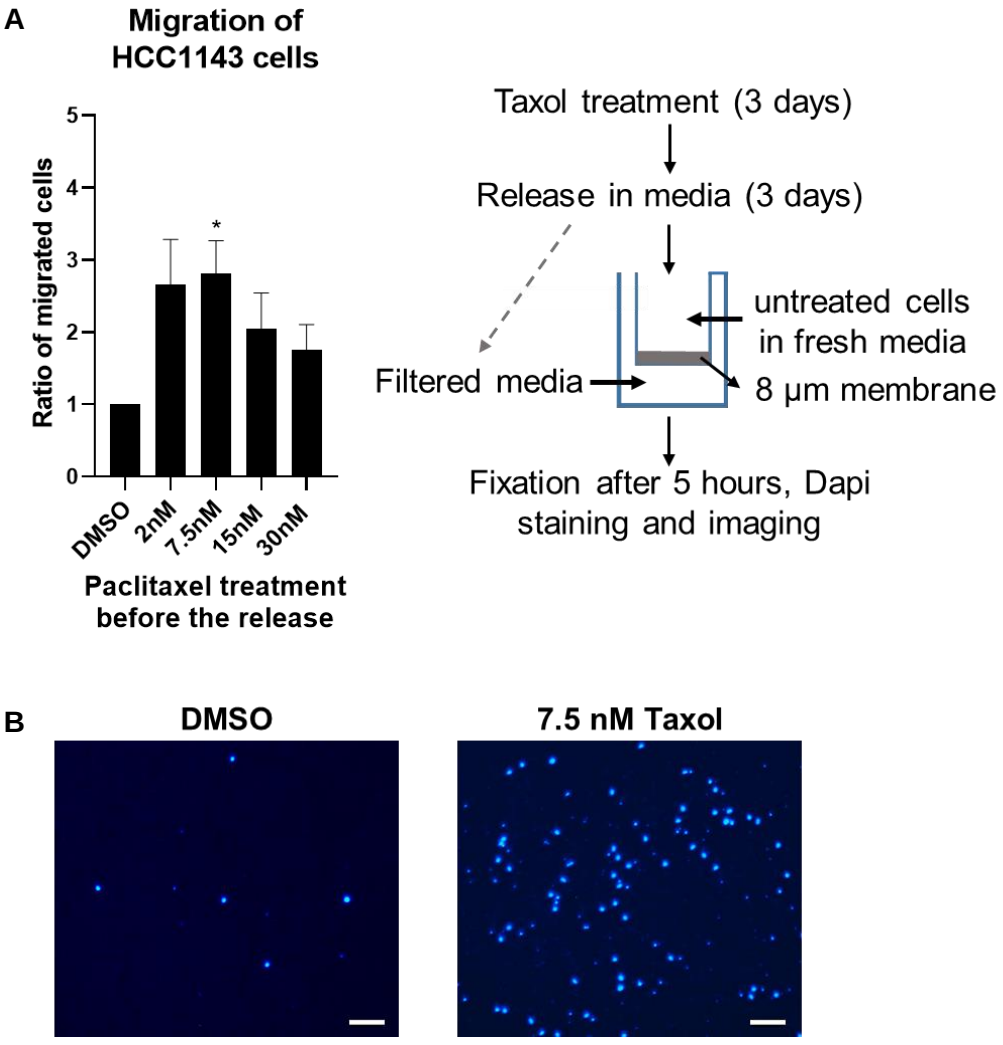

Figure 5.7: Cell migration when exposed to Taxol released media. (A) Faster migration when cells are exposed to 3 days released media of 3 days Taxol treated cells. Mean and SEM of three biological replicates are presented. t test analysis was performed, comparing each sample to the DMSO control, $P < 0.05$. **(B)** Illustration of migrated cells on the bottom of the membrane, in media released from DMSO and 7.5 nM Taxol. Four images/ condition were taken with 4x lens at EVOS. Blue demonstrates the dapi staining of the nuclei of the migrating cells. Scale bar at 100 µm.

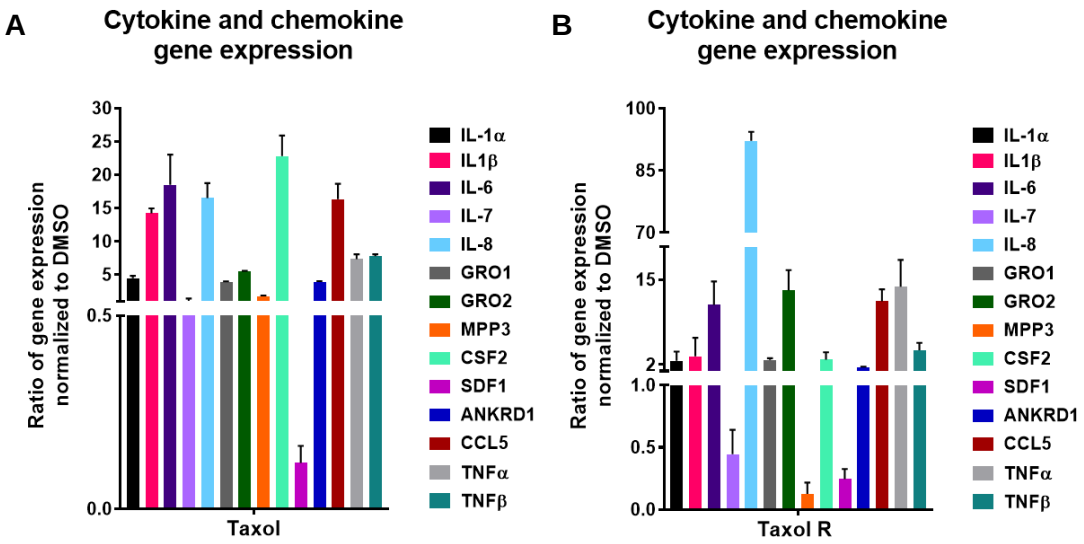

Figure 5.8: Cytokine and chemokine gene expression during and after Paclitaxel treatment. **(A)** Cytokine and chemokine gene expression after 3 days of 7.5 nM Taxol treatment, normalised to the DMSO control. **(B)** Cytokine and chemokine gene expression after 3 days of 7.5 nM Taxol treatment and 3 days of release in fresh media, normalised to the DMSO control. Mean and the range of two biological replicates are presented. R: Released.

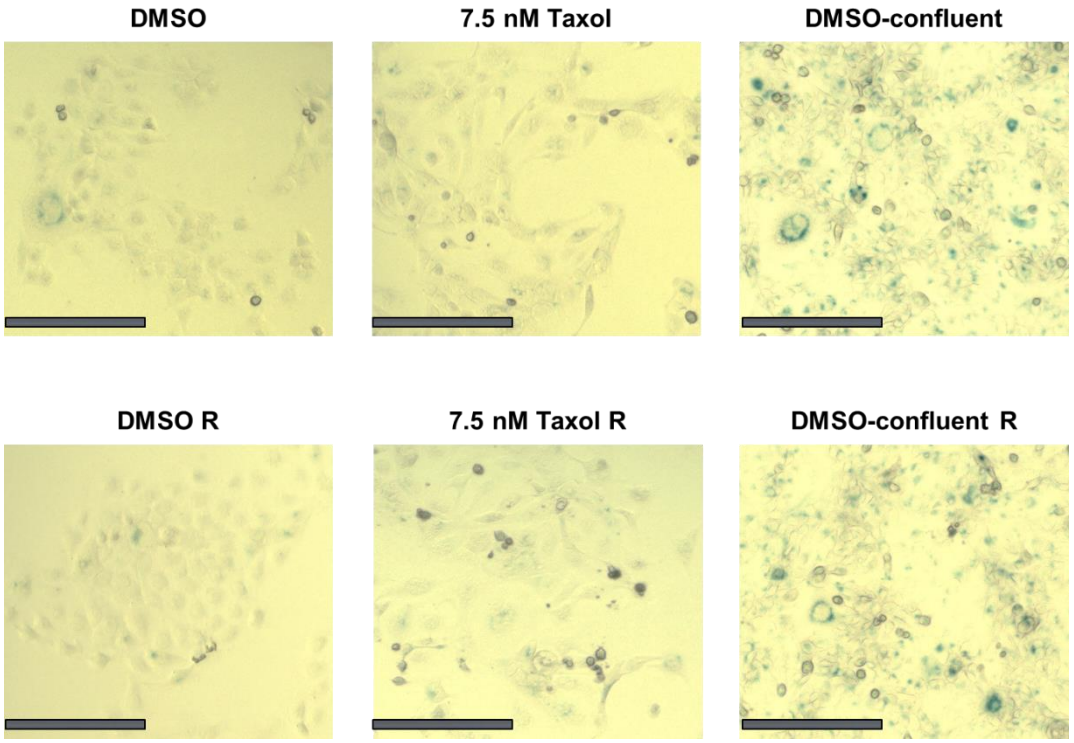

Figure 5.9: β-gal staining during and after Paclitaxel treatment. Illustration of β-gal staining after 3 days of 7.5 nM Taxol treatment and after 3 days of 7.5 nM Taxol treatment and 3 days of release in fresh media. Confluent cells were used as a technical control for β-gal staining. Images were taken with 10x lens at EVOS. Blue illustrates the β-gal staining. Scale bar at 250 µm.

5.2.3 Investigation of cell exodus as a cause of cell recovery after Paclitaxel treatment.

To investigate cell exodus events during Paclitaxel treatment and after its removal, a time-lapse experiment was set up containing samples with ongoing Taxol treatment or released from treatment, as previously explained. Thus, H2B-GFP and H2B-RFP HCC1143 cells were mixed and treated for 3 days with 7.5 nM of Taxol and released in fresh media on the day of the time-lapse or 7.5 nM of Taxol were added shortly before initiating the time-lapse in equally mixed H2B-GFP and H2B-RFP cells. Following the fate of the cells for 3 days, we observed that cell exodus events are doubled after the release of Paclitaxel (Figure 5.10 A). These results indicate a possible correlation between cell exodus events and cell population recovery after Paclitaxel treatment.

Based on the above evidence our hypothesis was that, by inhibiting cell exodus a reduction of cell recovery after paclitaxel treatment would be achieved, which could be the basis of a new therapeutic approach. In order to target the cell population recovery after Taxol treatment and further investigate the association of cell exodus with the recovered population, we initially performed a small molecule drug screening. HCC1143 cells were treated for 3 days with 7.5 nM of Taxol and were released in 100 nM of our annotated “drugs and tools” set which consists of 604 cancer-targeted compounds from the combined Selleckchem’s Cambridge Cancer Compound Library. This set covers the whole spectrum of known cancer targets involved in multiple oncogenic pathways and contains FDA approved drugs and drugs that are currently in clinical trials. They are structurally diverse, medicinally active, cell permeable, good in vitro and in vivo pharmacology and have rich annotation. Utilising a specialised, limited-sized library comprised of annotated compounds for their known mechanism of action will help narrow the number of potential drugs for any hit and aid in identification of candidate drugs. The cells were imaged and the confluence of the wells was analysed by CeligoS the day after the release in the library and once every week for 2 weeks in total. Every compound was present in duplicate and DMSO was used as a control. After 2 weeks in culture, the well’s cell covered area in μm^2 for each compound was normalised to the average value of all

the control values in the experiment in order to eliminate effects of plate-to-plate variation. Then, the average value of the two duplicates for each compound was calculated and the depth value for each compound was determined by subtracting the normalised average value for each compound from the average control value. As hits were considered compounds with depth value 3 times the STDEV of all the depth values of the compounds and the control samples included in the screening (Figure 5.10 B).

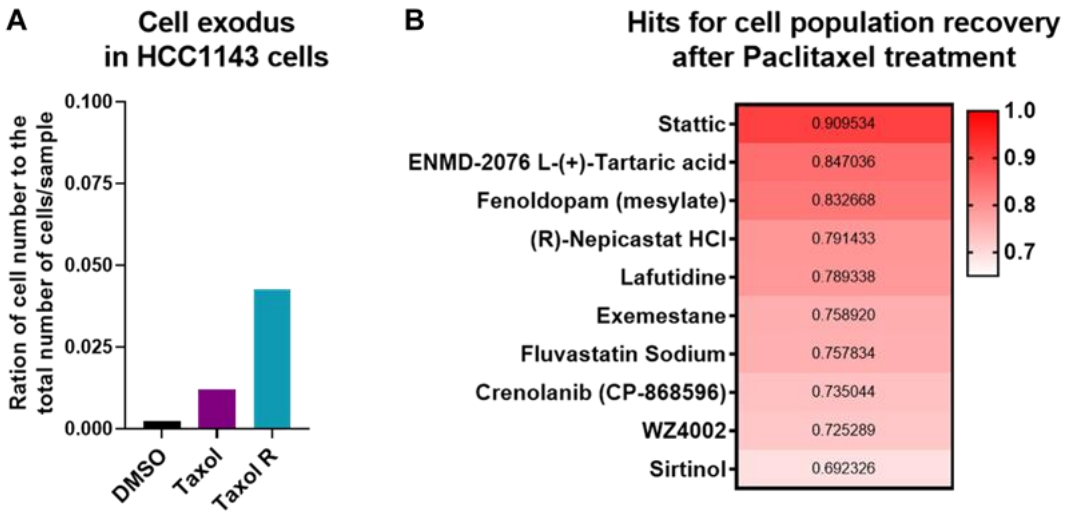

Figure 5.10: Cell exodus events during and after Paclitaxel treatment and hits for inhibition of cell population recovery after Paclitaxel treatment. (A) Ratio of exodus events observed during (Taxol) and after the release (Taxol R) of 7.5 nM Taxol treatment compared to the total number of cells per sample that were imaged. 8 positions per samples were imaged with Zeiss3i widefield microscope and the fate of at least 150 cells/ sample was followed for 3 days. R: Released. **(B)** Heatmap and depth values of the compounds that inhibit cell population recovery after Taxol treatment. The red gradient illustrates the hierarchy of the compound with depth values higher than 3 times the STDEV of all the depth values in the screening. R: Released.

From the hits identified, we noticed that two of them, Crenolanib and ENMD-2076 L-(+)-Tartaric acid, target FLT3 and Crenolanib is involved in multiple clinical trials (Table 5.2). Thus, initially we investigated the toxicity of Crenolanib in untreated cells and in cells that had undergone Paclitaxel treatment. By identifying the sensitivity of the cells after dose response of Crenolanib with viability assays (Figure 5.11 A), 150 nM were selected as a sub-lethal concentration of Crenolanib to test its effect in the cell viability in combination with Paclitaxel (Figure 5.11 B). Treatment of cells with Paclitaxel and 150

nM of Crenolanib modestly reduced the IC_{50} concentration of Taxol from 1.5 nM to 0.7 nM when Crenolanib was also present (Figure 5.11 B).

To investigate whether Crenolanib delays cell population recovery after paclitaxel treatment, HCC1143 cells were treated either with 7.5 nM Taxol or 150 nM Crenolanib or with 7.5 nM Taxol in combination with 150 nM Crenolanib. After three days of treatment the cells from each treatment group were separated in two groups. In the first the cells were released in fresh media, while in the second, the cells were released in 150 nM Crenolanib and the same number of cells from every group were seeded in 384 well plates. In addition, two more samples were added in the experiment. Cells that contained no treatment and cells treated with 150 nM of Crenolanib alone. The next day the cells were imaged and the confluence of the wells was measured by CeligoS. Imaging of the plates continued once per week for a period of three weeks. In order to avoid any technical errors with CeligoS that may intervene in the final confluence measurements, at least 32 replicates per sample were included. At the end of the 3 weeks we observed that all the samples have recovered completely apart from these in which Crenolanib was present regardless of concurrent treatment with Paclitaxel or after release from Paclitaxel (Figure 5.12 A). Illustration of the percentage of confluence for each replicate per sample, indicates that overall, the cells in each well per sample recovered at a similar rate (Figure 5.12 B).

Table 5.2: Targets of the drugs that were identified as hits in the compound screen.

Small molecule	Inhibitor/antagonist	Clinical Trial
Stattic	STAT3	No
ENMD-2076 L-(+)-Tartaric acid	Aurora A, **Flt3**	No
Fenoldopam (mesylate)	dopamine-1 receptor (DA1)	No
(R)-Nepicastat HCl	dopamine-β-hydroxylase	No
Lafutidine	histamine H(2)-receptor	Yes
Exemestane	aromatase	Yes
Fluvastatin Sodium	HMG-CoA reductase	Yes
Crenolanib (CP-868596)	**PDGFRα/β, Flt3**	**Yes**
WZ4002	EGFR(L858R)/(T790M)	No
Sirtinol	SIRT1 and SIRT2	No

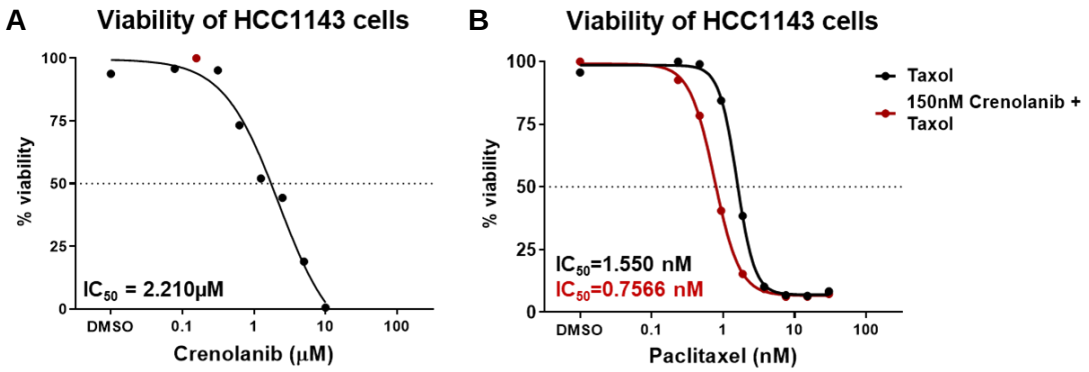

Figure 5.11: Sensitivity of HCC1143 to Crenolanib and to Paclitaxel in combination with Crenolanib. (A) Sensitivity to Crenolanib for six days with a highest concentration of 10 μM followed by 7 1/2 serial dilutions. **(B)** Sensitivity to Paclitaxel for six days with a highest concentration of 30 nM followed by 7 1/2 serial dilutions alone or in combination to 150 nM Crenolanib.

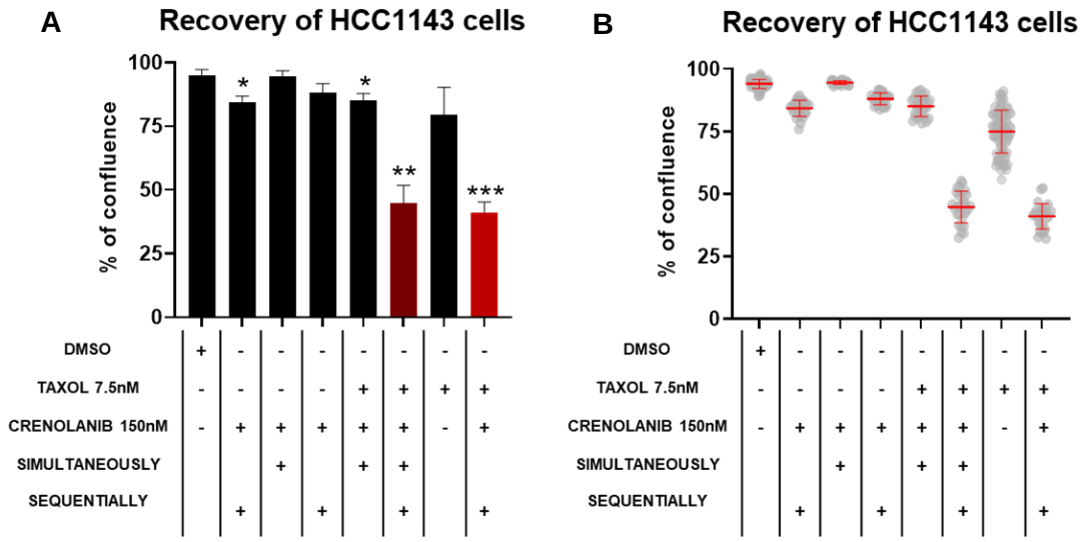

Figure 5.12: Recovery of HCC1143 cells after simultaneous or sequential treatment of Paclitaxel and Crenolanib. (A) Mean of all the confluence values for each sample after three weeks of recovery. Mean and SEM of three biological replicates are shown and t test analysis was performed, comparing each sample to DMSO. **(B)** Illustration of all the individual confluence values per sample. Mean and SD of three biological replicates are shown.

To elucidate the mechanism by which Crenolanib delays cell population recovery after Paclitaxel, a time-lapse experiment was performed. H2B-GFP and H2B-RFP HCC1143 cells were equally mixed and treated with 7.5 nM Taxol, 150 nM Crenolanib or combination of 7.5 nM Taxol and 150 nM Crenolanib. Additionally, cells were pre-treated for 3 days with 7.5 nM of Taxol and released the day of the time-lapse in fresh media or 150 nM Crenolanib. Following the fate of the cells for 3 days, we observed that simultaneous or sequential treatment of Paclitaxel and Crenolanib reduce the fusion events and almost completely inhibit cell exodus (Figure 5.13). However, the effect of Crenolanib on cell fusion is independent to cytokine expression, as sequential treatment with Paclitaxel and Crenolanib does not affect the cytokine gene expression compared to treatment only with Paclitaxel. Exception is the expression of CCL5 which is increased after sequential treatment of Paclitaxel with Crenolanib compared to Paclitaxel treatment alone (Figure 5.14). Thus, more experiments are needed to investigate the mechanism by which Crenolanib reduces the cell fusion and exodus events and the importance of CCL5 chemokine in these events. Nevertheless, our results indicate the significance of cell exodus for cell population recovery after Paclitaxel treatment and provide a potential

sequential treatment of Paclitaxel with Crenolanib as a new therapeutic approach in clinic, in order to delay tumour recovery after Paclitaxel treatment.

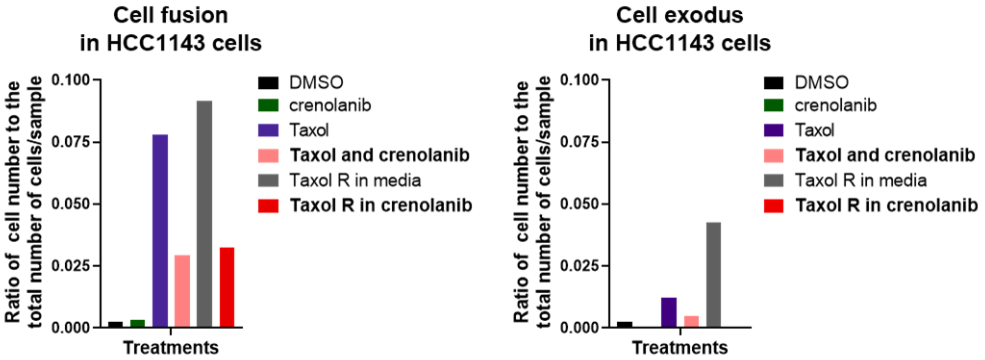

Figure 5.13: Cell fusion and cell exodus events after simultaneous or sequential treatment of Paclitaxel and Crenolanib. Ratio of fusion events observed during 7.5 nM Taxol, 150 nM Crenolanib and simultaneous or sequential treatment of Taxol and Crenolanib to the total number of cells per sample that were imaged. 8 positions per samples were imaged with Zeiss3i widefield microscope and the fate of at least 100 cells/sample was followed for 3 days. R: Released.

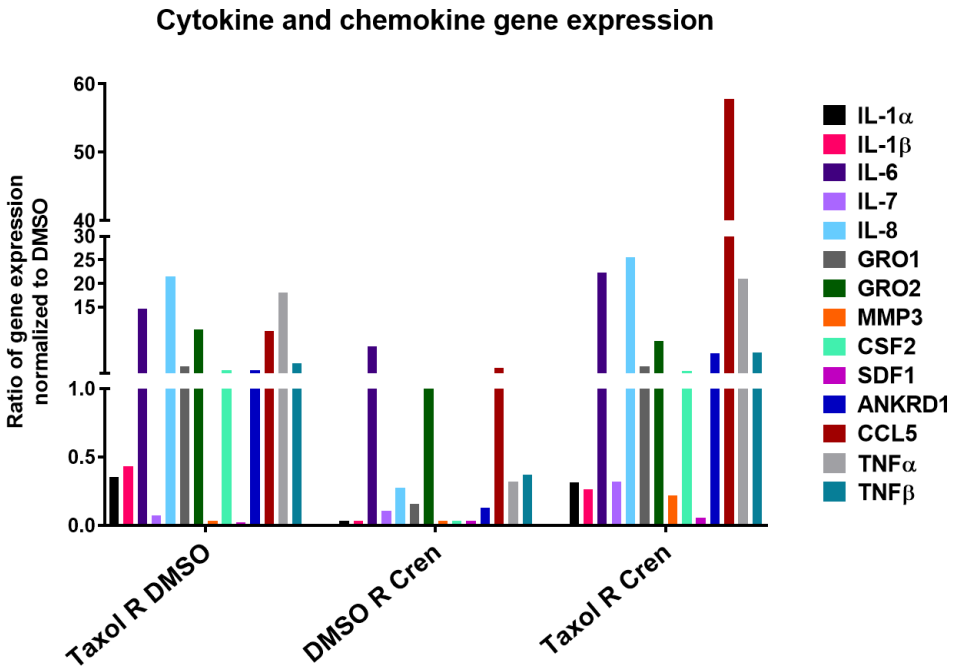

Figure 5.14: Cytokine and chemokine gene expression after sequential treatment with Paclitaxel and Crenolanib. Cytokine and chemokine gene expression by real-time PCR, after 3 days treatment with 7.5 nM Taxol and released (R) for 3 days in DMSO or 150 nM Crenolanib (Cren). Also, cells in DMSO were released in 150 nM of Crenolanib and as a control, cells with no treatment were included. All the CT values were normalised to β-ACTIN and the ratio to the DMSO with no extra treatments was calculated. Taxol: Paclitaxel, R: Released and Cren: Crenolanib.

5.3 Conclusions

During the generation of aneuploid clones, we noticed that the majority of the propagated clones contained similar DNA content to the parental cell line. Additionally, clones that were changing their DNA content from a near tetraploid to a near diploid, were observed. Thus, we hypothesized that cancer cells utilise mechanisms by which they can change their DNA content. In order to investigate the events by which the DNA content change is occurring, stable H2B-GFP and H2B-mCherry HCT116p53$^{-/-}$ cell lines were generated, were equally mixed and treated with Paclitaxel. Following the fate of the cells with time-lapse we identified that cells during Paclitaxel treatment can increase their DNA content by cytokinesis failure, abortive mitosis and cell fusion, while they can reduce their DNA content by cell exodus and independent nucleus catastrophe. Moreover, events of independent mitosis were observed, following cell fusion, which can increase the DNA content if the daughter cells remain in the fused cell or decrease it, if they exit the host cell. These events are not cell line specific and they were also observed in breast cancer cells.

In time-lapse experiments it was shown that Paclitaxel enables cell fusion but after its removal the cancer cells can continue to get fused. Furthermore, Paclitaxel treated cells can attract untreated cells potentially through cytokine and chemokine expression that are induced by Taxol treatment. Specifically, Taxol treated cells may attract other cells through expression of IL-8, GRO2, IL-6, CCL5 and/or TNFα. However, more experiments would be needed to confirm the importance of these cytokines for cell fusion.

In contrast to cell fusion, cell exodus events doubled after Paclitaxel release indicating a potential association of cell exodus with cell recovery, as it was demonstrated by time-lapse experiments. Targeting of cell population recovery after Paclitaxel treatment, with an annotated small molecule library screen, identified Crenolanib, a PDGFRα/β and FLT3 inhibitor, as a potential hit. Recovery experiments demonstrated that simultaneous or sequential treatment of Paclitaxel and Crenolanib

inhibit cell population recovery more than 50%. Finally, time-lapse experiments showed that the observed delayed recovery after sequential or simultaneous treatment of Paclitaxel and Crenolanib, is due to cell fusion and exodus reduction, indicating the importance of these events to cell recovery.

Overall, Paclitaxel treatment increases the expression of cytokines and chemokines in the cells, generating a persistent state that enables cell fusion through cell-cell attraction. After the removal of the treatment, the fused cells can undergo cell exodus that promotes cell population recovery. Sequential treatment of Paclitaxel with Crenolanib can delay the cell population recovery by inhibition of the exodus events. However, the effect of Crenolanib is independent of cytokine expression and further experiments would be needed to better elucidate the mechanisms by which Crenolanib reduces cell fusion events and inhibits cell exodus.

Chapter 6 - Discussion and future perspectives

6.1 Targeting CIN and aneuploidy in cancer

Aneuploidy and chromosomal instability (CIN) are distinct events that can coexist in a tumour and one can result from the other. Aneuploidy is present in 90% of solid tumours and 50-60% of blood cancers and it can promote tumour initiation and tumour progression through gains/losses of oncogenes/tumour suppressor genes or increased efficiency of cellular pathways (Ben-David and Amon, 2020, Santaguida and Amon, 2015). Although high degree of aneuploidy is associated with poor prognosis, excessive degree of aneuploidy results to increased cellular stress, such as metabolic and mitotic, and is detrimental to cell physiology (Ben-David and Amon, 2020, Sheltzer and Amon, Chunduri and Storchová, 2019, 2011, Hwang et al., 2017, Rodrigues-Ferreira and Nahmias, 2020). Similar to aneuploidy, only moderate levels of CIN in the tumour are linked with poor prognosis and decreased survival, while excessive degree of CIN is linked with better prognosis in cancer (Turajilic et al., 2019, McGrahan et al., 2012, Targa and Rancati, 2018, Lee et al., 2019). Moreover, CIN and aneuploidy can generate gene dependencies due to oxidative stress or DNA damage repair deficiency that did not exist previously (Slade, 2020). Thus, targeting CIN and aneuploidy either by driving excessive chromosomal alterations that cannot be tolerated by cancer cells or gene dependencies, may open novel avenues of anticancer therapies.

6.1.1 Generation of CIN models

In the context of this study, CIN models were generated to complement aneuploidy, as CIN can be a major cause of aneuploidy. CIN can generate mosaic aneuploidy in the tumour, providing the intratumour heterogeneity in which positive selection acts. Chromosomal instability is induced when persistent errors directly in mitosis or in DNA damage response/repair are present in the cells. For example,

persistence of CENP-E using selective chemical tools, intervenes with correct chromosome alignment in the metaphase plate and promotes errors in the kinetochore-microtubules attachments. Thus, SAC is activated, however, the cell can continue to anaphase, through SAC exhaustion, and the unattached kinetochores will lead to chromosome missegregation and CIN (Bennett et al., 2015).

Analysis of CENP-E mutations in The Cancer Genome Atlas (TCGA) cohort by ci-Bioportal, indicates that it is mutated in approximately 10% of skin and endometrial cancers and 5% of colon and lung cancers (Figure 6.1 A). Multiple missense and truncating mutations can occur throughout the gene, but missense mutation R2659C/L occurs in 9 of the 757 (~1%) cancers queried (Figure 6.1 B) (Cerami et al., 2012). However, the effect of this mutation in the function of the protein is not known.

Moreover, errors in DNA damage response and repair machineries, can indirectly generate CIN by allowing cells with damaged DNA to progress into mitosis, generating lagging or double minute chromosomes, which form micronuclei (Ye et al., 2019). ATM, a key protein in DNA damage response, has been shown to be highly mutated in many cancers, such as in approximately 20% of small bowel and endometrial cancers, 10% in melanoma, colorectal, lung and prostate cancers and in approximately 4% of breast cancers (Figure 6.2 A). The majority of these mutations are missense, however 30% (795/2622) of mutations on ATM gene are truncating mutations, which are very likely to have a deleterious effect on ATM function. In addition, R337C/H has been identified in 78 of the 2622 (~3%) cancers queried and is considered as a cancer mutation hotspot (Figure 6.2 B). R337C/H has not been functionally validated, however it is considered likely oncogenic by destabilising the protein (Jette et al., 2020).

Similarly, CHK1 and CHK2 are also involved in DNA damage response pathways and they are mutated in approximately 10% of lung and endometrial cancers, respectively (Figures 6.3 A and 6.4 A). Multiple missense and truncating mutations are occurring in either gene. Importantly, 20% (55/264) of CHK1 and 22% (104/471) are truncating, indicating a deleterious effect and have been annotated as potentially oncogenic. Point mutation I471V is present in CHK1 in 30 of the 264 (~11%) cancers

queried and K373E/N in CHK2, in 27 of the 471 (~6%) cancers (Figures 6.3 B and 6.4 B). It is not known how the I471V missense mutation affects the activity of CHK1, however, the K373E/N missense mutation in CHK2 is known to be oncogenic by disrupting CHK2 autophosphorylation and its kinase activity (Higashiguchi et al., 2016).

These data suggest, that ATM, CHK1 and CHK2 genes and to a lesser extent CENPE gene show a high frequency of potentially loss of function mutations in cancer. To target CIN, dependent or independent to specific gene interactions, we generated three different models either by promoting segregation errors in mitosis or by intervening in DNA damage response. Thus, we used chemical inhibition of ATM, CENP-E and CHK1/CHK2 in order to phenocopy the loss of function of these genes, seen in patient samples.

In chapter 3, we demonstrated that inhibition of CENP-E for three days using the selective CENP-E inhibitor compound GSK923295, increased the number of cells with at least one chromosome missegregation event, in agreement with previous studies (Figure 3.2 A) (Bennett et al., 2015). Furthermore, we showed that inhibition of ATM by KU60019 or CHK1/CHK2 by CCT241106, increased the presence of micronuclei in cells. Interfering with DNA damage response and forcing cell cycle progression even in the presence of unrepaired DNA damage, results to micronuclei formation, which are indicative of CIN (Figure 3.1 B and C) (Zhu et al., 2014, Golding et al., 2009, Chao et al., 2020). Nevertheless, because the effects of the compounds are reversible, the cells were always pre-treated for three days and the treatment continued until the end of the experiments, in order to continuously induce errors and CIN.

Finally, we included a fourth model for targeting CIN with impaired SWI/SNF complex. BRG1$^{-/-}$ and BAF180$^{-/-}$ cells were provided by Prof. Jessica Downs, who has previously shown that BAF180 is localised at the kinetochores and is essential for chromatin cohesion, while BRG1 is important in DSB-induced transcriptional silencing (Kakarougkas et al., 2014, Meisenberg et al., 2019, Brownlee, et al., 2014). In addition, their loss promotes chromosomal instability through micronuclei generation either by

chromosome missegregation after defects in cohesion at the centromere or impaired DSB repair and defects in DNA end resection (Brownlee, et al., 2014, Hays et al., 2020).

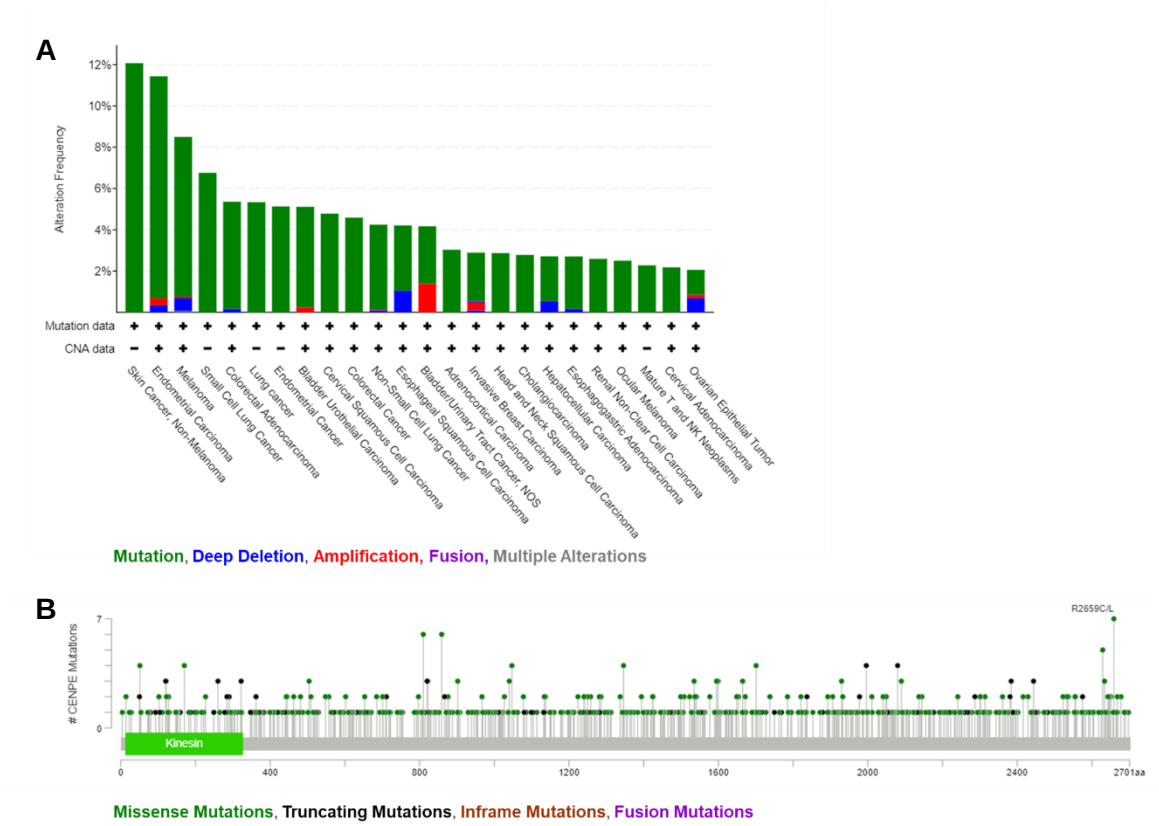

Figure 6.1: Frequency of Centromere Protein E (CENP-E) mutations in human cancer. (A) CENP-E was queried against all entries in the curated non-redundant data set on c-Bioportal, accessed November 2020. The frequency of CENP-E alteration in various cancers is shown. **(B)** The location of mutations in CENP-E from all samples in the curated non-redundant data site available on c-Bioportal, accessed November 2020.

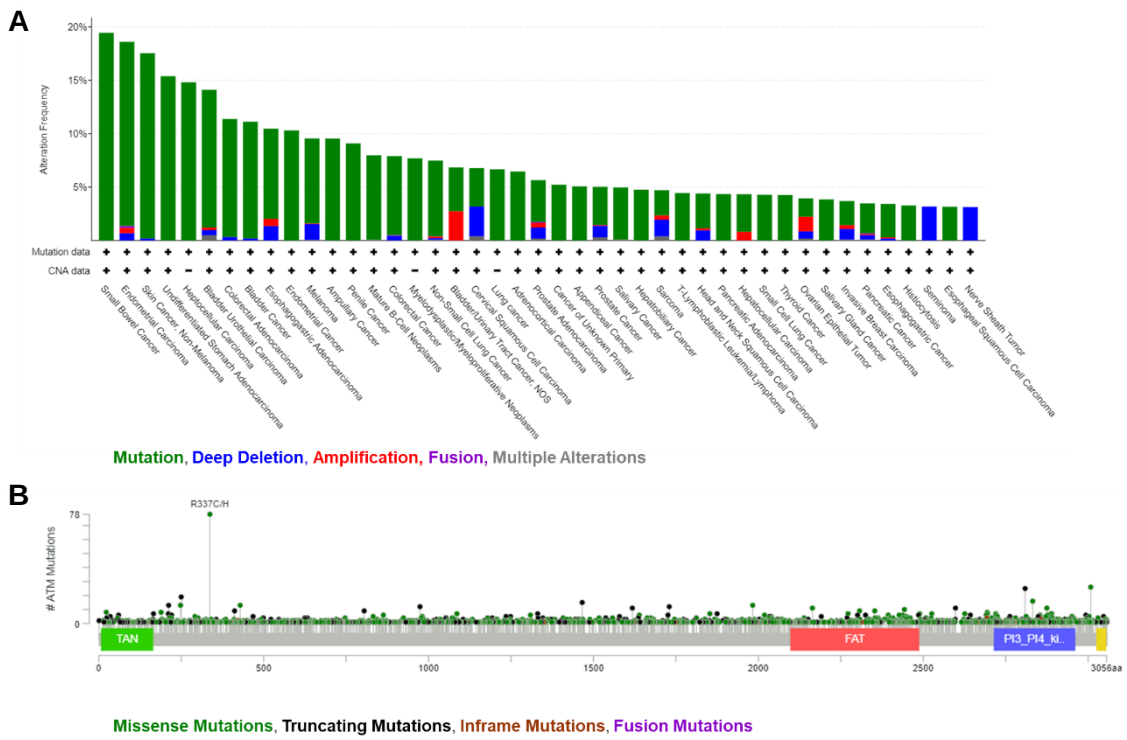

Figure 6.2: Frequency of Ataxia-Telangiectasia Mutated (ATM) mutations in human cancer. **(A)** ATM was queried against all entries in the curated non-redundant data set on c-Bioportal, accessed November 2020. The frequency of ATM alteration in various cancers is shown. **(B)** The location of mutations in ATM from all samples in the curated non-redundant data site available on c-Bioportal, accessed November 2020.

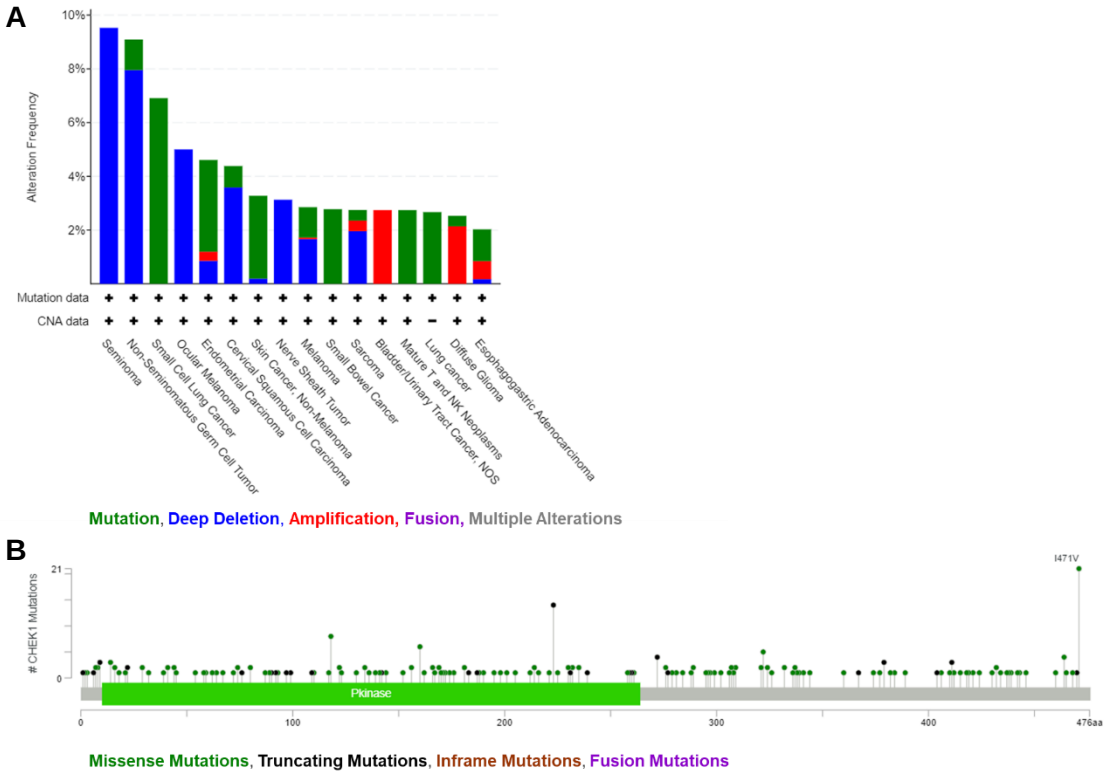

Figure 6.3: Frequency of Checkpoint Kinase 1 (CHK1) mutations in human cancer. (A) CHK1 was queried against all entries in the curated non-redundant data set on c-Bioportal, accessed November 2020. The frequency of CHK1 alteration in various cancers is shown. **(B)**

The location of mutations in CHK1 from all samples in the curated non-redundant data site available on c-Bioportal, accessed November 2020.

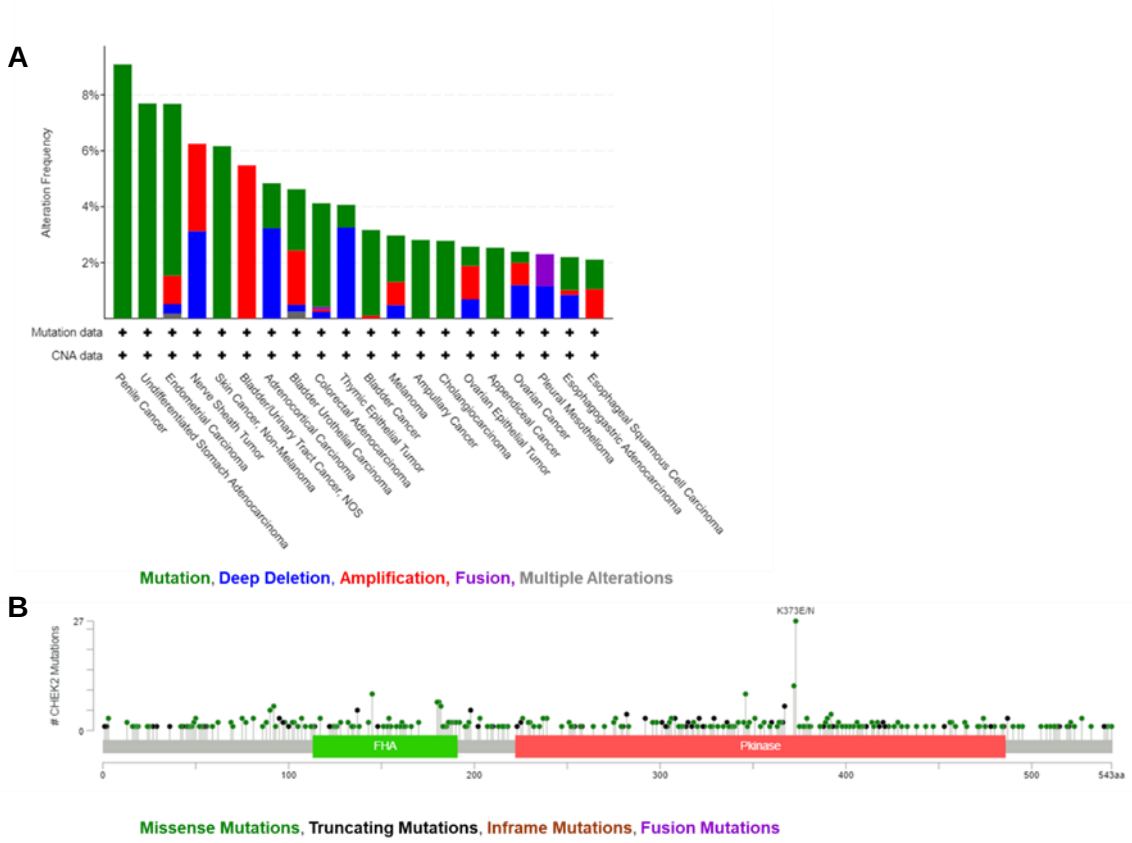

Figure 6.4: Frequency of Checkpoint Kinase 2 (CHK2) mutations in human cancer. (A) CHK2 was queried against all entries in the curated non-redundant data set on c-Bioportal, accessed November 2020. The frequency of CHK2 alteration in various cancers is shown. **(B)** The location of mutations in CHK2 from all samples in the curated non-redundant data site available on c-Bioportal, accessed November 2020.

6.1.2 Generation of aneuploid clones in a p53-deficient genetic background

A major cause of aneuploidy is errors during mitosis, such as chromosome missegregation through unattached kinetochores or impaired SAC activity (Simmonetti et al., 2019). Aneuploidy generated by SAC deficiency has been shown to be lethal in mouse embryonic fibroblasts (MEFs), at least partially, through p53 activation, but stable aneuploid MEFs express low levels of active p53 protein (Burds et al., 2005, Tang et al., 2011). Moreover, Thompson and Compton in 2010, showed that chromosome missegregation events promote cell cycle arrest in a p38/p53-dependent manner. These findings are in agreement with Aylon and Oren, who showed in 2011 that interruption of spindle formation generates tetraploid cells that get arrested in G1/S phase through p53

activation and eventually underwent apoptosis. In contrast, when p53 was inactive, the generated tetraploid cells were able to re-enter the cell cycle and promoted aneuploidy through lagging chromosomes and segregation errors (Aylon and Oren, 2011, Ganem et al., 2009). However, it was first shown by Li et al. in 2010 that only cells with high degree of aneuploidy generated by SAC impairment, are led to apoptosis through p53 activation because of the increased metabolic stress and ROS levels. Similarly, it was shown that whole chromosome missegregation by SAC dysfunction, can partially generate aneuploidy in p53-proficient cells that can actively proliferate, generating aneuploid clones with whole chromosome alterations (Soto et al., 2017). Thus, because of the controversial role of p53 in the tolerance of aneuploidy and the elevated mutation rate of p53 in cancer, mainly inactivating the function of the protein, we focused on identifying targets in aneuploidy, independently of p53 activity (Donehower et al., 2019).

To generate aneuploidy in cells, we selected the stable near diploid cell lines HCT116p53$^{-/-}$ and DLD1 that expresses a mutant inactive p53. To induce aneuploidy, the cells were treated with nocodazole that blocks them in mitosis and were released in Taxol, the Eg5 inhibitor Monastrol or the CENP-E inhibitor GSK923295 that promote errors in the spindle formation and the kinetochore-microtubule attachments. In parallel, SAC was abrogated by MPS1 inhibition, in order to allow metaphase to anaphase transition even in the presence of unaligned chromosomes or unattached kinetochores. Wash out of the compounds and Hoeschst cell cycle profile by FACS, demonstrated the presence of aneuploid cells in the cell population and single cell isolation of these cells by FACS sorting was performed (Figure 4.2). As expected, single cell isolation after the G2/M phases of a generally diploid cell population and before the G1 phase of a tetraploid cell population, generated clones either with chromosomal gains or chromosomal losses, respectively. Nevertheless, by CGH and SNPs microarrays, we observed that the generated aneuploid clones contained mainly small structural chromosomal alterations and only two clones contained a large gain of one chromosome each, which resembled to whole chromosome amplification (Figure 4.10). These results are opposing previous studies suggesting that when kinetochore-microtubule

attachments and SAC activity are impaired, the majority of p53 deficient cells display whole chromosome aneuploidies and can tolerate high levels of aneuploidy (Soto et al., 2017, Li et al., 2010). In contrast, our results propose that more mechanisms, independent to p53 activity, may control the degree of aneuploidy and that even in p53 deficient cells, high degree of aneuploidy with multiple numerical and structural aneuploidies cannot be tolerated.

Interestingly, we observed by FACS PI cell cycle profile that the majority of the generated clones contained a DNA content similar to the parental cell line (Table 5.1). Clones that transitioned from a near tetraploid DNA content to a near diploid, while in culture, were observed (Figure 4.4). CGH analysis demonstrated that the final near diploid clones that were generated after the transition, contained minor chromosomal aberrations compared to the parental cell lines (clones UN16 and UN10 in Figure 4.10 A). These findings further support the existence of additional mechanisms, independent to p53, by which cells can control aneuploidy to a low degree or reduce their DNA content to a near diploid with minimal chromosomal alterations.

6.1.3 Targeting CIN and aneuploidy by CRISPR/Cas9 loss of function screening

To identify new targets in aneuploidy and CIN, we performed a loss of function screen using a custom sgRNA library against 200 genes identified as potential hits in aneuploidy or CIN in the literature and genes involved in DNA damage response/repair pathways, metabolic pathways and chromosomal instability. The library is based on a two-vector system that utilizes a lentiviral vector for inducible Cas9 expression and a gene-specific lentiviral vector for constitutively expressed sgRNA. A blasticidin resistance gene is included in the inducible Cas9 lentiviral vector and a puromycin resistance gene in the sgRNA lentiviral vector, which they provide the infected cells with resistance in each antibiotic, respectively (Figures 2.2 and 2.3).

The functional titer for each cell line was identified and cas9-inducible cells were generated. Although no blasticidin resistant population of cells in the uninfected controls was observed, Cas9 expression in the transduced cells was only present in 45-65% of

the HCT116p53$^{-/-}$ parental cells, aneuploid clones and the HCT116 cells and BRG1 isogenic cell line. It is possible that the TRE3G inducible promoter is more prone to methylation or may be sensitive to the DNA locus the Cas9 vector integrates (Figure 2.1). In the Cas9 vector, the blasticidin resistance gene and the transactivator protein, which is essential, for Cas9 induction, are driven by the constitutive promoter hEF1α in a single mRNA. It is therefore also possible that some cells cannot process the mRNA as normally, resulting in a truncated (and inactive) transactivator protein. To overcome these problems, we transduced for a second time the aneuploid clones and the cell lines that contained less than 60% of cells expressing Cas9. Second transduction with the virus demonstrated that approximately all the cell lines contained more than 75% of Cas9 expressing cells. Thus, we continued with transduction of the library and the loss of function sgRNA screening.

6.1.3.1 SETD7 as a potential target in CIN, induced by BRG1 deletion

In the sgRNA loss of function screening, SETD1A was identified as a potential hit in CIN induced through impaired SWI/SNF complex (Figure 3.10). Hit confirmation by siRNA screening, using four different siRNAs for SETD1A, confirmed its selectivity towards BAF180 impaired cells and CIN cells induced by ATM or CHK1/CHK2 inhibition (Figure 3.11). Because no specific inhibitor exists for SETD1A, we used (R)-PFI 2 hydrochloride, as a potential SETD1A inhibitor, which is inhibiting at least 19 methyltransferases, some of which belong to the same family of SETD1A (Barsyte-Lovejoy et al., 2014). Interestingly, (R)-PFI-2HCl was selective only towards BRG1$^{-/-}$ cells with an IC50 of 12.2 μM, while the parental cells demonstrated an IC50 of 32.9 μM. The selectivity of (R)-PFI-2HCl towards BRG1$^{-/-}$ cells was confirmed by its 500-fold less active enantiomer (S)-PFI-2HCl (Table 3.6 and Figure 3.20 E). From the methyltransferases that (R)-PFI-2HCl inhibits, it is 1000-fold more selective for SETD7 (Barsyte-Lovejoy et al., 2014). Thus, inhibition of SETD7 is selective towards CIN induced by BRG1 deletion.

SETD7 is a SET domain-containing methyltransferase 7, also known as SET7, SET7 or KMT7 and its monomethyltransferase activity on H3K4 is catalysed by the

interaction of its SET domain with the cofactor S-adenosylmethionine (SAM). (R)-PFI-2HCl not only binds to the peptide-binding site and interferes with the enzymatic activity of SETD7 but also interacts with SAM, explaining its high potency (Barsyte-Lovejoy et al., 2014, Batista and Helguero, 2018). In contrast, (S)-PFI-2HCl interacts with less residues in SETD7 than (R)-PFI-2HCl, reducing its binding efficacy (Niu et al., 2017).

H3K4 is a marker of transcriptional activation and SETD7 substrates are involved in multiple cellular pathways, such as cell cycle regulation (E2F, CYCLIN E, p53, MPS1) or DNA damage response (PARP) (Batista and Helguero, 2018, Pradhan et al., 2009). Of note, in the mesoderm stage of cardiac differentiation, SETD7 interacts with BRG1 or BAF60A and p300 histone acetyltransferase and recruit them to the promoters of genes to facilitate RNA-PolII dependent transcription (Lee et al., 2018, Alexander et al., 2015, Bultman, 2019). In addition, in early 2000, it was shown that SETD7 is recruited with RNA-PolII in the promoter of the collagenase type I gene and promote di- and trimethylation of H3K4. Then, p300 and RSK2 are recruited that promote histone acetylation and phosphorylation and finally BRG1 is recruited, which signals the transcription initiation (Martens et al., 2003). Nevertheless, more studies have shown interaction and recruitment of BRG1 by p300 in promoters of thyroid and androgen receptors or at sites of DSBs repair, where both proteins are needed for KU70 recruitment (Huang et al., 2003, Ogiwara et al., 2011). Finally, it was recently shown that BRG1 interacts with p300 and transcriptionally activate genes involved in cell cycle progression and DNA replication (CDK2, CDK4, CCNB, CHK2, PCNA) (Sobczak et al., 2020).

Thus, we suggest that SETD7 may be important for recruitment of SWI/SNF chromatin remodelling complex and transcription factors in the promoters of cell cycle progression genes. Inactivation of BRG1 or SETD7 does not impair transcription, possibly through interaction with other SWI/SNF proteins (such as BAF60A) or other histone lysine methyltransferases (KMT). However, when both SETD7 and BRG1 activities are lost, the cells cannot counterpart their function and cell proliferation is inhibited, indicating synthetic lethal interactions between SETD7 and BRG1 (Figure 6.5).

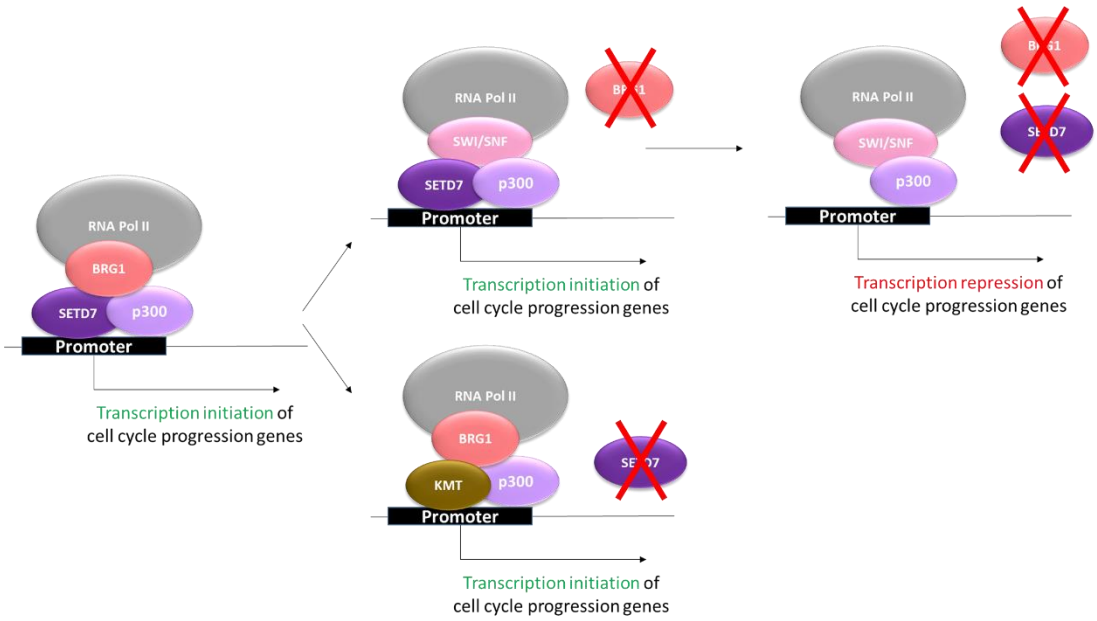

Figure 6.5: Schematic illustration of SETD7 and BRG1 interaction for cell proliferation. Interaction of SETD7 and BRG1 is essential for transcriptional activation of cell cycle progression and loss of both may lead to inhibition of cell proliferation. However, when only one of the two proteins is lost, the cell can balance the transcriptional activity with the function of other chromatin remodellers.

In addition to (S)-PFI-2HCl as inactive control, inhibition of SETD7 and its selectivity towards BRG1 deletion should be further confirmed by insertion of mutations in SETD7 that do not affect its activity but interfere with the binding of the inhibitor. For example, mutation of H252 to tryptophan that results in an active SETD7, (R)-PFI-2HCl activity is reduced 1000-fold (Barsyte-Lovejoy et al., 2014). Thus, treatment of BRG1 deleted cells containing the active mutant SETD7 with (R)-PFI-2HCl should not affect their viability. Moreover, mutations in the catalytic activity of SETD7 should inhibit the proliferation of BRG1 deleted cells but should not affect the parental cells. Secondly, the mechanism by which loss of SETD7 and BRG1 inhibit cell proliferation should be identified by investigating the expression of genes involved in cell cycle progression, such as CDK2 or CDK4, or the presence of p300 and other proteins involved in transcriptional activation, by SETD7 and BRG1 immunoprecipitation. Finally, *in vivo* experiments are needed to confirm that inhibition of SETD7 reduced the growth of tumours generated by BRG1 deleted cells while does not affect the growth of tumours generated by $BRG1^{wt}$ cancer cells.

6.1.3.2 PRIM1 as a potential target in CIN, induced by CHK1,CHK2 or SWI/SNF impairment

PRIM1 was identified as a hit in the sgRNA screening, in CIN cells generated after CHK1/CHK2 inhibition and it was the only hit in which three of four siRNAs were confirmed to reduce the viability of CHK1/CHK2 inhibitor-treated cells, by the siRNA screening (Figures 3.10 and 3.11). Moreover, we showed that PRIM1 knockdown reduces the ability of CHK1/CHK2 inhibitor-treated or mutated cells to form colonies, identifying PRIM1 as a potential target for CHK1, CHK2 inactivation (Figures 3.33 and 3.36).

In addition, we found that PRIM1-depletion was also able to inhibit the formation of colonies in cell lines with mutations in different members of the SWI/SNF complex. Interestingly, these cell lines (SKOV3 and IGROV1) did not contained mutations in CHK1 or CHK2 genes, demonstrating PRIM1 as a potential target also against impaired SWI/SNF complex (Table 3.7 and Figure 3.36). However, expansion of the cell line panel as well as rescue experiments are needed in order to confirm dependency of CHK1/CHK2 inactive or SWI/SNF impaired cells on PRIM1 activity.

During DNA replication, DNA primase polypeptide 1 (PRIM1) is responsible for the generation of the RNA primers that DNA polymerase α is using, to elongate them to generate the Okazaki fragments in the lagging strand. The DNA primase complex is consisted of DNA polymerase α, PRIM1 and PRIM2, however the primase activity is carried by PRIM1 and not PRIM2 (Lee et al., 2018, Xu et al., 2016). In 2016, Hocke et al., performed a siRNA screen for 288 genes involved in DNA damage repair in order to identify synthetic lethal interactions with ATR. PRIM1 was one of the identified hits for which they further showed also synthetic lethal interaction with CHK1. Synthetic lethality between PRIM1 and ATR was induced through S phase arrest and WEE1-mediated caspase-8 apoptosis. However, it was shown that PRIM1 depletion in ATR reduced cells did not reduce CHK1 phosphorylation, indicating an ATR-independent CHK1 activation (Hocke et al., 2016, Job et al., 2018). In addition, Lee et al., in 2018, shown that PRIM1

knockdown, disrupts DNA replication and activates CHK1 and CDC25C as well as WEE1 that drive cells to G2/M cell cycle arrest.

These studies are in agreement with our results demonstrating synthetic lethal interaction of PRIM1 with CHK1. However, more experiments are needed to validate the potential synthetic lethal interaction by introducing mutations in PRIM1, in areas of the gene that will prevent the siRNAs from silencing the gene, and therefore maintaining the function of the protein (rescue experiments). Secondly, following the *in vitro* experiments, PRIM1 and CHK1 potential lethal interactions should be investigated *in vivo* by generating inducible PRIM1 and CHK1 knockouts and confirm that only when both knockouts are induced, tumour growth is reduced. Finally, the mechanism by which depletion of PRIM1 and CHK1 promote cell death should be elucidated by investigation of WEE1 and caspase-8 expression as a starting point.

Nevertheless, we showed that mutations in SWI/SNF might also promote synthetic lethal interactions with PRIM1. Interactions of SWI/SNF with PRIM1 have not been extensively studied. In 2005, Gresh et al., showed that hepatocytes with SMARCAB1 deletion overexpress PRIM1, which promotes cell proliferation possible through partial inactivation of G1/S checkpoint. A recent study suggested that PRIM1 is overexpressed in breast and liver cancers and is correlated with poor patient prognosis, while a gene set enrichment analysis demonstrated that PRIM1 is correlated with cell growth and death pathways (Zhang et al., 2020). Moreover, previous studies have shown that SWI/SNF complex transcriptionally regulates ATR and CHK1 (Sethy et al., 2018, Zhang et al., 2013).

Thus, a potential synthetic lethal interaction of PRIM1 with SWI/SNF complex should be further investigated in a larger panel of cancer cell lines with mutations in the SWI/SNF complex but not in ATR, CHK1 or WEE1 proteins as well as in vivo, by inducible knockout of PRIM1 in impaired SWI/SNF tumours. Finally, it will be interesting to investigate the effect of SWI/SNF impairment in PRIM1 expression and if synthetic lethality of PRIM1 and SWI/SNF complex is induced through transcriptional repression of ATR and CHK1.

6.1.3.3 HELQ as a potential target in CIN, induced by SWI/SNF impairment

HELQ is a superfamily II (SF2) DNA helicase and exhibits an ATP dependent 3'-5' DNA helicase activity. It has been shown that HELQ is recruited in the area of stalked replication forks, which have been generated through interstrand crosslinks (ICLs) by mitomycin-C or Captothesin treatment, to unwind the parental strands for loading of factors required for DNA damage repair or replication re-start (Tafel et al., 2011, HAN et al., 2016). Multiple pathways are involved in the repair of ICLs, with Fanconi anaemia (FA) being one of the main repair networks. However, the interactions of HELQ with FA pathway is controversial. It has been shown that HELQ co-localizes with mono-ubiquitinated FANCD2 under ICLs conditions, however other studies have shown that HELQ deletion does not affect FANCD2 mono-ubiquitination, while deletion of FANCC, another FA protein, affects FANCD2 mono-ubiquitination (Tafel et al. 2014, Luebben et al., 2011). Moreover, loss of HELQ increases stalled replication forks and micronuclei formation, independent to FANCC, suggesting that HELQ acts in parallel but independent to FA pathway (Luebben et al., 2011, Takata et al., 2013).

Additionally, ATR is also recruited in the area of stalled replication forks and has been shown to promote mono-ubiquitination of FANCD2 but also phosphorylates and activates CHK1 for cells cycle delay until the DNA damages is repaired, or cell death to prevent damaged DNA to progress through cell cycle (Han et al., 2016). Previous studies have shown that HELQ interacts with ATR and RAD51 for repair of ICLs and that HELQ deletion reduces the expression of phosphorylated CHK1, which also interacts with RAD51, indicating a role of HELQ in the repair of ICLs through CHK1-RAD51 signaling (Liu et al., 2017, Takata et al., 2013).

Nevertheless, our results oppose this hypothesis as HELQ gene silencing showed no selectivity towards ATM or CHK1/CHK2 inhibition (Figure, 3.26). In contrast, in chapter 3, we presented selectivity of HELQ-depletion only towards SWI/SNF defects (Figures 3.22 and 3.26). Our results indicate that HELQ may act independently of CHK-RAD51 interactions. Moreover, no interaction of SWI/SNF complex with RAD51 has been shown, however, BRG1 interacts with RAD52, which together with BRCA2 replace

RPA with RAD51 on SSBs in order to initiate DNA strand invasion and repair of the damaged DNA (Qi et al., 2015). Interestingly, it is shown that repair of DSBs generated by ICLs after cisplatin treatment, is impaired in BRG1 or BRM deleted cells. The cells present impaired DNA damage repair through reduced ERCC1 expression, abnormal checkpoint activation with accumulation of cells in G1 phase and enhanced apoptosis (Kothandapani et al., 2012).

In summary, HELQ deletion may promote DNA damage during DNA replication, through increase of ICLs and stalled replication forks. In cells with functional SWI/SNF complex, CIN may be generated but the DNA damage will be repaired through NER or other repair mechanisms. However, when SWI/SNF complex is inactive, HELQ deletion generates DNA damage that cannot be repaired, promoting cell death through altered checkpoint activation or excessive degree of CIN.

This hypothesis needs to be investigated initially by validating HELQ selectivity towards SWI/SNF *in vitro* (by rescue experiments) and *in vivo* (by inducible HELQ knockout and impaired SWI/SNF complex). Secondly, the effect of HELQ-depletion in CIN should be further investigated, focusing on the presence of micronuclei and the pathway that is activated in order to repair the generated DNA damage that. For example, the pathway and the mechanism that induces the localisation and the expression of ERCC1. Finally, reduction of the repair pathway needs to be confirmed in cells with impaired SWI/SNF complex.

6.1.3.4 TEX14 as a potential target in CIN, induced by CENP-E inhibition

Testis-expressed gene 14 (TEX14) is mainly expressed in germ cell lines and its deletion it has been shown to promote infertility but only in male mice. In germ cells, TEX14 is localised in the midbody and is essential for the correct and stable formation of intercellular bridges during cytokinesis (Greenbaum et al., 2007, Boroujeni et al., 2018, Greenbaum et al., 2006). However, TEX14 expression has been also reported in other cells. Mondal et al., in 2012, showed in HeLa cells that TEX14 is recruited in the KT in prometaphase by PLK1, which is also essential for TEX14 removal at late metaphase

for metaphase to anaphase transition. In addition, they presented that TEX14 localisation at the outer kinetochores when no microtubules are attached promotes the expression and localisation of CENP-E and SAC proteins in the area, such as MAD1, MAD2 and MPS1. Deletion of TEX14 reduces the expression of CENP-E and weakens SAC, which is not enough to resolve the defects in KT-MT attachments and promotes chromosome missegregations and CIN (Mondal et al., 2012).

Our results from the sgRNA screening and confirmation by gene silencing in CENP-E inhibited or mutated cancer cell lines, indicate synthetic lethal interactions of TEX14 and CENP-E (Figures 3.10, 3.11, 3.29 and 3.35). In the presence of unattached kinetochores, CENP-E activates BUBR1 and SAC, delaying metaphase to anaphase transition, until CENP-E is captured by microtubules and silences BUBR1. Thus, inhibition of CENP-E activates SAC, however through a potential weakened or exhausted SAC, cells with unaligned chromosomes can transition to anaphase and generate segregation errors (Bennett et al., 2015). TEX14 depletion in a CENP-E loss of function background, may reduce SAC activity and allow anaphase transition with unaligned chromosomes that can lead to major chromosome missegregations and excessive degree of CIN, which cannot be tolerated by the cells (Figure 6.6).

However, synthetic lethal interactions of TEX14 and CENP-E should be further validated *in vitro*, by generation of TEX14 mutations that cannot be recognised by the siRNAs, but also do not affect the function of the protein. Thus, transduction with the TEX14 siRNAs should not affect the viability of CENP-E inhibited or deleted cells. In addition, quantification of chromosome missegregation in TEX14 depleted cells in combination with CENPE inhibition or alone should be investigated to determine whether loss of function in both proteins acts cooperatively to induce gross chromosome missegregation that may lead to cell death. Moreover, it will be interesting to investigate the activity of SAC and the degree of chromosome missegregations and CIN that is generated by deletion of TEX14 and CENP-E. Finally, *in vivo* experiments are needed, by using inducible TEX14 knockout and CENP-E deleted cancer cell lines, to confirm that TEX14 knockout reduces the growth of CENP-E deleted tumours.

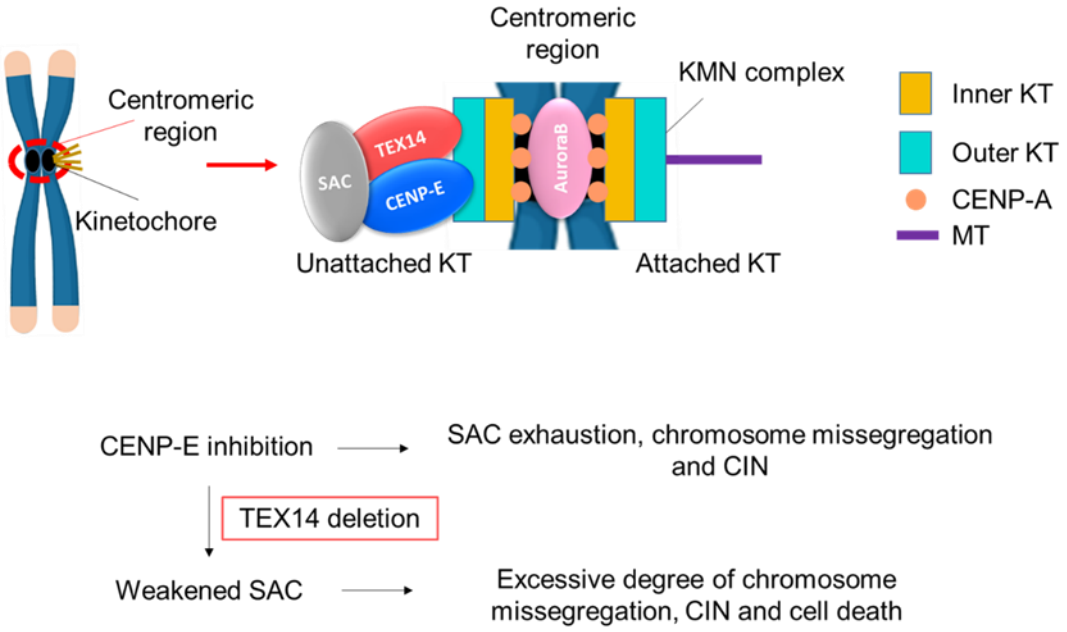

Figure 6.6: Schematic illustration of TEX14 and CENP-E localisation at the outer KT. TEX14 localises with CENP-E in unattached kinetochores promoting SAC activation until KT-MT attachments occur. Reduction of TEX14 and CENP-E results to an erroneous SAC that allows anaphase to metaphase transition, even in the presence of unattached kinetochores, generating chromosome missegregations and excessive degree of CIN. MT: Microtubules, KT: Kinetochore.

6.1.3.5 Targeting aneuploidy

The aim of this part of the study was to identify novel targets in aneuploidy, dependent or independent to specific chromosomal gains or losses. Therefore, after generation and characterisation of clones by FACS and CGH or SNPs microarrays, we selected a panel of aneuploid clones with different chromosomal alterations to continue with the loss of function sgRNA screening. Despite our efforts, because of technical limitations in the quality control assays at the outsourced company (Horizon Discovery) in the vast majority of the samples and unfortunately in the parental cell lines, we weren't able to identify any hits. Interestingly, we did not observe any resistant cell population during selection with puromycin, while the presence of the sgRNAs was confirmed by PCR amplification, according to the library protocol (Appendices figures 7.1 and 7.2).

In tumours or in a cancer cell population, CIN can generate stable aneuploid clones, thus, it would be interesting to investigate if gene silencing of the potential targets that were identified in CIN are also affecting the viability of the aneuploid clones. In particular, TEX14 deletion has been shown to induce aneuploidy by elevated

chromosome segregation errors (Mondal et al., 2012). Moreover, low or moderate degree of numerical or structural chromosomal alterations can be better tolerated by cancer cells (Chunduri and Storchová, 2019). As discussed in the section 6.1.2, our results also indicate that high degree of chromosomal alterations cannot be tolerated in the cells. Thus, deletion of TEX14 in an already aneuploid genetic background may lead to excessive aneuploidy and cell death.

6.2 Targeting the mechanisms of DNA content reduction

As discussed in the section 6.1.2, generation of aneuploid clones, reviled potential mechanisms by which cancer cells can alter their DNA content and transition from a near tetraploid to a near diploid, similar to the parental cell, DNA content. To gain further insight into the mechanisms by which cells can alter their DNA content, we conducted time-lapse microscopy experiments using Paclitaxel treated H2B-RFP and H2B-GFP cells and investigating their fate. Our results, in chapter 5, demonstrate that apart from multinucleation occurred through microtubule stabilisation, cancer cells could increase their DNA content by cell fusion. Following fusion, the cells were able to reduce their DNA content by either undergoing cell exodus or independent nucleus catastrophe. In addition, events of independent mitosis were observed, in which the fused cells could undergo mitosis independently from each other. The daughter cells could remain in the initial fused cell, increasing its DNA content or ‘escape’, generating mononucleated cells and reducing the DNA content of the host cell.

These events were previously observed in different studies investigating cancer cell invasion or regulation of nuclear division in multinucleated cells (Durgan and Florey, 2018, Overholtzer et al., 2007). Our study suggests that the observed events may also play a role in chemotherapeutic drug resistance. Also, we identify them as potential mechanisms by which cancer cells avoid deleterious gross aneuploidy. Indeed, treatment of cancer cells with chemotherapeutic agents or irradiation can generate PGCCs through neosis and escaping mononucleated cells that are resistant to the initial

treatment (Sundaram et al., 2004, Rajaraman et al., 2006, Fei et al., 2019, Sirois et al., 2019, Puig et al., 2008). In this study, we present for the first time evidence that cell-cell fusion plays a role in resistance of cells to Paclitaxel treatment and the combination of independent mitosis, cell exodus and independent nucleus catastrophe as mechanisms by which cells can reduce their DNA content after the treatment.

However, the mechanism by which cell-cell fusion occurs is not yet well understood. For example, in myoblasts, apoptotic cells have been suggested to induce cell fusion of alive neighbouring cells activating the cascade of phospatidylserine receptor BAI1 which results in activation of Rac pathway and generation of new actin filaments (Hochreiter-Hufford et al., 2013). Our results indicate a novel mechanism of cell attraction and cell-cell fusion, after Paclitaxel treatment, through cytokine and chemokine expression. We propose that chemotherapy treatment enables cell fusion through induction of cytokines and chemokines in the treated cells that compose them able to attract other cells (treated or untreated). This hypothesis is supported by previous studies showing that epirubicin treatment increase the percentage of fused cells in tumours from 6% to 12%, in breast cancer xenografts (Yan et al., 2016). Moreover, Paclitaxel treatment increases the expression of cytokines and chemokines (such as IL-6, IL-8 and CCF2) in the plasma of patients or in breast cancer cells (Jia et al., 2017, Pusztai et al., 2004). However, this hypothesis needs to be further confirmed by knockout or blocking of cytokines and chemokines such as IL-8, IL-6 or CCL5, and investigate their effect in cell-cell fusion during and after Taxol treatment. Moreover, it would be interesting to investigate the addition of these cytokines and chemokines in untreated cells and their effect in cell fusion.

Furthermore, our results demonstrate the importance of cell exodus in cell population recovery after paclitaxel treatment and importantly, we targeted cell exodus and cell recovery by sequential treatment of Paclitaxel with Crenolanib. This is the first study demonstrating that release of Paclitaxel to Crenolanib reduces cell fusion and inhibits cell exodus, resulting to more than 50% inhibition in the recovery of the cell population. Previous studies have shown that inhibition of ROCK pathway with Y-27632

or H-1152 compounds, blocks entosis, but allows cell fusion to occur, and treatment of MCM7 cells with Y-27632 does not reduce the cells' colony size in soft agar (Sottile et al., 2016, Hamann et al., 2017, Overholtzer et al., 2007).

Crenolanib is a PDGFRα/β and FLT3 inhibitor and is involved in approximately 20 clinical trials, mostly as FLT3 inhibitor, in Acute Myeloid Leukaemia (AML), in which an internal tandem duplication of FLT3 is present, hyper-activating the receptor (Clinical Trials.gov, Galanis et al., 2014). Moreover, Crenolanib can inhibit FLT3 receptor, even in the presence of mutations such as D835H/Y, which may arise after treatment with other FLT3 inhibitors (Galanis et al., 2014, Zimmerman et al., 2013). In addition, ongoing clinical trials in AML are investigating the effect of Crenolanib after chemotherapy treatment, such as Mitoxantrone or Etoposide (Clinical Trials.gov). However, Crenolanib was initially designed as a selective PDGFR inhibitor and it is currently also involved in clinical trials for amplified or mutated PDGFRα in glioblastomas and gastrointestinal tumours (Clinical trials.gov, Berndsen et al., 2019).

PDGFRα/β and FLT3 receptors are tyrosine kinase receptors and while inhibitors have been designed to specifically affect a small number of signalling pathways, it is becoming clear that these tyrosine kinase inhibitors generate off-target interactions. For example, it has been shown that Crenolanib prevents angiogenesis independently of PDGFR, although the latter is known for its role in angiogenesis. However, it was noticed that Crenolanib reduced the cadherin junctions and generated intercellular gaps (Berndsen et al., 2019). Moreover, Crenolanib has been shown to inhibit centrosome clustering, inducing multipolar divisions without SAC activation or mitotic delay. This ability of Crenolanib has been allocated to activation of Cofilin that dissociates F-actin filaments (Konotop et al., 2016).

To investigate the mechanism by which Crenolanib affects cell fusion and cell exodus, initially it needs to be examined if inhibition of cell exodus is a result of PDGFR or FLT3 inhibition, or combination of both. Secondly, it needs to be investigated the downstream pathways of the causative receptor, focusing on Crenolanib effect in cadherin junctions and in actin cytoskeleton that may be key regulators of cell fusion and

exodus. Previously has been described that cells need to be positioned in close proximity in order to be fused and deregulation of actin cytoskeleton by Cenolanib may affect the ability of fused cells to exit the host cells (Hernández and Podbilewicz, 2017). Additionally, the transcriptional signature of cells treated with Paclitaxel and released in Crenolanib should be investigated in order to identify the direct or indirect pathways that are affected by Crenolanib.

Finally, *in vivo* experiments are needed to confirm that sequential treatment of Paclitaxel with Crenolanib delay tumour recovery in comparison with tumours treated only with Paclitaxel.

6.3 Statement of impact

Due to Covid19 and the resulted disruption that occurred in the last months of this PhD study, we were unable to completely validate the confirmed hits *in vitro* and *in vivo*. In particular, the significant delay occurred by the lockdown due to Covid19 and the ventor in which we outsourced the samples for NGS, it was impossible to initiate confirmation of the hits by chemical inhibition and clonogenic assays before June 2020. Moreover, while we were able to validate the potential targets in a small panel of cancer cell lines with inactivation mutations in the genes of interest, time limitations prohibit us from including more cancel cell lines in the panel, or investigate the effect of silencing these genes in the aneuploid clones.

Additionally, to further validate the confirmed hits, we have generated constructs for HELQ, PRIM1 and TEX14 with specific targeted mutations that although they would not interfere with the function of the proteins, they would be resistant to the corresponding siRNAs. Thus, gene silencing of the hits in the corresponding CIN models containing these mutations, should rescue the detrimental phenotype. In addition, we have also generated constructs for hit-protein overexpression with the rational that the siRNAs will not be able to suppress entirely the expression of the exogenous and the

endogenous proteins. Due to vendor's delay and time limitations, we haven't used the above constructs but they will be useful for continuation of this project in the lab.

Combination of these delays, prevented us from investigating the molecular mechanisms by which deletion of the potential targets promotes synthetic lethality with the genes of interest. For example, to perform immunoprecipitation assays for the potential targets and the genes of interest and identify common proteins by which they may interact or immunoblotting and immunofluorescent assays to investigate the expression and the localisation of the potential proteins that are involved in the pathways. Additionally, we would perform immunofluorescence assays to identify the degree of CIN after deletion of the potential targets and the genes of interest, in order to investigate if the observed synthetic lethality is a result of excessive CIN that cannot be tolerated by the cancer cells.

During the NGS waiting period, we focused on investigating and targeting the mechanisms by which Paclitaxel treatment enables cell fusion, which in turn promotes cell population recovery. However, because of Covid19 we were not able to initiate *in vivo* experiments and confirm cell fusion occurrence after Paclitaxel treatment that can lead to tumour relapse or that sequential treatment of Paclitaxel and Crenolanib delays tumour relapse. We were aiming to perform *in vivo* experiments, using mixed H2B-GFP and H2B-RFP HCC1143 cells after subcutaneous injection into athymic mice. Treatment with paclitaxel alone or sequentially with Crenolanib will be followed to investigate tumour growth. This approach would confirm our *in vitro* findings that sequential treatment of Paclitaxel with Crenolanib delays tumour relapse. Sections from tumours would be used to further investigate percentage of fused cells.

In summary, despite the significant delays that were presented during this PhD project, we were able to perform confirmation clonogenic assays for multiple potential hits and investigate the effect of their chemical inhibition, when available, in the viability of the CIN models and a small panel of cancer cell lines. We confirmed three potential targets selective towards SWI/SNF mutated complex, one towards CENP-E defects and one towards CHK1 defects, which would be interesting to further validate and elucidate

the mechanism by which they can promote synthetic lethal interactions. Finally, we uncovered the mechanisms by which cell fusion enables cell recovery after Paclitaxel treatment and target for a first time cell recovery through these mechanisms, by sequential treatment of Paclitaxel and Crenolanib.

6.4 Conclusions

The data presented in this thesis, demonstrate potential targets in CIN by inducing synthetic lethal interactions with genes that drive the CIN phenotype. In particular, we identified synthetic lethality between SETD7 and BRG1 defects, TEX14 depletion and CENP-E defects, HELQ depletion and SWI/SNF-impaired complex and PRIM1 depletion and CHK1-defective or SWI/SNF-mutated complex. Moreover, we showed that high degree of aneuploidy with large chromosomal alterations cannot be tolerated in cancer cells. We presented cell fusion, followed by independent mitosis, cell exodus and independent nucleus separation as the causative events for generating cells with DNA content similar to the parental cell line, after treatment with Paclitaxel. In addition, we showed that cell exodus is essential for cell recovery after Paclitaxel treatment and we targeted the phenotype by sequential treatment of Paclitaxel and Crenolanib. The findings of this PhD will inform future investigations into potential therapeutic targets in CIN and mechanisms of DNA content alteration after Paclitaxel treatment, to improve cancer patient outcome.

Chapter 7 - Appendices

7.1 Supplementary videos

Video 7.1: PGCCs generation. Polyploid giant cancer cells were generated after equal mixing of H2B-GFP and H2B-mCherry HCT116p53$^{-/-}$ cells, treatment with 5nM of Taxol for three days and release in fresh media. The PGCC with one or two big nuclei initially underwent abortive mitosis but also mononucleated red nuclei can be seen around the big nuclei. Moreover, other H2B-GFP and H2B-RFP cells are getting fused in the initial cell, can undergo independent mitosis and cell exodus. Red illustrates H2B-mCherry nuclei, green the H2B-GFP nuclei and blue the phase contrast. Time-lapse was performed with 20x lens in Zeiss3i widefield microscope.

Video 7.2: Event of independent mitosis. Independent mitosis of a fused HCT116p53$^{-/-}$ cell with H2B-GFP and H2B-mcherry nuclei after 5 nM of Taxol treatment for three days. Only the H2B-mcherry nucleus undergoes mitosis and the two daughter cells remain in the original fused cell. Red illustrates H2B-mCherry nuclei, green the H2B-GFP nuclei and blue the phase contrast. Time-lapse was performed with 20x lens in Zeiss3i widefield microscope.

Video 7.3: Events of cell fusion and cell exodus. Cell fusion and cell exodus of H2B-GFP and H2B-mCherry HCT116p53$^{-/-}$ cells, after treatment with 5nM of Taxol for three days. A fused cell with five H2B-GFP nuclei and one H2B-mCherry nucleus is entering the video on the left. The red nucleus is undergoing cell exodus and another cell with red nucleus is entering the initial host cell. The H2B-mCherry nucleus that got fused is trying to undergo independent mitosis and by the same time is exiting the host cell. Red illustrates H2B-mCherry nuclei, green the H2B-GFP nuclei and blue the phase contrast. Time-lapse was performed with 20x lens in Zeiss3i widefield microscope.

Video 7.4: Events of cell fusion and independent nucleus catastrophe. Cell fusion and independent nucleus catastrophe in HCT116p53$^{-/-}$ cells. Illustration of a cell with two H2B-GFP nuclei and one H2B-mcherry nucleus (at the centre of the video) after 5 nM of Taxol treatment for three days. The red nucleus is undergoing independent catastrophe but it continues to remain in the fused cell as micronuclei. Red illustrates H2B-mCherry nuclei, green the H2B-GFP nuclei and blue the phase contrast. Time-lapse was performed with 20x lens in Zeiss3i widefield microscope.

7.2 Supplementary figures

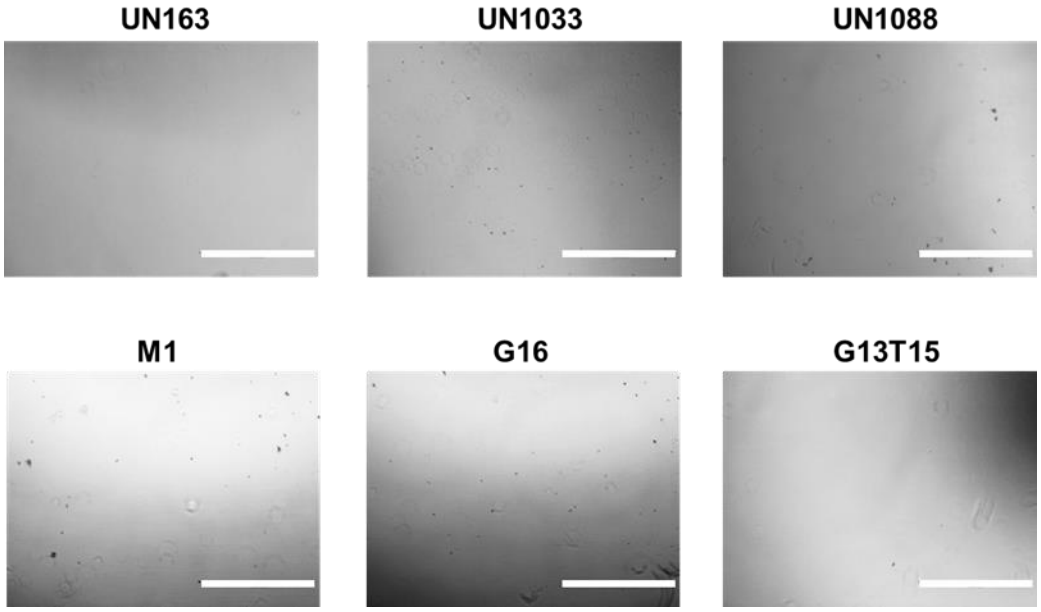

Figure 7.1: Treatment of untransduced aneuploid clones with puromycin. Illustration of untransduced cells, as control, during selection of the sgRNA transduced cells. Selection was made with 1 µg/ ml puromycin for 5 days. Photographs were taken by 4x lens of EVOS FL microscope. Scale bar 100 µm.

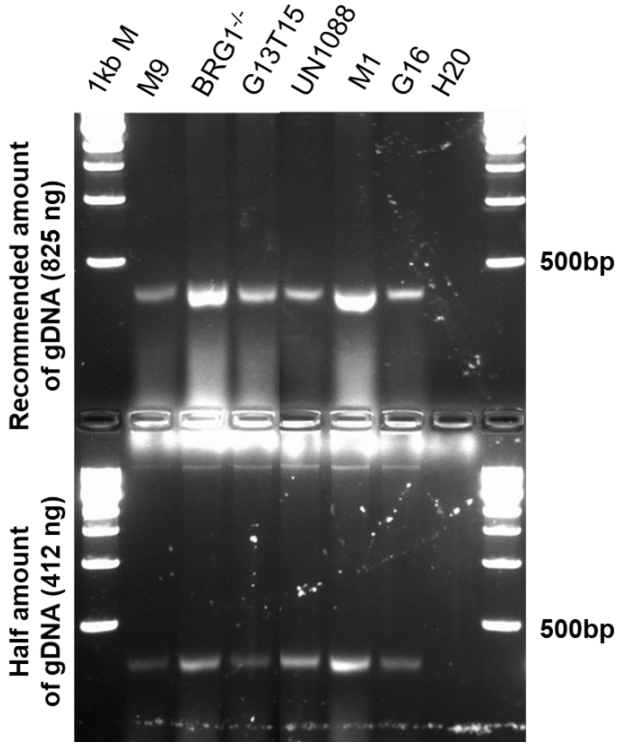

Figure 7.2: PCR amplification of the Edit-R pooled sgRNA construct. Illustration of the PCR amplification product by nucleic acid electrophoresis following the protocol provided by Dharmacon/Horizon. The amount recommended as well as double the amount needed was used. The baseline DNA for each cell line is illustrated. H2O was used as negative control. The expected size of the amplicon is 357 bp.

Bibliography

Abbas, T., and A. Dutta. 2009. 'p21 in cancer: intricate networks and multiple activities', *Nat Rev Cancer*, 9: 400-14.

Aguilera, A., and B. Gomez-Gonzalez. 2008. 'Genome instability: a mechanistic view of its causes and consequences', *Nat Rev Genet*, 9: 204-17.

Ahmed, M., and N. Rahman. 2006. 'ATM and breast cancer susceptibility', *Oncogene*, 25: 5906-11.

Aichel, O. 1911. *Über Zellverschmelzung mit qualitativ abnormer Chromosomenverteilung als Ursache der Geschwulstbildung* (W. Engelmann).

Al-Ejeh, F., P. T. Simpson, J. M. Sanus, K. Klein, M. Kalimutho, W. Shi, M. Miranda, J. Kutasovic, A. Raghavendra, J. Madore, L. Reid, L. Krause, G. Chenevix-Trench, S. R. Lakhani, and K. K. Khanna. 2014. 'Meta-analysis of the global gene expression profile of triple-negative breast cancer identifies genes for the prognostication and treatment of aggressive breast cancer', *Oncogenesis*, 3: e100-e00.

Alberts, Bruce. 2003. 'DNA replication and recombination', *Nature*, 421: 431-35.

Alexander, J. M., S. K. Hota, D. He, S. Thomas, L. Ho, L. A. Pennacchio, and B. G. Bruneau. 2015. 'Brg1 modulates enhancer activation in mesoderm lineage commitment', *Development*, 142: 1418-30.

Alhumaydhi, F. A., O. Lopes D. de, D. L. Bordin, A. S. M. Aljohani, C. B. Lloyd, M. D. McNicholas, L. Milano, C. F. Charlier, I. Villela, J. A. P. Henriques, K. E. Plant, R. M. Elliott, and L. B. Meira. 2020. 'Alkyladenine DNA glycosylase deficiency uncouples alkylation-induced strand break generation from PARP-1 activation and glycolysis inhibition', *Sci Rep*, 10: 2209.

AlQranei, Mohammed S., Hanan Aljohani, Sunipa Majumdar, Linda T. Senbanjo, and Meenakshi A. Chellaiah. 2020. 'C-phycocyanin attenuates RANKL-induced osteoclastogenesis and bone resorption in vitro through inhibiting ROS levels, NFATc1 and NF-κB activation', *Sci Rep*, 10: 2513.

Amend, S. R., G. Torga, K. C. Lin, L. G. Kostecka, A. de Marzo, R. H. Austin, and K. J. Pienta. 2019. 'Polyploid giant cancer cells: Unrecognized actuators of tumorigenesis, metastasis, and resistance', *Prostate*, 79: 1489-97.

Andor, N., C. C. Maley, and H. P. Ji. 2017. 'Genomic Instability in Cancer: Teetering on the Limit of Tolerance', *Cancer Res*, 77: 2179-85.

Andor, Noemi, Trevor A. Graham, Marnix Jansen, Li C. Xia, C. Athena Aktipis, Claudia Petritsch, Hanlee P. Ji, and Carlo C. Maley. 2016. 'Pan-cancer analysis of the extent and consequences of intratumor heterogeneity', *Nature Medicine*, 22: 105-13.

Armanios, M., and E. H. Blackburn. 2012. 'The telomere syndromes', *Nat Rev Genet*, 13: 693-704.

Aylon, Y., and M. Oren. 2011. 'p53: guardian of ploidy', *Mol Oncol*, 5: 315-23.

Bakhoum, S. F., and D. A. Compton. 2012. 'Chromosomal instability and cancer: a complex relationship with therapeutic potential', *J Clin Invest*, 122: 1138-43.

Bakhoum, S. F., L. Kabeche, J. P. Murnane, B. I. Zaki, and D. A. Compton. 2014. 'DNA-damage response during mitosis induces whole-chromosome missegregation', *Cancer Discov*, 4: 1281-9.

Bakhoum, S. F., and D. A. Landau. 2017. 'Chromosomal Instability as a Driver of Tumor Heterogeneity and Evolution', *Cold Spring Harb Perspect Med*, 7.

Balmus, G., D. Pilger, J. Coates, M. Demir, M. Sczaniecka-Clift, A. C. Barros, M. Woods, B. Fu, F. Yang, E. Chen, M. Ostermaier, T. Stankovic, H. Ponstingl, M. Herzog, K. Yusa, F. M. Martinez, S. T. Durant, Y. Galanty, P. Beli, D. J. Adams, A. Bradley, E. Metzakopian, J. V. Forment, and S. P. Jackson. 2019. 'ATM orchestrates the DNA-damage response to counter toxic non-homologous end-joining at broken replication forks', *Nat Commun*, 10: 87.

Balvan, J., J. Gumulec, M. Raudenska, A. Krizova, P. Stepka, P. Babula, R. Kizek, V. Adam, and M. Masarik. 2015. 'Oxidative Stress Resistance in Metastatic Prostate Cancer: Renewal by Self-Eating', *PLoS One*, 10: e0145016.

Bartlett, C., T. J. Orvis, G. S. Rosson, and B. E. Weissman. 2011. 'BRG1 mutations found in human cancer cell lines inactivate Rb-mediated cell-cycle arrest', *J Cell Physiol*, 226: 1989-97.

Barra, V., and D. Fachinetti. 2018. 'The dark side of centromeres: types, causes and consequences of structural abnormalities implicating centromeric DNA', *Nat Commun*, 9: 4340.

Barsyte-Lovejoy, Dalia, Fengling Li, Menno J. Oudhoff, John H. Tatlock, Aiping Dong, Hong Zeng, Hong Wu, Spencer A. Freeman, Matthieu Schapira, Guillermo A. Senisterra, Ekaterina Kuznetsova, Richard Marcellus, Abdellah Allali-Hassani, Steven Kennedy, Jean-Philippe Lambert, Amber L. Couzens, Ahmed Aman, Anne-Claude Gingras, Rima Al-Awar, Paul V. Fish, Brian S. Gerstenberger, Lee Roberts, Caroline L. Benn, Rachel L. Grimley, Mitchell J. S. Braam, Fabio M. V. Rossi, Marius Sudol, Peter J. Brown, Mark E. Bunnage, Dafydd R. Owen, Colby Zaph, Masoud Vedadi, and Cheryl H. Arrowsmith. 2014. '(R)-PFI-2 is a potent and selective inhibitor of SETD7 methyltransferase activity in cells', *Proceedings of the National Academy of Sciences*, 111: 12853.

Bastida-Ruiz, D., K. Van Hoesen, and M. Cohen. 2016. 'The Dark Side of Cell Fusion', *Int J Mol Sci*, 17.

Batista, Inês de Albuquerque Almeida, and Luisa Alejandra Helguero. 2018. 'Biological processes and signal transduction pathways regulated by the protein methyltransferase SETD7 and their significance in cancer', *Signal Transduction and Targeted Therapy*, 3: 19.

Beck, M., J. F. Peterson, J. McConnell, M. McGuire, M. Asato, J. E. Losee, U. Surti, S. Madan-Khetarpal, A. Rajkovic, and S. A. Yatsenko. 2015. 'Craniofacial abnormalities and developmental delay in two families with overlapping 22q12.1 microdeletions involving the MN1 gene', *Am J Med Genet A*, 167a: 1047-53.

Ben-David, U., and A. Amon. 2020. 'Context is everything: aneuploidy in cancer', *Nat Rev Genet*, 21: 44-62.

Ben-David, U., R. Beroukhim, and T. R. Golub. 2019. 'Genomic evolution of cancer models: perils and opportunities', *Nat Rev Cancer*, 19: 97-109.

Ben-David, U., B. Siranosian, G. Ha, H. Tang, Y. Oren, K. Hinohara, C. A. Strathdee, J. Dempster, N. J. Lyons, R. Burns, A. Nag, G. Kugener, B. Cimini, P. Tsvetkov, Y. E. Maruvka, R. O'Rourke, A. Garrity, A. A. Tubelli, P. Bandopadhayay, A. Tsherniak, F. Vazquez, B. Wong, C. Birger, M. Ghandi, A. R. Thorner, J. A. Bittker, M. Meyerson, G. Getz, R. Beroukhim, and T. R. Golub. 2018. 'Genetic and transcriptional evolution alters cancer cell line drug response', *Nature*, 560: 325-30.

Ben-David, Uri, Gal Arad, Uri Weissbein, Berhan Mandefro, Adva Maimon, Tamar Golan-Lev, Kavita Narwani, Amander T. Clark, Peter W. Andrews, Nissim Benvenisty, and Juan Carlos Biancotti. 2014. 'Aneuploidy induces profound changes in gene expression, proliferation and tumorigenicity of human pluripotent stem cells', *Nat Commun*, 5: 4825.

Benetti, R., S. Gonzalo, I. Jaco, G. Schotta, P. Klatt, T. Jenuwein, and M. A. Blasco. 2007. 'Suv4-20h deficiency results in telomere elongation and derepression of telomere recombination', *J Cell Biol*, 178: 925-36.

Bennett, A., B. Bechi, A. Tighe, S. Thompson, D. J. Procter, and S. S. Taylor. 2015. 'Cenp-E inhibitor GSK923295: Novel synthetic route and use as a tool to generate aneuploidy', *Oncotarget*, 6: 20921-32.

Berndsen, Robert H., Cédric Castrogiovanni, Andrea Weiss, Magdalena Rausch, Marchien G. Dallinga, Marijana Miljkovic-Licina, Ingeborg Klaassen, Patrick Meraldi, Judy R. van Beijnum, and Patrycja Nowak-Sliwinska. 2019. 'Anti-angiogenic effects of crenolanib are mediated by mitotic modulation independently of PDGFR expression', *British Journal of Cancer*, 121: 139-49.

Bharadwaj, Rajnish, and Hongtao Yu. 2004. 'The spindle checkpoint, aneuploidy, and cancer', *Oncogene*, 23: 2016-27.

Biancotti, J. C., K. Narwani, B. Mandefro, T. Golan-Lev, N. Buehler, D. Hill, C. N. Svendsen, and N. Benvenisty. 2012. 'The in vitro survival of human monosomies and trisomies as embryonic stem cells', *Stem Cell Res*, 9: 218-24.

Birkbak, N. J., A. C. Eklund, Q. Li, S. E. McClelland, D. Endesfelder, P. Tan, I. B. Tan, A. L. Richardson, Z. Szallasi, and C. Swanton. 2011. 'Paradoxical relationship between chromosomal instability and survival outcome in cancer', *Cancer Res*, 71: 3447-52.

Bjerregaard, B., S. Holck, I. J. Christensen, and L. I. Larsson. 2006. 'Syncytin is involved in breast cancer-endothelial cell fusions', *Cellular and Molecular Life Sciences CMLS*, 63: 1906-11.

Blackford, A. N., and S. P. Jackson. 2017. 'ATM, ATR, and DNA-PK: The Trinity at the Heart of the DNA Damage Response', *Mol Cell*, 66: 801-17.

Bolhaqueiro, Ana C. F., Bas Ponsioen, Bjorn Bakker, Sjoerd J. Klaasen, Emre Kucukkose, Richard H. van Jaarsveld, Judith Vivié, Ingrid Verlaan-Klink, Nizar Hami, Diana C. J. Spierings, Nobuo Sasaki, Devanjali Dutta, Sylvia F. Boj, Robert G. J. Vries, Peter M. Lansdorp, Marc van de Wetering, Alexander van Oudenaarden, Hans Clevers, Onno Kranenburg, Floris Foijer, Hugo J. G. Snippert, and Geert J. P. L. Kops. 2019. 'Ongoing chromosomal instability and karyotype evolution in human colorectal cancer organoids', *Nature Genetics*, 51: 824-34.

Bondy, Carolyn A., and Clara Cheng. 2009. 'Monosomy for the X chromosome', *Chromosome Research*, 17: 649-58.

Boroujeni, P. B., M. Sabbaghian, M. Totonchi, N. Sodeifi, H. Sarkardeh, A. Samadian, M. A. Sadighi-Gilani, and H. Gourabi. 2018. 'Expression analysis of genes encoding TEX11, TEX12, TEX14 and TEX15 in testis tissues of men with non-obstructive azoospermia', *JBRA Assist Reprod*, 22: 185-92.

Bouchet, B. P., J. Bertholon, N. Falette, C. Audoynaud, C. Lamblot, A. Puisieux, and C. M. Galmarini. 2007. 'Paclitaxel resistance in untransformed human mammary epithelial cells is associated with an aneuploidy-prone phenotype', *British Journal of Cancer*, 97: 1218-24.

Bourgo, R. J., H. Siddiqui, S. Fox, D. Solomon, C. G. Sansam, M. Yaniv, C. Muchardt, D. Metzger, P. Chambon, C. W. Roberts, and E. S. Knudsen. 2009. 'SWI/SNF deficiency results in aberrant chromatin organization, mitotic failure, and diminished proliferative capacity', *Mol Biol Cell*, 20: 3192-9.

Boveri, T. 1902. *Über mehrpolige Mitosen als Mittel zur Analyse des Zellkerns*.

Boveri, T. 1914. *Zur Frage der Entstehung maligner Tumoren* (Fischer).

Bower, Jacquelyn J., Leah D. Vance, Matthew Psioda, Stephanie L. Smith-Roe, Dennis A. Simpson, Joseph G. Ibrahim, Katherine A. Hoadley, Charles M. Perou, and William K. Kaufmann. 2017. 'Patterns of cell cycle checkpoint deregulation associated with intrinsic molecular subtypes of human breast cancer cells', *npj Breast Cancer*, 3: 9.

Brison, Olivier, Sami El-Hilali, Dana Azar, Stéphane Koundrioukoff, Mélanie Schmidt, Viola Nähse, Yan Jaszczyszyn, Anne-Marie Lachages, Bernard Dutrillaux, Claude Thermes, Michelle Debatisse, and Chun-Long Chen. 2019. 'Transcription-mediated organization of the replication initiation program across large genes sets common fragile sites genome-wide', *Nat Commun*, 10: 5693.

Brownlee, P. M., A. L. Chambers, R. Cloney, A. Bianchi, and J. A. Downs. 2014. 'BAF180 promotes cohesion and prevents genome instability and aneuploidy', *Cell Rep*, 6: 973-81.

Brownlee, P. M., C. Meisenberg, and J. A. Downs. 2015. 'The SWI/SNF chromatin remodelling complex: Its role in maintaining genome stability and preventing tumourigenesis', *DNA Repair (Amst)*, 32: 127-33.

Brukman, N. G., B. Uygur, B. Podbilewicz, and L. V. Chernomordik. 2019. 'How cells fuse', *J Cell Biol*, 218: 1436-51.

Bultman, S. J. 2019. 'SETD7 interacts with other chromatin-modifying factors to regulate cardiac development', *Stem Cell Investig*, 6: 14.

Burds, Aurora A., Annegret Schulze Lutum, and Peter K. Sorger. 2005. 'Generating chromosome instability through the simultaneous deletion of Mad2 and p53', *Proc Natl Acad Sci U S A*, 102: 11296.

Burrell, Rebecca A., Nicholas McGranahan, Jiri Bartek, and Charles Swanton. 2013. 'The causes and consequences of genetic heterogeneity in cancer evolution', *Nature*, 501: 338-45.

Cahill, D. P., K. W. Kinzler, B. Vogelstein, and C. Lengauer. 1999. 'Genetic instability and darwinian selection in tumours', *Trends Cell Biol*, 9: M57-60.

Cao, Wanlu, Meng Li, Jiaye Liu, Shaoshi Zhang, Lisanne Noordam, Monique M. A. Verstegen, Ling Wang, Buyun Ma, Shan Li, Wenshi Wang, Michiel Bolkestein, Michael Doukas, Kan Chen, Zhongren Ma, Marco Bruno, Dave Sprengers, Jaap Kwekkeboom, Luc J. W. van der Laan, Ron Smits, Maikel P. Peppelenbosch, and Qiuwei Pan. 2020. 'LGR5 marks targetable tumor-initiating cells in mouse liver cancer', *Nat Commun*, 11: 1961.

Ceccaldi, Raphael, Prabha Sarangi, and Alan D. D'Andrea. 2016. 'The Fanconi anaemia pathway: new players and new functions', *Nature Reviews Molecular Cell Biology*, 17: 337-49.

Cerami, E., J. Gao, U. Dogrusoz, B. E. Gross, S. O. Sumer, B. A. Aksoy, A. Jacobsen, C. J. Byrne, M. L. Heuer, E. Larsson, Y. Antipin, B. Reva, A. P. Goldberg, C. Sander, and N. Schultz. 2012. 'The cBio cancer genomics portal: an open platform for exploring multidimensional cancer genomics data', *Cancer Discov*, 2: 401-4.

Cereda, A., and J. C. Carey. 2012. 'The trisomy 18 syndrome', *Orphanet J Rare Dis*, 7: 81.

Cermak, V., V. Dostal, M. Jelinek, L. Libusova, J. Kovar, D. Rosel, and J. Brabek. 2020. 'Microtubule-targeting agents and their impact on cancer treatment', *Eur J Cell Biol*: 151075.

Chan, Y. W., C. So, K. L. Yau, K. C. Chiu, X. Wang, F. L. Chan, and S. Y. Tsang. 2020. 'Adipose-derived stem cells and cancer cells fuse to generate cancer stem cell-like cells with increased tumorigenicity', *J Cell Physiol*.

Chao, Hann-Hsiang, Ilias V. Karagounis, Christoforos Thomas, Noëlle B. François, Andrea Facciabene, Constantinos Koumenis, and Amit Maity. 2020. 'Combination of CHEK1/2 inhibition and ionizing radiation results in abscopal tumor response through increased micronuclei formation', *Oncogene*, 39: 4344-57.

Chatterjee, N., and G. C. Walker. 2017. 'Mechanisms of DNA damage, repair, and mutagenesis', *Environ Mol Mutagen*, 58: 235-63.

Chen, Elizabeth H., and Eric N. Olson. 2005. 'Unveiling the Mechanisms of Cell-Cell Fusion', *Science*, 308: 369.

Chen, G., W. A. Mulla, A. Kucharavy, H. J. Tsai, B. Rubinstein, J. Conkright, S. McCroskey, W. D. Bradford, L. Weems, J. S. Haug, C. W. Seidel, J. Berman, and R. Li. 2015. 'Targeting the adaptability of heterogeneous aneuploids', *Cell*, 160: 771-84.

Chen, J., N. Niu, J. Zhang, L. Qi, W. Shen, K. V. Donkena, Z. Feng, and J. Liu. 2019. 'Polyploid Giant Cancer Cells (PGCCs): The Evil Roots of Cancer', *Curr Cancer Drug Targets*, 19: 360-67.

Chen, W., J. Dong, J. Haiech, M. C. Kilhoffer, and M. Zeniou. 2016. 'Cancer Stem Cell Quiescence and Plasticity as Major Challenges in Cancer Therapy', *Stem Cells Int*, 2016: 1740936.

Chen, Yalei, and William O. Hancock. 2015. 'Kinesin-5 is a microtubule polymerase', *Nat Commun*, 6: 8160.

Choi, E., P. G. Park, H. O. Lee, Y. K. Lee, G. H. Kang, J. W. Lee, W. Han, H. C. Lee, D. Y. Noh, S. Lekomtsev, and H. Lee. 2012. 'BRCA2 fine-tunes the spindle assembly checkpoint through reinforcement of BubR1 acetylation', *Dev Cell*, 22: 295-308.

Chou, E. J., L. Y. Hung, C. J. Tang, W. B. Hsu, H. Y. Wu, P. C. Liao, and T. K. Tang. 2016. 'Phosphorylation of CPAP by Aurora-A Maintains Spindle Pole Integrity during Mitosis', *Cell Rep*, 14: 2975-87.

Chunduri, Narendra Kumar, and Zuzana Storchová. 2019. 'The diverse consequences of aneuploidy', *Nature Cell Biology*, 21: 54-62.

Clapier, Cedric R., Janet Iwasa, Bradley R. Cairns, and Craig L. Peterson. 2017. 'Mechanisms of action and regulation of ATP-dependent chromatin-remodelling complexes', *Nature Reviews Molecular Cell Biology*, 18: 407-22.

Clynes, D., C. Jelinska, B. Xella, H. Ayyub, C. Scott, M. Mitson, S. Taylor, D. R. Higgs, and R. J. Gibbons. 2015. 'Suppression of the alternative lengthening of telomere pathway by the chromatin remodelling factor ATRX', *Nat Commun*, 6: 7538.

Cohen, S. M., P. D. Chastain, 2nd, G. B. Rosson, B. S. Groh, B. E. Weissman, D. G. Kaufman, and S. J. Bultman. 2010. 'BRG1 co-localizes with DNA replication factors and is required for efficient replication fork progression', *Nucleic Acids Res*, 38: 6906-19.

Conomos, D., H. A. Pickett, and R. R. Reddel. 2013. 'Alternative lengthening of telomeres: remodeling the telomere architecture', *Front Oncol*, 3: 27.

Cortés-Ciriano, Isidro, Jake June-Koo Lee, Ruibin Xi, Dhawal Jain, Youngsook L. Jung, Lixing Yang, Dmitry Gordenin, Leszek J. Klimczak, Cheng-Zhong Zhang, David S. Pellman, Kadir C. Akdemir, Eva G. Alvarez, Adrian Baez-Ortega, Rameen Beroukhim, Paul C. Boutros, David D. L. Bowtell, Benedikt Brors, Kathleen H. Burns, Peter J. Campbell, Kin Chan, Ken Chen, Isidro Cortés-Ciriano, Ana Dueso-Barroso, Andrew J. Dunford, Paul A. Edwards, Xavier Estivill, Dariush Etemadmoghadam, Lars Feuerbach, J. Lynn Fink, Milana Frenkel-Morgenstern, Dale W. Garsed, Mark Gerstein, Dmitry A. Gordenin, David Haan, James E. Haber, Julian M. Hess, Barbara Hutter, Marcin

Imielinski, David T. W. Jones, Young Seok Ju, Marat D. Kazanov, Leszek J. Klimczak, Youngil Koh, Jan O. Korbel, Kiran Kumar, Eunjung Alice Lee, Jake June-Koo Lee, Yilong Li, Andy G. Lynch, Geoff Macintyre, Florian Markowetz, Iñigo Martincorena, Alexander Martinez-Fundichely, Satoru Miyano, Hidewaki Nakagawa, Fabio C. P. Navarro, Stephan Ossowski, Peter J. Park, John V. Pearson, Montserrat Puiggròs, Karsten Rippe, Nicola D. Roberts, Steven A. Roberts, Bernardo Rodriguez-Martin, Steven E. Schumacher, Ralph Scully, Mark Shackleton, Nikos Sidiropoulos, Lina Sieverling, Chip Stewart, David Torrents, Jose M. C. Tubio, Izar Villasante, Nicola Waddell, Jeremiah A. Wala, Joachim Weischenfeldt, Lixing Yang, Xiaotong Yao, Sung-Soo Yoon, Jorge Zamora, Cheng-Zhong Zhang, Peter J. Park, Pcawg Structural Variation Working Group, and Pcawg Consortium. 2020. 'Comprehensive analysis of chromothripsis in 2,658 human cancers using whole-genome sequencing', *Nature Genetics*, 52: 331-41.

Dagogo-Jack, Ibiayi, and Alice T. Shaw. 2018. 'Tumour heterogeneity and resistance to cancer therapies', *Nature Reviews Clinical Oncology*, 15: 81-94.

Das, K., and P. Tan. 2013. 'Molecular cytogenetics: recent developments and applications in cancer', *Clin Genet*, 84: 315-25.

de Cubas, Aguirre A., and W. Kimryn Rathmell. 2018. 'Epigenetic modifiers: activities in renal cell carcinoma', *Nature Reviews Urology*, 15: 599-614.

Delespaul, Lucile, Candice Merle, Tom Lesluyes, Pauline Lagarde, Sophie Le Guellec, Gaëlle Pérot, Jessica Baud, Martina Carlotti, Coralie Danet, Murielle Fèvre, Benoit Rousseau, Stéphanie Durrieu, Martin Teichmann, Jean-Michel Coindre, Lydia Lartigue, and Frédéric Chibon. 2019. 'Fusion-mediated chromosomal instability promotes aneuploidy patterns that resemble human tumors', *Oncogene*, 38: 6083-94.

Deng, W., S. W. Tsao, G. W. Y. Mak, C. M. Tsang, Y. P. Ching, X. Y. Guan, M. S. Y. Huen, and A. L. M. Cheung. 2011. 'Impact of G2 checkpoint defect on centromeric instability', *Oncogene*, 30: 1281-89.

Díaz-Carballo, D., S. Saka, J. Klein, T. Rennkamp, A. H. Acikelli, S. Malak, H. Jastrow, G. Wennemuth, C. Tempfer, I. Schmitz, A. Tannapfel, and D. Strumberg. 2018. 'A Distinct Oncogenerative Multinucleated Cancer Cell Serves as a Source of Stemness and Tumor Heterogeneity', *Cancer Res*, 78: 2318-31.

Ding, L., M. J. Ellis, S. Li, D. E. Larson, K. Chen, J. W. Wallis, C. C. Harris, M. D. McLellan, R. S. Fulton, L. L. Fulton, R. M. Abbott, J. Hoog, D. J. Dooling, D. C. Koboldt, H. Schmidt, J. Kalicki, Q. Zhang, L. Chen, L. Lin, M. C. Wendl, J. F. McMichael, V. J. Magrini, L. Cook, S. D. McGrath, T. L. Vickery, E. Appelbaum, K. Deschryver, S. Davies, T. Guintoli, L. Lin, R. Crowder, Y. Tao, J. E. Snider, S. M. Smith, A. F. Dukes, G. E. Sanderson, C. S. Pohl, K. D. Delehaunty, C. C. Fronick, K. A. Pape, J. S. Reed, J. S. Robinson, J. S. Hodges, W. Schierding, N. D. Dees, D. Shen, D. P. Locke, M. E. Wiechert, J. M. Eldred, J. B. Peck, B. J. Oberkfell, J. T. Lolofie, F. Du, A. E. Hawkins, M. D. O'Laughlin, K. E. Bernard, M. Cunningham, G. Elliott, M. D. Mason, D. M. Thompson, Jr., J. L. Ivanovich, P. J. Goodfellow, C. M. Perou, G. M. Weinstock, R. Aft, M. Watson, T. J. Ley, R. K. Wilson, and E. R. Mardis. 2010. 'Genome remodelling in a basal-like breast cancer metastasis and xenograft', *Nature*, 464: 999-1005.

Dodgson, S. E., S. Santaguida, S. Kim, J. Sheltzer, and A. Amon. 2016. 'The pleiotropic deubiquitinase Ubp3 confers aneuploidy tolerance', *Genes Dev*, 30: 2259-71.

Donehower, L. A., T. Soussi, A. Korkut, Y. Liu, A. Schultz, M. Cardenas, X. Li, O. Babur, T. K. Hsu, O. Lichtarge, J. N. Weinstein, R. Akbani, and D. A. Wheeler. 2019. 'Integrated Analysis of TP53 Gene and Pathway Alterations in The Cancer Genome Atlas', *Cell Rep*, 28: 1370-84.e5.

Donne, Romain, Maëva Saroul-Aïnama, Pierre Cordier, Séverine Celton-Morizur, and Chantal Desdouets. 2020. 'Polyploidy in liver development, homeostasis and disease', *Nature Reviews Gastroenterology & Hepatology*.

Donnelly, N., V. Passerini, M. Dürrbaum, S. Stingele, and Z. Storchová. 2014. 'HSF1 deficiency and impaired HSP90-dependent protein folding are hallmarks of aneuploid human cells', *Embo j*, 33: 2374-87.

Dörnen, J., M. Sieler, J. Weiler, S. Keil, and T. Dittmar. 2020. 'Cell Fusion-Mediated Tissue Regeneration as an Inducer of Polyploidy and Aneuploidy', *Int J Mol Sci*, 21.

Drosopoulos, Konstantinos, Chan Tang, William C. H. Chao, and Spiros Linardopoulos. 2014. 'APC/C is an essential regulator of centrosome clustering', *Nat Commun*, 5: 3686.

Drosos, Y., D. Escobar, M. Y. Chiang, K. Roys, V. Valentine, M. B. Valentine, J. E. Rehg, V. Sahai, L. A. Begley, J. Ye, L. Paul, P. J. McKinnon, and B. Sosa-Pineda. 2017. 'ATM-deficiency increases genomic instability and metastatic potential in a mouse model of pancreatic cancer', *Sci Rep*, 7: 11144.

Duch, Alba, Berta Canal, Sonia I. Barroso, María García-Rubio, Gerhard Seisenbacher, Andrés Aguilera, Eulàlia de Nadal, and Francesc Posas. 2018. 'Multiple signaling kinases target Mrc1 to prevent genomic instability triggered by transcription-replication conflicts', *Nat Commun*, 9: 379.

Durgan, J., and O. Florey. 2018. 'Cancer cell cannibalism: Multiple triggers emerge for entosis', *Biochim Biophys Acta Mol Cell Res*, 1865: 831-41.

Durgan, J., Y. Y. Tseng, J. C. Hamann, M. C. Domart, L. Collinson, A. Hall, M. Overholtzer, and O. Florey. 2017. 'Mitosis can drive cell cannibalism through entosis', *Elife*, 6.

Ertych, Norman, Ailine Stolz, Albrecht Stenzinger, Wilko Weichert, Silke Kaulfuß, Peter Burfeind, Achim Aigner, Linda Wordeman, and Holger Bastians. 2014. 'Increased microtubule assembly rates influence chromosomal instability in colorectal cancer cells', *Nature Cell Biology*, 16: 779-91.

Faisal, Amir, Grace W. Y. Mak, Mark D. Gurden, Cristina P. R. Xavier, Simon J. Anderhub, Paolo Innocenti, Isaac M. Westwood, Sébastien Naud, Angela Hayes, Gary Box, Melanie R. Valenti, Alexis K. De Haven Brandon, Lisa O'Fee, Jessica Schmitt, Hannah L. Woodward, Rosemary Burke, Rob L. M. vanMontfort, Julian Blagg, Florence I. Raynaud, Suzanne A. Eccles, Swen Hoelder, and Spiros Linardopoulos. 2017. 'Characterisation of CCT271850, a selective, oral and potent MPS1 inhibitor, used to directly measure in vivo MPS1 inhibition vs therapeutic efficacy', *British Journal of Cancer*, 116: 1166-76.

Fei, F., C. Li, X. Wang, J. Du, K. Liu, B. Li, P. Yao, Y. Li, and S. Zhang. 2019. 'Syncytin 1, CD9, and CD47 regulating cell fusion to form PGCCs associated with cAMP/PKA and

JNK signaling pathway', *Cancer Med*, 8: 3047-58.

Foijer, F. 2010. 'CINister thoughts', *Biochem Soc Trans*, 38: 1715-21.

Forment, Josep V., Abderrahmane Kaidi, and Stephen P. Jackson. 2012. 'Chromothripsis and cancer: causes and consequences of chromosome shattering', *Nature Reviews Cancer*, 12: 663-70.

Fu, D., J. A. Calvo, and L. D. Samson. 2012. 'Balancing repair and tolerance of DNA damage caused by alkylating agents', *Nat Rev Cancer*, 12: 104-20.

Fukumoto, T., E. Magno, and R. Zhang. 2018. 'SWI/SNF Complexes in Ovarian Cancer: Mechanistic Insights and Therapeutic Implications', *Mol Cancer Res*, 16: 1819-25.

Gaillard, Hélène, Tatiana García-Muse, and Andrés Aguilera. 2015. 'Replication stress and cancer', *Nature Reviews Cancer*, 15: 276-89.

Galanis, A., H. Ma, T. Rajkhowa, A. Ramachandran, D. Small, J. Cortes, and M. Levis. 2014. 'Crenolanib is a potent inhibitor of FLT3 with activity against resistance-conferring point mutants', *Blood*, 123: 94-100.

Ganem, N. J., S. A. Godinho, and D. Pellman. 2009. 'A mechanism linking extra centrosomes to chromosomal instability', *Nature*, 460: 278-82.

Ganem, N. J., Z. Storchova, and D. Pellman. 2007. 'Tetraploidy, aneuploidy and cancer', *Curr Opin Genet Dev*, 17: 157-62.

Gao, P., and J. Zheng. 2010. 'High-risk HPV E5-induced cell fusion: a critical initiating event in the early stage of HPV-associated cervical cancer', *Virol J*, 7: 238.

García-Muse, Tatiana, and Andrés Aguilera. 2016. 'Transcription–replication conflicts: how they occur and how they are resolved', *Nature Reviews Molecular Cell Biology*, 17: 553-63.

Gast, C. E., A. D. Silk, L. Zarour, L. Riegler, J. G. Burkhart, K. T. Gustafson, M. S. Parappilly, M. Roh-Johnson, J. R. Goodman, B. Olson, M. Schmidt, J. R. Swain, P. S. Davies, V. Shasthri, S. Iizuka, P. Flynn, S. Watson, J. Korkola, S. A. Courtneidge, J. M. Fischer, J. Jaboin, K. G. Billingsley, C. D. Lopez, J. Burchard, J. Gray, L. M. Coussens, B. C. Sheppard, and M. H. Wong. 2018. 'Cell fusion potentiates tumor heterogeneity and reveals circulating hybrid cells that correlate with stage and survival', *Sci Adv*, 4: eaat7828.

Gerbaud, P., and G. Pidoux. 2015. 'Review: An overview of molecular events occurring in human trophoblast fusion', *Placenta*, 36 Suppl 1: S35-42.

Giam, M., and G. Rancati. 2015. 'Aneuploidy and chromosomal instability in cancer: a jackpot to chaos', *Cell Div*, 10: 3.

Girard, Pierre-Marie, Enriqueta Riballo, Adrian C. Begg, Alastair Waugh, and Penny A. Jeggo. 2002. 'Nbs1 promotes ATM dependent phosphorylation events including those required for G1/S arrest', *Oncogene*, 21: 4191-99.

Giraudo, C. G., C. Hu, D. You, A. M. Slovic, E. V. Mosharov, D. Sulzer, T. J. Melia, and J. E. Rothman. 2005. 'SNAREs can promote complete fusion and hemifusion as alternative outcomes', *J Cell Biol*, 170: 249-60.

Glotzer, M. 2017. 'Cytokinesis in Metazoa and Fungi', *Cold Spring Harb Perspect Biol*, 9.

Godinho, Susana A., Remigio Picone, Mithila Burute, Regina Dagher, Ying Su, Cheuk T. Leung, Kornelia Polyak, Joan S. Brugge, Manuel Théry, and David Pellman. 2014. 'Oncogene-like induction of cellular invasion from centrosome amplification', *Nature*, 510: 167-71.

Golding, S. E., E. Rosenberg, N. Valerie, I. Hussaini, M. Frigerio, X. F. Cockcroft, W. Y. Chong, M. Hummersone, L. Rigoreau, K. A. Menear, M. J. O'Connor, L. F. Povirk, T. van Meter, and K. Valerie. 2009. 'Improved ATM kinase inhibitor KU-60019 radiosensitizes glioma cells, compromises insulin, AKT and ERK prosurvival signaling, and inhibits migration and invasion', *Mol Cancer Ther*, 8: 2894-902.

Gordon, David J., Benjamin Resio, and David Pellman. 2012. 'Causes and consequences of aneuploidy in cancer', *Nature Reviews Genetics*, 13: 189-203.

Greenbaum, M. P., L. Ma, and M. M. Matzuk. 2007. 'Conversion of midbodies into germ cell intercellular bridges', *Dev Biol*, 305: 389-96.

Greenbaum, M. P., W. Yan, M. H. Wu, Y. N. Lin, J. E. Agno, M. Sharma, R. E. Braun, A. Rajkovic, and M. M. Matzuk. 2006. 'TEX14 is essential for intercellular bridges and fertility in male mice', *Proc Natl Acad Sci U S A*, 103: 4982-7.

Gregan, J., S. Polakova, L. Zhang, I. M. Tolic-Norrelykke, and D. Cimini. 2011. 'Merotelic kinetochore attachment: causes and effects', *Trends Cell Biol*, 21: 374-81.

Gresh, L., B. Bourachot, A. Reimann, B. Guigas, L. Fiette, S. Garbay, C. Muchardt, L. Hue, M. Pontoglio, M. Yaniv, and A. Klochendler-Yeivin. 2005. 'The SWI/SNF chromatin-remodeling complex subunit SNF5 is essential for hepatocyte differentiation', *Embo j*, 24: 3313-24.

Gronroos, E., and C. López-García. 2018. 'Tolerance of Chromosomal Instability in Cancer: Mechanisms and Therapeutic Opportunities', *Cancer Res*, 78: 6529-35.

Gupta, D., and C. D. Heinen. 2019. 'The mismatch repair-dependent DNA damage response: Mechanisms and implications', *DNA Repair (Amst)*, 78: 60-69.

Gupta, Deepesh Kumar, Siamak A. Kamranvar, Jian Du, Liangwen Liu, and Staffan Johansson. 2019. 'Septin and Ras regulate cytokinetic abscission in detached cells', *Cell Division*, 14: 8.

Gurden, M. D., I. M. Westwood, A. Faisal, S. Naud, K. M. Cheung, C. McAndrew, A. Wood, J. Schmitt, K. Boxall, G. Mak, P. Workman, R. Burke, S. Hoelder, J. Blagg, R. L. Van Montfort, and S. Linardopoulos. 2015. 'Naturally Occurring Mutations in the MPS1 Gene Predispose Cells to Kinase Inhibitor Drug Resistance', *Cancer Res*, 75: 3340-54.

H. Dehkordi, Mahshid, Amin Tashakor, Enda O'Connell, and Howard O. Fearnhead. 2020. 'Apoptosome-dependent myotube formation involves activation of caspase-3 in differentiating myoblasts', *Cell Death & Disease*, 11: 308.

Hamann, J. C., A. Surcel, R. Chen, C. Teragawa, J. G. Albeck, D. N. Robinson, and M. Overholtzer. 2017. 'Entosis Is Induced by Glucose Starvation', *Cell Rep*, 20: 201-10.

Han, J., C. Ruan, M. S. Y. Huen, J. Wang, A. Xie, C. Fu, T. Liu, and J. Huang. 2017. 'BRCA2 antagonizes classical and alternative nonhomologous end-joining to prevent gross genomic instability', *Nat Commun*, 8: 1470.

Han, X., L. Zhao, and X. Li. 2016. 'HELQ in cancer and reproduction', *Neoplasma*, 63: 825-35.

Hanahan, D., and R. A. Weinberg. 2000. 'The hallmarks of cancer', *Cell*, 100: 57-70.

Hanahan, D., and R. A. Weinberg. 2011. 'Hallmarks of cancer: the next generation', *Cell*, 144: 646-74.

Hansemann, David. 1890. 'Ueber asymmetrische Zelltheilung in Epithelkrebsen und deren biologische Bedeutung', *Archiv für pathologische Anatomie und Physiologie und für klinische Medicin*, 119: 299-326.

Hardy, P. A., and H. Zacharias. 2005. 'Reappraisal of the Hansemann-Boveri hypothesis on the origin of tumors', *Cell Biol Int*, 29: 983-92.

Hass, R., J. von der Ohe, and H. Ungefroren. 2019. 'Potential Role of MSC/Cancer Cell Fusion and EMT for Breast Cancer Stem Cell Formation', *Cancers (Basel)*, 11.

Hays, Emily, Elizabeth Nettleton, Caitlin Carter, Mariangel Morales, Lynn Vo, Max Passo, and Renier Vélez-Cruz. 2020. 'The SWI/SNF ATPase BRG1 stimulates DNA end resection and homologous recombination by reducing nucleosome density at DNA double strand breaks and by promoting the recruitment of the CtIP nuclease', *Cell Cycle*: 1-19.

Heaphy, C. M., W. L. Bi, S. Coy, C. Davis, G. L. Gallia, S. Santagata, and F. J. Rodriguez. 2020. 'Telomere length alterations and ATRX/DAXX loss in pituitary adenomas', *Mod Pathol*.

Helmrich, Anne, Monica Ballarino, Evgeny Nudler, and Laszlo Tora. 2013. 'Transcription-replication encounters, consequences and genomic instability', *Nature Structural & Molecular Biology*, 20: 412-18.

Heng, H. H., S. W. Bremer, J. B. Stevens, S. D. Horne, G. Liu, B. Y. Abdallah, K. J. Ye, and C. J. Ye. 2013. 'Chromosomal instability (CIN): what it is and why it is crucial to cancer evolution', *Cancer Metastasis Rev*, 32: 325-40.

Hernández, J. M., and B. Podbilewicz. 2017. 'The hallmarks of cell-cell fusion', *Development*, 144: 4481-95.

Hernandez, Javier M., Alexander Stein, Elmar Behrmann, Dietmar Riedel, Anna

Cypionka, Zohreh Farsi, Peter J. Walla, Stefan Raunser, and Reinhard Jahn. 2012. 'Membrane Fusion Intermediates via Directional and Full Assembly of the SNARE Complex', *Science*, 336: 1581.

Hieronymus, H., R. Murali, A. Tin, K. Yadav, W. Abida, H. Moller, D. Berney, H. Scher, B. Carver, P. Scardino, N. Schultz, B. Taylor, A. Vickers, J. Cuzick, and C. L. Sawyers. 2018. 'Tumor copy number alteration burden is a pan-cancer prognostic factor associated with recurrence and death', *Elife*, 7.

Higashiguchi, M., I. Nagatomo, T. Kijima, O. Morimura, K. Miyake, T. Minami, S. Koyama, H. Hirata, K. Iwahori, T. Takimoto, Y. Takeda, H. Kida, and A. Kumanogoh. 2016. 'Clarifying the biological significance of the CHK2 K373E somatic mutation discovered in The Cancer Genome Atlas database', *FEBS Lett*, 590: 4275-86.

Hindi, Sajedah M., Jonghyun Shin, Yann S. Gallot, Alex R. Straughn, Adriana Simionescu-Bankston, Lubna Hindi, Guangyan Xiong, Robert P. Friedland, and Ashok Kumar. 2017. 'MyD88 promotes myoblast fusion in a cell-autonomous manner', *Nat Commun*, 8: 1624.

Hochreiter-Hufford, Amelia E., Chang Sup Lee, Jason M. Kinchen, Jennifer D. Sokolowski, Sanja Arandjelovic, Jarrod A. Call, Alexander L. Klibanov, Zhen Yan, James W. Mandell, and Kodi S. Ravichandran. 2013. 'Phosphatidylserine receptor BAI1 and apoptotic cells as new promoters of myoblast fusion', *Nature*, 497: 263-67.

Hocke, S., Y. Guo, A. Job, M. Orth, A. Ziesch, K. Lauber, E. N. De Toni, T. M. Gress, A. Herbst, B. Göke, and E. Gallmeier. 2016. 'A synthetic lethal screen identifies ATR-inhibition as a novel therapeutic approach for POLD1-deficient cancers', *Oncotarget*, 7: 7080-95.

Hoevenaar, Wilma H. M., Aniek Janssen, Ajit I. Quirindongo, Huiying Ma, Sjoerd J. Klaasen, Antoinette Teixeira, Bastiaan van Gerwen, Nico Lansu, Folkert H. M. Morsink, G. Johan A. Offerhaus, René H. Medema, Geert J. P. L. Kops, and Nannette Jelluma. 2020. 'Degree and site of chromosomal instability define its oncogenic potential', *Nat Commun*, 11: 1501.

Holland, Andrew J., and Don W. Cleveland. 2009. 'Boveri revisited: chromosomal instability, aneuploidy and tumorigenesis', *Nature Reviews Molecular Cell Biology*, 10: 478-87.

Horton, J. K., M. Watson, D. F. Stefanick, D. T. Shaughnessy, J. A. Taylor, and S. H. Wilson. 2008. 'XRCC1 and DNA polymerase beta in cellular protection against cytotoxic DNA single-strand breaks', *Cell Res*, 18: 48-63.

Hu, Chuan, Mahiuddin Ahmed, Thomas J. Melia, Thomas H. Söllner, Thomas Mayer, and James E. Rothman. 2003. 'Fusion of Cells by Flipped SNAREs', *Science*, 300: 1745.

Huang, Yuejia, Lin Lin, Xing Liu, Sheng Ye, Phil Y. Yao, Wenwen Wang, Fengrui Yang, Xinjiao Gao, Junying Li, Yin Zhang, Jiancun Zhang, Zhihong Yang, Xu Liu, Zhenye Yang, Jianye Zang, Maikun Teng, Zhiyong Wang, Ke Ruan, Xia Ding, Lin Li, Don W. Cleveland, Rongguang Zhang, and Xuebiao Yao. 2019. 'BubR1 phosphorylates CENP-E as a switch enabling the transition from lateral association to end-on capture of spindle microtubules', *Cell Res*, 29: 562-78.

Huang, Z. Q., J. Li, L. M. Sachs, P. A. Cole, and J. Wong. 2003. 'A role for cofactor-cofactor and cofactor-histone interactions in targeting p300, SWI/SNF and Mediator for transcription', *Embo j*, 22: 2146-55.

Hwang, S., H. T. Gustafsson, C. O'Sullivan, G. Bisceglia, X. Huang, C. Klose, A. Schevchenko, R. C. Dickson, P. Cavaliere, N. Dephoure, and E. M. Torres. 2017. 'Serine-Dependent Sphingolipid Synthesis Is a Metabolic Liability of Aneuploid Cells', *Cell Rep*, 21: 3807-18.

Ichijima, Y., K. Yoshioka, Y. Yoshioka, K. Shinohe, H. Fujimori, J. Unno, M. Takagi, H. Goto, M. Inagaki, S. Mizutani, and H. Teraoka. 2010. 'DNA lesions induced by replication stress trigger mitotic aberration and tetraploidy development', *PLoS One*, 5: e8821.

Iliakis, George, Ya Wang, Jun Guan, and Huichen Wang. 2003. 'DNA damage checkpoint control in cells exposed to ionizing radiation', *Oncogene*, 22: 5834-47.

Itoh, Go, Masanori Ikeda, Kenji Iemura, Mohammed Abdullahel Amin, Sei Kuriyama, Masamitsu Tanaka, Natsuki Mizuno, Hiroko Osakada, Tokuko Haraguchi, and Kozo Tanaka. 2018. 'Lateral attachment of kinetochores to microtubules is enriched in prometaphase rosette and facilitates chromosome alignment and bi-orientation establishment', *Sci Rep*, 8: 3888.

Jang, Sang-Min, Jenny F. Nathans, Haiqing Fu, Christophe E. Redon, Lisa M. Jenkins, Bhushan L. Thakur, Lőrinc S. Pongor, Adrian M. Baris, Jacob M. Gross, Maura J. O'Neill, Fred E. Indig, Steven D. Cappell, and Mirit I. Aladjem. 2020. 'The RepID–CRL4 ubiquitin ligase complex regulates metaphase to anaphase transition via BUB3 degradation', *Nat Commun*, 11: 24.

Janssen, A., and R. H. Medema. 2013. 'Genetic instability: tipping the balance', *Oncogene*, 32: 4459-70.

Jazayeri, Ali, Jacob Falck, Claudia Lukas, Jiri Bartek, Graeme C. M. Smith, Jiri Lukas, and Stephen P. Jackson. 2006. 'ATM- and cell cycle-dependent regulation of ATR in response to DNA double-strand breaks', *Nature Cell Biology*, 8: 37-45.

Jette, N. R., M. Kumar, S. Radhamani, G. Arthur, S. Goutam, S. Yip, M. Kolinsky, G. J. Williams, P. Bose, and S. P. Lees-Miller. 2020. 'ATM-Deficient Cancers Provide New Opportunities for Precision Oncology', *Cancers (Basel)*, 12.

Jia, D., L. Li, S. Andrew, D. Allan, X. Li, J. Lee, G. Ji, Z. Yao, S. Gadde, D. Figeys, and L. Wang. 2017. 'An autocrine inflammatory forward-feedback loop after chemotherapy withdrawal facilitates the repopulation of drug-resistant breast cancer cells', *Cell Death Dis*, 8: e2932.

Jing, Anqi, Frederick S. Vizeacoumar, Sreejit Parameswaran, Bjorn Haave, Chelsea E. Cunningham, Yuliang Wu, Roland Arnold, Keith Bonham, Andrew Freywald, Jie Han, and Franco J. Vizeacoumar. 2018. 'Expression-based analyses indicate a central role for hypoxia in driving tumor plasticity through microenvironment remodeling and chromosomal instability', *npj Systems Biology and Applications*, 4: 38.

Jiricny, J. 2006. 'The multifaceted mismatch-repair system', *Nat Rev Mol Cell Biol*, 7: 335-46.

Job, A., L. M. Schmitt, L. von Wenserski, B. Lankat-Buttgereit, T. M. Gress, M. Buchholz, and E. Gallmeier. 2018. 'Inactivation of PRIM1 Function Sensitizes Cancer Cells to ATR and CHK1 Inhibitors', *Neoplasia*, 20: 1135-43.

Kabeche, Lilian, Hai Dang Nguyen, Rémi Buisson, and Lee Zou. 2018. 'A mitosis-specific and R loop–driven ATR pathway promotes faithful chromosome segregation', *Science*, 359: 108.

Kakarougkas, A., A. Ismail, A. L. Chambers, E. Riballo, A. D. Herbert, J. Künzel, M. Löbrich, P. A. Jeggo, and J. A. Downs. 2014. 'Requirement for PBAF in transcriptional repression and repair at DNA breaks in actively transcribed regions of chromatin', *Mol Cell*, 55: 723-32.

Kapoor, T. M., M. A. Lampson, P. Hergert, L. Cameron, D. Cimini, E. D. Salmon, B. F. McEwen, and A. Khodjakov. 2006. 'Chromosomes can congress to the metaphase plate before biorientation', *Science*, 311: 388-91.

Kaur, Ekjot, Jacinth Rajendra, Shailesh Jadhav, Epari Shridhar, Jayant Sastri Goda, Aliasgar Moiyadi, and Shilpee Dutt. 2015. 'Radiation-induced homotypic cell fusions of innately resistant glioblastoma cells mediate their sustained survival and recurrence', *Carcinogenesis*, 36: 685-95.

Kehinde, F. I., C. E. Anderson, J. E. McGowan, R. N. Jethva, M. A. Wahab, A. R. Glick, M. R. Sterner, Jr., J. M. Pascasio, H. H. Punnett, and J. Liu. 2014. 'Co-occurrence of non-mosaic trisomy 22 and inherited balanced t(4;6)(q33;q23.3) in a liveborn female: case report and review of the literature', *Am J Med Genet A*, 164a: 3187-93.

Kim, I. W., A. C. Khadilkar, E. Y. Ko, and E. S. Sabanegh, Jr. 2013. '47,XYY Syndrome and Male Infertility', *Rev Urol*, 15: 188-96.

Knudson, A. G. 2001. 'Two genetic hits (more or less) to cancer', *Nat Rev Cancer*, 1: 157-62.

Koh, K. H., H. J. Kang, L. S. Li, N. G. Kim, K. T. You, E. Yang, H. Kim, H. J. Kim, C. O. Yun, K. S. Kim, and H. Kim. 2005. 'Impaired nonhomologous end-joining in mismatch repair-deficient colon carcinomas', *Lab Invest*, 85: 1130-8.

Kompus, K., R. Westerhausen, L. G. Nilsson, K. Hugdahl, S. Jongstra, A. Berglund, S. Arver, and I. Savic. 2011. 'Deficits in inhibitory executive functions in Klinefelter (47, XXY) syndrome', *Psychiatry Res*, 189: 135-40.

Konotop, G., E. Bausch, T. Nagai, A. Turchinovich, N. Becker, A. Benner, M. Boutros, K. Mizuno, A. Krämer, and M. S. Raab. 2016. 'Pharmacological Inhibition of Centrosome Clustering by Slingshot-Mediated Cofilin Activation and Actin Cortex Destabilization', *Cancer Res*, 76: 6690-700.

Kothandapani, A., K. Gopalakrishnan, B. Kahali, D. Reisman, and S. M. Patrick. 2012. 'Downregulation of SWI/SNF chromatin remodeling factor subunits modulates cisplatin cytotoxicity', *Exp Cell Res*, 318: 1973-86.

Krenn, V., and A. Musacchio. 2015. 'The Aurora B Kinase in Chromosome Bi-Orientation and Spindle Checkpoint Signaling', *Front Oncol*, 5: 225.

Kumar, A., and R. Purohit. 2012. 'Computational screening and molecular dynamics simulation of disease associated nsSNPs in CENP-E', *Mutat Res*, 738-739: 28-37.

Kwon, S. J., J. H. Park, E. J. Park, S. A. Lee, H. S. Lee, S. W. Kang, and J. Kwon. 2015. 'ATM-mediated phosphorylation of the chromatin remodeling enzyme BRG1 modulates DNA double-strand break repair', *Oncogene*, 34: 303-13.

Lambert, Sarah, and Antony M. Carr. 2013. 'Impediments to replication fork movement: stabilisation, reactivation and genome instability', *Chromosoma*, 122: 33-45.

Lans, H., J. H. J. Hoeijmakers, W. Vermeulen, and J. A. Marteijn. 2019. 'The DNA damage response to transcription stress', *Nat Rev Mol Cell Biol*, 20: 766-84.

Laubert, Tilman, Sandra Freitag-Wolf, Michael Linnebacher, Alexandra König, Brigitte Vollmar, Jens K. Habermann, and consortium on behalf of the North German Tumorbank of Colorectal Cancer. 2015. 'Stage-specific frequency and prognostic significance of aneuploidy in patients with sporadic colorectal cancer—a meta-analysis and current overview', *International Journal of Colorectal Disease*, 30: 1015-28.

Lee, A. J., D. Endesfelder, A. J. Rowan, A. Walther, N. J. Birkbak, P. A. Futreal, J. Downward, Z. Szallasi, I. P. Tomlinson, M. Howell, M. Kschischo, and C. Swanton. 2011. 'Chromosomal instability confers intrinsic multidrug resistance', *Cancer Res*, 71: 1858-70.

Lee, J., N. Y. Shao, D. T. Paik, H. Wu, H. Guo, V. Termglinchan, J. M. Churko, Y. Kim, T. Kitani, M. T. Zhao, Y. Zhang, K. D. Wilson, I. Karakikes, M. P. Snyder, and J. C. Wu. 2018. 'SETD7 Drives Cardiac Lineage Commitment through Stage-Specific Transcriptional Activation', *Cell Stem Cell*, 22: 428-44.e5.

Lee, K., H. J. Kim, M. H. Jang, S. Lee, S. Ahn, and S. Y. Park. 2019. 'Centromere 17 copy number gain reflects chromosomal instability in breast cancer', *Sci Rep*, 9: 17968.

Lee, W. H., L. C. Chen, C. J. Lee, C. C. Huang, Y. S. Ho, P. S. Yang, C. T. Ho, H. L. Chang, I. H. Lin, H. W. Chang, Y. R. Liu, C. H. Wu, and S. H. Tu. 2019. 'DNA primase polypeptide 1 (PRIM1) involves in estrogen-induced breast cancer formation through activation of the G2/M cell cycle checkpoint', *Int J Cancer*, 144: 615-30.

Lens, S. M. A., and R. H. Medema. 2019. 'Cytokinesis defects and cancer', *Nat Rev Cancer*, 19: 32-45.

Levine, M. S., B. Bakker, B. Boeckx, J. Moyett, J. Lu, B. Vitre, D. C. Spierings, P. M. Lansdorp, D. W. Cleveland, D. Lambrechts, F. Foijer, and A. J. Holland. 2017. 'Centrosome Amplification Is Sufficient to Promote Spontaneous Tumorigenesis in Mammals', *Dev Cell*, 40: 313-22.e5.

Leylek, Tarik R., Lucile M. Jeusset, Zelda Lichtensztejn, and Kirk J. McManus. 2020. 'Reduced Expression of Genes Regulating Cohesion Induces Chromosome Instability that May Promote Cancer and Impact Patient Outcomes', *Sci Rep*, 10: 592.

Li, G. M. 2008. 'Mechanisms and functions of DNA mismatch repair', *Cell Res*, 18: 85-98.

Li, M., X. Fang, D. J. Baker, L. Guo, X. Gao, Z. Wei, S. Han, J. M. van Deursen, and P. Zhang. 2010. 'The ATM-p53 pathway suppresses aneuploidy-induced tumorigenesis', *Proc Natl Acad Sci U S A*, 107: 14188-93.

Li, Y., X. Sun, and S. K. Dey. 2015. 'Entosis allows timely elimination of the luminal epithelial barrier for embryo implantation', *Cell Rep*, 11: 358-65.

Li, Z., W. Zhang, Y. Chen, W. Guo, J. Zhang, H. Tang, Z. Xu, H. Zhang, Y. Tao, F. Wang, Y. Jiang, F. L. Sun, and Z. Mao. 2016. 'Impaired DNA double-strand break repair contributes to the age-associated rise of genomic instability in humans', *Cell Death Differ*, 23: 1765-77.

List, A., B. L. Ebert, and P. Fenaux. 2018. 'A decade of progress in myelodysplastic syndrome with chromosome 5q deletion', *Leukemia*, 32: 1493-99.

Liu, D., G. Keijzers, and L. J. Rasmussen. 2017. 'DNA mismatch repair and its many roles in eukaryotic cells', *Mutat Res*, 773: 174-87.

Liu, D. N., Y. F. Zhou, A. F. Peng, X. H. Long, X. Y. Chen, Z. L. Liu, and H. Xia. 2017. 'HELQ reverses the malignant phenotype of osteosarcoma cells via CHK1-RAD51 signaling pathway', *Oncol Rep*, 37: 1107-13.

Liu, Yu, Chong Chen, Zhengmin Xu, Claudio Scuoppo, Cory D. Rillahan, Jianjiong Gao, Barbara Spitzer, Benedikt Bosbach, Edward R. Kastenhuber, Timour Baslan, Sarah Ackermann, Lihua Cheng, Qingguo Wang, Ting Niu, Nikolaus Schultz, Ross L. Levine, Alea A. Mills, and Scott W. Lowe. 2016. 'Deletions linked to TP53 loss drive cancer through p53-independent mechanisms', *Nature*, 531: 471-75.

Löbrich, Markus, and Penny A. Jeggo. 2007. 'The impact of a negligent G2/M checkpoint on genomic instability and cancer induction', *Nature Reviews Cancer*, 7: 861-69.

Lok, Tsun Ming, Yang Wang, Wendy Kaichun Xu, Siwei Xie, Hoi Tang Ma, and Randy Y. C. Poon. 2020. 'Mitotic slippage is determined by p31comet and the weakening of the spindle-assembly checkpoint', *Oncogene*, 39: 2819-34.

London, Nitobe, and Sue Biggins. 2014. 'Signalling dynamics in the spindle checkpoint response', *Nature Reviews Molecular Cell Biology*, 15: 736-48.

Lopez-Sánchez, L. M., C. Jimenez, A. Valverde, V. Hernandez, J. Peñarando, A. Martinez, C. Lopez-Pedrera, J. R. Muñoz-Castañeda, J. R. De la Haba-Rodríguez, E. Aranda, and A. Rodriguez-Ariza. 2014. 'CoCl2, a mimic of hypoxia, induces formation of polyploid giant cells with stem characteristics in colon cancer', *PLoS One*, 9: e99143.

Lord, Christopher J., and Alan Ashworth. 2012. 'The DNA damage response and cancer therapy', *Nature*, 481: 287-94.

Lu, Xin, and Yibin Kang. 2009. 'Cell Fusion as a Hidden Force in Tumor Progression', *Cancer Res*, 69: 8536.

Luebben, S. W., T. Kawabata, M. K. Akre, W. L. Lee, C. S. Johnson, M. G. O'Sullivan, and N. Shima. 2013. 'Helq acts in parallel to Fancc to suppress replication-associated

genome instability', *Nucleic Acids Res*, 41: 10283-97.

Lukas, J., C. Lukas, and J. Bartek. 2004. 'Mammalian cell cycle checkpoints: signalling pathways and their organization in space and time', *DNA Repair (Amst)*, 3: 997-1007.

Ly, P., and D. W. Cleveland. 2017. 'Rebuilding Chromosomes After Catastrophe: Emerging Mechanisms of Chromothripsis', *Trends Cell Biol*, 27: 917-30.

Maia, Ana Rita R., Simon Linder, Ji-Ying Song, Chantal Vaarting, Ute Boon, Colin E. J. Pritchard, Arno Velds, Ivo J. Huijbers, Olaf van Tellingen, Jos Jonkers, and René H. Medema. 2018. 'Mps1 inhibitors synergise with low doses of taxanes in promoting tumour cell death by enhancement of errors in cell division', *British Journal of Cancer*, 118: 1586-95.

Maliga, Z., T. M. Kapoor, and T. J. Mitchison. 2002. 'Evidence that monastrol is an allosteric inhibitor of the mitotic kinesin Eg5', *Chem Biol*, 9: 989-96.

Marangos, Petros, Michelle Stevense, Konstantina Niaka, Michaela Lagoudaki, Ibtissem Nabti, Rolf Jessberger, and John Carroll. 2015. 'DNA damage-induced metaphase I arrest is mediated by the spindle assembly checkpoint and maternal age', *Nat Commun*, 6: 8706.

Maréchal, A., and L. Zou. 2013. 'DNA damage sensing by the ATM and ATR kinases', *Cold Spring Harb Perspect Biol*, 5.

Margolis, R. L., O. D. Lohez, and P. R. Andreassen. 2003. 'G1 tetraploidy checkpoint and the suppression of tumorigenesis', *J Cell Biochem*, 88: 673-83.

Mariappan, A., K. Soni, K. Schorpp, F. Zhao, A. Minakar, X. Zheng, S. Mandad, I. Macheleidt, A. Ramani, T. Kubelka, M. Dawidowski, K. Golfmann, A. Wason, C. Yang, J. Simons, H. G. Schmalz, A. A. Hyman, R. Aneja, R. Ullrich, H. Urlaub, M. Odenthal, R. Buttner, H. Li, M. Sattler, K. Hadian, and J. Gopalakrishnan. 2019. 'Inhibition of CPAP-tubulin interaction prevents proliferation of centrosome-amplified cancer cells', *Embo j*, 38.

Markov, D., S. Ivanov, and P. Popivanova. 2007. '[Warkany syndrome associated with agenesis of the corpus callosum]', *Akusherstvo i ginekologiia*, 46: 48-50.

Marteijn, J. A., H. Lans, W. Vermeulen, and J. H. Hoeijmakers. 2014. 'Understanding nucleotide excision repair and its roles in cancer and ageing', *Nat Rev Mol Cell Biol*, 15: 465-81.

Martens, J. H., M. Verlaan, E. Kalkhoven, and A. Zantema. 2003. 'Cascade of distinct histone modifications during collagenase gene activation', *Mol Cell Biol*, 23: 1808-16.

Martinez, P., D. Mallo, T. G. Paulson, X. Li, C. A. Sanchez, B. J. Reid, T. A. Graham, M. K. Kuhner, and C. C. Maley. 2018. 'Evolution of Barrett's esophagus through space and time at single-crypt and whole-biopsy levels', *Nat Commun*, 9: 794.

Mashtalir, N., A. R. D'Avino, B. C. Michel, J. Luo, J. Pan, J. E. Otto, H. J. Zullow, Z. M. McKenzie, R. L. Kubiak, R. St Pierre, A. M. Valencia, S. J. Poynter, S. H. Cassel, J. A.

Ranish, and C. Kadoch. 2018. 'Modular Organization and Assembly of SWI/SNF Family Chromatin Remodeling Complexes', *Cell*, 175: 1272-88.e20.

Matsuno, Yusuke, Yuko Atsumi, Atsuhiro Shimizu, Kotoe Katayama, Haruka Fujimori, Mai Hyodo, Yusuke Minakawa, Yoshimichi Nakatsu, Syuzo Kaneko, Ryuji Hamamoto, Teppei Shimamura, Satoru Miyano, Teruhisa Tsuzuki, Fumio Hanaoka, and Ken-ichi Yoshioka. 2019. 'Replication stress triggers microsatellite destabilization and hypermutation leading to clonal expansion in vitro', *Nat Commun*, 10: 3925.

McArdle, T. J., B. M. Ogle, and F. K. Noubissi. 2016. 'An In Vitro Inverted Vertical Invasion Assay to Avoid Manipulation of Rare or Sensitive Cell Types', *J Cancer*, 7: 2333-40.

McGranahan, N., R. A. Burrell, D. Endesfelder, M. R. Novelli, and C. Swanton. 2012. 'Cancer chromosomal instability: therapeutic and diagnostic challenges', *EMBO Rep*, 13: 528-38.

McIntosh, J. R. 2016. 'Mitosis', *Cold Spring Harb Perspect Biol*, 8.

McKinney, J. A., G. Wang, A. Mukherjee, L. Christensen, S. H. S. Subramanian, J. Zhao, and K. M. Vasquez. 2020. 'Distinct DNA repair pathways cause genomic instability at alternative DNA structures', *Nat Commun*, 11: 236.

Meisenberg, C., S. I. Pinder, S. R. Hopkins, S. K. Wooller, G. Benstead-Hume, F. M. G. Pearl, P. A. Jeggo, and J. A. Downs. 2019. 'Repression of Transcription at DNA Breaks Requires Cohesin throughout Interphase and Prevents Genome Instability', *Mol Cell*, 73: 212-23.e7.

Meunier, S., and I. Vernos. 2016. 'Acentrosomal Microtubule Assembly in Mitosis: The Where, When, and How', *Trends Cell Biol*, 26: 80-87.

Mirzayans, R., and D. Murray. 2020. 'Intratumor Heterogeneity and Therapy Resistance: Contributions of Dormancy, Apoptosis Reversal (Anastasis) and Cell Fusion to Disease Recurrence', *Int J Mol Sci*, 21.

Mittal, K., S. Donthamsetty, R. Kaur, C. Yang, M. V. Gupta, M. D. Reid, D. H. Choi, P. C. G. Rida, and R. Aneja. 2017. 'Multinucleated polyploidy drives resistance to Docetaxel chemotherapy in prostate cancer', *Br J Cancer*, 116: 1186-94.

Mittal, Priya, and Charles W. M. Roberts. 2020. 'The SWI/SNF complex in cancer — biology, biomarkers and therapy', *Nature Reviews Clinical Oncology*.

Mladenov, Emil, Xiaoxiang Fan, Rositsa Dueva, Aashish Soni, and George Iliakis. 2019. 'Radiation-dose-dependent functional synergisms between ATM, ATR and DNA-PKcs in checkpoint control and resection in G2-phase', *Sci Rep*, 9: 8255.

Mondal, G., A. Ohashi, L. Yang, M. Rowley, and F. J. Couch. 2012. 'Tex14, a Plk1-regulated protein, is required for kinetochore-microtubule attachment and regulation of the spindle assembly checkpoint', *Mol Cell*, 45: 680-95.

Mondal, G., M. Rowley, L. Guidugli, J. Wu, V. S. Pankratz, and F. J. Couch. 2012.

'BRCA2 localization to the midbody by filamin A regulates cep55 signaling and completion of cytokinesis', *Dev Cell*, 23: 137-52.

Mortensen, K., J. Lichtenberg, P. D. Thomsen, and L. I. Larsson. 2004. 'Spontaneous fusion between cancer cells and endothelial cells', *Cellular and Molecular Life Sciences CMLS*, 61: 2125-31.

Mukherjee, Chirantani, Vivek Tripathi, Eleni Maria Manolika, Anne Margriet Heijink, Giulia Ricci, Sarra Merzouk, H. Rudolf de Boer, Jeroen Demmers, Marcel A. T. M. van Vugt, and Arnab Ray Chaudhuri. 2019. 'RIF1 promotes replication fork protection and efficient restart to maintain genome stability', *Nat Commun*, 10: 3287.

Muller, Patricia A. J., and Karen H. Vousden. 2013. 'p53 mutations in cancer', *Nature Cell Biology*, 15: 2-8.

Nalepa, Grzegorz, and D. Wade Clapp. 2018. 'Fanconi anaemia and cancer: an intricate relationship', *Nature Reviews Cancer*, 18: 168-85.

Naumenko, A. N., V. A. Timoshevskiy, N. A. Kinney, A. A. Kokhanenko, B. S. deBruyn, D. D. Lovin, V. N. Stegniy, D. W. Severson, I. V. Sharakhov, and M. V. Sharakhova. 2015. 'Mitotic-chromosome-based physical mapping of the Culex quinquefasciatus genome', *PLoS One*, 10: e0115737.

Negrini, S., V. G. Gorgoulis, and T. D. Halazonetis. 2010. 'Genomic instability--an evolving hallmark of cancer', *Nat Rev Mol Cell Biol*, 11: 220-8.

Nicholson, J. M., J. C. Macedo, A. J. Mattingly, D. Wangsa, J. Camps, V. Lima, A. M. Gomes, S. Dória, T. Ried, E. Logarinho, and D. Cimini. 2015. 'Chromosome mis-segregation and cytokinesis failure in trisomic human cells', *Elife*, 4.

Nigg, Erich A., and Andrew J. Holland. 2018. 'Once and only once: mechanisms of centriole duplication and their deregulation in disease', *Nature Reviews Molecular Cell Biology*, 19: 297-312.

Niu, N., J. Zhang, N. Zhang, I. Mercado-Uribe, F. Tao, Z. Han, S. Pathak, A. S. Multani, J. Kuang, J. Yao, R. C. Bast, A. K. Sood, M. C. Hung, and J. Liu. 2016. 'Linking genomic reorganization to tumor initiation via the giant cell cycle', *Oncogenesis*, 5: e281-e81.

Niu, Yuzhen, Danfeng Shi, Lanlan Li, Jingyun Guo, Huanxiang Liu, and Xiaojun Yao. 2017. 'Revealing inhibition difference between PFI-2 enantiomers against SETD7 by molecular dynamics simulations, binding free energy calculations and unbinding pathway analysis', *Sci Rep*, 7: 46547.

Noubissi, F. K., T. Harkness, C. M. Alexander, and B. M. Ogle. 2015a. 'Apoptosis-induced cancer cell fusion: a mechanism of breast cancer metastasis', *Faseb j*, 29: 4036-45.

Noubissi, Felicite K., Ty Harkness, Caroline M. Alexander, and Brenda M. Ogle. 2015b. 'Apoptosis-induced cancer cell fusion: a mechanism of breast cancer metastasis', *The FASEB Journal*, 29: 4036-45.

Ogiwara, H., A. Ui, A. Otsuka, H. Satoh, I. Yokomi, S. Nakajima, A. Yasui, J. Yokota, and T. Kohno. 2011. 'Histone acetylation by CBP and p300 at double-strand break sites facilitates SWI/SNF chromatin remodeling and the recruitment of non-homologous end joining factors', *Oncogene*, 30: 2135-46.

Ogle, Brenda M., Marilia Cascalho, and Jeffrey L. Platt. 2005. 'Biological implications of cell fusion', *Nature Reviews Molecular Cell Biology*, 6: 567-75.

Ohashi, Akihiro, Momoko Ohori, Kenichi Iwai, Yusuke Nakayama, Tadahiro Nambu, Daisuke Morishita, Tomohiro Kawamoto, Maki Miyamoto, Takaharu Hirayama, Masanori Okaniwa, Hiroshi Banno, Tomoyasu Ishikawa, Hitoshi Kandori, and Kentaro Iwata. 2015. 'Aneuploidy generates proteotoxic stress and DNA damage concurrently with p53-mediated post-mitotic apoptosis in SAC-impaired cells', *Nat Commun*, 6: 7668.

Ohta, S., L. Wood, J. C. Bukowski-Wills, J. Rappsilber, and W. C. Earnshaw. 2011. 'Building mitotic chromosomes', *Curr Opin Cell Biol*, 23: 114-21.

Oike, T., H. Ogiwara, Y. Tominaga, K. Ito, O. Ando, K. Tsuta, T. Mizukami, Y. Shimada, H. Isomura, M. Komachi, K. Furuta, S. Watanabe, T. Nakano, J. Yokota, and T. Kohno. 2013. 'A synthetic lethality-based strategy to treat cancers harboring a genetic deficiency in the chromatin remodeling factor BRG1', *Cancer Res*, 73: 5508-18.

Oren-Suissa, M., and B. Podbilewicz. 2010. 'Evolution of programmed cell fusion: common mechanisms and distinct functions', *Dev Dyn*, 239: 1515-28.

Oren-Suissa, Meital, and Benjamin Podbilewicz. 2007. 'Cell fusion during development', *Trends Cell Biol*, 17: 537-46.

Orr, B., K. M. Godek, and D. Compton. 2015. 'Aneuploidy', *Curr Biol*, 25: R538-42.

Orthwein, Alexandre, Amélie Fradet-Turcotte, Sylvie M. Noordermeer, Marella D. Canny, Catherine M. Brun, Jonathan Strecker, Cristina Escribano-Diaz, and Daniel Durocher. 2014. 'Mitosis Inhibits DNA Double-Strand Break Repair to Guard Against Telomere Fusions', *Science*, 344: 189.

Overholtzer, M., A. A. Mailleux, G. Mouneimne, G. Normand, S. J. Schnitt, R. W. King, E. S. Cibas, and J. S. Brugge. 2007. 'A nonapoptotic cell death process, entosis, that occurs by cell-in-cell invasion', *Cell*, 131: 966-79.

Paim, Lia Mara Gomes, and Greg FitzHarris. 2019. 'Tetraploidy causes chromosomal instability in acentriolar mouse embryos', *Nat Commun*, 10: 4834.

Paolella, B. R., W. J. Gibson, L. M. Urbanski, J. A. Alberta, T. I. Zack, P. Bandopadhayay, C. A. Nichols, P. K. Agarwalla, M. S. Brown, R. Lamothe, Y. Yu, P. S. Choi, E. A. Obeng, D. Heckl, G. Wei, B. Wang, A. Tsherniak, F. Vazquez, B. A. Weir, D. E. Root, G. S. Cowley, S. J. Buhrlage, C. D. Stiles, B. L. Ebert, W. C. Hahn, R. Reed, and R. Beroukhim. 2017. 'Copy-number and gene dependency analysis reveals partial copy loss of wild-type SF3B1 as a novel cancer vulnerability', *Elife*, 6.

Pasanen, A., M. Loukovaara, and R. Butzow. 2020. 'Clinicopathological significance of deficient DNA mismatch repair and MLH1 promoter methylation in endometrioid

endometrial carcinoma', *Mod Pathol*.

Passerini, Verena, Efrat Ozeri-Galai, Mirjam S. de Pagter, Neysan Donnelly, Sarah Schmalbrock, Wigard P. Kloosterman, Batsheva Kerem, and Zuzana Storchová. 2016. 'The presence of extra chromosomes leads to genomic instability', *Nat Commun*, 7: 10754.

Patel, Nirmesh, Daniel Weekes, Konstantinos Drosopoulos, Patrycja Gazinska, Elodie Noel, Mamun Rashid, Hasan Mirza, Jelmar Quist, Fara Brasó-Maristany, Sumi Mathew, Riccardo Ferro, Ana Mendes Pereira, Cynthia Prince, Farzana Noor, Erika Francesch-Domenech, Rebecca Marlow, Emanuele de Rinaldis, Anita Grigoriadis, Spiros Linardopoulos, Pierfrancesco Marra, and Andrew N. J. Tutt. 2018. 'Integrated genomics and functional validation identifies malignant cell specific dependencies in triple negative breast cancer', *Nat Commun*, 9: 1044.

Pavelka, Norman, Giulia Rancati, Jin Zhu, William D. Bradford, Anita Saraf, Laurence Florens, Brian W. Sanderson, Gaye L. Hattem, and Rong Li. 2010. 'Aneuploidy confers quantitative proteome changes and phenotypic variation in budding yeast', *Nature*, 468: 321-25.

Pellman, David. 2007. 'Aneuploidy and cancer', *Nature*, 446: 38-39.

Peng, G., and S. Y. Lin. 2011. 'Exploiting the homologous recombination DNA repair network for targeted cancer therapy', *World J Clin Oncol*, 2: 73-9.

Permata, T. B. M., Y. Hagiwara, H. Sato, T. Yasuhara, T. Oike, S. Gondhowiardjo, K. D. Held, T. Nakano, and A. Shibata. 2019. 'Base excision repair regulates PD-L1 expression in cancer cells', *Oncogene*, 38: 4452-66.

Petry, S. 2016. 'Mechanisms of Mitotic Spindle Assembly', *Annu Rev Biochem*, 85: 659-83.

Petsalaki, E., and Zachos G. 2014. 'Chk2 prevents mitotic exit when the majority of kinetochores are unattached', *J Cell Biol*, 205: 339-56.

Petsalaki, E and Zachos, G. 2020. 'DNA damage response proteins regulating mitotic cell division: double agents preserving genome stability', *Febs j*.

Pikor, Larissa, Kelsie Thu, Emily Vucic, and Wan Lam. 2013. 'The detection and implication of genome instability in cancer', *Cancer and Metastasis Reviews*, 32: 341-52.

Pilié, Patrick G., Chad Tang, Gordon B. Mills, and Timothy A. Yap. 2019. 'State-of-the-art strategies for targeting the DNA damage response in cancer', *Nature Reviews Clinical Oncology*, 16: 81-104.

Pittis, Alexandros A., and Toni Gabaldón. 2016. 'Late acquisition of mitochondria by a host with chimaeric prokaryotic ancestry', *Nature*, 531: 101-04.

Pradhan, S., H. G. Chin, P. O. Estève, and S. E. Jacobsen. 2009. 'SET7/9 mediated methylation of non-histone proteins in mammalian cells', *Epigenetics*, 4: 383-7.

Puig, P. E., M. N. Guilly, A. Bouchot, N. Droin, D. Cathelin, F. Bouyer, L. Favier, F. Ghiringhelli, G. Kroemer, E. Solary, F. Martin, and B. Chauffert. 2008. 'Tumor cells can escape DNA-damaging cisplatin through DNA endoreduplication and reversible polyploidy', *Cell Biol Int*, 32: 1031-43.

Pusztai, L., T. R. Mendoza, J. M. Reuben, M. M. Martinez, J. S. Willey, J. Lara, A. Syed, H. A. Fritsche, E. Bruera, D. Booser, V. Valero, B. Arun, N. Ibrahim, E. Rivera, M. Royce, C. S. Cleeland, and G. N. Hortobagyi. 2004. 'Changes in plasma levels of inflammatory cytokines in response to paclitaxel chemotherapy', *Cytokine*, 25: 94-102.

Qi, W., R. Wang, H. Chen, X. Wang, T. Xiao, I. Boldogh, X. Ba, L. Han, and X. Zeng. 2015. 'BRG1 promotes the repair of DNA double-strand breaks by facilitating the replacement of RPA with RAD51', *J Cell Sci*, 128: 317-30.

Qu, Yang, Li Zhang, Zhe Rong, Tao He, and Sai Zhang. 2013. 'Number of glioma polyploid giant cancer cells (PGCCs) associated with vasculogenic mimicry formation and tumor grade in human glioma', *Journal of Experimental & Clinical Cancer Research*, 32: 75.

Raff, J. W., and R. Basto. 2017. 'Centrosome Amplification and Cancer: A Question of Sufficiency', *Dev Cell*, 40: 217-18.

Rafique, M., S. AlObaid, and D. Al-Jaroudi. 2019. '47, XXX syndrome with infertility, premature ovarian insufficiency, and streak ovaries', *Clin Case Rep*, 7: 1238-41.

Rajaraman, R., D. L. Guernsey, M. M. Rajaraman, and S. R. Rajaraman. 2006. 'Stem cells, senescence, neosis and self-renewal in cancer', *Cancer Cell Int*, 6: 25.

Ratajczak, Mariusz Z., Kamila Bujko, Aaron Mack, Magda Kucia, and Janina Ratajczak. 2018. 'Cancer from the perspective of stem cells and misappropriated tissue regeneration mechanisms', *Leukemia*, 32: 2519-26.

Reisman, D., S. Glaros, and E. A. Thompson. 2009. 'The SWI/SNF complex and cancer', *Oncogene*, 28: 1653-68.

Ribeiro-Silva, C., W. Vermeulen, and H. Lans. 2019. 'SWI/SNF: Complex complexes in genome stability and cancer', *DNA Repair (Amst)*, 77: 87-95.

Ribeiro-Silva, Cristina, Özge Z. Aydin, Raquel Mesquita-Ribeiro, Jana Slyskova, Angela Helfricht, Jurgen A. Marteijn, Jan H. J. Hoeijmakers, Hannes Lans, and Wim Vermeulen. 2018. 'DNA damage sensitivity of SWI/SNF-deficient cells depends on TFIIH subunit p62/GTF2H1', *Nat Commun*, 9: 4067.

Richeson, Katherine V., Tatyana Bodrug, Katharine L. Sackton, Masaya Yamaguchi, Joao A. Paulo, Steven P. Gygi, Brenda A. Schulman, Nicholas G. Brown, and Randall

W. King. 2020. 'Paradoxical mitotic exit induced by a small molecule inhibitor of APC/CCdc20', *Nature Chemical Biology*.

Roake, Caitlin M., and Steven E. Artandi. 2020. 'Regulation of human telomerase in homeostasis and disease', *Nature Reviews Molecular Cell Biology*.

Roberts, Charles W. M., and Stuart H. Orkin. 2004. 'The SWI/SNF complex — chromatin and cancer', *Nature Reviews Cancer*, 4: 133-42.

Rodrigues-Ferreira, S., and C. Nahmias. 2020. 'From tumorigenesis to cell death: the aneuploidy paradox', *Mol Cell Oncol*, 7: 1709390.

Roylance, R., D. Endesfelder, P. Gorman, R. A. Burrell, J. Sander, I. Tomlinson, A. M. Hanby, V. Speirs, A. L. Richardson, N. J. Birkbak, A. C. Eklund, J. Downward, M. Kschischo, Z. Szallasi, and C. Swanton. 2011. 'Relationship of extreme chromosomal instability with long-term survival in a retrospective analysis of primary breast cancer', *Cancer Epidemiol Biomarkers Prev*, 20: 2183-94.

Rutledge, S. D., and D. Cimini. 2016. 'Consequences of aneuploidy in sickness and in health', *Curr Opin Cell Biol*, 40: 41-46.

Sajesh, B. V., Z. Lichtensztejn, and K. J. McManus. 2013a. 'Sister chromatid cohesion defects are associated with chromosome instability in Hodgkin lymphoma cells', *BMC Cancer*, 13: 391.

Sajesh, Babu V., Zelda Lichtensztejn, and Kirk J. McManus. 2013b. 'Sister chromatid cohesion defects are associated with chromosome instability in Hodgkin lymphoma cells', *BMC Cancer*, 13: 391.

Sansregret, L., and C. Swanton. 2017. 'The Role of Aneuploidy in Cancer Evolution', *Cold Spring Harb Perspect Med*, 7.

Sansregret, Laurent, Charles Vadnais, Julie Livingstone, Nicholas Kwiatkowski, Arif Awan, Chantal Cadieux, Lam Leduy, Michael T. Hallett, and Alain Nepveu. 2011. 'Cut homeobox 1 causes chromosomal instability by promoting bipolar division after cytokinesis failure', *Proceedings of the National Academy of Sciences*, 108: 1949.

Sansregret, Laurent, Bart Vanhaesebroeck, and Charles Swanton. 2018. 'Determinants and clinical implications of chromosomal instability in cancer', *Nature Reviews Clinical Oncology*, 15: 139-50.

Santaguida, S., and A. Amon. 2015. 'Short- and long-term effects of chromosome mis-segregation and aneuploidy', *Nat Rev Mol Cell Biol*, 16: 473-85.

Santaguida, S., C. Vernieri, F. Villa, A. Ciliberto, and A. Musacchio. 2011. 'Evidence that Aurora B is implicated in spindle checkpoint signalling independently of error correction', *Embo j*, 30: 1508-19.

Santen, G. W., M. Kriek, and H. van Attikum. 2012. 'SWI/SNF complex in disorder: SWItching from malignancies to intellectual disability', *Epigenetics*, 7: 1219-24.

Schukken, K. M., and F. Foijer. 2018. 'CIN and Aneuploidy: Different Concepts, Different Consequences', *Bioessays*, 40.

Searles, S. C., E. K. Santosa, and J. D. Bui. 2018. 'Cell-cell fusion as a mechanism of DNA exchange in cancer', *Oncotarget*, 9: 6156-73.

Sethy, R., R. Rakesh, K. Patne, V. Arya, T. Sharma, D. T. Haokip, R. Kumari, and R. Muthuswami. 2018. 'Regulation of ATM and ATR by SMARCAL1 and BRG1', *Biochim Biophys Acta Gene Regul Mech*, 1861: 1076-92.

She, Zhen-Yu, Kai-Wei Yu, Ning Zhong, Yu Xiao, Ya-Lan Wei, Yang Lin, Yue-Ling Li, and Ming-Hui Lu. 2020. 'Kinesin-7 CENP-E regulates chromosome alignment and genome stability of spermatogenic cells', *Cell Death Discovery*, 6: 25.

Sheahan, S., C. O. Bellamy, D. R. Dunbar, D. J. Harrison, and S. Prost. 2007. 'Deficiency of G1 regulators P53, P21Cip1 and/or pRb decreases hepatocyte sensitivity to TGFbeta cell cycle arrest', *BMC Cancer*, 7: 215.

Sheltzer, J. M., and A. Amon. 2011. 'The aneuploidy paradox: costs and benefits of an incorrect karyotype', *Trends Genet*, 27: 446-53.

Sheltzer, Jason M., Heidi M. Blank, Sarah J. Pfau, Yoshie Tange, Benson M. George, Timothy J. Humpton, Ilana L. Brito, Yasushi Hiraoka, Osami Niwa, and Angelika Amon. 2011. 'Aneuploidy Drives Genomic Instability in Yeast', *Science*, 333: 1026.

Shen, T., and S. Huang. 2012. 'The role of Cdc25A in the regulation of cell proliferation and apoptosis', *Anticancer Agents Med Chem*, 12: 631-9.

Shi, Lei, Adel Qalieh, Mandy M. Lam, Jason M. Keil, and Kenneth Y. Kwan. 2019. 'Robust elimination of genome-damaged cells safeguards against brain somatic aneuploidy following Knl1 deletion', *Nat Commun*, 10: 2588.

Shiloh, Yosef. 2003. 'ATM and related protein kinases: safeguarding genome integrity', *Nature Reviews Cancer*, 3: 155-68.

Shiozawa, Y., B. Nie, K. J. Pienta, T. M. Morgan, and R. S. Taichman. 2013. 'Cancer stem cells and their role in metastasis', *Pharmacol Ther*, 138: 285-93.

Simonetti, G., S. Bruno, A. Padella, E. Tenti, and G. Martinelli. 2019. 'Aneuploidy: Cancer strength or vulnerability?', *Int J Cancer*, 144: 8-25.

Sirois, I., A. Aguilar-Mahecha, J. Lafleur, E. Fowler, V. Vu, M. Scriver, M. Buchanan, C. Chabot, A. Ramanathan, B. Balachandran, S. Légaré, E. Przybytkowski, C. Lan, U. Krzemien, L. Cavallone, O. Aleynikova, C. Ferrario, M. C. Guilbert, N. Benlimame, A. Saad, M. Alaoui-Jamali, H. U. Saragovi, S. Josephy, C. O'Flanagan, S. D. Hursting, V.

R. Richard, R. P. Zahedi, C. H. Borchers, E. Bareke, S. Nabavi, P. Tonellato, J. A. Roy, A. Robidoux, E. A. Marcus, C. Mihalcioiu, J. Majewski, and M. Basik. 2019. 'A Unique Morphological Phenotype in Chemoresistant Triple-Negative Breast Cancer Reveals Metabolic Reprogramming and PLIN4 Expression as a Molecular Vulnerability', *Mol Cancer Res*, 17: 2492-507.

Slade, D. 2020. 'PARP and PARG inhibitors in cancer treatment', *Genes Dev*, 34: 360-94.

Sobczak, M., J. Pietrzak, T. Płoszaj, and A. Robaszkiewicz. 2020. 'BRG1 Activates Proliferation and Transcription of Cell Cycle-Dependent Genes in Breast Cancer Cells', *Cancers (Basel)*, 12.

Sobczak, M., A. R. Pitt, C. M. Spickett, and A. Robaszkiewicz. 2019. 'PARP1 Co-Regulates EP300-BRG1-Dependent Transcription of Genes Involved in Breast Cancer Cell Proliferation and DNA Repair', *Cancers (Basel)*, 11.

Sotillo, R., E. Hernando, E. Díaz-Rodríguez, J. Teruya-Feldstein, C. Cordón-Cardo, S. W. Lowe, and R. Benezra. 2007. 'Mad2 overexpression promotes aneuploidy and tumorigenesis in mice', *Cancer Cell*, 11: 9-23.

Sotillo, Rocio, Juan-Manuel Schvartzman, Nicholas D. Socci, and Robert Benezra. 2010. 'Mad2-induced chromosome instability leads to lung tumour relapse after oncogene withdrawal', *Nature*, 464: 436-40.

Soto, M., J. A. Raaijmakers, B. Bakker, D. C. J. Spierings, P. M. Lansdorp, F. Foijer, and R. H. Medema. 2017. 'p53 Prohibits Propagation of Chromosome Segregation Errors that Produce Structural Aneuploidies', *Cell Rep*, 19: 2423-31.

Sottile, Francesco, Francesco Aulicino, Ilda Theka, and Maria Pia Cosma. 2016. 'Mesenchymal stem cells generate distinct functional hybrids in vitro via cell fusion or entosis', *Sci Rep*, 6: 36863.

Srikanth, Srimari, Srimathy Ramachandran, and Suma Mohan S. 2020. 'Construction of the gene regulatory network identifies MYC as a transcriptional regulator of SWI/SNF complex', *Sci Rep*, 10: 158.

Stathis, A., and A. Oza. 2010. 'Targeting Wee1-like protein kinase to treat cancer', *Drug News Perspect*, 23: 425-9.

Stolz, Ailine, Norman Ertych, Anne Kienitz, Celia Vogel, Verena Schneider, Barbara Fritz, Ralf Jacob, Gunnar Dittmar, Wilko Weichert, Iver Petersen, and Holger Bastians. 2010. 'The CHK2–BRCA1 tumour suppressor pathway ensures chromosomal stability in human somatic cells', *Nature Cell Biology*, 12: 492-99.

Storchova, Z., and C. Kuffer. 2008. 'The consequences of tetraploidy and aneuploidy', *J Cell Sci*, 121: 3859-66.

Storchova, Zuzana, and David Pellman. 2004. 'From polyploidy to aneuploidy, genome instability and cancer', *Nature Reviews Molecular Cell Biology*, 5: 45-54.

Sundaram, M., D. L. Guernsey, M. M. Rajaraman, and R. Rajaraman. 2004. 'Neosis: a novel type of cell division in cancer', *Cancer Biol Ther*, 3: 207-18.

Swanton, C., B. Nicke, M. Schuett, A. C. Eklund, C. Ng, Q. Li, T. Hardcastle, A. Lee, R. Roy, P. East, M. Kschischo, D. Endesfelder, P. Wylie, S. N. Kim, J. G. Chen, M. Howell, T. Ried, J. K. Habermann, G. Auer, J. D. Brenton, Z. Szallasi, and J. Downward. 2009. 'Chromosomal instability determines taxane response', *Proc Natl Acad Sci U S A*, 106: 8671-6.

Täckholm, G. 1922. *Zytologische Studien Über Die Gattung Rosa*.

Tafel, A. A., L. Wu, and P. J. McHugh. 2011. 'Human HEL308 localizes to damaged replication forks and unwinds lagging strand structures', *J Biol Chem*, 286: 15832-40.

Taglialatela, A., S. Alvarez, G. Leuzzi, V. Sannino, L. Ranjha, J. W. Huang, C. Madubata, R. Anand, B. Levy, R. Rabadan, P. Cejka, V. Costanzo, and A. Ciccia. 2017. 'Restoration of Replication Fork Stability in BRCA1- and BRCA2-Deficient Cells by Inactivation of SNF2-Family Fork Remodelers', *Mol Cell*, 68: 414-30.e8.

Takata, Kei-ichi, Shelley Reh, Junya Tomida, Maria D. Person, and Richard D. Wood. 2013. 'Human DNA helicase HELQ participates in DNA interstrand crosslink tolerance with ATR and RAD51 paralogs', *Nat Commun*, 4: 2338.

Tanaka, K., H. Goto, Y. Nishimura, K. Kasahara, A. Mizoguchi, and M. Inagaki. 2018. 'Tetraploidy in cancer and its possible link to aging', *Cancer Sci*, 109: 2632-40.

Tang, Y. C., B. R. Williams, J. J. Siegel, and A. Amon. 2011a. 'Identification of aneuploidy-selective antiproliferation compounds', *Cell*, 144: 499-512.

Tang, Y. C., H. Yuwen, K. Wang, P. M. Bruno, K. Bullock, A. Deik, S. Santaguida, M. Trakala, S. J. Pfau, N. Zhong, T. Huang, L. Wang, C. B. Clish, M. T. Hemann, and A. Amon. 2017. 'Aneuploid Cell Survival Relies upon Sphingolipid Homeostasis', *Cancer Res*, 77: 5272-86.

Tang, Yun-Chi, Bret R. Williams, Jake J. Siegel, and Angelika Amon. 2011b. 'Identification of Aneuploidy-Selective Antiproliferation Compounds', *Cell*, 144: 499-512.

Tanudji, M., J. Shoemaker, L. L'Italien, L. Russell, G. Chin, and X. M. Schebye. 2004. 'Gene silencing of CENP-E by small interfering RNA in HeLa cells leads to missegregation of chromosomes after a mitotic delay', *Mol Biol Cell*, 15: 3771-81.

Targa, A., and G. Rancati. 2018. 'Cancer: a CINful evolution', *Curr Opin Cell Biol*, 52: 136-44.

Taylor, A. Malcolm R., Cynthia Rothblum-Oviatt, Nathan A. Ellis, Ian D. Hickson, Stefan

Meyer, Thomas O. Crawford, Agata Smogorzewska, Barbara Pietrucha, Corry Weemaes, and Grant S. Stewart. 2019. 'Chromosome instability syndromes', *Nature Reviews Disease Primers*, 5: 64.

Thompson, S. L., S. F. Bakhoum, and D. A. Compton. 2010. 'Mechanisms of chromosomal instability', *Curr Biol*, 20: R285-95.

Thompson, S. L., and D. A. Compton. 2010. 'Proliferation of aneuploid human cells is limited by a p53-dependent mechanism', *J Cell Biol*, 188: 369-81.

Tolić, I. M. 2018. 'Mitotic spindle: kinetochore fibers hold on tight to interpolar bundles', *Eur Biophys J*, 47: 191-203.

Torres, Eduardo M., Tanya Sokolsky, Cheryl M. Tucker, Leon Y. Chan, Monica Boselli, Maitreya J. Dunham, and Angelika Amon. 2007. 'Effects of Aneuploidy on Cellular Physiology and Cell Division in Haploid Yeast', *Science*, 317: 916.

Tsai, Hung-Ji, Anjali R. Nelliat, Mohammad Ikbal Choudhury, Andrei Kucharavy, William D. Bradford, Malcolm E. Cook, Jisoo Kim, Devin B. Mair, Sean X. Sun, Michael C. Schatz, and Rong Li. 2019. 'Hypo-osmotic-like stress underlies general cellular defects of aneuploidy', *Nature*, 570: 117-21.

Turajlic, S., H. Xu, K. Litchfield, A. Rowan, T. Chambers, J. I. Lopez, D. Nicol, T. O'Brien, J. Larkin, S. Horswell, M. Stares, L. Au, M. Jamal-Hanjani, B. Challacombe, A. Chandra, S. Hazell, C. Eichler-Jonsson, A. Soultati, S. Chowdhury, S. Rudman, J. Lynch, A. Fernando, G. Stamp, E. Nye, F. Jabbar, L. Spain, S. Lall, R. Guarch, M. Falzon, I. Proctor, L. Pickering, M. Gore, T. B. K. Watkins, S. Ward, A. Stewart, R. DiNatale, M. F. Becerra, E. Reznik, J. J. Hsieh, T. A. Richmond, G. F. Mayhew, S. M. Hill, C. D. McNally, C. Jones, H. Rosenbaum, S. Stanislaw, D. L. Burgess, N. R. Alexander, and C. Swanton. 2018. 'Tracking Cancer Evolution Reveals Constrained Routes to Metastases: TRACERx Renal', *Cell*, 173: 581-94.e12.

Turajlic, Samra, Andrea Sottoriva, Trevor Graham, and Charles Swanton. 2019. 'Resolving genetic heterogeneity in cancer', *Nature Reviews Genetics*, 20: 404-16.

Uygur, Berna, Kamran Melikov, Anush Arakelyan, Leonid B. Margolis, and Leonid V. Chernomordik. 2019. 'Syncytin 1 dependent horizontal transfer of marker genes from retrovirally transduced cells', *Sci Rep*, 9: 17637.

Van de Peer, Yves, Eshchar Mizrachi, and Kathleen Marchal. 2017. 'The evolutionary significance of polyploidy', *Nature Reviews Genetics*, 18: 411-24.

van den Bos, H., B. Bakker, D. C. J. Spierings, P. M. Lansdorp, and F. Foijer. 2018. 'Single-cell sequencing to quantify genomic integrity in cancer', *Int J Biochem Cell Biol*, 94: 146-50.

van Jaarsveld, R. H., and Gjpl Kops. 2016. 'Difference Makers: Chromosomal Instability versus Aneuploidy in Cancer', *Trends Cancer*, 2: 561-71.

Vargas-Rondon, N., V. E. Villegas, and M. Rondon-Lagos. 2017. 'The Role of Chromosomal Instability in Cancer and Therapeutic Responses', *Cancers (Basel)*, 10.

Vasudevan, A., P. S. Baruah, J. C. Smith, Z. Wang, N. M. Sayles, P. Andrews, J. Kendall, J. Leu, N. K. Chunduri, D. Levy, M. Wigler, Z. Storchová, and J. M. Sheltzer. 2020. 'Single-Chromosomal Gains Can Function as Metastasis Suppressors and Promoters in Colon Cancer', *Dev Cell*, 52: 413-28.e6.

Vitale, I., L. Galluzzi, L. Senovilla, A. Criollo, M. Jemaà, M. Castedo, and G. Kroemer. 2011. 'Illicit survival of cancer cells during polyploidization and depolyploidization', *Cell Death & Differentiation*, 18: 1403-13.

Vitale, I., M. Jemaà, L. Senovilla, L. Galluzzi, S. Rello-Varona, D. Metivier, H. Ripoche, V. Lazar, P. Dessen, M. Castedo, and G. Kroemer. 2010. 'Involvement of p38alpha in the mitotic progression of p53(-/-) tetraploid cells', *Cell Cycle*, 9: 2823-9.

Vogel, Celia, Anne Kienitz, Irmgard Hofmann, Rolf Müller, and Holger Bastians. 2004. 'Crosstalk of the mitotic spindle assembly checkpoint with p53 to prevent polyploidy', *Oncogene*, 23: 6845-53.

Wang, Mengdie, Raymond B. Nagle, Beatrice S. Knudsen, Anne E. Cress, and Gregory C. Rogers. 2020. 'Centrosome loss results in an unstable genome and malignant prostate tumors', *Oncogene*, 39: 399-413.

Wang, Ran, Shuxun Chen, Changxian Li, Kevin Tak Pan Ng, Chi-wing Kong, Jinping Cheng, Shuk Han Cheng, Ronald A. Li, Chung Mau Lo, Kwan Man, and Dong Sun. 2016. 'Fusion with stem cell makes the hepatocellular carcinoma cells similar to liver tumor-initiating cells', *BMC Cancer*, 16: 56.

Wang, Y., L. Hoang, J. X. Ji, and D. G. Huntsman. 2020. 'SWI/SNF Complex Mutations in Gynecologic Cancers: Molecular Mechanisms and Models', *Annu Rev Pathol*, 15: 467-92.

Watson, J. D., and F. H. C. Crick. 1953. 'Molecular Structure of Nucleic Acids: A Structure for Deoxyribose Nucleic Acid', *Nature*, 171: 737-38.

Watts, C. A., F. M. Richards, A. Bender, P. J. Bond, O. Korb, O. Kern, M. Riddick, P. Owen, R. M. Myers, J. Raff, F. Gergely, D. I. Jodrell, and S. V. Ley. 2013. 'Design, synthesis, and biological evaluation of an allosteric inhibitor of HSET that targets cancer cells with supernumerary centrosomes', *Chem Biol*, 20: 1399-410.

Weaver, B. A., A. D. Silk, C. Montagna, P. Verdier-Pinard, and D. W. Cleveland. 2007. 'Aneuploidy acts both oncogenically and as a tumor suppressor', *Cancer Cell*, 11: 25-36.

Weiler, J., and T. Dittmar. 2019. 'Cell Fusion in Human Cancer: The Dark Matter Hypothesis', *Cells*, 8.

Whelan, D. R., W. T. C. Lee, Y. Yin, D. M. Ofri, K. Bermudez-Hernandez, S. Keegan, D.

Fenyo, and E. Rothenberg. 2018. 'Spatiotemporal dynamics of homologous recombination repair at single collapsed replication forks', *Nat Commun*, 9: 3882.

Wieser, S., and J. Pines. 2015. 'The biochemistry of mitosis', *Cold Spring Harb Perspect Biol*, 7: a015776.

Wilhelm, T., M. Said, and V. Naim. 2020. 'DNA Replication Stress and Chromosomal Instability: Dangerous Liaisons', *Genes (Basel)*, 11.

Wilhelm, Therese, Anna-Maria Olziersky, Daniela Harry, Filipe De Sousa, Helène Vassal, Anja Eskat, and Patrick Meraldi. 2019. 'Mild replication stress causes chromosome mis-segregation via premature centriole disengagement', *Nat Commun*, 10: 3585.

Williams, Bret R., Vineet R. Prabhu, Karen E. Hunter, Christina M. Glazier, Charles A. Whittaker, David E. Housman, and Angelika Amon. 2008. 'Aneuploidy Affects Proliferation and Spontaneous Immortalization in Mammalian Cells', *Science*, 322: 703.

Wong, S., P. Hui, and N. Buza. 2020. 'Frequent loss of mutation-specific mismatch repair protein expression in nonneoplastic endometrium of Lynch syndrome patients', *Mod Pathol*.

Wood, K. W., L. Lad, L. Luo, X. Qian, S. D. Knight, N. Nevins, K. Brejc, D. Sutton, A. G. Gilmartin, P. R. Chua, R. Desai, S. P. Schauer, D. E. McNulty, R. S. Annan, L. D. Belmont, C. Garcia, Y. Lee, M. A. Diamond, L. F. Faucette, M. Giardiniere, S. Zhang, C. M. Sun, J. D. Vidal, S. Lichtsteiner, W. D. Cornwell, J. D. Greshock, R. F. Wooster, J. T. Finer, R. A. Copeland, P. S. Huang, D. J. Morgans, Jr., D. Dhanak, G. Bergnes, R. Sakowicz, and J. R. Jackson. 2010. 'Antitumor activity of an allosteric inhibitor of centromere-associated protein-E', *Proc Natl Acad Sci U S A*, 107: 5839-44.

Worrall, J. T., N. Tamura, A. Mazzagatti, N. Shaikh, T. van Lingen, B. Bakker, D. C. J. Spierings, E. Vladimirou, F. Foijer, and S. E. McClelland. 2018. 'Non-random Mis-segregation of Human Chromosomes', *Cell Rep*, 23: 3366-80.

Wu, J., A. Springett, and J. K. Morris. 2013. 'Survival of trisomy 18 (Edwards syndrome) and trisomy 13 (Patau Syndrome) in England and Wales: 2004-2011', *Am J Med Genet A*, 161a: 2512-8.

Xie, Y., A. Wang, J. Lin, L. Wu, H. Zhang, X. Yang, X. Wan, R. Miao, X. Sang, and H. Zhao. 2017. 'Mps1/TTK: a novel target and biomarker for cancer', *J Drug Target*, 25: 112-18.

Xu, H., J. Ma, J. Wu, L. Chen, F. Sun, C. Qu, D. Zheng, and S. Xu. 2016. 'Gene expression profiling analysis of lung adenocarcinoma', *Braz J Med Biol Res*, 49.

Xu, R., Y. Xu, W. Huo, Z. Lv, J. Yuan, S. Ning, Q. Wang, M. Hou, G. Gao, J. Ji, J. Chen, R. Guo, and D. Xu. 2018. 'Mitosis-specific MRN complex promotes a mitotic signaling cascade to regulate spindle dynamics and chromosome segregation', *Proc Natl Acad Sci U S A*, 115: E10079-e88.

Xu, Xiaowei, Shijiao Huang, Boyan Zhang, Fan Huang, Wangfei Chi, Jingyan Fu, Gang Wang, Si Li, Qing Jiang, and Chuanmao Zhang. 2017. 'DNA replication licensing factor Cdc6 and Plk4 kinase antagonistically regulate centrosome duplication via Sas-6', *Nat Commun*, 8: 15164.

Xuan, B., D. Ghosh, E. M. Cheney, E. M. Clifton, and M. R. Dawson. 2018. 'Dysregulation in Actin Cytoskeletal Organization Drives Increased Stiffness and Migratory Persistence in Polyploidal Giant Cancer Cells', *Sci Rep*, 8: 11935.

Yahara, Yasuhito, Tomasa Barrientos, Yuning J. Tang, Vijitha Puviindran, Puviindran Nadesan, Hongyuan Zhang, Jason R. Gibson, Simon G. Gregory, Yarui Diao, Yu Xiang, Yawar J. Qadri, Tomokazu Souma, Mari L. Shinohara, and Benjamin A. Alman. 2020. 'Erythromyeloid progenitors give rise to a population of osteoclasts that contribute to bone homeostasis and repair', *Nature Cell Biology*, 22: 49-59.

Yan, Bingyu, Jianguo Wang, and Li Liu. 2016. 'Chemotherapy promotes tumour cell hybridization in vivo', *Tumor Biology*, 37: 5025-30.

Yan, Ting-Lin, Meng Wang, Zhi Xu, Chun-Ming Huang, Xiao-Cheng Zhou, Er-Hui Jiang, Xiao-Ping Zhao, Yong Song, Kai Song, Zhe Shao, Ke Liu, and Zheng-Jun Shang. 2017. 'Up-regulation of syncytin-1 contributes to TNF-α-enhanced fusion between OSCC and HUVECs partly via Wnt/β-catenin-dependent pathway', *Sci Rep*, 7: 40983.

Yanagida, M. 2014. 'The role of model organisms in the history of mitosis research', *Cold Spring Harb Perspect Biol*, 6: a015768.

Yang, C., X. Tang, X. Guo, Y. Niikura, K. Kitagawa, K. Cui, S. T. Wong, L. Fu, and B. Xu. 2011. 'Aurora-B mediated ATM serine 1403 phosphorylation is required for mitotic ATM activation and the spindle checkpoint', *Mol Cell*, 44: 597-608.

Yang, Liqun, Pengfei Shi, Gaichao Zhao, Jie Xu, Wen Peng, Jiayi Zhang, Guanghui Zhang, Xiaowen Wang, Zhen Dong, Fei Chen, and Hongjuan Cui. 2020. 'Targeting cancer stem cell pathways for cancer therapy', *Signal Transduction and Targeted Therapy*, 5: 8.

Yao, Xuebiao, Ariane Abrieu, Yun Zheng, Kevin F. Sullivan, and Don W. Cleveland. 2000. 'CENP-E forms a link between attachment of spindle microtubules to kinetochores and the mitotic checkpoint', *Nature Cell Biology*, 2: 484-91.

Yart, Lucile, Daniel Bastida-Ruiz, Christine Wuillemin, Pascale Ribaux, Mathilde Allard, Pierre-Yves Dietrich, Patrick Petignat, and Marie Cohen. 2020. 'Linking endoplasmic reticulum stress to polyploidy in ovarian cancer cells', *bioRxiv*: 2020.01.24.918029.

Ye, C. J., Z. Sharpe, S. Alemara, S. Mackenzie, G. Liu, B. Abdallah, S. Horne, S. Regan, and H. H. Heng. 2019. 'Micronuclei and Genome Chaos: Changing the System Inheritance', *Genes (Basel)*, 10.

Yi, Q., X. Zhao, Y. Huang, T. Ma, Y. Zhang, H. Hou, H. J. Cooke, D. Q. Yang, M. Wu, and Q. Shi. 2011. 'p53 dependent centrosome clustering prevents multipolar mitosis in

tetraploid cells', *PLoS One*, 6: e27304.

Yin, Liyuan, Peizhen Hu, Xianping Shi, Weiping Qian, Haiyen E. Zhau, Stephen J. Pandol, Michael S. Lewis, Leland W. K. Chung, and Ruoxiang Wang. 2020. 'Cancer cell's neuroendocrine feature can be acquired through cell-cell fusion during cancer-neural stem cell interaction', *Sci Rep*, 10: 1216.

Yu, Y., W. Jia, Y. Lyu, D. Su, M. Bai, J. Shen, J. Qiao, T. Han, W. Liu, J. Chen, W. Chen, D. Ye, X. Guo, S. Zhu, J. Xi, R. Zhu, X. Wan, S. Gao, J. Zhu, and J. Kang. 2019. 'Pwp1 regulates telomere length by stabilizing shelterin complex and maintaining histone H4K20 trimethylation', *Cell Discov*, 5: 47.

Zasadil, L. M., K. A. Andersen, D. Yeum, G. B. Rocque, L. G. Wilke, A. J. Tevaarwerk, R. T. Raines, M. E. Burkard, and B. A. Weaver. 2014. 'Cytotoxicity of paclitaxel in breast cancer is due to chromosome missegregation on multipolar spindles', *Sci Transl Med*, 6: 229ra43.

Zhang, L., H. Chen, M. Gong, and F. Gong. 2013. 'The chromatin remodeling protein BRG1 modulates BRCA1 response to UV irradiation by regulating ATR/ATM activation', *Front Oncol*, 3: 7.

Zhang, Qiao, Ajay A. Vashisht, Jason O'Rourke, Stéphane Y. Corbel, Rita Moran, Angelica Romero, Loren Miraglia, Jia Zhang, Eric Durrant, Christian Schmedt, Srinath C. Sampath, and Srihari C. Sampath. 2017. 'The microprotein Minion controls cell fusion and muscle formation', *Nat Commun*, 8: 15664.

Zhang, S., I. Mercado-Uribe, and J. Liu. 2014. 'Tumor stroma and differentiated cancer cells can be originated directly from polyploid giant cancer cells induced by paclitaxel', *Int J Cancer*, 134: 508-18.

Zhang, S., I. Mercado-Uribe, Z. Xing, B. Sun, J. Kuang, and J. Liu. 2014. 'Generation of cancer stem-like cells through the formation of polyploid giant cancer cells', *Oncogene*, 33: 116-28.

Zhang, S., D. Zhang, Z. Yang, and X. Zhang. 2016. 'Tumor Budding, Micropapillary Pattern, and Polyploidy Giant Cancer Cells in Colorectal Cancer: Current Status and Future Prospects', *Stem Cells Int*, 2016: 4810734.

Zhang, W., J. H. Mao, W. Zhu, A. K. Jain, K. Liu, J. B. Brown, and G. H. Karpen. 2016. 'Centromere and kinetochore gene misexpression predicts cancer patient survival and response to radiotherapy and chemotherapy', *Nat Commun*, 7: 12619.

Zhang, Y., L. Li, R. Liu, and C. Zeng. 2020. 'DNA Primase Subunit 1 Expression in Hepatocellular Carcinoma and Its Clinical Implication', *Biomed Res Int*, 2020: 9689312.

Zhou, X., K. Merchak, W. Lee, J. P. Grande, M. Cascalho, and J. L. Platt. 2015. 'Cell Fusion Connects Oncogenesis with Tumor Evolution', *Am J Pathol*, 185: 2049-60.

Zhu, Y., C. Mao, J. Wu, S. Li, R. Ma, H. Cao, M. Ji, C. Jing, and J. Tang. 2014. 'Improved ataxia telangiectasia mutated kinase inhibitor KU60019 provides a promising treatment strategy for non-invasive breast cancer', *Oncol Lett*, 8: 2043-48.

Zielinski, Daniel C., Neema Jamshidi, Austin J. Corbett, Aarash Bordbar, Alex Thomas, and Bernhard O. Palsson. 2017. 'Systems biology analysis of drivers underlying hallmarks of cancer cell metabolism', *Sci Rep*, 7: 41241.

Zimmerman, E. I., D. C. Turner, J. Buaboonnam, S. Hu, S. Orwick, M. S. Roberts, L. J. Janke, A. Ramachandran, C. F. Stewart, H. Inaba, and S. D. Baker. 2013. 'Crenolanib is active against models of drug-resistant FLT3-ITD-positive acute myeloid leukemia', *Blood*, 122: 3607-15.

Cancer research UK statistics, accessed November 2020: https://www.cancerresearchuk.org/health-professional/cancer-statistics-for-the-uk

c-Bioportal for cancer genomics, accessed November 2020: https://www.cbioportal.org/

World health organisation statistics, accessed November 2020: https://www.who.int/health-topics/cancer#tab=tab_1